NASA TECHNICAL TRANSLATION NASA TT F-16,148

# THE THERMAL AND STRESSED STATES OF ROTORS OF CENTRIPETAL GAS TURBINES

Ya. M. Gusak et al.

(NASA-TT-F-16148) THE THERMAL AND STRESSED STATES OF ROTORS OF CENTRIPETAL GAS TURBINES (Kanner (Leo) Associates)

N75-16855

Unclas
G3/37 10242

Translation of Teplovoye i napryazhennoye sostoyaniya rotorov radial'no-osevykh gasovykh turbin, Kiev, Naukova Dumka Press, 1973, 184 pp.

Reproduced by
NATIONAL TECHNICAL
INFORMATION SERVICE
U.S. Department of Commerce
Springfield, VA. 22151

NATIONAL AERONAUTICS AND SPACE ADMINISTRATION
WASHINGTON, D.C. 20546 FEBRUARY 1975

STANDARD TITLE PAGE

| 1. Report No. NASA TT F-16,148 | 2. Government Accession No. | 3. Recipient's Catalog No. |
|---|---|---|
| 4. Title and Subtitle THE THERMAL AND STRESSED STATES OF ROTORS OF CENTRIPETAL GAS TURBINES | | 5. Report Date February 1975<br>6. Performing Organization Code |
| 7. Author(s) Ya. M. Gusak, Ye. P. Dyban, A. F. Koles-nichenko, S. A. Mokrushin, and M. V. Stradomskiy | | 8. Performing Organization Report No.<br>10. Work Unit No. |
| 9. Performing Organization Name and Address Leo Kanner Associates Redwood City, California 94063 | | 11. Contract or Grant No. NASw-2481<br>13. Type of Report and Period Covered Translation |
| 12. Sponsoring Agency Name and Address National Aeronautics and Space Administration, Washington, D.C. 20546 | | 14. Sponsoring Agency Code |

15. Supplementary Notes

Translation of Teplovoye i napryazhennoye sostoyaniya rotorov radial'no-osevykh gasovykh turbin, Kiev, Naukova Dumka Press, 1973, 184 pp. (A-74-45270)

16. Abstract

Theoretical and experimental data on rotors of small turbines of the type used in superchargers of internal combustion engines are examined and generalized. Engineering methods of calculating the thermal and stressed states of rotors with different types of cooling are proposed.

Reproduced by
NATIONAL TECHNICAL INFORMATION SERVICE
US Department of Commerce
Springfield, VA. 22151

| 17. Key Words (Selected by Author(s)) | 18. Distribution Statement |
|---|---|
| | Unclassified - Unlimited |

| 19. Security Classif. (of this report) | 20. Security Classif. (of this page) | 21. |
|---|---|---|
| Unclassified | Unclassified | |



NASA-HQ

## AUTHORS' ABSTRACT

/2*

Generalized findings of experimental and theoretical investigations of the thermal and stressed states of rotors of centripetal gas turbines used in turbo-supercharging units in internal combustion engines are presented in the book. Engineering methods of calculating the thermal and stressed states of rotors of centripetal turbines are proposed for various methods of rotor cooling.

The book is written for scientific and engineering-technical personnel working in gas turbine-building and also for instructors, and graduate and undergraduate students in senior courses of the related specialties.

Chief Editor:
Academician of the UkSSR Academy of Sciences I. T. Shvets

Reviewers:
Doctor of Technical Sciences L. A. Kozdoba, and
Candidate of Technical Sciences S. S. Rusakov

* Numbers in the margin indicate pagination in the foreign text.

# FOREWORD

/3

Single-stage centripetal gas turbines are used as compressor drives in turbo-supercharging sets in internal combustion engines. Also, small, high-rpm, low-power centripetal gas turbines are used as autonomous engines for driving various auxiliary mechanisms where compactness of installation is required in conjunction with rapid startup and operation over a wide range of variable loads. In these applications, centripetal turbines compete successfully with axial turbines, naturally assuming equal power rating.

Centripetal turbines have a number of advantages compared to axial.

1. The net efficiency of a low-power centripetal turbine (up to 1000 kW) is higher than for an axial low-power turbine and can attain, according to data in the studies /33, 59/, 0.85-0.88. This high efficiency of a centripetal gas turbine is combined with good manufacturability of the rotor, which can be made monolithic.

2. The adjustable nozzle box in centripetal turbines is simpler and more reliable than in axial.

3. Greater heat transfer can be generated in the stage of a centripetal turbine with fairly high efficiency than in an axial.

Drawbacks of centripetal turbines include these: high running speeds, owing to which the demands on the bearing assemblies and shaft couplings are intensified; relatively high rotor temperatures caused by the fact that most of the disk is swept by heated gases; and large temperature drops along the radius and thickness of the rotor, causing unacceptable stresses.

The last two disadvantages often are of decisive weight when selecting a turbine type. These disadvantages can be eliminated when the cooling system is successfully chosen. Intensive rotor cooling systems in centripetal gas turbines ensure longer service life and reliability of installations operating at initial gas temperature above 700° C.

As shown by theoretical and experimental studies /26, 33, 46, 59, 79, 90/, use of air cooling in gas turbine engines /GTE/ with centripetal turbines is most effective. When air is used as the coolant, simple and reliable turbine impeller cooling systems can be built, not complicating operating conditions and design of the remaining components. Intensive rotor cooling lowers overall disk

temperatures (and thus increases the allowable limit of long-term strength) and markedly lowers temperature drops over different parts of the disk. This latter advantage favorably affects the stressed state of the disk and enhances its strength, especially in frequent starts and stops. /4

The periodical literature contains a number of studies on problems in calculating the thermal and stressed states of rotors of centripetal gas turbines. Of late studies have been published giving the results of the direct determination of temperatures and stresses in full-scale and model centripetal turbines. The drawback common to these studies is their partial coverage, and sometimes contradictoriness; this greatly hampers designing new engines and adds to the volume (and therefore, the workload) in revising prototypes of centripetal turbines.

This monogram attempts to sum up many years of theoretical and experimental work on the thermal and stressed states of rotors of centripetal gas turbines (mainly, turbo-supercharger sets in internal combustion engines) carried out at the Institute of Technical Heat-Physics (ITTF), Ukrainian SSR Academy of Sciences, and at the Ural'sk Turbomotor Plant imeni K. Ye. Voroshilov /TMZ/.

In the preparation of this book, some results of work done at the ITTF, AN UkSSR /Ukrainian SSR Academy of Sciences/ on air-cooling systems for parts of axial gas turbines were also used. Moreover, results of similarly oriented work published in the domestic and foreign periodical literature were drawn upon.

Based on the accumulated experience of research and design-calculation work, plus critical analysis of literature sources, in the book are suggested engineering methods of calculating the thermal and stressed states of rotors of centripetal gas turbines, and for determining the main characteristics of currently used air-cooling systems for these turbines; also given are recommendations on optimizing these systems.

Chapter One briefly reviews designs of the most representative centripetal gas turbines and describes test beds and instruments used in investigating cooling systems in turbines of this class.

Chapter Two sets forth the main results of studies of rotor cooling systems of centripetal turbines in series-produced domestic supercharging turbocompressors of internal combustion engines both in stand conditions and directly in the engine.

Chapter Three contains results of experimental and design work on determining the effectiveness of the most common systems of rotor air cooling in centripetal gas turbines. Included in the same chapter are the regularities of heat transfer in rotor-cooling systems of centripetal turbines and in their blading.

Chapter Four presents the main principles of the techniques of the engineering calculation of air-cooling systems in centripetal gas turbines. The recommended method sums up experience accumulated in allied fields, as well as in developing air-cooling systems of axial turbines.

The last two chapters deal with problems arising in evaluating the stressed state and strength characteristics of impellers of centripetal gas turbines.

Chapter Five gives the results of calculating stresses induced /5 in rotors acted on by centrifugal forces. Stress calculations were done on a digital computer. This made it possible to examine the influence on the stressed rotor state of numerous design and regime parameters. Included in this same chapter are the findings of experimental work on the strength of rotors, turbines, and compressors; failure rpm values are determined for these components.

Chapter Six sets forth the results of investigations of the stressed state and strength of rotors when steady-state and nonsteady temperature fields are present along with centrifugal forces. Most of these studies were conducted with the use of calculation methods.

The primary attention in the book is given to engineering methods of calculation that have suitable precision and workload requirements. The limited size of the book did not permit inclusion of more complicated and laborious methods of calculating cooling systems and the stressed state of rotors.

Chapters One through Four of the book were written by Doctor of Technical Sciences Ye. P. Dyban, and Candidates of Technical Sciences M.V. Stradomskiy and A. F. Kolesnichenko; Chapter Five was written by Candidate of Technical Sciences Ya. M. Gusak; Chapter Six -- by Candidate of Technical Sciences S. A. Mokrushin (Section 3 of Chapter Six -- by Ya. M. Gusak). Overall scientific editing of the manuscript was done by Academician of the Ukrainian SSR Academy of Sciences, I. T. Shvets and Doctor of Technical Sciences Ye. P. Dyban.

The authors are deeply grateful to the staff members of the thermal conductivity department of the ITTF AN UkSSR for assistance in readying the manuscript.

The authors are most appreciative of Doctor of Technical Sciences L. Kozdoba and Candidate of Technical Sciences S. S. Rusakov for a number of valuable suggestions and advice in their review of the manuscript.

All comments, suggestions, and ideas should be sent to: Kiev-57, Zhelyabova 2-A, Institute of Technical Heat-Physics, Ukrainian SSR Academy of Sciences.

## LIST OF SYMBOLS

$a = \frac{\lambda}{C_p \rho}$ is coefficient of thermal diffusivity, $m^2/sec$

B is wetted perimeter, m

$C_p$ is heat capacity, J/kg·deg

$D_g = 4F/B$ is hydraulic diameter, m

D is maximum disk diameter, m

C is absolute gas velocity, m/sec

f, F is cross sectional area, $m^2$

G is the mass flow of gas through turbine, compressor capacity, kg/sec

g is mass flow of cooland, kg/sec

$\bar{g} = g/G$ is relative mass flow of coolant

h, h' is thickness of rotor blade at tip and in root section, mm

$K = Cp/Cv$ is adiabatic index

i is the number of grooves in labyrinth seal

$L_o$ is the available specific work, J/kg

$\ell$ is the characteristic dimension, m

$\bar{m} = \rho_{i.a} C_{i.a} / \rho_g W_1$ is the coefficient of intercooler air when film cooling is used

$m = g_{rad}/g_{i.a}$ is the ratio of the mass flow of cooling air in radial blowoff to total mass flow of air in combination cooling

n is number of revolutions, 1/sec, rpm

N is power, kW

P is pressure, $N/m^2$, bar

r is radius, mm

$\bar{r} = r/r'$ is relative radius

R is gas constant, J/kg·deg

s is height of slot, width of clearance, mm

$\bar{s} = s + 0.5\,h$ is standard slot height, m

T* is total stream temperature, °C

$T$ is temperature, $^{\circ}C$

$t$ is blade spacing, mm

$u$ is rotor tip speed, m/sec

$u_1$ is velocity of intercooler air, m/sec

$x$ is coordinate measured from the leading edge or coordinate of cross section under consideration, m

$g$ is acceleration due to gravity, $m/sec^2$

$w$ is velocity in given section or relative gas velocity, m/sec /7

$v$ is specific volume, $kg/m^3$

$z$ is number of blades

$\bar{z} = z/D_{str}$ is relative number of blades, 1/m

$\alpha$ is heat transfer coefficient, $W/m^2 \cdot deg$

$\alpha_{av} = (\alpha_{i.a} + \alpha_g)/2$ is the mean heat transfer coefficient for an asymmetrically cooled disk, $W/m^2 \cdot deg$

$\delta$ is thickness of blade tip, mm

$\delta^*$ is displacement thickness of boundary layer, m

$\varepsilon_\ell$ is corrective factor allowing for relative ducting length

$\varepsilon_\phi$ is the relative elongation in the peripheral direction, 1/deg

$\varepsilon_r$ is the relative elongation in the radial direction, 1/deg

$\xi$ is the coefficient of hydraulic losses

$\theta_1 = T_{i.a}/T_1$ is the ratio of intercooler temperature to temperature of gas in channel

$\theta = T-T_{i.a}/T_g-T_{i.a}$ is relative excess temperature

$\bar{\lambda}$ is coefficient of friction

$\lambda$ is coefficient of thermal conductivity, $W/m \cdot deg$

$\nu_s = \frac{\sigma}{\alpha E(T_g - T_{s.d})}$ is dimensionless temperature stress

$\nu$ is coefficient of kinematic viscosity, $m^2/sec$

$\rho$ is density

$\tau$ is time, sec

$\bar{\tau} = \frac{\tau}{\tau_{st}}$ is dimensionless time

$\sigma_r$ is radial stress in disk, $kg/cm^2$

$\sigma_{r_b}$ is radial stresses in blades, $kg/cm^2$

$\sigma_t$ is tangential stresses in disk, $kg/cm^2$

$\eta = (T_{w.ad}-T_g)/T_{i.a}-T_g)$ is efficiency of film cooling

$\eta$ is diffuser efficiency

$\omega$ is angular velocity, 1/sec

$a_k$ is speed of sound, m/sec

## SIMILARITY CRITERIA

$Bi = \alpha\ell/\lambda|_w$ is Biot number

$Re = w\ell\rho/\mu$ is Reynolds number

$Nu = \alpha\ell/\lambda|$ is Nusselt number

$Re_1 = \rho_g\omega_g s/\mu$ is Reynolds number calculated from parameters of main stream and standard slot height

$Re_\omega = \omega r^2/v$ is Reynolds number calculated from angular speed of disk

$Re_o = wr/v$ is Reynolds number calculated from stream velocity during blowoff /8

$Fr = \omega^2 r/g$ is Froude number

$Fo = a^2 r/\ell^2$ is Fourier number

$M = w/a_k$ is compressibility criterion (Mach number)

$Pr = \mu/\rho a$ is Prandtl number

$St = \alpha/C_p\rho w$ is Stanton number

Tu is degree of turbulence

## SUBSCRIPTS

ad is adiabatic temperature
atm is ambient atmosphere
w is water
g is gas
en is engine
d is disk
ed is edge
c is compressor
b is blade

i.a is intercooler air
o is entry section
fi is air film
rad is mass flow in radial direction
rup is number of revolutions or tip speed corresponding to disk rupture
wor is working value of parameters
cal is calculated value of quantity
av is mean value of quantity
jet is jet blowoff
wa is wall
t is turbine
tc is turbocompressor
ci is circulation component
nod is nodal point
rd is reduced value of parameter for rated regime
se is seal
r is radial component
$\rho$ is radial direction
$\phi$ is peripheral direction
1 stands for parameters upstream of impeller
2 stands for parameters downstream of turbine
i stands for parameters in inlet section
j stands for parameters in outlet section
i-j is the mean value of a parameter between the inlet and outlet sections

TABLE OF CONTENTS


| | Page |
|---|---|
| Chapter One. Methods and Installations for Experimental Investigation of Rotor Cooling Systems of Centripetal Turbines | 1 |
| 1.1. Designs of centripetal turbines of turbo-supercharging sets and autonomous GTE | 1 |
| 1.2. Main problems of investigation | 11 |
| 1.3. Objects of investigations and test stands | 17 |
| 1.4. Method of measurements and measuring equipment | 21 |
| Chapter Two. Results of Experimental Investigations of Cooling Systems of Rotors of Centripetal Turbines of Series-Produced Turbocompressors | 28 |
| 2.1. Stand test | 28 |
| 2.2. Tests with combined operation of turbocompressor and internal combustion engine | 36 |
| 2.3. Nonsteady thermal regimes | 49 |
| Chapter Three. Effectiveness of Rotor Cooling Systems and Heat Transfer in Rotor Elements | 58 |
| 3.1. Main characteristics of cooling systems | 58 |

Page

3.2. Estimating effectiveness of air-cooling methods examined 72

3.3. Heat transfer in cooling system elements 75

Chapter Four. Main Principles of Method of Calculating Air-Cooling Systems of Rotors in Centripetal Gas Turbines 92

4.1. Hydraulic calculation 93

4.2. Thermal calculation 103

4.3. Examples of calculations 116

Chapter Five. Stressed State and Strength of Rotors of Centripetal Turbines and of Centrifugal Compressors When Acted on by Centrifugal Forces 121

5.1. Background on the stressed state of rotors of radial turbo-machines 121

5.2. Survey of methods of stressed calculation 123

5.3. Main premises of the method of calculating stresses in rotors using computers 126

5.4. Design study of stressed state of rotors 137

5.5. Method of investigating strength of rotors in acceleration tests of full-scale turbocompressors 141

5.6. Main results of investigating rotor strength 146

5.7. Calculation of limit stress. Criteria and margins of safety 156

5.8. Approximate determination of rupture revolution for rotors 162

Chapter Six. Stressed State and Strength of Rotors in Centrifugal Turbines When Steady and Nonsteady Temperature Fields Are Present 168

6.1. Stressed state of rotors when acted on by thermal stresses and stresses induced by centrifugal forces 168

6.2. Thermal stresses in rotors of centrifugal turbines 170

6.3. Experimental studies of rotor thermal fatigue 179

References 188

# THERMAL AND STRESSED STATES OF CENTRIPETAL GAS TURBINES

Ya. M. Gusak, Ye. P. Dyban, A. F. Kolesnichenko,
S. A. Mokrushin, and M. V. Stradomskiy,
Institute of Technical Heat-Physics,
Ukrainian SSR Academy of Sciences

## CHAPTER ONE

/9

## METHODS AND INSTALLATIONS FOR EXPERIMENTAL INVESTIGATION OF ROTOR COOLING SYSTEMS OF CENTRIPETAL TURBINES

### 1. Designs of Centripetal Turbines of Turbo-Supercharging Sets and Autonomous GTE /Gas Turbine Engines/

Depending on the function, gas turbine power plants with centripetal turbines are built with uncooled or cooled turbines.

Uncooled rotors of centripetal turbines are used as a rule in gas turbine power plants with short service life (100-1000 hours) and relatively low gas temperatures upstream of turbine (500-650° C).

In uncooled turbines, high quality heat-resistant alloys and austenite class steels are used in making the impellers /59, 107/. In this case, an effort is made to develop a rotor design with minimum disk service in contact with hot gases /98, 101/. For this purpose, unshrouded-type rotors are used in some turbine designs, even at the cost of turbine operating economy. Thus, unshrouded rotors made from nimonic 90-type alloys were used in GTE and turbocompressors for super charging internal combustion engines /71, 114, 120/ (Fig. 1). Unshrouded rotors (Fig. 1) operate in the region of temperatures that are quite low for this alloy -- 700-720° C. Since the efficiency of the turbo-supercharger set containing these rotors is low, the rotors have not found wide use in modern turboprop engines. However, in unshrouded rotors it was possible to avoid successive temperature stresses in nonsteady regimes.

Uncooled semishrouded rotors are used in several turbocompressors produced by our domestic industry. They include the TKR-8.5 and TKR-11 turbocompressors with turbine rotor diameters of 85 and 110 mm, and also the YaMZ turbocompressor (Fig. 2), whose impellers are made monolithic from the austenite class

steel EI-572 /7, 42/. These turbocompressors are designed for supercharging truck and tractor-type engines and have a service life of 1500-2000 hours /86/.

Ordinarily in these turbocompressors there is no need to use special air-cooling systems since their rotors have fairly high strength safety factors owing to their small size.

The appearance of more powerful turbocompressors with centripetal turbines ( rotor diameters of 140, 230 mm, and higher) and the conversion from low supercharging to moderate and high levels demanded a large expansion of investigations into the thermal and stressed states of turbine rotors. Accumulated experience in designing and operating these turbocompressors showed that to ensure the required service life and operating reliability of an installation intensive turbine rotor cooling was vital. So modern centripetal turbines have some system of cooling rotors and casings. /10

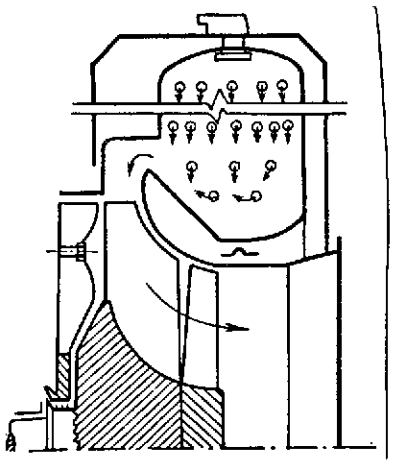

Fig. 1. Longitudinal section of turbine of Airsearch GTE (United States)

The temperature of the turbine rotor can be markedly lowered with monorotors /104/ (Fig. 3). In rotors of this type, heat from the turbine section is removed into the compressor section through thermal conductivity. Air in the blading of the compressor is additionally warmed, appreciably lowering its efficiency. This latter factor, as well as large technological difficulties in manufacturing rotors and bearing assemblies (in this case the rotor as a rule is made in the cantilever type) meant this design failed to gain wide acceptance.

The effort to increase the manufacturability of monorotors and lower their weight led to compound rotors being used in GTE with centripetal turbines (Fig. 4) /107/. This rotor is made of two parts: a turbine part, commonly cast of heat-resistant steel, and a compressor part made of light alloys. Both rotor parts are abutted tightly against each other in different ways. In this case, owing to the contact thermal resistance at the contiguous surfaces, the heat flows from turbine rotor to compressor rotor are somewhat smaller than in the monorotor, although the cooling efficiency of the turbine rotor is also less.

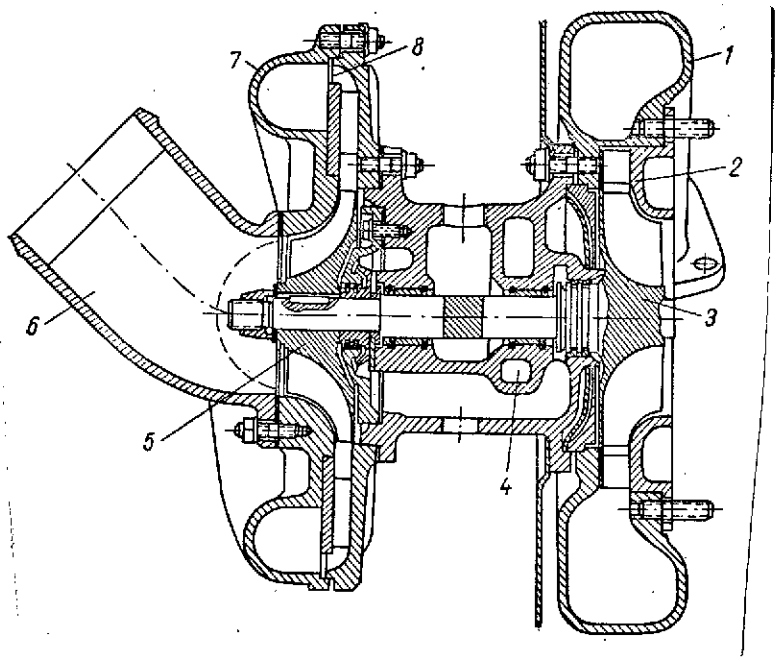


Fig. 2. YaMZ Turbocompressor:
1. Turbine case
2. Nozzle rim
3. Turbine rotor
4. Bearing case
5. Compressor rotor
6. Inlet
7. Compressor case
8. Diffuser

Compound turbine rotors and less often, rotor blades can be made partially hollow, thus providing so-called internal rotor cooling /107/. Turbocompressors with partially hollow disks are made in large lots by the Swedish DeLevalle company, and also by American and European licensees of this company /98, 103, 107, 112/. Turbocompressors of this type, models S-8, S-10, S-13, and S-17, provide an air capacity of 0.5-10 kg/sec, a pressure rise $\pi_c$ = 1.4-3.0 and operate at an upstream-turbine gas temperature of up to 700° C. Some of the /11 turbocompressors listed are provided with feed of compressed air into the internal cavity of the rotor to produce a film over the rotor surface swept by the gases (Fig. 5).

One of the most important problems -- ensuring appropriate stressed state of roots of turbine rotor blades at which there are maximum temperature drops -- has been solved quite uniquely: the ends of the rotor blades are not connected to the disk. In addition, this design permits quite high efficiencies, since losses in disk friction are slight.

Successes in building effective systems for air cooling of rotors of axial gas turbine promoted the adoption of analogous solutions also in designs of low-power GTE and in turbocompressors with centripetal turbines /21, 79, 90/. In the latter, generally air-cooled solid rotors are used, since they have the highest manufacturability. As a rule, air for rotor cooling is bled from the compressor unit; rotor blades are not specifically cooled in this case.

At the present time the following ways of cooling rotors of centripetal gas turbines are widely in use:

/12

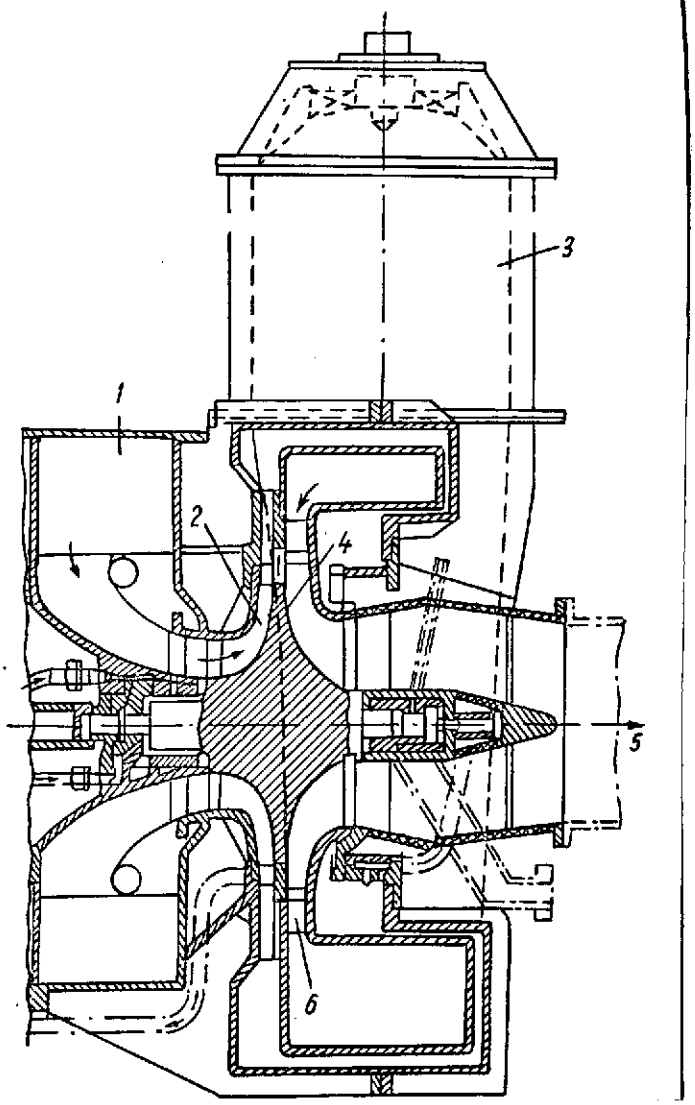


Fig. 3. Allen-Sont GTE (United States):
1. Inlet
2. Compressor rotor
3. Combustor /combustion chamber/
4. Turbine rotor
5. Outlet
6. Nozzle box

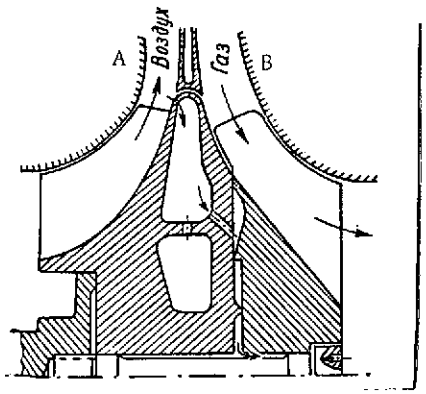


Fig. 4. Layout of compound rotor of centripetal turbine of GTE with internal cooling
Key: A. Air
B. Gas

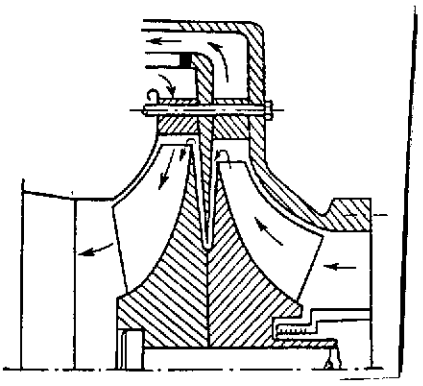

Fig. 5. Flow pattern of cooling air in composite Badword GTE (Great Britain)

a) radial blowoff of back side of disk, which can be made either smooth or with sealing grooves, and with balancing collars;

b) jet blowoff of back side of disk (as a rule, jet blowoff is combined with radial);

c) shielded cooling of back side both without forced flow, as well as with flowing of air along radius of back side of disk;

d) film cooling of working surface of disk; and

e) combination of above-listed cooling methods (radial or jet blowoff with film cooling, and so on).

Let us examine each of these methods in detail.

Radial blowoff of the back side of the disk often is not even provided for in the engine design but is implemented perforce due to flowing of air from the compressor part of the unit to the turbine. Thus, in the Badword engine (Great Britain) /103/, the Titan GTE (United States) /71/, and the Deutz GTE (FRG) /103/, part of the air from the inlet of the vaneless diffuser of the compressor flows through the clearances between the compressor impeller and the turbine rotor and, sweeping over its back side, mixes in the blading with the working gases (Fig. 6).

In some earlier designs of turbocompressors (TKR-14 and TKR-11) produced by the domestic industry, air was bled from the compressor to protect the bearing assembly against the gases bursting from the blading /61/.

Part of the air in this case was led into the oil cavity of the bearing assembly and part of it cooled the back side of the disk.

Results of investigating temperature fields of rotors cooled in this manner showed that by feeding air specifically for blow-off of the disk, its temperature can be considerably lowered /11, 22, 23, 44, 49/.

/14

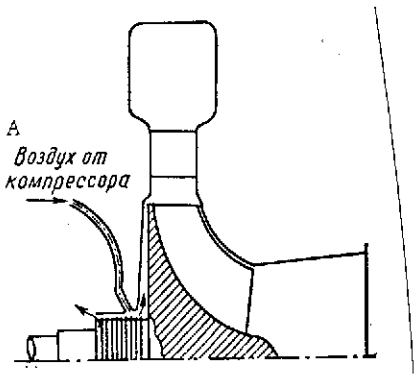


Fig. 6. Feed of cooling air for radial blowoff of turbocompressor rotor
Key: A. Air from compressor

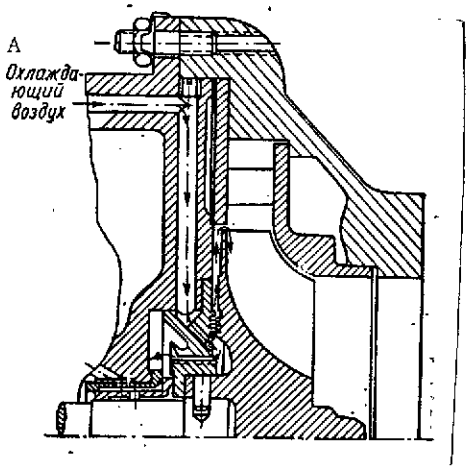


Fig. 7. Longitudinal section of turbine of TKR-14-2a turbocompressor and flow pattern of air-cooling rotor
Key: A. Cooling air

In all the latest designs of domestic turbocompressors with centripetal turbines, a provision is made for the feed of cooling air not only for cutting off the bearing assembly, but also to cool the turbine rotor. Generally the cooling air is fed into the cavity between the axial and radial labyrinth seals (Fig. 7). Most (65-80 percent) of the cooling air bathes the turbine rotor, while the rest, traversing the axial labyrinth seal, departs into the middle case. To lower this fraction of the cooling air, some modifications of the TKR-14 TMZ turbocompressor have, instead of axial labyrinth seals, steel sealing rings.

In the TKR-23-1 TMZ turbocompressor, the cooling air is fed into the space between the sections of the radial labyrinth seal and is divided into two flows (Fig. 8). One part of the air is

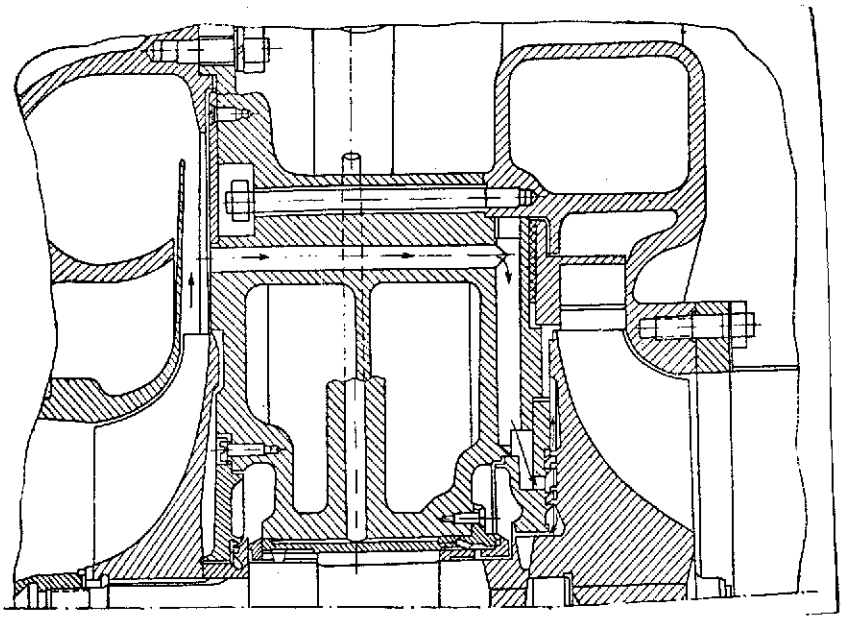

Fig. 8. Longitudinal section of TKR-23-1 turbocompressor

directed toward the periphery of the disk and enters the blading, while the other, traversing the radial and axial seals, is led into the bearing case. Similar methods of directing cooling air are provided for in turbocompressors built by the Eberspracher-Bosch Company (FRG) in which the air is directed into the axial labyrinth seal (see Fig. 6).

Thus, this method of cooling cantilever semishrouded rotors of centripetal turbines provides both for cooling of the disk as well as the bearing assembly.

Jet blowoff in centripetal turbines was borrowed from axial-type gas turbines, where at the present time it is widespread /73/. In cooling by jet blowoff, air bled from the compressor stage (usually, just beyond the impeller) is fed in jets to the back side of the turbine rotor (Fig. 9). Then this air flows /15
into the axial clearance along the back side of the disk and is mixed with the working gases. In the case of jet blowoff, after spreading out of the jets, as a rule there is also radial blowoff of the outer sections of the disk. Since by this cooling method a substantial (by 150-200 degrees) drop in the rotor metal temperatures is possible /73/, the technique is used in turbines with initial gas temperature to 750° C.

In shielded cooling, the heat flow from the back side of the turbine rotor is transferred via convection across an air

or gas interlayer to the less heated fixed turbine elements (the water or air-cooled walls of the crank case, deflectors, and so on). The fraction of the heat flow due to radiation here is 3-6 percent of the total heat flow.

The intensity of heat rejection from the back surface of the turbine rotor is increased with additional feed of air to the clearance between the rotor and the shielding surface /21, 73/.

As for radial blowoff, shielded cooling of a rotor usually is employed when the engine design does not provide for special cooling of the rotor. Cooling of the turbine disk due to heat being rejected into the deflector bathed by air from without was employed in the BMW-6002 GTE /100, 113/ (Fig. 10). In this engine, the combustor with rotating injectors lies in the space between the compressor impeller and the turbine rotor. Air from /16
the vaneless diffuser of the compressor enters a jacket embracing the entire turbo-unit and cools the nozzle box and the combustion can. Passing to the sections of the combustion can where the flame is formed, air intensively cools the deflector located opposite the back side of the turbine disk. Thus, heat from the rotor is transferred through the axial clearance to the relatively cold deflector. In addition to shielded cooling, the BMW-6002 engine is provided with intensive heat rejection to the rotating fuel injectors coupled to the bearing assembly.

Shielded cooling is also employed in domestic turbocompressors of the TKR type and in turbocompressors built by Eberspacher-Bosch /98/ in which the case walls opposite the back side of the disk are water-cooled. The system of water cooling of the turbocompressor case in this instance as a rule is related to the overall engine cooling system. The effectiveness of shielded cooling of /17
rotors will be high if the shielding walls are swept by water and not by air or oil vapor.

The above-considered radial and jet blowoff as well as shielded cooling and their various combinations make it possible to abstract heat from the disk only from the back side. This raises the temperature drops in the disk body, which in some cases may adversely affect the strength of the turbine rotor. Recently, attention has been drawn to cooling methods according to which the reduction of heat from gas to disk would be reduced. The so-called film cooling of a disk appeared, where the cooling air flows along the working (bladed) rotor surface swept by the hot gas. Between the hot gas and the rotor surface a film of cold air is formed, markedly lowering the intensity of heat flow to the rotor.

Designwise, film-type cooling in centripetal turbines is commonly implemented by feeding air into the radial clearance

/16

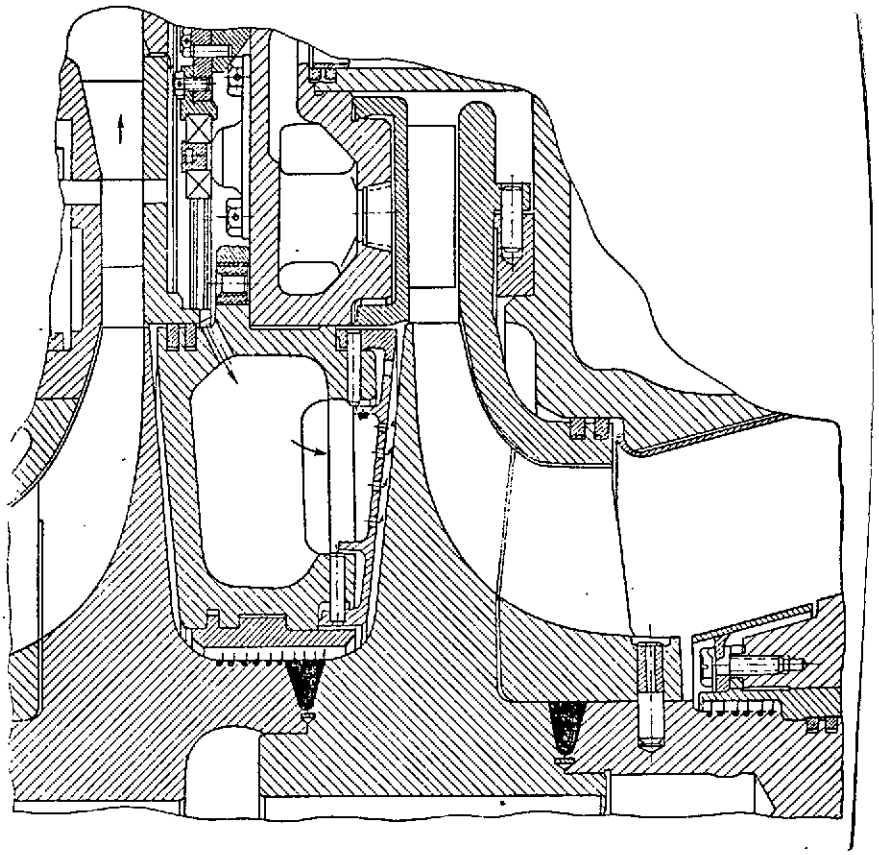

Fig. 9. Longitudinal section of TKR-40 turbocompressor

between the disk rim and the components of the nozzle box (Fig. /17
11). The effectiveness of film cooling of a rotor in a centripetal turbine increases with decrease in the blow angle, that is, the angle between the direction of the main stream (gas) and the secondary stream (air). Therefore, in later models of the TKR-14-2b turbocompressors, along the periphery of the turbine disk is provided a crest entering the corresponding passage in the cheek /side-plate/ of the nozzle box. This lowers the blow angle from /18
90 to 30° and, as well be shown below, greatly raises cooling efficiency. It bears noting that when a rotor is cooled by radial or jet blowoff, air flowing along the back side of the rotor ultimately will still arrive in the blading of the turbine. In this case, a film of relatively cold air will be formed along the periphery of the rotor; this cold air markedly lowers the heat flow to the rotor from the gases. The effectiveness of film cooling of the rotor in a centripetal turbine, in addition to the above-listed factors, also depends on the temperature of the cooling air and the blow zone; therefore it is reduced when air appreciably warmed through the removal of heat from the back side of the rotor is blown into the blading.

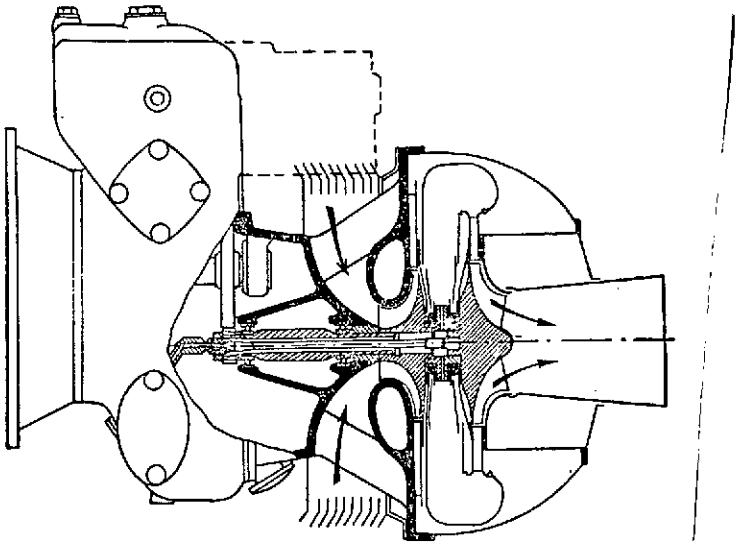

Fig. 10. Layout of BMW-6002 GTE (FRG)

These methods of /17
air-cooling of rotors /18
of centripetal gas
engines are classified
quite arbitrarily in
order to reveal the main
processes determining
heat removal. Actually,
it is virtually impossible
to imagine a cooling system
in which two or more of the
above-described cooling
methods are not combined.
Thus, in particular, in
the case of air cooling
of a case shielded cooling
develops, combined with /19
radial or jet blowoff
of its back side (turbo-
compressors TKR-14-2a
and TKR-23-1) (see Figs.
7 and 8); a combination of blowoff, shielded, and film-type
cooling is to be found in the TKR-14-2b turbocompressor (see
Fig. 11), and so on.

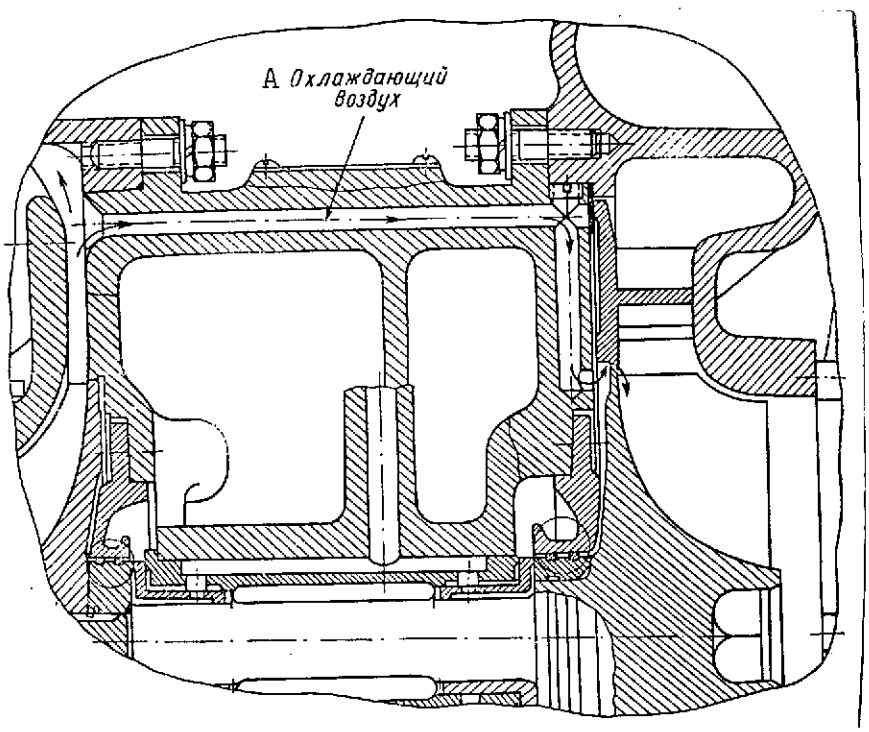


Fig. 11. Longitudinal section of TKR-14-2b turbocompressor
Key: A. Cooling air

## 2. Main Problems of Investigation

We know that depending on the purpose and operating conditions of gas turbine engines, various methods of protecting their rotors against overheating are used. The specific details of design and operating conditions of gas turbine supercharging sets with centripetal turbines account for the kind of cooling systems they employ. First of all, this stems from the necessity of providing internal cooling of rotor blades in the rotors of centripetal turbines. Designers have to find compromisory solutions, by intensively cooling, for example, the back side of the turbine rotor and thus providing for heat to be removed from the vanes via thermal-conductivity to the disk. The leading edges of the blades in the rim area of the rotor are additionally cooled by intercooler blow into the turbine blading.

The effectiveness of operation of the cooling system of rotors in centripetal turbines, as well as the temperature field of the rotors differs markedly from those prevailing in axial turbines. Therefore experience accumulated in the development, investigation, and operation of air-cooled axial turbines can only partially be utilized in turbines of the centripetal type. Wide use in recent years of centripetal turbines in turbo-supercharging sets of diesels and to a lesser extent as autonomous GTE required solutions to a whole series of problems arising in the designing and calculation of rotor cooling systems in these gas turbine engines.

The quality of the rotor cooling system of a gas turbine (that is, its effectiveness) is usually characterized by the temperature of the disk (blades), the temperature drops in the disk and rotor blades, the mass flow of cooling air, and by the power losses caused by employing cooling [73, 79, 90].

The first two of the above-listed parameters characterize the effect coming from using cooling. In turn, the disk temperatures and the temperature drops responsible for the disk stressed state are the starting data for evaluating the stressed state of the rotor. Existing methods of determining the thermal endurance of disks of centripetal turbines do not make it possible to relate with sufficiently simple relationships these indicators of the rotor cooling system and their strength characteristics. An estimate of the latter is possible only on the basis of extremely laborious calculations, generally conducted on digital computers.

To the first approximation, the quality of cooling systems is usually determined from the disk temperatures, the temperature drops, and the mass flows of cooling air for assigned strength properties of the rotor material and the gas temperatures upstream of the turbine. Determining these quantities for rotor cooling /20

systems in gas turbines in general and centripetal gas turbines in particular by analytical or numerical methods is an extremely complicated matter. In this case one must jointly solve a three-dimensional thermal conductivity problem with boundary conditions that are variable along the contour. The latter can be quantitatively determined only on the basis of experimental data. Still, by the appropriate generalization of experimental data based on regularities of heat transfer in cooling systems approximate methods can be devised that permit estimating the efficiency of the rotor cooling system, as well as the reliability and efficiency of its design with an accuracy sufficient for practical purposes. Therefore, to get general criteria for estimating the operating efficiency of rotor cooling systems in centripetal turbines and starting data for their design necessitates comprehensive experimental investigations of full-sized turbosupercharging sets. Experimental investigations can be conducted both in special test stands and installations, as well as directly in internal combustion engines.

Usually, in the experimental investigation of cooling systems the following problems are solved.

1. Developing the design of the cooling system of a gas turbine engine prepared for mass production or in mass production.

2. Determining the comparative effectiveness of various schemes and methods of cooling for the engine being designed with specified working parameters, and finding the optimal variant of the cooling system.

3. Establishing or revising regularities of heat transfer in the components of the cooling line and in the blading of the rotor used in calculations of the cooling system.

4. Verifying the method of calculating the cooling system used in designing the engine.

In the first case, the effectiveness of the existing design of the cooling system is investigated, that is, the variables of the temperatures of the rotor metal, and the mass flows and parameters of the cooling air are determined. An estimate is made concerning how the thermal state of the rotor is affected by the shape of the rotor, mass flow of oil to the bearings, rejection of heat into the water-cooled fixed components, and so on, the design parameters. Also investigated is the effect of the regime factors -- load, rpm, and so on -- on the thermal state of the rotor. In addition, the effect of the engine operating regimes overall on the performance of the turbine rotor cooling system is determined. Usually if the system of measurements permits, these experiments are conducted both in the steady-state thermal regimes

as well as in the regimes of startup, shutdown, and change of loads. Results of the investigations are used for the comprehensive analysis of the thermal and stressed states of the rotor. /21

When solving the second problem, quantities characterizing the effectiveness of the varying cooling systems used for the same, specified type of gas turbine engine are compared. The experiments are conducted on a single engine whose operating regime for all cooling variants remains unchanged. Experimental data are used for the final selection of the cooling system for the engine being built.

The third problem in general reduces to determining the coefficients of heat transfer from gas to rotor and from rotor to cooling air, and also to determining the hydraulic characteristics of the components of the cooling line for the maximum possible number of turbine operating regimes. Experimental data thus obtained can be generalized by the theory of similarity, and the corresponding empirical equations can later be used when calculating the thermal and stressed states of rotors.

In the fourth case, one finds the temperature field of the rotor and the mass-flow characteristics of the cooling system for the largest possible number of engine operating regimes, including during startup, shutdown, and transition from one load to another. The resulting data are compared with the results of calculating the cooling system according to one or several methods, which when necessary are revised based on experimental data.

The method ensuring the most complete accord of the calculation results with experimental findings can subsequently be used in designing other centripetal turbines.

Problems arising in generalizing experimental data and applying them for calculations of other analogous rotor cooling systems of centripetal turbines are extremely important, therefore we will dwell on them in somewhat greater detail.

When investigating temperature fields of rotors of centripetal turbines, of practical interest is the possibility of extending the data obtained to other regimes, as well as to rotors of other types and sizes. This problem, as well as the problems of selecting the operating regimes of the experimental gas turbine can be solved by using the fundamental premises of similarity theory /58/. For example, steady-state temperature fields of geometrically similar rotors proved to be similar if the criteria of thermal similarity will be numerically equal. If at rotor surfaces on the gas side and on the air-cooling side (on the working and back /pressure and suction/ sides) boundary conditions of the third kind are assigned:

$$\frac{\partial\theta}{\partial n} = \mathrm{Bi}_g(\theta_g - \theta); \qquad (I.1)$$

$$\frac{\partial\theta}{\partial n} = \mathrm{Bi}_{i.a}(\theta - \theta_{i.a}), \qquad (I.2)$$

then the similarity conditions of the rotor temperature fields can be represented in the form: /22

$$\mathrm{Bi}_g(r) = \text{idem}; \quad \mathrm{Bi}_{i.a}(r) = \text{idem}; \quad \theta(r) = \text{idem}; \quad \theta_{i.a}(r) = \text{idem}.$$

In order to ensure that the thermal similarity criteria are equal, there must be gas-dynamic similarity, that is, similarity of the fields of gas and air flow rates at the rotor surfaces; in the first approximation gas-dynamic similarity reduces to the equality of the Reynolds and Froude criteria at the heated and cooled surfaces:

$$\begin{aligned} &\mathrm{Re}_g(r) = \text{idem}; \quad \mathrm{Fr}_g = \text{idem}; \quad \frac{u}{c_1} = \text{const}; \\ &\mathrm{Re}_{i.a}(r) = \text{idem}; \quad \mathrm{Fr}_{i.a} = \text{idem}; \quad z = \text{const}. \end{aligned} \qquad (I.3)$$

Usually, in gas turbine power plants being compared, interdependent variation of most parameters is carried out and very rarely is there total thermal similarity. Most often it is possible to satisy only approximate gas-dynamic and thermal similarity. The solution of this problem is somewhat simplified due to the presence in centripetal turbine (in full and moderate operating regimes) of nearly automodeling regimes in terms of Biot numbers as for air and gas. Calculations of the temperature fields of rotors of centripetal gas turbines showed that they contain regions of automodeling character in $\mathrm{Bi}_g$ (and thus also in $\mathrm{Re}_g$) if $\mathrm{Bi}_g \gg \mathrm{Bi}_{i.a}$ and in $\mathrm{Bi}_{i.a}$ (and thus, in $\mathrm{Re}_{i.a}$) if $\mathrm{Bi}_{i.a} \gg \mathrm{Bi}_g$.

The temperatures of uncooled rotor blades are negligibly affected by the coefficients of heat transfer from gas, as a rule, which is due to the incommensurability of the thermal stresses at the blade roots and at the gas-swept surfaces. Because of this, generalization of data on the thermometry of rotors of centripetal turbines as applied to steady thermal regimes is greatly simplified.

In particular, when the comparative characteristics of various methods of air cooling of rotors of centripetal turbines are obtained experimentally[1], one must keep only the criteria of thermal similarity at the heating side constant. This makes it possible by varying the thermal similarity criteria on the heat rejection side to estimate the comparative effectiveness of any particular cooling method.

Expanding the values of $Bi_g$ for the turbulent regime of gas flow, in accordance with the typical criterial equation for heat exchange for turbulent gas flow, we get the expression

$$Bi_g = Nu_g \frac{\lambda_g}{\lambda_{cr}} = C Re_g^{0,8} Pr^{0,4}. \qquad (I.4)$$

Since in the 400-550° C temperature range the Prandtl number is virtually constant for the gas, in order to ensure that the boundary conditions of the third kind are identical on the gas side, the following must be satisfied[2]: /23

$$\frac{w_g d\rho}{\mu} = \text{idem}; \quad \frac{u}{c_1} = \text{const}$$

or

$$\frac{Gg}{\nu_g} = \text{idem}; \quad \frac{P_0 n}{G_g T_g} = \text{const}. \qquad (I.5)$$

The values of the Reynolds number on the gas side obtained in a study of the cooling systems of the TKR-14-2a turbocompressor in the ITTF /Institute of Technical Heat-Physics/ of the UkSSR AN /Ukrainian SSR Academy of Sciences/ differed from their nominal values by 15 percent, while the difference in the velocity ratios $u_1/c_1$ was 10 percent, with respect to their nominal values.

However, data obtained experimentally in less stressed regimes only approximately characterize the thermal state of a

---

[1] These investigations are commonly conducted on a single turbine adapted for implementation of the various cooling methods.

[2] The condition $u_1/c_1$ = const also requires constancy of $w_{ci}/w_1$, since the circulation component of the gas velocity in the working channel of a rotor $w_{ci}$ depends on the angular velocity of rotation.

rotor in total power regimes, since the magnitudes of the parameters determining the temperature field of the rotor (Biot number) in several cases can depend strongly on the turbine operating regime.

When experimental data from thermometry of rotors of centripetal gas turbines in nonsteady thermal regimes are generalized, the experimental results are usually given in the coordinates $\theta = f(F_o)$ or $\theta = f(\tau/\tau_{st})$, where $\tau$ and $\tau_{st}$ are the instantaneous time and time of arrival at the steady thermal rotor regime.

In full-scale turbocompressors and GTE the number of revolutions of the rotor, mass flow and pressure of air are quite closely interrelated; therefore it is virtually impossible to conduct experiments in less stressed regimes by preserving total thermal similarity on the heating side or on the side at which the disk is being cooled. In those cases when the turbine and the compressor in the experimental installations are not linked with the gas-air line, the possibilities of modeling the regimes increase. So experimental studies of the operating efficiency of a cooling system are desirably conducted in regimes of gas turbine set operation as closely as possible to full-scale regimes. Results of these experimental studies, that is, the absolute values of temperatures and the trend of their distribution in the rotor, will in this case correspond to the true values. However, owing to the complexity of conducting experimental studies it is not always possible to carry them out in regimes that are near-full-scale, especially when we are talking about the most stressed regimes in terms of the initial gas temperatures upstream of the turbine and when the rotor rpm is up to 60,000. Therefore experiments on stands are conducted in less stressed regimes and during the course of the experiments all parameters of the working gas and cooling air determining the operating efficiency of the cooling system and the temperature field of the rotor are measured. /24 Based on the values measured in the experiments, the heat exchange coefficients at the rotor surfaces and the hydraulic characteristics of the cooling system are calculated. The resulting data are generalized as dimensionless complexes, which on the basis of similarity theory, are reduced to criterial equations used then to calculate heat transfer at rotor surfaces and to calculate the hydraulic characteristics of the cooling system. Results of calculating temperature fields are compared with experimental data for the corresponding regimes, and their agreement is a unique criterion for estimating the reliability of equations resulting from generalizing numerous experimental studies. The equations found permit estimating the operating efficiency of the rotor cooling system of the turbine also for the regimes for which no investigations were carried out. Therefore obtaining data needed to develop the method of calculating the operating efficiency of the rotor cooling system of centripetal turbines and verifying these data and the overall technique is the paramount aim of the experimental investigations conducted on model installations and in full-scale units.

In the following chapters will be presented the results of experimental studies of the cooling systems of the most widely series-produced turbo-supercharger sets with centripetal turbines, the method of generalizing experimental results, and the method of engineering calculation of the efficiency of cooling systems based on these results.

## 3. Objects of Investigations and Test Stands

Investigations of the thermal state of rotors of centripetal gas turbines and their cooling systems are carried out either on full-scale sets with combined operation with internal combustion engines, or on specially built test beds. The earliest work in this area was done directly on internal combustion engines, however methodological difficulties arising during the thermometry of high-speed rotors promoted the building of special experimental stands for testing cooling systems of centripetal turbines. Investigations of the thermal state of rotors of centripetal turbines were carried out in the ITTF AN UkSSR jointly with several turbine-making plants [22-25, 49, 78, 91]. Both the objects of the tests and the experimental stands for investigating cooled centripetal turbines used in the ITTF AN UkSSR can be viewed as typical for this kind of research (Table 1).

Cooling systems of the turbocompressors TKR-14-2a and TKR-23-1 were investigated on a stand specifically designed in the ITTF AN UkSSR for testing low-power gas turbine power plants; cooling systems of the turbocompressors TKR-40 and TKR-14-2b were investigated at test stands of plants (see Figs. 7 and 8).

Gas entered the nozzle cascade of the turbocompressor turbines/25 through nozzle boxes divided into two sections in the TKR-14-2a and into four in the TKR-23-1. In the TKR-14-2a turbocompressor mounted on the test stand gas was exhausted via a special exhaust outlet, while in the TKR-23-1 -- directly through an exhaust pipe.

Cooled air is fed to the rotor in both turbocompressors via a system of drilled passages and grooves from the slotted diffuser of a centrifugal compressor. In the case of the TKR-14-2a turbocompressor, special air intakes were installed for utilizing the velocity head of the main stream. Radial blowoff of the back side of the turbine rotor was used in both turbocompressors. In basic tests, the cooling air was fed from the institute's pressurized air line through a special tubing with a measuring diaphragm and control valves. Here the openings for the direction of air into the vaneless diffuser of the centrifugal compressor were carefully overlapped.

TABLE 1

CHARACTERISTICS OF TURBOCOMPRESSORS TESTED BY THE ITTF AN UkSSR JOINTLY WITH MANUFACTURING PLANTS

| Quantities | Type of turbocompressors | | | |
|---|---|---|---|---|
| | TKR-14-2a | TKR-23-1 | TKR-40 | TKR-14-2b |
| Supercharging pressure, bar | 1.41 | 1.62 | 3.0 | 1.46 |
| Compressor capacity, kg/sec | 0.37 | 1.35 | - | 0.40 |
| Initial temperature of short (up to 20 min) operating regime, °C | 600 | 600 | 650 | 550 |
| Number of rotor revolutions, rps | 530-600 | 367-370 | 370 | 600-660 |
| Gas pressure upstream of turbine, bar | 1.31 | 1.20 | 1.8-2.3 | 1.34 |
| Outer diameter of turbine and compressor rotors, mm/mm | 140/140 | 230/230 | 400/400 | 140/140 |
| Temperature of air downstream of compressor, °C | 78 | 89 | 180-100 | 87 |

Remark. Initial temperature of the extended operating regime for all types of compressors was 550° C.

The cooling line was redesigned in the TKR-14-2a turbocompressor (Fig. 12); it was thus found possible to feed measured amounts of air either directly into the blading on the gas side or in radial blowoff of the back side of the rotor.

To carry out the second admission of cooling air directly into the peripheral part of the rotor, the water cavity of the bearing housing was used. Cooling air was fed through the control valve and a measuring washer into this cavity, whence through 28 2.3 mm diameter openings it was admitted to an annular chamber formed by the passage of the housing wall and a specially built bronze deflector. From this chamber the air passed into the /26
clearance between the disk rim and the flange of the nozzle cascade, whence it arrived in the blading of the rotor.

In a turbocompressor with a 400 mm diameter rotor, the cooling air arrives from the diffuser of the centrifugal compressor through slotted clearances and cavities of the internal case to a fixed deflector covering the back side of the disk (see Fig. 9).

The deflector has four rows of openings, 4 mm in diameter, through which the air blows off the turbine disk in jets. Part of the air from the air from the compressor passes through the axial labyrinth seal between the turbine and compressor rotors. Combination disk cooling was used in the TKR-14-2b turbocompressor: film cooling and jet-radial blowoff. To boost the efficiency of film cooling, a ridge was provided on the rotor for deflecting the secondary stream of the coolant in the direction close to the main stream. The cooling air, as in the earlier designs considered, was fed from the vaneless diffuser of the centrifugal compressor through two passages to the disk and blown off in jets, after which in the form of a film the air was injected along the working surface of the rotor into the turbine blading.

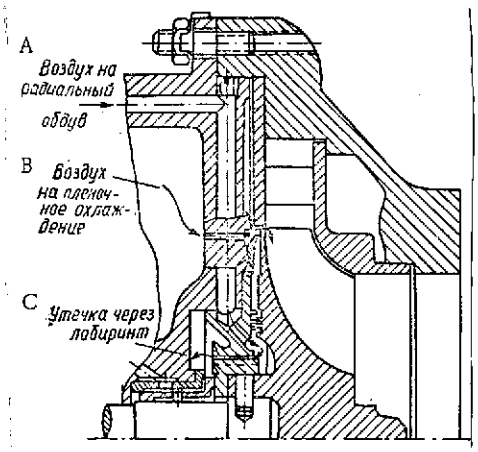


Fig. 12. Longitudinal profile of redesigned cooling line of TKR-14-2a turbocompressor

Key: A. Air for radial blowoff
B. Air for film cooling
C. Leakage through labyrinth

The test stand of the ITTF AN UkSSR was typical of such installations /30, 32, 33, 84/ and consisted of a test turbocompressor with an auxiliary combustion chamber, a fuel supply and regulation system, a lubrication system, control panel, and monitoring instrumentation (Fig. 13). The stand was connected to an independent compressor station, permitting the additional admission into the combustion chambers of up to 0.36 kg/sec of air at pressures of up to 6 bar. This air was enough to bring the TKR-14-2a turbocompressor into the rated regime in rpm, head, and compressor capacity. The TKR-23-1 compressor needed supplementary air only during its startup period, and in the TMZ test stands it could be used in the layout of an ordinary GTE. However, owing to large pressure losses in the annular combustion chamber used in the ITTF AN UkSSR stand, it was not possible to bring this turbocompressor to the nominal regime in terms of compressor capacity and to ensure its operation without air replenishment.

In the TKR-14-2a turbocompressor the compressor was used as an external load for the turbine; this permitted varying the number of revolutions, gas temperature, and gas mass flow over wide limits. /27

In the TKR-23-1 it was not possible to independently vary these parameters and the experiments were conducted only within a very narrow range of rpm with the simultaneous variation of gas temperature and mass flow.

In the combustion chambers installed on the ITTF AN UkSSR the number of injectors was varied as a function of the gas temperatures required in the experiments. This ensured their stable operation at pressures in the fuel line of not less than 2.0-3.0 bar. The nonuniformity of the gas temperatures in the nozzle cascade of the turbine was 5-7 percent in the TKR-14-2a turbocompressor, and 7-12 percent in the TKR-23-1. The greatest deviation with time in the gas temperature downstream of the combustion chamber did not exceed $\pm$ 1.5 percent from the assigned value.

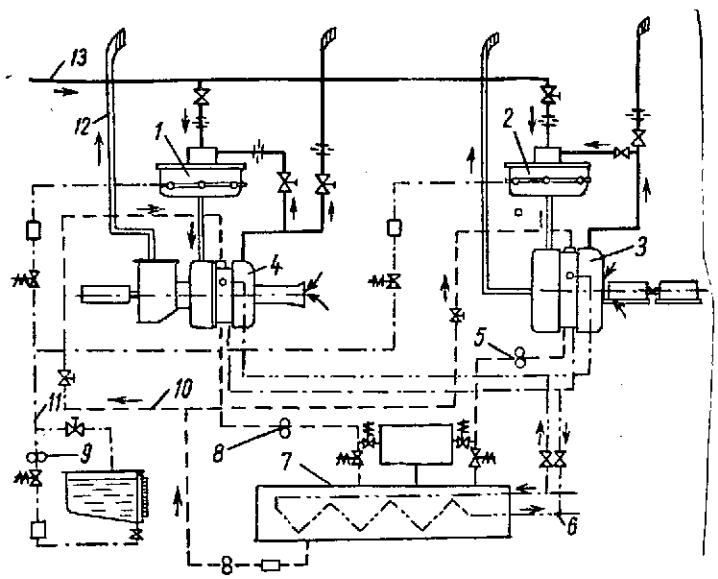


Fig. 12. Layout of ITTF AN UkSSR test stand for investigating rotor cooling systems in centripetal gas turbines:
1, 2. Combustion chambers
3, 4. Turbocompressor
5, 8. Oil pumps
6. Water
7. Oil tank
9. Fuel tank
10. Oil
11. Fuel
12. Gas
13. Air

In the ITTF AN UkSSR test stand, T-1 kerosene was used as fuel; it was admitted by gravity flow through a filter into a geared pump mounted on the gearbox of the pump unit. The drive of the reduction gear to which the oil pump and the combustion chamber ignition system were also connected was provided with a 4.5 kW electric motor. Past the pump, at pressures up to 100 bar the fuel was admitted through a system of coarse and fine filters to the working injectors of the combustion chambers. Fuel mass flow was regulated with a needle valve at a bypass line and was measured by the drop in pressures at the fuel injectors, which had been calibrated before being installed on the combustion chambers. /28

The fuel system was equipped with pressurizing fittings with remote drives, which were controlled from a common panel. The combustion chambers were provided with ignition by means of a fuel starter system consisting of starter injectors and electromagnetic cocks blocked together with an induction ignition coil. The primary dc voltage in the ignition system and in the operating line of the panel was 24 V. The stand lubrication system consisted of a geared pressurizing pump to which oil was admitted through a filter from the oil block with a built-in oil cooler, and then through a system of filters and lines with pressurizing fittings the oil was fed to lubricate the bearings of both turbocompressors, current collector drive, and pump unit reduction gear. Overflow of oil from the TKR-23-1 turbocompressor took place into an intermediate container, whence via an automatic weighing device (see Fig. 13) the oil was fed by means of a suction pump into the main oil tank. Oil overflow[3] from the crankcase of the TKR-14-2a into the main oil tank was provided by means of the same pump with electric drive.

The stand control panel consisted of devices for controlling the pumps, fuel system fittings, and instruments (class 1-1.5) for monitoring the working parameters of the installation (frequency meter, galvanometers, and manometers). Built into the housing of the control panel was an automatic weighing dispenser designed in the ITTF AN UkSSR to determine the mass flow of oil to the turbocompressor bearings. The dispenser consisted of a periodically filled vessel mounted on a spring. With filling, a system of valves controlled by means of contacts secured to a sliding capacitance was triggered. All the parameters (temperatures of metal, gas, and air, gas and air pressures, and so on) necessary to estimate the efficiency of the cooling systems were measured with the special measuring /monitoring instrumentation/ system.

## 4. Method of Measurements and Measuring Equipment

Air was fed into the combustion chambers of the ITTF AN UkSSR test stand both from centrifugal pumps of the turbocompressors as well as from outside sources. The mass flow of air fed to the combustion chambers of both turbocompressors from the institute's air line was measured with normal measuring diaphragms built in accordance with existing regulations /55/.

---

[3] Type L turbine oil was used in the ITTF AN UkSSR installation.

The capacity of the centrifugal pumps of the turbocompressors being tested was measured with a diaphragm installed on the pressure line in the TKR-14-2a turbocompressor, and with a special metering valve in the suction line of the TKR-23-1 turbocompressor.

The mass flows of cooling air fed from the outside compressor station were measured with double diaphragms; the temperature of this air was measured with a mercury thermometer.

Mass flows of cooling air through the branches of the cooling line and through the axial labyrinth seal of the TKR-14-2a and TKR-23-1 turbocompressors were determined from their calibration characteristics found from special adjustment experiments. /29

Mass flows of cooling air were measured volumetrically and were monitored by pressure in the water cavities.

Temperatures in the stator part of the TKR-23-1 and the TKR-14-2a turbocompressors were measured with class KhA-0.5 thermocouples. The total number of thermocouples in both turbocompressors in the various series of the experiments was 150-180. Gas temperatures upstream and downstream of the turbines were measured at 20 points in the TKR-14-2a, at 18 points in the TKR-23-1, and in four points at the TKR-40; the temperatures of the cooling air were measured in all branches of the cooling line. In addition, the temperatures in the stator part of the turbines (nozzle vanes and nozzle boxes), bearings, oil upstream and downstream of the bearings, as well as the water at the inlet and outlet from the water cavities were measured. The thermocouples were made of standard thermoelectric wire, 0.5 mm in diameter. The wire was carefully isolated with silica or glass filament or with glass braiding.

The working parts of the thermocouples installed in the action zone of high temperatures were additionally wound with KN-11 silica filament and were coated with FG-9 lacquer.

To measure the temperature of the gas in the inlet and outlet lines, use was made of shielded flow-type thermocouples /32, 63, 66/; thermocouples measuring the gas temperatures in the blading of the turbine (upstream and downstream of the nozzles) had no shields. Since the temperatures of the elements of the nozzle cascade were close to the gas temperatures, here the errors arising were minor /89, 110/. When the measurements were interpreted, the recovery coefficients for the flow-type thermocouples were taken as 0.85, and for the exposed thermocouples -- 0.65 /43, 66/.

The cold junctions of all thermocouples were thermostatted in heat-insulated jackets. The emf generated by the thermo-

couples were measured with EPP-09 type self-recording potentiometers of accuracy class 0.5. In several experiments, the emf of some of the thermocouples were measured with a PPTV-1 type laboratory potentiometer.

The thermocouples with which the metal temperature was determined were mounted by means of point capacitative welding or were caulked in.

The most complicated procedural problem in testing the rotor cooling systems of centripetal turbines was measuring the temperatures of the metal of a rotor spinning at high rpms (40,000-60,000). Since the reliability and accuracy of measurements of rotor metal temperatures basically determine the value of the experiment, naturally priority attention was given to selecting the method of measurements in these experiments.

We can regard as the earliest work done on the direct thermometry of rotors of centripetal gas turbines to be [104], in /30
which the temperatures were measured with heat-sensitive paints applied to rotor surfaces. After normal startup lasting not more than 1.5 min, the engine was brought to the regime of rated power. Measurements under this method corresponded to the maximum temperature values occurring during the experiment, that is, the inevitable scattering of gas temperature values during startups were taken into account, as the result of which it was difficult to judge the actual values of the temperatures of the rotor and the rotor blades in the rated regime. In addition, the heat-sensitive paint method had a substantial error, usually exceeding 10 percent. The advantages of this method were reliability and simplicity.

Besides heat-sensitive paint for measuring rotor temperature, ferro-diamond transducers were used. The crystal lattice of a ferro-diamond transducer -- a small crystal 1-2 $mm^3$ in size -- was first subjected to deformation by a fairly lengthy (20-30 hours) irradiation with gamma-rays. Upon subsequent action of temperatures on the transducers, reverse deformation (recovery to initial state) of the crystal lattice occurred, which was recorded by x-ray diffraction analysis. From the results of x-ray diffraction analysis the temperature of the transducer at the point of the object measured was determined. The transducer reading was affected not only by the temperature but also by the duration of its exposure. Since the duration of measurement of the steady temperatures is several hours, the reliability of the temperatures measured was much reduced. During this time it is usually difficult to keep the working regime unchanged in the engine being tested. Naturally, both these methods do not /31
permit recording the temperatures in the transient thermal processes. It is possible to reliably and quite precisely measure temperatures of spinning parts with thermocouples

TABLE 2

CHARACTERISTICS OF CURRENT COLLECTORS OF THE ITTF AN UkSSR INTENDED FOR THERMOMETRY OF ROTORS FOR HIGH-SPEED GAS TURBINES

| Type of current collector | Number of pairs of rings | Outside diameter of ring, mm | Roller diameter, mm | Bearing model number | Spacing between bearing axes, mm | Maximum rpm | Error, mV | Overall dimensions, mm |
|---|---|---|---|---|---|---|---|---|
| SK-8 | 10 | 20 | 15 | V-203 B | 185 | 36 000 | ±0.10 | 295×55 |
| SK-13 | 20 | 16 | 11 | V201<br>V1008 | 198 | 22 000 | ±0.05 | 240×80 |
| SK-14 | 21 | 19 | 14 | V201<br>V200 | 210 | 23 000 | ±0.05 | 260×80 |
| SK-15 | 21 | 19 | 14 | V201 | 210 | 24 000 | ±0.05 | 278×80 |
| SK-16 | 12 | 19 | 14 | V-201 B | 134 | 36 000 | ±0.10 | 210×80 |
| SK-17 | 21 | 24 | 19 | V-201 B | 208 | 40 000 | ±0.10 | 280×80 |
| SK-19 | 32 | 26 | 20 | V202 | 297 | 15 000 | ±0.10 | 370×96 |

Remark. The contact rings of the current collectors were made of copper. The brushes were copper-graphite, 2.5 x 4 x 6 mm; for SK-8 -- -- 3 x 4 x 6 mm; the clamping of the brushes was pneumatic. The height of the centers for all current collectors was 55 mm, and for SK-8 -- 28 mm.

whose emf is being transmitted to a fixed measuring instrument by means of special contact systems (slip rings). Developing and building contact slip rings of devices operating at high rpm (20,000-60,000) is a complicated problem. Slip-ring devices for thermometry of rotors of centripetal turbines are complicated by difficulties that are purely technological, coming from the connection of slip rings to overhanging rotors of centripetal turbines of small geometrical size and often of low power /109, 116/. This necessitated building special compact slip rings with small moment of drag /118/.

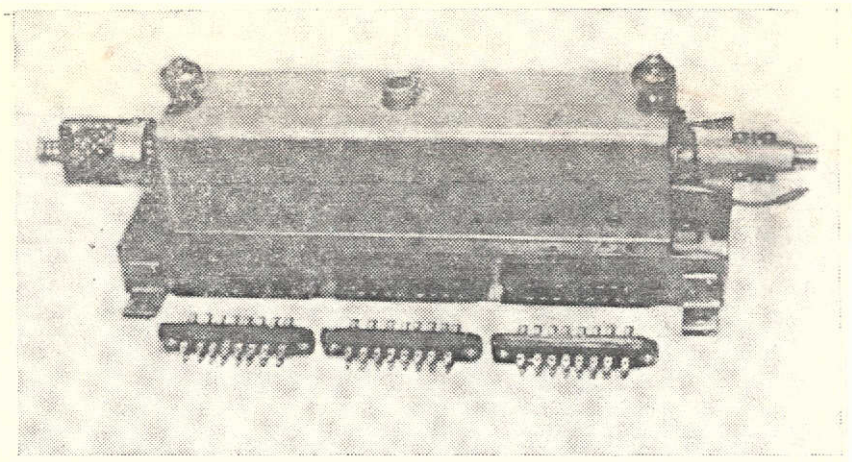

Fig. 14. SK-13 current collector of ITTF AN UkSSR for 20 pairs of contact rings

In the experiments on the ITTF AN UkSSR and at the turbomotor plant, use was made of ten- and twelve-point contact brush current collectors designed in the Institute (Table 2) (Fig. 14). The operating time of these current collectors is 20-25 hours for maximum rpm and increases 3-5 times when the rpm is 50-70 percent of these maximum values[4].

When the TKR-40 turbocompressor was tested, a 12-point mercury current collector was used: its operating time when $n_{tc}$ = 20,000 rpm was 1.5-2 hours.

The number of thermocouples arranged on rotors of turbines of the turbocompressors TKR-14-2a, TKR-23-1, and TKR-14-2b are 22, 32, and 20, respectively. The technology of manufacturing rotating thermocouples is analogous to that described above. The diameter of the thermoelectrode wire was 0.20 mm. /32

When the thermocouples were installed on a rotor, attention was given to the careful insulation of the thermocouple against exposure of gases and air sweeping the rotor surface. To do this, the surface of the soldered thermocouple near the cold junction was covered for a length of 10-15 mm with a layer of mica, after

---

[4] One has in mind the operating time of the current collector between the inspections of the contact assembly and the bearings; at the present time it is more than 100 hours for SK-16 current collectors.

which the thermocouple was projected by means of capacitive welding with a heat-resistant steel foil ($\delta$ = 0.05 mm). In the blading part of the rotor the thermocouples were placed on its working surface at the blade insertion points. The leadout of the thermocouples to the current collecting devices was via hollow shafts of the TKR-23-1 and the TKR-14-2b; this made it possible to arrange the current collectors on the compressor side. In the TKR-14-2a turbocompressor the diameter of the shaft did not permit this method of thermocouple leadout to be employed. In this case the leadout was on the turbine exhaust side via an intermediate hollow spindle mounted on slide bearings in the exhaust outlet. In the first experiments on the TKR-14-2a turbocompressor, an SK-8 current collector was positioned in a special water-cooled housing immediately in the exhaust pipe of the turbine.

During tests of the TKR-40 turbocompressor, 30 thermocouples made of chromel-copel thermoelectrode wire, 0.1 mm in diameter, were positioned on the rotor. The thermoelectrode wires during placement were completely protected with 0.05 mm thick heat-resistant foil. The thermocouple ends were brought out into a special heat-insulated rotating plate positioned on the coupling of the current collector drive. Similar rotating plates were used in the TKR-14-2a and TKR-23-1 turbocompressors. In the TKR-14-2a, the cold junctions of the rotor thermocouples were arranged between the rotor of the turbocompressor and an extension spindle (drive), while in the TKR-23-1 -- between the rotor and the current collector.

The temperature of the cold junctions of the rotor thermocouples was measured with semiconductor resistance thermometers (thermistors) of types MMT-6 and MMT-1, which were placed along with the cold junctions on the rotating plates[5]. The lead to the thermistors, like the cold junctions of the thermocouples, were connected to contact rings of the current collectors. The resistance of the thermistors was determined with a dc bridge specially designed for these kinds of measurements and developed in the ITTF AN UkSSR. The measuring bridge was built with constant resistance in both arms of 9 kilo-ohms, and an R33 potentiometer was used as the variable resistance. The bridge was supplied from a 1.5 V stabilized voltage source. Reference standard /33
spring manometers of classes 0.4 and 0.5 were used in measuring the pressure of the cooling air and the working gas. Pressures and drops not exceeding 0.2 bar were measured with U-type water

---

[5] The initial resistance of the thermistors at 20° C was of the order of 16 kilo-ohms.

manometers, while the pressures and drops to 200 mm $H_2O$ were measured with type MMN-250 alcohol micromanometers. In all cases static pressures were measured. Besides these instruments, the GRM-5 self-recording manometer was used in measuring air and gas pressures at 20 points with a minimum measurement limit of 0.6 ata.

## CHAPTER TWO

/34

# RESULTS OF EXPERIMENTAL INVESTIGATIONS OF COOLING SYSTEMS OF ROTORS OF CENTRIPETAL TURBINES OF SERIES-PRODUCED TURBOCOMPRESSORS

## 1. Stand Test

This chapter gives the results of experimental studies of cooling systems of series-produced domestic turbocompressors. As a rule, these investigations were carried out in specially equipped stands that permitted determination of mass flows and parameters of media, temperatures and rpm of rotor, and temperature of several turbine elements adjacent to the rotor, with sufficient accuracy.

Accumulated experience in investigating cooling systems of gas turbines showed that using thermocouples to measure temperatures of a spinning rotor provides the most reliable and quite accurate results.

However, these measurements on rotors of centripetal turbines running at $n_{tc}$ = 20,000-50,000 rpm can be carried out only if equipment is well-designed, first of all current-collecting devices. Therefore early work in investigating cooling systems of centripetal turbines as a rule were carried out on fixed rotors or at reduced rpm, determined by the capabilities of the instrumentation. The results of these experimental studies are also of practical interest since they enable one to estimate the qualitative and, to a lesser extent, the quantitative nature of the distribution of temperatures in rotors of centripetal turbines of different designs.

In reference /12/, the nonsteady thermal state of the rotor in a TKR-11 turbocompressor was measured, in which there was no special air cooling. The temperature was measured with thermocouples on a fixed (braked) and on a spinning rotor. In the

steady thermal regime the rotor was nearly uniformly heated, indicating the absence of intensive rejection of heat from its back side. Results of the investigations established that rotor blades exhibit low thermal inertia with variation in thermal regime, but in the root sections of the rotor blades significant temperature drops are produced in this case. Heating curves of the disk of the centripetal turbine in a TKR-11 turbocompressor are given in Fig. 15 /11/.

At the Ural'skiy turbomotor plant, in 1965-1967 /12, 14-16/ studies were made of the thermal state and the heat resistance /35
of the rotor in the series-built TKR-23-1 turbocompressor at 2400-6000 rpm (rated rpm of this turbocompressor is 22,000). The turbocompressor turbine was driven by gas admitted from an external combustion chamber, and air from the compressor was discharged into the atmosphere. The rotor temperatures were measured during startups, shutdowns, and in the steady thermal regime. The results of the experiments showed that for the rotor the most dangerous operating regime from the standpoint of the considerable temperature drops induced is a rapid startup from the cold state (not longer than 1.5 min). A variation in the operating regime of the turbine accompanied by rapid (40-60 sec) change in the initial gas temperature is characterized by an abrupt change in the temperature of the rotor blades and by a smoother change in disk temperature. As a result, considerable alternating temperature gradients are induced in the root sections of the rotor blades. The experiments showed that in radial blow-off of the back side of the disk, disk temperature is 150-160° below the gas temperature in the rotor blading, while the temperatures of the rotor blades are 65-80° below the gas temperature in the blading part of the rotor.

Results of measuring the temperature fields of the rotor of the TKR-23-1 were compared with the calculated data in /106/ (Fig. 16). It was noted in reference /12/ that presentation of experimental results in dimensionless quantities permits comparison of the temperature drops at rotors with different geometrical dimensions and boundary conditions.

One way of overcoming the difficulties arising when measuring rotor temperatures of high speed centripetal turbines using thermocouples placed on the disk and on the rotor blades is the use of the so-called methods of physical modeling. This approach as applied to centripetal gas turbines was proposed and elaborated in /50/. The test regimes are characterized by the fact that the temperatures of the main stream (working body /reaction mass/) must be below the temperatures of the secondary stream (coolant), while the turbine rpm values at which "reversed" thermal similarity is attained are much lower than the nominal rpm. It is shown in

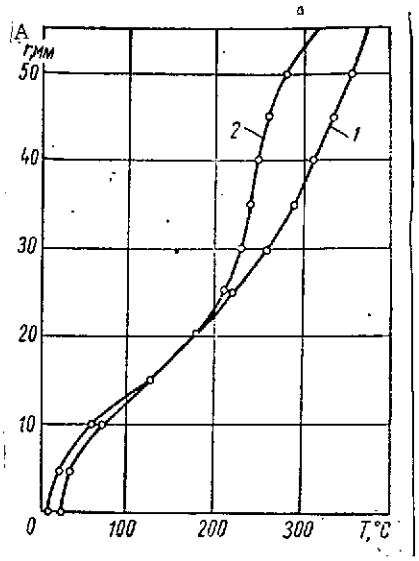


Fig. 15. Distribution over radius of mean (with respect to thickness) temperatures during heating of rotor of TKR-11 /12/:

1. $T_o$ = 700° C, $G_g$ = 0.24 kg/sec
2. $T_o$ = 600° C, $G_g$ = 0.19 kg/sec

Key: A. mm

/50/ that the conditions for similarity of the steady temperature field of a rotor in a centripetal gas turbine reduced to constancy of the boundary conditions (in this case, boundary conditions of the third kind): /36

$$\mathrm{Bi}' = \mathrm{Bi}'' = \text{idem}; \quad \theta'_g = \theta''_g = \text{idem};$$

$$\theta'_{i.a} = \theta''_{i.a} = \text{idem}, \qquad \text{(II.1)}$$

where the marks ' and '' pertain to full-scale and model situations, respectively.

In the experimental investigation of the thermal state of a rotor of a model centripetal gas turbine, cold ($t_{i.a}$ = 15-25° C) air was admitted into its blading, while air warmed in special heaters to 230-200° C was admitted into the cooling line. The main results of these experiments are in Fig. 17.

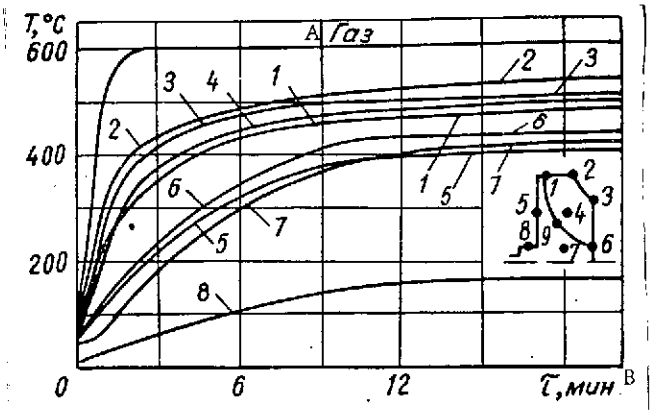


Fig. 16. Variation of temperatures at characteristic points of the rotor of the TKR-23-1 turbocompressor during warmup

Key: A. Gas; B. Minutes

The above-presented results of direct measurements of temperature fields of rotors of centripetal turbines are characterized by the fact that to obtain them use was made of different kinds of procedural techniques; ultimately these techniques do not make it possible to estimate with full reliability the actual operating conditions of the cooling systems. These kinds of disadvantages are eliminated as the instrumentation is improved.

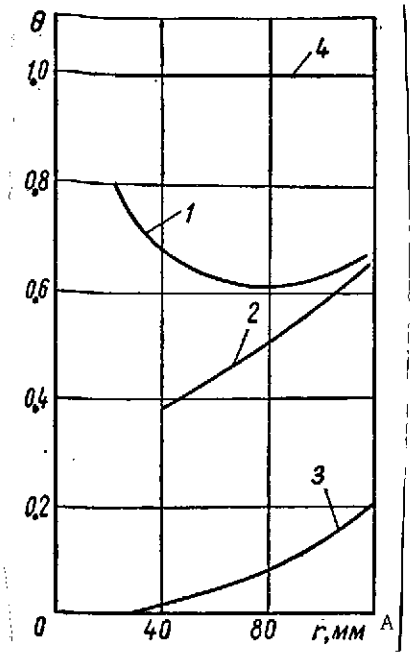


Fig. 17. Results of investigating temperatures of rotor in centripetal turbine by physical modeling based on data in /50/:
1. Temperature of pressure /working/ side of rotor
2. Temperature of back side of rotor
3. Temperature of cooling air
4. Gas temperature

Key: A. mm

The thermal state of rotors in centripetal turbines and their cooling systems was investigated in ITTF AN UkSSR under a broad program on special experimental stands. The test program included measuring not only the temperature fields of rotors of turbines of series-produced turbocompressors, but also the detailed investigation of the hydraulics of the cooling systems, as well as evaluating the effect of heat rejection into oil and water cooling the crankcase on the thermal state of a rotor. A full-scale turbocompressor was tested on a stand whose diagram is shown in Fig. 7, while the basic data of the turbocompressor are presented in Table 1. To determine the true mass flows of air in the cooling system, all the components of the cooling line were calibrated.

In the first years of experiments, the pressures in the cooling line were measured at the terminal and nodal points with normal admission of cooling air (from a centrifugal compressor). Then the openings for bleeding of cooling air from the compressor diffuser were carefully closed, and the cooling air was fed into the line through a measuring diaphragm from an outside source. With variation in the mass flow of this air, the former pressure was achieved (reduced to normal atmospheric conditions) at the nodal point of the cooling line (see Fig. 7). /37

Test results showed that in the rated regime the pressure of the cooling air of the nodal point was 1.187 bar. The total mass flow of cooling air in this case was $3.55 \cdot 10^{-3}$ kg/sec, from which $1.88 \cdot 10^{-3}$ kg/sec was expended in radial blowoff of the disk, while the rest, $1.67 \cdot 10^{-3}$ kg/sec, passed through the axial labyrinth seal into the turbocompressor casing.

The leakage of cooling air through the axial labyrinth was determined from its calibration data preceding this experiment.

The seal was calibrated with the rotor still. The openings in the air intake located in the slotted diffuser of the centrifugal compressor and the clearance in the radial labyrinth seal were reliably closed. During calibration air was admitted through the measuring diaphragm. This leakage through the axial seal was typical of new turbocompressors that had been run 20-50 hours. Extended operation of the turbocompressor can lead to the breakdown of the axial seal and to increase in its clearances. A consequence of this is the redistribution of the mass flows of cooling air through the branches of the cooling line. Thus, after 150-200 hours of operation the clearances in the axial seal of the TKR-14-2a turbocompressor rose[1] from 0.23 to 0.45-0.50 mm, a consequence of which was the air leakage through the seal and the total mass flow of cooling air rising to, respectively, $3.4 \cdot 10^{-3}$ and $5.0 \cdot 10^{-3}$ kg/sec. $1.64 \cdot 10^{-3}$ kg/sec was expended in blowoff of the disk in this case. /38

Thus, when the size of the clearance in the axial seal was varied, the total mass flow of cooling air rose considerably (by 47 percent in this case); however its mass flow for radial disk blowoff changed to a lesser extent -- from $1.88 \cdot 10^{-3}$ to $1.64 \cdot 10^{-3}$ kg/sec, that is, 15 percent.

Rotor temperatures in the rated operating regime of the TKR-14-2a turbocompressor were measured for a mass flow of cooling air in radial blowoff of $1.88 \cdot 10^{-3}$ kg/sec and for a total mass flow of air of $3.55 \cdot 10^{-3}$ kg/sec (0.9 percent of gas mass flow).

As follows directly from analysis of the measurements, the highest disk temperatures occurred over sections of relative rotor radii of 1.0 and 0.25-0.30 (the working side of the disk) and were 423 and 410-415° C, respectively. The section of the working side of the disk located at $\bar{r}$ = 0.35-0.65 proved to be the least heated. This was due to the proximity of the injection point of the cooling air, the quite intense heat rejection in the radial labyrinth seal, and also heat rejection into the bearing assembly (Fig. 18).

---

[1] This axial seal accrued operating time here was significantly caused by some unbalancing of the rotor owing to the presence of thermocouples in it. Obviously, a similar enlargement of clearances in the turbocompressor installed on a diesel will occur after a much longer time interval.

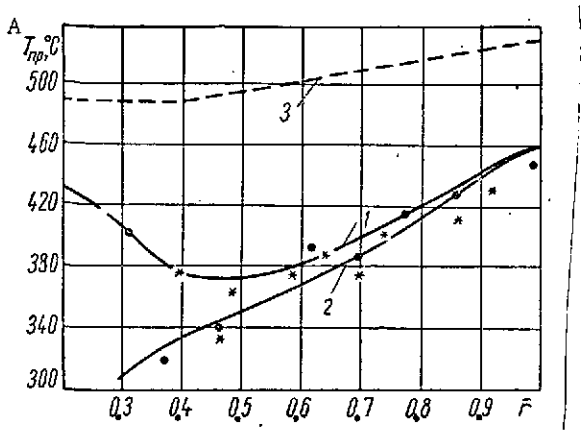


Fig. 18. Change of temperature of rotor in TKR-14-2a turbocompressor in rated regime:
1. Working surface of rotor
2. Back surface of rotor
3. Gas in working channel. Asterisks denote rated regime for $n_{tc} = 34 \cdot 10^3$ rpm; $G_g = 0.37$ g/sec; the points denote thc regime when $n_{tc} = 18 \cdot 10^3$ rpm; $G_g = 0.185$ kg/sec

Key: A. $T_{rd}$

The radial temperature gradients averaged over the disk sections at $\bar{r} = 0.5$-$1.0$ did not exceed 1.5 deg/mm (a temperature drop of 50 deg), and the axial gradients in the cross sections of the section $\bar{r} = 0.2$-$0.6$ were 4.0-4.5 deg/mm (temperature gradient 112 deg). The maximum disk temperature was 65 deg below the gas temperature in the rotor blading.

The greatest temperature drops occurring in the root sections of the rotor blades, which in this case were cooled only by heat rejection to the disk, at $\bar{r} = 1.0$ and $\bar{r} = 0.5$ were 7 and 12 deg/mm, respectively. /39

Under a similar program, tests were conducted, on an experimental stand, of the cooling system of another series-produced turbocompressor, model TKR-23-1 (see Table 1).

The experimental stand permitted testing this turbocompressor at operating rotor rpm, and the regimes in terms of mass flow of gas, cooling air, and initial gas temperature were close to the rated regimes, differing from them by 12-20 percent. As in the case of the TKR-14-2a turbocompressor, initially the air-cooling system line was calibrated. Results of experiments to experimentally determine the mass flow of cooling air showed that in the regime investigated the mass flow of air was $12.4 \cdot 10^{-3}$ kg/sec, of which $6.1 \cdot 10^{-3}$ kg/sec (0.92 percent) went to the turbine bearing, while the rest, $6.3 \cdot 10^{-3}$ kg/sec went to the disk periphery.

Increasing the dimensions of the clearances in the axial labyrinth seal during extended operation, in contrast to the earlier-examined TKR-14-2a turbocompressor, changed the mass flow of cooling air much less, since in the TKR-23-1 the main seal was preceded (along air flow) by the radial labyrinth.

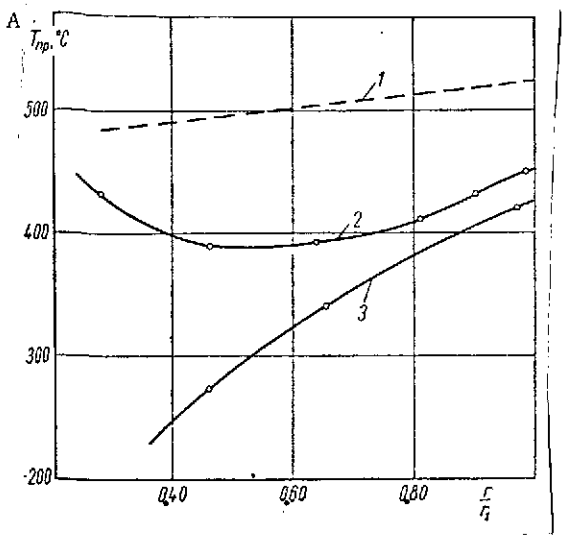


Fig. 19. Change in temperature of rotor of TKR-23-1 at near-rated regime:
1. $T^*_g$
2. Working side of rotor
3. Back side of rotor
Key: A. $T_{rd}$

Fig. 19 shows the distribution of temperatures in the rotor disk, and Fig. 20 -- in the rotor blades for the regime studied. The trend of temperature variation along the radii of the disk of the TKR-23-1 is similar to the above-considered distribution of temperatures in the disk of the TKR-14-2a. The highest temperatures occurred along the peripheral part of the rotor ($\bar{r}$ = 0.85-1.0) and amounted to 450° C when the gas temperature upstream of the rotor was 522° C. The face of the rotor directed toward the exhaust outlet was 65° lower than the gas temperature at the exit from the turbine rotor, while the temperature of the opposite face adjoining the bearing was 120-140° C. The axial temperature gradient induced here reached, as in the TKR-14-2a, a value of roughly 4 deg/mm (temperature drop of 220°). Radial temperature gradients along the disk periphery were 1-1.5 deg/mm and were reduced to zero over the sections $\bar{r}$ = 0.45-0.8 on the disk working side. On the back side of the rotor these gradients had a positive sign[2] and did not exceed 2.5 deg/mm (temperature drop 100 deg). On the working side of the disk within the limits of the ($\bar{r}$ = 0.3-0.45) the temperature gradient, as in the TKR-14-2a, bore a negative sign and was 2.7 deg/mm (temperature gradient of 44 deg). /40

By comparing the curves of temperature distribution in the rotor of the TKR-14-2a and TKR-23-1 (see Figs. 18 and 19), one can note their qualitative similarity: the temperature drop from the periphery ($\bar{r}$ = 1) to the injection site of the cooling air. The more extended section with minimum temperatures of working rotor surface in the TKR-23-1 is due to the displacement toward the periphery of the injection site of the cooling air ($\bar{r}$ = 0.49 in the TKR-23-1 and $\bar{r}$ = 0.4 in the TKR-14-2a) and by the presence of highly elaborated radial seals.

---

[2] Here and in the following the positive sign of the temperature gradient was assumed to correspond to the case when the disk temperatures at larger radii are higher.

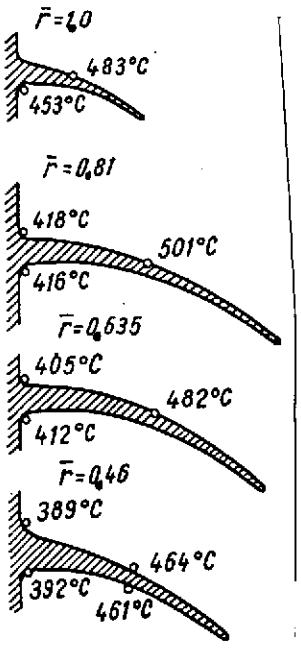


Fig. 20. Temperatures of rotor blades of TKR-23-1 in near-rated regimes

It can be assumed that these temperature fields of the TKR-23-1 and TKR-14-2a are characteristic of overhanging-type rotors when they are cooled by radial blowoff.

The temperatures of the blades of the rotor in the TKR-23-1 in the regimes studied were 100-120 deg higher than the disk temperatures even at a distance 6-10 mm from rotor surface (Fig. 20). Temperature gradients in the root section of blades in this case were 10-15 deg/mm. The highest values of these gradients (15 deg/mm) occurred over the sections of minimum temperatures of rotor working surfaces, that is, at $\bar{r}$ = = 0.45-0.65. At the ends of the leading and trailing blade edges cooling is not at all evident and their temperature is equal to the gas temperature.

The cooling system of the TKR-23-1 turbocompressor makes it possible to lower the temperature of the disk at near-rated regimes 80-130 deg with respect to the gas temperature in the working channel. Here a fairly high uniformity of disk heating is ensured, advantageously distinguishing the cooling system of the TKR-23-1 from the cooling system of the TKR-14-2a. However, as in the TKR-14-2a cooling system, rotor blades in the TKR-23-1 remain practically uncooled. /41

Tests of the TKR-14-2b turbocompressor in which film cooling of rotor and jet blowoff of its back side was employed were conducted at regimes embracing the entire working range of the turboprop engine. In the rated-power regime the mass flow of cooling air was 0.0088 kg/sec, with $n_{tc}$ = 31,200 rpm and the initial gas temperature $T_g$ = 575° C (Fig. 21).

The cooling method used in the turbocompressor made it possible, with this mass flow of cooling air (2.3 percent of $G_g$), to lower to overall temperature level 80-145 deg relative to the gas temperature in the rotor blading. However, the nonuniformity of disk heating was found to be quite high and over the sections $\bar{r}$ = 0.43-0.57 the radial temperature gradients reached 2.5 deg/mm,

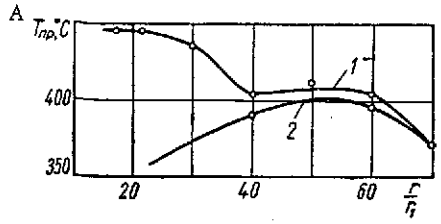


Fig. 21. Temperature field of rotor of TKR-14-2b in rated regime:
1. Working side of rotor
2. Back side of rotor
Key: A. $T_{rd}$

and 3.8-4.0 deg/mm with an opposite sign[3] -- over the peripheral sections. This trend of the temperature field is caused, on the one hand, by intensive film cooling of the peripheral parts, and on the other -- -- by the geometrical shape of the rotor and the marked changes in the boundary conditions of heat exchange radiuswise on the heating and cooling sides that occur at rated or near-rated regimes. The results of thermometry of the rotor of this turbocompressor model allow us to conclude that the intensity of film cooling must be reduced, by somewhat shifting toward the rotor axis the casing opening for the admission of cooling air.

## 2. Tests With Combined Operation of Turbocompressor and Internal Combustion Engine

The above-presented data on the temperature regimes of rotors of centripetal turbines correspond to one operating regime of the turbocompressor that is at the rated level in terms of rpm and power. At the same time, when both the turbocompressor and the internal combustion engine are operating at the same time, the cycle parameters change over very broad limits. Therefore it is natural to propose the question of determining the operating regimes of the turbocompressor cooling system that are the most thermally stressed when both the turbocompressor and the engine are operating. /42

Besides the regime factors determining the diesel characteristics, the operating conditions of the cooling system of a turbocompressor is strongly affected also by the type of diesel and, primarily by its stroke cycle. Rotors of centripetal turbines in which these cooling systems are used are cooled by air in supercharging two-stroke diesels in all possible regimes,

---

[3] These temperature gradients here and in the following (with the exception of specially stipulated cases) can be recalculated for the temperature drops in the earlier sections under consideration. The relative radii and the geometrical dimensions of the rotors required are given in the text only in the figures.

since the necessity of reliable scavenging of cylinders necessitates the supercharging pressure always exceeding the pressure of gases upstream of the turbine /9, 80/. In schemes of combination supercharging of two-stroke diesels where a driven supercompressor is used as the first stage, the ratio of the supercharging pressure to the gas pressure upstream of the turbine proves to be even higher.

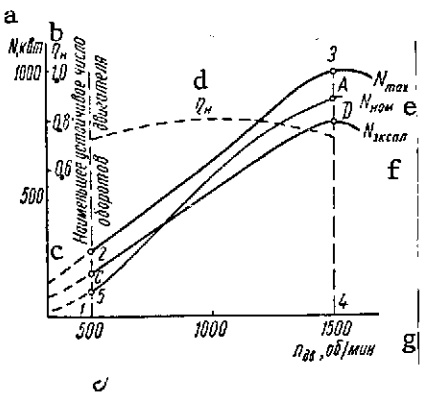


Fig. 22. Velocity characteristics of 124N 18/20 engine:
5 - A. External characteristics of engine /18/
$\eta_f$ = Filling factor /9/

Key: a. N, kW
b. $\eta_f$
c. Lowest stable engine rpm
d. $\eta_f$
e. $N_{rat}$
f. $N_{oper}$

When four-stroke diesels are provided with gas-turbine supercharging, leakage of gas instead of air in the cooling line of the turbine rotor is not precluded. This is observed in diesel operating regimes in which the supercharging pressure, that is, the pressure at the initial point of the cooling line proves to be lower than the pressure upstream of the turbine rotor (at the terminal point of the cooling line).

As an example, let us examine the operating characteristics of the joint operation of a TKR-23-1 turbocompressor with a four-stroke locomotive diesel (124N 18/20 according to the nomenclature of the Council of Mutual Economic Assistance), whose working parameters are these: $n_{en}$ = 1500 rpm, maximum power 735 kW, $\pi_{en}$ = 13.5 /18/ (Fig. 22). The range of all possible operating regimes for this diesel is characterized by the region 1-2-3-4-1. The line 1-2 corresponds to diesel loading at minimum stable rpms ($n_{en}$ = 500 rpm), line 2-3 corresponds to the acceleration of the diesel with simultaneous maximum loading over the entire range of rpm values, the 4-3 line corresponds to loading of the diesel in idling with $n_{en} = n_{max}$ = 1500 rpm up to $N_{max}$ = 735 kW and, finally, the line of diesel acceleration in idling from $n_{en} = n_{min}$ = 500 rpm to $n_{en} = n_{max}$ = 1500 rpm.

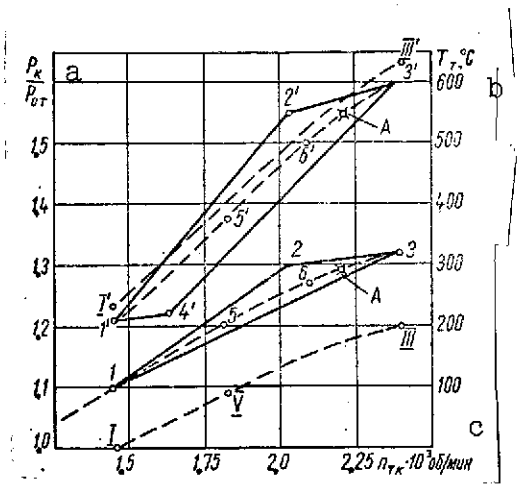


Fig. 23. Variation in ratio of pressures $P_c/P_{0t}$ /t = turbine/ and gas temperature upstream of turbine $T_0$ for different diesel operating regimes:

1-6. Variation in $P_c/P_{0t}$ ratios for different diesel operating regimes

1', 2', 3'. Change in gas temperature upstream of turbocompressor under the same diesel operating conditions

I-V-III and I'-III'. Change in $P_c/P_{0t}$ ratios and $T_o$ for back-pressure of 1.18 bar

A. Nominal diesel operating regime

Key: a. $P_c/P_{0t}$
b. $T_t$
c. $n_{tc} \cdot 10^3$ rpm

To determine the main parameters of the gas and cooling air in the blading part of a centripetal turbine, an approximate calculation was made of the conditions of joint operation of diesel and turbocompressor at each point of the diagram in Fig. 22. The results of these calculations are presented graphically as the functions $P_c/P_{1t} = f(n_{tc})$ and $T_g = f(n_{tc})$ in Fig. 23. They are characteristics of the turbine cooling system of a TKR-23-1 turbocompressor when it is operating simultaneously with a 12ЧN 18/20 diesel ($P_c$ = supercharging pressure; $P_{1t}$ = pressure of gas upstream of turbine rotor; $T_g$ = temperature of gas upstream of turbine; $n_{tc}$ is the rpm of the turbocompressor). /43

As we can see in Figs. 22 and 23, the maximum rpm of the turbocompressor rotor (point 1) is 14,500 rpm, while the maximum (point 3) is 24,000 rpm.

Corresponding to the total diesel power is the maximum value of the gas temperature upstream of the turbine, mass flows of cooling air, and rpm of turbocompressor rotor. By comparing the parameters at points 2 and 3 we can note that the maximum mass flow of cooling air (point 3) proves to be only 2-3 percent higher[4] than at point 2 corresponding to the maximum power of diesel when $n_{en} = n_{min} =$

[4] The small $P_c/P_{1t}$ ratios in passing from regime 2 to regime 3 give grounds for assuming that the change in the mass flow is proportional to the square root of this ratio.

= 500 rpm. In this case the initial gas temperature in the nominal regime is 50 deg higher than at regime 2. Thus, the most stressed operating condition of the cooling system of this turbocompressor in the absence of back pressure on the turbine must be regarded as the regime of total (rated /nominal/) power.

An increase in back pressure is accompanied by an increase in gas pressures in the blading of the turbine, and also in the compressor turbodrive of the diesel. The effect of back pressure is more evident in the changes in the turbine parameter and less evident in the change in the supercharging pressure.

Curves 1-5-A (see Fig. 22) and I-V-III (see Fig. 23) correspond to loading of the diesel locomotive according to the external characteristic with a 10 percent rise in back pressure. The reduction in the mass flow of cooling air is about 5 percent, while the rpm of the turbocompressors at which gas begins to enter the cooling line from the blading is 18,500 rpm. /44

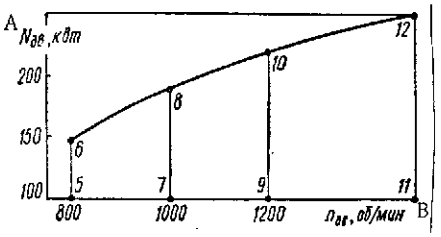


Fig. 24. Velocity characteristics of D-6 engine. Points on the graph correspond to the regime number in the experiments.
Key: A. $N_{en}$, kW
B. $n_{en}$, rpm

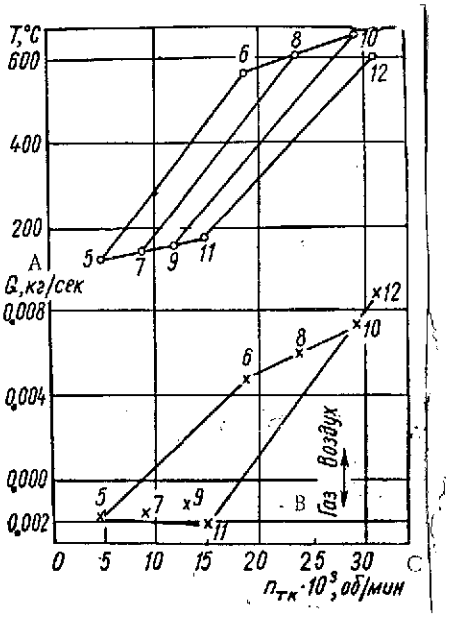


Fig. 25. Gas temperatures and mass flows of air in the rotor cooling system when turbocompressor TKR-14-2b is running together with D-6 diesel. The regime numbers correspond to Fig. 24.
Key: A. kg/sec
B. Gas Air
C. $n_{tc} \cdot 10^3$, rpm

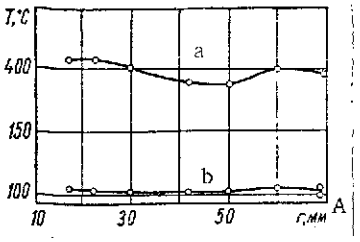


Fig. 26. Temperature field of rotor of TKR-14-2b in regime 6 (a) and 7 (b) of control characteristic of D-6 diesel. The regime numbers correspond to Fig. 25.
Key: A. mm

When two-stroke engines are supercharged, the supercharging pressure is always 15-20 percent higher than the pressure of the gas upstream of the turbine [7, 9, 34]. In this case it should be expected that in all the possible regimes the turbine rotor of the turbocompressor will be air-cooled. Here the pressure ratios $P_c/P_0$ with increase in turbocompressor rpm rises more slowly than gas temperature. As in four-stroke diesels, the most stressed regime in two-stroke diesels is the total power regime.

To determine the temperature field of the turbine rotor in the most stressed regime of turbocompressor operation and to compare the results of testing the cooling system in stand conditions and when both the turbocompressor and the diesel are running together, special experimental studies were conducted.

Tests of the cooling system of the turbine of the series-produced TKR-14-2b turbocompressor were run on the six-cylinder D-6 engine. The limiting operating regimes of the engine during the test process were determined by two control characteristics of the diesel: at minimum stable rpm ($n_{en}$ = 800 rpm) and at the rated rpm ($n_{en}$ = 1500 rpm). Between these two extreme regimes tests were conducted further in four more regimes (Fig. 24, points 7-10), which are the limiting regimes at the intermediate control characteristics for rpm values of 1000 and 1200. The first regime was idling at the lowest stable rpm ($n_{en}$ = 800 rpm) at which the diesel is capable of bearing a load. At these same rpm of the engine operating under the control characteristics it was loaded to its maximum power (Fig. 24, point 6). During the [45] loading, all parameters were measured. After the conclusion of heating of the turbine rotor, all parameters were measured in the steady regime and a sudden release of load to idling was performed. Then the diesel rpm in idling was increased (Fig. 24, point 7), and a new idling regime was provided, after which sudden loading under the control characteristic was put into effect up to the next regime in power level (point 8). Further alternation of the regimes took place in similar fashion all the way until the rated power level at $n_{en}$ = 1500 rpm was achieved.

Fig. 25 presents the gas temperatures and mass flows of cooling air for several turbocompressor rpm values. The mass

flows of cooling air were determined from the equation

$$g_{en} = \sqrt{\frac{2\rho\Delta P F^2}{\xi}}. \qquad (II.2)$$

The numbering of the points in Fig. 25 corresponds to the numbering of the diesel operating regimes.

From an analysis of the data in Fig. 25, to the same turbocompressor rpm there may correspond different gas temperatures, different $(P_c - P_{i.a})/P_c$ ratios, and different mass flows of cooling air. To illustrate, when $n_{tc}$ = 15,000 rpm the gas temperature is 175-450° C, and the $(P_c - P_{i.a})/P_c$ ratio = -0.017 - + 0.36. Both cooling air whose mass flow can reach 0.003 kg/sec as well as gas (up to 0.002 kg/sec) can flow in the cooling line in this case. Thus, in contrast to an autonomous gas turbine engine or a turbocompressor driven from a combustion chamber in an experimental stand, in a turboprop engine the interrelationship of parameters characterizing the efficiency of the turbocompressor cooling system and the diesel engine regime is strongly complicated.

Let us look at the operation of the turbocompressor cooling system first in the idling regime (Fig. 25, points 5-7-9-11). As Fig. 25 shows, for diesel idling rpm the gas temperature upstream of the turbine does not go above 170° C, while $n_{tc}$ varies from 5000 to 15,000 rpm. Gas flows in the cooling line at these regimes. The temperature field of the rotor is quite uniform (Fig. 26 b, Fig. 27 b, and Fig. 28 b), while the temperature drops between the rotor blade and the disk do not exceed 20 deg. Characteristic of these diesel operating regimes are low gas temperatures in the blading (not above 150-160° C), but the danger is present that the cooling line will be plugged by carbon deposits and mineral residues of combustion products. This danger mounts when the diesel is run at idling regimes with increased rpm. /46

When the diesel is being loaded, air begins to enter the cooling system. Thus, even when $n_{en}$ = 800 rpm and $n_{tc}$ = 6000 rpm the cooling system begins operating normally. In those cases when loading is carried out at higher engine rpms, air enters the cooling line already when $n_{tc}$ = 17,000-18,000 rpm. When the diesel is being run according to the external characteristic of maximum power (Fig. 25, points 5-6-8-10-12), the temperatures of gas and rotor along the section 5-6 climb most steeply, where the diesel is being loaded at $n_{en}$ = const. Along the characteristic sections 6-8-10 the intensity of the rise in these temperatures is somewhat reduced. This is so because the rise in diesel power along the

section 6-8-10 occurs owing to an increase in diesel rpm at near-constant indicated pressure. Maximum gas and rotor temperatures occurred at a regime when $n_{en}$ = 1200 rpm and $N_{en}/N_{rat}$ = 0.87. The rpm of the turbocompressor here corresponded to 29,400, while the mass flow of cooling air was 0.0069 kg/sec.

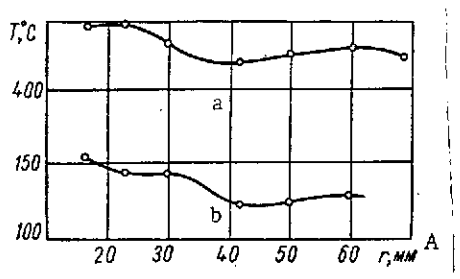


Fig. 27. Temperature field of rotor of TKR-14-2b in regimes 8 (a) and 9 (b) of control characteristic of D-6 diesel. Regime numbers correspond to those in Fig. 25.
Key: A. mm

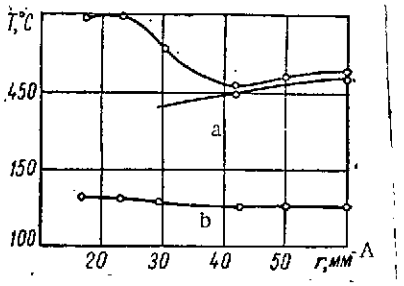


Fig. 28. Temperature field of rotor of TKR-14-2b in regimes 10 (a) and 11 (b) of control characteristic of D-6 diesel. Regime numbers correspond to those in Fig. 25.
Key: A. mm

The regime of maximum (in our experiments) turbocompressor rpm proved less thermally stressed (Fig. 25, point 10). In this regime the gas temperature was 50 degrees lower, while the mass flow of cooling air was 29 percent higher (0.0088 kg/sec). As a result, rotor disk temperatures were 60-80 deg lower. However, when the diesel[5] was overloaded to N = 188.5 kW (where $N_{rat}$ = = 185 kW) this regime will be most stressed, since both gas temperatures as well as turbocompressor rpm will be at their maximum values. Mass flows of cooling air in this case will rise less than will gas temperature and rotor rpm.

Let us look more closely at the temperature fields of the turbine rotor for load regimes.

After the diesel has been loaded at $n_{en}$ = 800 rpm to $N_{en}/N_{rat}$ = 0.57 (Fig. 25, point 6), the turbocompressor rpm is 18,600 rpm, /47 the mass flow of cooling air is 0.0048 kg/sec, and the temperature of the gas upstream of the turbine is 565° C. The trend of the temperature field (Fig. 26 a) corresponds in large measure to the trend already obtained for the turbocompressor TKR-14-2a with the line adapted for film cooling.

[5] In the experiments the maximum attained diesel power was 185 kW.

The highest disk temperatures occur for $\bar{r}$ = 60-65 mm and at the rotor face. Along the section $\bar{r}$ = 0.7-0.75 the temperatures are lower, due to the shape of the turbine. Along the disk periphery the effect of film cooling is marked. Overall, in this regime the temperature field is characterized by relative uniformity. Thus, the maximum radial gradients occur along the sections $\bar{r}$ = 0.75-0.82 and amount to 1 deg/mm (the temperature drop is within a 5 deg range). The drop in disk temperatures relative to gas temperatures in the blading is 100 deg at the disk face and 140-145 deg along the periphery.

In the diesel operating regime corresponding to point 8 in Fig. 25, when $N/N_{rat}$ = 0.76 and $n_{en}$ = 1000 rpm, the initial gas temperature reached 605° C, while the mass flow of cooling air was 0.00585 kg/sec. The trend of the temperature field (Fig. 27 a) and the radial temperature gradients remained as before, while the reduction in the disk temperatures relative to the gas temperatures was 95-100 deg at the disk face and 150 deg along the periphery. The axial temperature gradients did not exceed 3-4 deg/mm for $\bar{r}$ = 0.6 (temperature drop 66-88 deg).

In passing to regime 10 (Fig. 28 a) (along the external diesel characteristic), the effectiveness of film cooling rises sharply. The trend of the temperature field along the periphery changes: the temperatures of the disk ridge fall off sharply compared to the disk temperatures over the remaining sections. Radial temperature gradients along the disk radius 60-70 mm change sign and reach 5 deg/mm. Also rising strongly are the inverse gradients along the section $\bar{r}$ = 0.35-0.50 of the working disk surface, reaching 3 deg/mm (temperature drop 32 deg). The level of disk temperatures is 80 deg (disk face) below the gas temperatures in the rotor blading, and 160 deg below the gas temperatures in the rotor blading for $\bar{r}$ = 0.85.

In the most stressed operating regime of the turbocompressor ($n_{tc}$ = 31,200 rpm; $N/N_{rat}$ = 1; $n_{en}$ = 1500 rpm, regime 12, see Fig. 25), nonuniformity of disk heating at r = 30-50 mm and along its periphery rises appreciably (Fig. 29). Thus, the sign-inverse temperature gradients along the disk ridge and its periphery reach 4-5 deg/mm, 3.8-4 deg/mm along the section $\bar{r}$ = 0.43-0.52, and along the section $\bar{r}$ = 0.52-0.72 the gradients have a positive sign and their value is 2.5 deg/mm (the temperature drop in this case is 35 deg).

Thus, the temperature field of the rotor of the TKR-14-2b turbine at low and moderate loads is quite uniform and corresponds in trend to the fields examined earlier when film cooling is present. With increase in the diesel load to the rated value, nonuniformity of the temperature field rises, temperature drops /48

appear along the working surface of the disk along the radii $\bar{r}$ = = 0.5-0.7 and along the peripheral sections of the disk. This is caused both by intensive film cooling and the geometrical shape of the turbine and by the appreciable change in the boundary conditions of heat transfer on the heating and cooling sides.

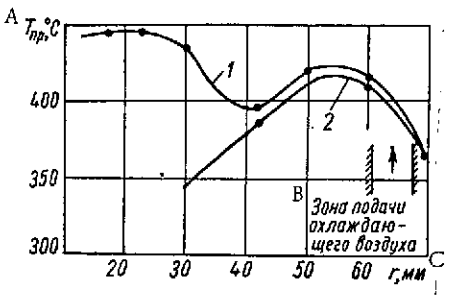


Fig. 29. Temperature field of rotor of TKR-14-2b in the rated regime when running together with D-6 diesel:
1. Working surface of rotor
2. Back /suction/ rotor surface

Key: A. $T_{rd}$
B. Zone of feed of cooling air
C. mm

To compare the results of experimental studies of the cooling systems of turbocompressors like TKR-23-1, and stand tests and when run jointly with the diesel, experiments were conducted on the turbocompressor in a combination turbine rotor cooling system (radial blowoff in conjunction with jet cooling). The layout of the turbine rotor cooling system is shown in Fig. 9. Tests of the cooling system of the turbocompressor were run together with an internal combustion engine. The test regimes of the turbocompressor were dictated by the characteristic regimes of the engine on which it was installed. The feed of diesel exhaust gases to the turbine was via four exhaust pipes.

Suction of air into the turbine was through a metering diaphragm if there was no current-collecting device, and through a regular muffler when the rotor underwent thermometry. In the latter case, compressor characteristics were used to determine air mass flow. A mercury current collector /slip ring/ was installed in the casing of a special drive placed in the suction duct of the turbocompressor. The oil systems of the drive and the turbocompressor were unified.

From results of these experiments, the operating conditions of the turbocompressor cooling system depend significantly on gas pressure at the turbine outlet. When the gas pressure at the turbine outlet is 1.5 bar, hot gas flowing through the labyrinth seals into the compressor cavity flows into the cooling line.

In this case, the temperatures of the peripheral part of the turbine disk and the rotor blades are very close to the temperatures of the gas in the blading (Fig. 30). The difference in

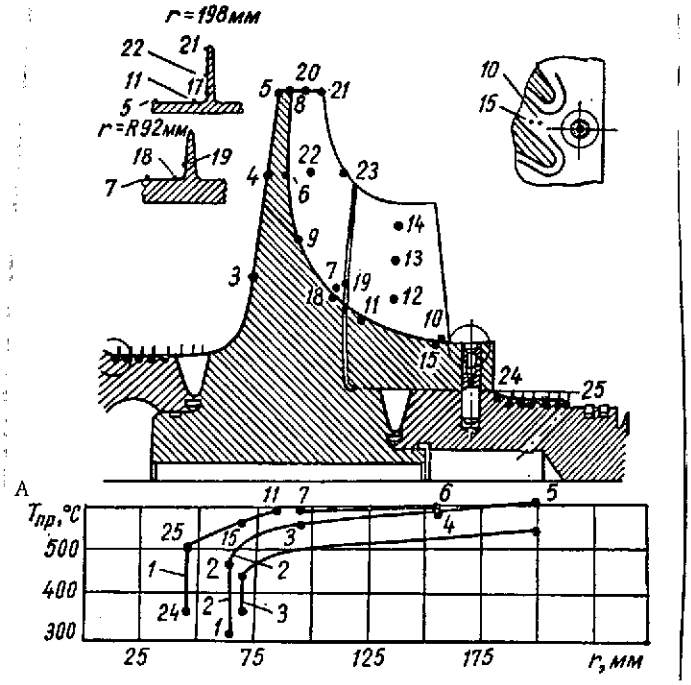


Fig. 30. Temperature field of uncooled rotor of the TKR-40 turbocompressor
1. Temperature of rotor working surface
2. Temperature of back surface of rotor
3. Gas temperature in clearance between rotor casing and back side

Key: MM = mm
A. $T_{rd}$

these temperatures does not exceed 15-18 deg, that is, the difference is a much smaller value than in the TKR-14-2a and TKR-23-1 turbocompressors. This is accounted for by the design features of the stator part of this turbocompressor, in which the central part of the deflector is heated by the gas to avoid high temperatures. Heat is rejected from the peripheral part of the disk mainly via thermal conductivity into the rotor hub and turbine bearing (see Fig. 9). This is shown by the large (up to 3 deg/mm) axial temperature gradients over these sections. The heat rejection from the back side of the disk to the gas delivered from the blading into the clearance present to a small extent is caused by a small drop in gas temperature through cooling in the casing of the spacer. It can be assumed that the gas penetrates through the peripheral series of openings into the spacer and then is swept toward the disk surface through the central opening rows. The temperature jump along the section $\bar{r}$ - 0.32 of the working rotor side is due to the presence of the nozzle rim of the exhaust rectifying device, which due to its considerable distance from the heat current sends the added contact resistance is virtually uncooled.

/49

The temperature field of the rotor in the rated regime of turbocompressor operating together with the diesel is shown in Fig. 31.

Four series of openings from which the cooled air flows to the back side of the disk provide for a smooth reduction in the temperature of the rotor metal over the sections swept by the air. /50 The radial gradients over the disk sections from $\bar{r} = 0.5$ to $r = 1.0$ vary slightly and amount to 0.8-1.0 deg/mm (temperature drop is 80-100 deg). Analysis of test results showed the mass flow of cooling air in the rotor cooling system during tests to be 80 percent below the design value. Inspection of the turbocompressor after the tests established that openings for air bleeding from the compressor were clogged with carbon and oil. In the subsequent startups of the turbocompressors of this type, the openings for air bleeding were enlarged, leading to a higher mass flow of cooling air compared with the first tests, by a factor of 2-2.2. Here the intensity of rotor cooling was much increased.

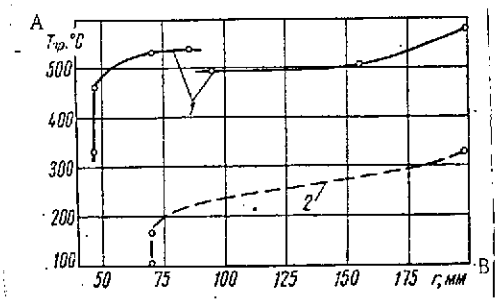


Fig. 31. Temperature field of rotor of TKR-40 in rated regime:
1. Temperature of working surface
2. Temperature of cooling air

Key: A. $T_{rd}$
B. mm

Estimation of the disk temperatures by opalescence colors make it possible to assume that the temperature of the disk at the air injection site was 160-170 deg below the gas temperature upstream of the rotor. Overall it had to be assumed that the trend of the temperature field of the rotor of this turbine is like that of the temperature fields we have examined for the rotors of TKR-14-2a and TKR-23-1 turbocompressors cooled by radial blowoff, with similar values of the relative mass flows of cooling air.

To determine the effect of periodic pulsations of the parameters of the gas upstream of the turbine on the efficiency of the rotor cooling system when the diesel was run with the turbocompressor, a special series of experimental studies was conducted.

Initially the cooling system of the turbine rotor of the TKR-14-2a turbocompressor was tested on an experimental stand with a combustion chamber. Here, at a series of regimes measurements were made of the main parameters of the working gas, cooling air, rpm of turbocompressor rotor, and the temperature field of turbine rotor. Then this same turbocompressor was installed in a six-cylinder D-6 diesel and all the regimes used for test stand experiments were reproduced. In reproducing the regimes in the diesel, it was possible to quite exactly reproduce the mean supercharging pressure, pressure of gas upstream of the turbocompressor

TABLE 3

MAIN RESULTS OF TESTING COOLING SYSTEMS OF TKR-14-2a TURBOCOMPRESSOR IN STAND CONDITIONS AND IN DIESEL

| Reg. Nr. | Oper. Regime | $n_{en}$ rpm | $T_g$ °C | $T_{i.a}$ °C | $g_{i.a}$ kg/sec | $\frac{Bi_{i.a}}{Bi_g}$ | $\frac{P_c - P_t}{P_c}$ |
|---|---|---|---|---|---|---|---|
| 1 | W/chamber | 15 000 | 430 | 105 | 0,00404 | 3,321 | 0,0389 |
| 15 | On diesel | 15 000 | 490 | 115 | 0,00445 | 3,972 | 0,0383 |
| 2 | W/chamber | 18 180 | 470 | 103 | 0,00475 | 4,101 | 0,0605 |
| 6 | On diesel | 18 600 | 540 | 125 | 0,00457 | 3,932 | 0,0560 |
| 3 | W/chamber | 20 000 | 510 | 103 | 0,00505 | 4,123 | 0,0705 |
| 13 | On diesel | 20 400 | 530 | 125 | 0,00560 | 3,867 | 0,0758 |
| 4 | W/chamber | 25 000 | 535 | 123 | 0,00644 | 4,848 | 0,1090 |
| 14 | On diesel | 25 000 | 546 | 127 | 0,00640 | 4,648 | 0,0910 |

(a deviation of 3-5 percent), and revolutions per minute (a deviation of 3-4 percent). However, the diesel control system did not permit reproducing the exhaust gas temperature with sufficient accuracy. So the temperature fields of the rotor were compared in their dimensionless representation. The main parameters of the regimes compared are shown in Table.3. /51

Since the dimensionless temperatures of the disk for these regimes were caused only by the heat transfer coefficients of the rotor surfaces, the ratio of the Biot numbers on the inner and gas sides ($Bi_{i.a}/Bi_g$) is also used as the comparison parameter.

The temperature of the working surface of the disk for combined operation with diesel was found to be 5-7 percent higher than for its operation on the test stand with the combustion chamber. It can be assumed that the higher temperatures of the turbine rotor when run with the diesel compared with performance on the stand with combustion chamber under the same conditions of turbocompressor rotor rpm, mass flows of gas through the turbine, and initial gas temperature were due to pulsations in the parameters in the gas stream upstream of the turbine. In one crankshaft revolution of the engine the gas pressure upstream of the turbine $P_0$ proved to be higher for certain time intervals than the supercharging pressure. Here the discharge of heated gases into the cooling line is inevitable. Thus, during one crankshaft revolution of the diesel successively hot gas, a mixture of hot gases and cooling air, and cooling air can enter the cooling line. The frequency of these changes in the cooling system were thus proportional to the diesel rpm.

In the hydraulic and thermal calculations of the rotor cooling system these factors are usually not allowed for, and the calculations

as such are conducted based on averaged (in time) pressures and temperatures of the gas upstream of the turbine. So the actual air mass flows turn out to be lower than those determined by mean parameters, while the temperatures of the air-gas mixture in the cooling line are higher than those assumed in the calculations even those measured by the thermocouples during testing. The combined action of these factors brings about an increase in rotor temperatures during operation with the diesel compared to the case when the turbocompressor is driven from the combustion chamber.

During the testing on the diesel, pulsations of gas pressure in the diesel exhaust pipe were measured. From these data the instantaneous values of cooling air mass flow were calculated, assuming that the coefficients of hydraulic drag, coefficients of losses in the nozzle cascade and blading cascade remained constant for the indicated operating regime. Results of calculations for one of the regimes (see Fig. 24, point 6) are in Fig. 32. /52

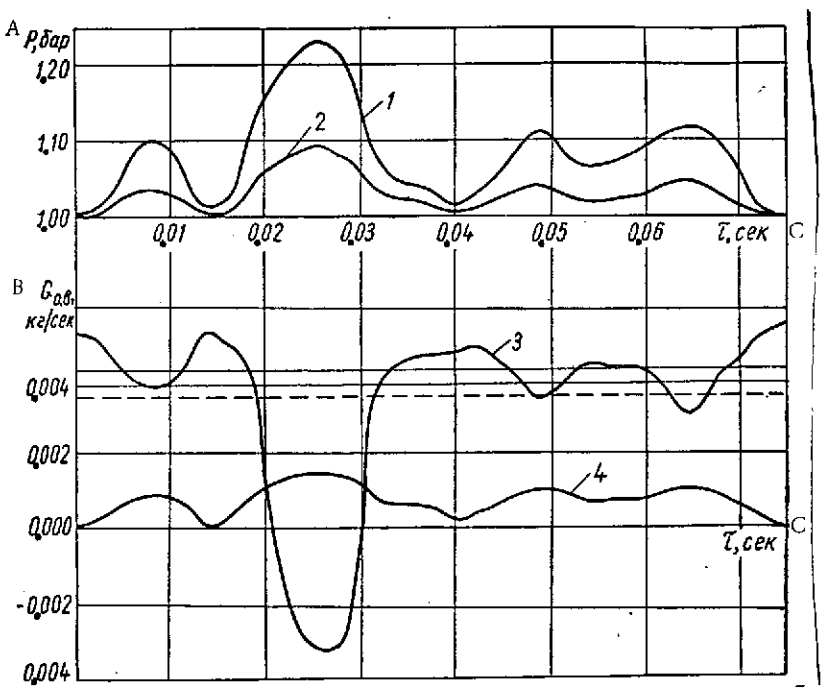


Fig. 32. Time-based variation of gas and air parameters in cooling line of TKR-14-2b when run together with D-6 diesel:
1. Initial gas pressure $P_0$; 2. Pressure of gas upstream of rotor $P_{1t}$; 3. Total mass flow of cooling air in line; 4. Leakage into labyrinth
Key: A. P, bar; B. $G_{i.a}$, kg/sec; C. sec

As follows from Fig. 32, the time-averaged mass flow of cooling air

$$g_{i.a} = \frac{1}{\tau} \int_{\tau_1}^{\tau_2} g_{i.a}(\tau)\, d\tau \qquad \text{(II.3)}$$

is much (by 10-20 percent) below the mass flow based on mean pressures:

$$\bar{g}_{i.a} = f(\bar{P}_{i_g}),$$

where $\bar{P}_{1g}$ is the mean pressure upstream of the rotor.

## 3. Nonsteady Thermal Regimes /53

Low-power gas turbine sets with centripetal turbines operate for much of their life in nonsteady thermal regimes. This is essentially true of turbocompressors used in supercharging tractive internal combustion engines, which for most of their service life operate in conditions of variable loads with rapid stops and starts from idling to the maximum-load regimes. In these conditions operating reliability of a centripetal turbine is due to the ability of the turbine to withstand a certain number of heat cycles, by the overall averaged temperature level of the rotor, and by the values of the radial and axial gradients. Therefore in recent years much attention has been paid to studying nonsteady thermal regimes of rotors. The goal of these investigations is estimating the effect of heat cycles on the strength characteristics of rotors in centripetal turbines.

It is noted in the references /11, 12/ that the peak temperature gradients along the disk radius in nonsteady regimes is much higher (by 1.5-2 times) than in steady thermal regimes. However these studies do not give specific quantitative data on the operating features of the cooling systems of rotors of centripetal turbines during rapid startups and shutdowns of the turbocompressor.

During the testing of cooling systems of the series-built turbocompressors TKR-14-2a, TKR-23-1, and TKR-14-2b, also determined were the main characteristics of the cooling system and the temperature fields of rotors of turbines during starting, stopping, and switching from one regime to another. These investigations were conducted both on test stands with combustion chamber as well as in the turbocompressor running with the diesel.

The TKR-14-2a turbocompressor was tested in most severe conditions affording deliberately overstated temperature gradients compared with the actual heating conditions of the rotor of a centripetal gas turbine when the turbocompressor is run together with the diesel. On the test stand during stopping of the TKR--14-2a turbocompressor, the delivery of fuel to the combustion chamber was halted virtually instantaneously, and both through the turbine blading and the cooling system cold air flowed for a certain time, whose mass flow differed only slightly from the mass flow of gas and cooling air in the rated operating regime of the turbocompressor. When this turbocompressor was started up on the stand, gas flowed through the blading of the turbine continuously at a mass flow virtually the same as the rated mass flow, while the gas temperature reached peak values for a few seconds. The mass flow of air through the cooling system in this case was also near-rated.

When the turbocompressor was run together with the diesel, simultaneously with stopping the delivery of fuel was halted, and the gas and air mass flows dropped quickly to zero. In this case the cooling of the turbine rotor occurred under conditions /54
of natural convection, but not in the stream of cold air as was the case during the stand tests of the TKR-14-2a. During diesel starts, at first the turbocompressor ran at regimes corresponding to idling, and then its loading began; when operating on the stand, the turbocompressor at once became virtually under total load.

Essentially, the regimes of turbocompressors startup and stopping on the stand are extremely close to those of an autonomous GTE.

The curves of rotor heating and cooling of the TKR-14-2a turbocompressor with constant mass flows of gas and air are in Fig. 33. During starting the rate of change in temperature of the peripheral parts of the rotor cooled by radial blowoff reached 1.9-2.0 deg/sec, while the heating rate of the central rotor areas went up to 1.5 deg/sec. This raised the radial temperature gradient 70-90 percent compared with the gradients in the steady thermal regimes. The axial temperature gradient during starting rose monotonely and reached peak values in steady thermal regimes.

When the combustion chamber was cut out the gas temperature at the combustion chamber outlet was 550° C and the peripheral part cooled off faster; air slowly cooling off was the
the rotor facing the exhaust pipe (the massive area of the disk). /55
Because of this, a radial test gradient developed in the disk; 60-70 sec after cutout the gradient reached 3.8-4.0 deg/mm, then began falling off and became zero in 9-10 min (Fig. 33).

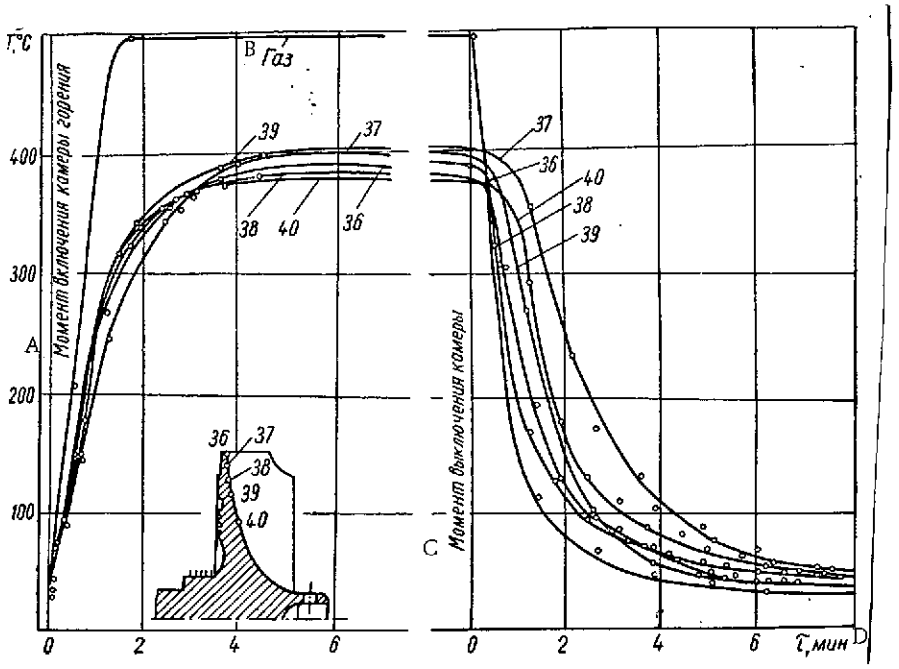


Fig. 33. Variation of temperatures at characteristic points of the rotor in a TKR-14-2b during starting and stopping with constant delivery of cooling air mass flow from outside source

Key: A. Moment of cut-in at combustion chamber
B. Gas
C. Moment of chamber cut-out
D. Minutes

In contrast to the TKR-14-2a turbocompressor with the centripetal compressor acting as a load device (the air was discharging to the atmosphere), in the TKR-23-1 the compressors and turbine were joined by an air-gas duct through the combustion chamber. In this case during starting and stopping the gas mass flow changed markedly, which in turn provided less intense rise in the temperature gradients of the turbine rotor. During the starting period the gas temperature was brought by the fuel mass flow regulator to 550° C in 30-35 sec and thereupon was kept constant. Fig. 34 shows the temperature fields of the turbine rotor in a TKR-23-1 turbocompressor during starting and stopping. From the instant the combustion chamber was cut in, roughly 60-65 sec later the radial gradients of the rotor temperature reached 2.8 deg/mm, but then they began to drop and roughly 1.6 min from the beginning of startup they were found to be at 1.5-1.6 deg/mm. The temperature gradients along the heart of the rotor vanes during the same interval were reduced to 6-8 deg/mm. The trend of variation in the axial temperature gradients and their magnitude both during startup and upon stopping remained the same as in the TKR-14-2a (see Fig. 33). /56

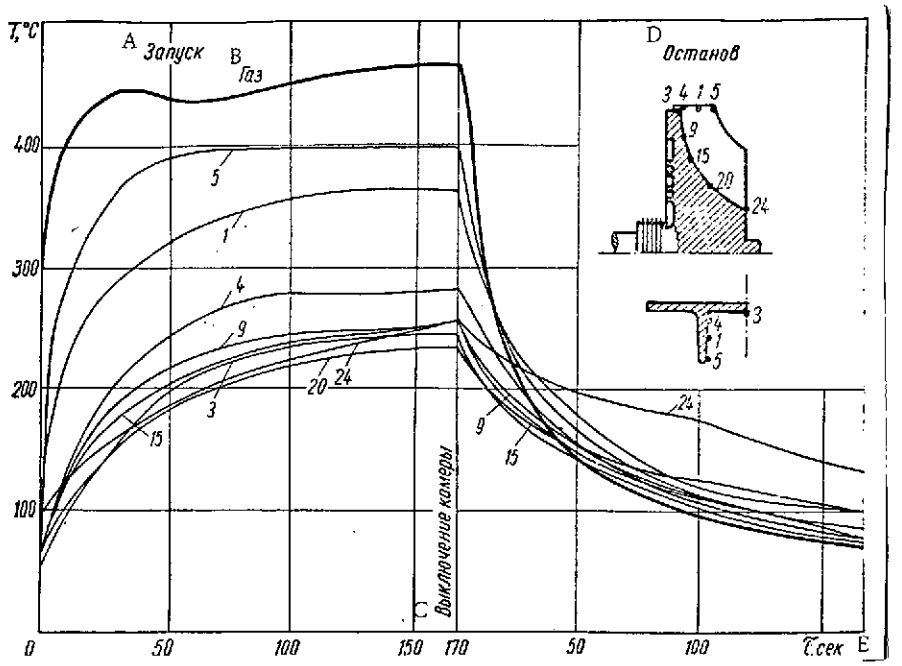


Fig. 34. Variation in temperatures at characteristic points of rotor of TKR-23-1 turbocompressor during starting and stopping with cooling air delivered from its own compressor

$(\bar{r}_1 = \bar{r}_3 = \bar{r}_4 = \bar{r}_5 = 1.0;\ \bar{r}_9 = 0.83;\ \bar{r}_{15} = 0.63;\ \bar{r}_{20} = 0.46;\ \bar{r}_{24} = 0.28)$.

Key:
A. Starting
B. Gas
C. Cut-out of chamber
D. Stopping
E. Seconds

In the shutdown regimes when the pure injectors were cut off, the temperature of the edges of the rotor blades fell fastest, differing from the gas temperature by not more than 10-15 deg. The rotor faced toward the exhaust proved to be highest in inertia, thermally speaking. The temperature gradients along the height of the rotor blades, beginning from the instant of chamber cutout dropped sharply -- in 20 sec they changed their sign and thereupon reached 2-2.2 deg/mm. The radial temperature gradients in remained nearly unchanged over the entire interval of shutdown and did not exceed the values obtained in the steady thermal regime (1.8-1.2 deg/mm).

The fullest investigations of the rotor cooling system in a centripetal gas turbine in nonsteady regimes were conducted for a TKR-14-2b turbocompressor installed on a D-6 diesel.

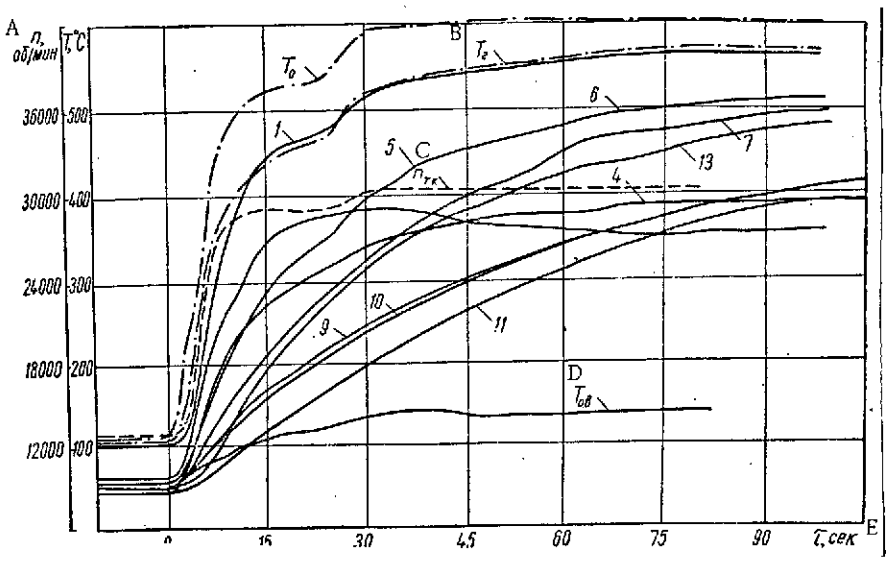


Fig. 35. Variation in temperatures at characteristic points of rotor in a TKR-14-2b turbocompressor, and changes in revolutions per minute, and in temperatures of gas and cooling air in passing from idling regime at $n_{tc}$ = 10,400 rpm, $N_{en}$ = 0, to the regimes with $n_{tc}$ = 29,400 rpm and $N_{en}$ = 0.89 $N_{rat}$:
$T_0$ is the temperature of the gas in the exhaust manifold at the diesel;
$T_g$ is the temperature of the gas at the rotor;
$T_{i.a}$ is the temperature of the cooling air in the cooling line;
1. Blade temperature, $\bar{r}$ = 0.98.
Working side of disk: Back /section/ side of disk:
4. $\bar{r}$ = 0.86 10. $\bar{r}$ = 0.33
5. $\bar{r}$ = 0.78 13. $\bar{r}$ = 0.60
7. $\bar{r}$ = 0.60 on/ side of
9. $\bar{r}$ = 0.43
Key: A. n, rpm D. $T_{i.a}$
B. $T_g$ E. sec
C. $n_{tc}$

The operating efficiency of the cooling system is determined not only from the temperature fields of the rotor, but also by the time-varying mass flows and parameters of the cooling air. To get the peak rates of change in the turbocompressor parameters, /57 the diesel was loaded at the rate that was the highest permitted by the control elements.

Results of the experiments (variation with time of the gas temperature, cooling air, rotor metal, pressures $P_c$ and $P_{1g}$, rotor rpm $n_{tc}$, and mass flow of cooling air) are shown in Fig. 35. The mass flow of cooling air is determined, as in the preceding chapters, by the drop $P_c - P_{1g}$. Here the independence of functional losses in the line from the mass flow of air was assumed, since the fraction of these losses is small compared with the losses for the remaining hydraulic drags.

With rapid diesel loading, the temperatures of the gas upstream and downstream of the turbine and the turbocompressor rotor rpms change most intensively with time. Thus, for example, in the first 20-25 sec after beginning of loading the initial gas temperature reached virtually steady values. The rate of its increase here is 50 deg/sec (during the first 5-7 sec) and is entirely due to the dynamic qualities of the diesel. A somewhat lower rate of gas temperature rise downstream of the turbine is caused both by an increase in heat transfer occurring in the turbine when the rpm is raised, and by substantial heat rejection to the turbocompressor elements. The rpm of the turbocompressor rotor stabilized already 5-7 sec from the beginning of power buildup. During this same time the pressure in the air-gas duct of the turbocompressor becomes stabilized and, virtually speaking, so do the mass flows of cooling air. The air temperature becomes stabilized in a more extended time interval (30-40 sec), however this change is small and has virtually no effect on the mass flows of cooling air.

The nature of the heating of rotor elements, as Fig. 35 shows, is determined by rotor shape and the medium flowing past it. Massive disk elements proved to be most subject to inertia. The effect of cooling on these sections in transient processes naturally is slight. It is also slight for the blades (see Fig. 35, curve for point 1 on blade), whose temperatures with time virtually follow the pattern of gas temperature in the blading. The temperature of the rotor blade proves to be dependent on the degree of heating of the elements of the turbocompressor stator: it rises on their arrival in the steady thermal regime. The heating rate of the turbine rotor radiuswise differs and depends on the thickness of the rotor and naturally on the method of cooling. In particular, if the disk temperatures at the section $\bar{r} \leqslant 0.4$ and the rotor blade temperatures throughout the heating period have the same temperature rise, over the section $\bar{r} = 0.8$--0.9 the pattern of temperature changes is more complex. The maximum temperatures are attained by the peripheral parts of the disk directly by the moment of stabilization of the revolutions per minute, after which with increase in mass flow cooling air they drop to stationary values. This is accounted for both by /58

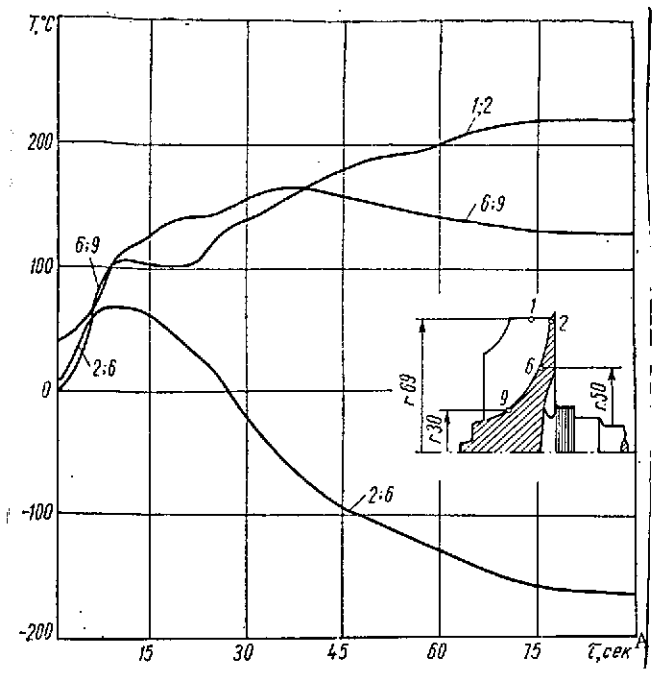


Fig. 36. Temperature drops between characteristic points of rotor of TKR-14-2b turbocompressor when D-6 diesel is loaded from idling to $N_d$ = 0.87 $N_{rat}$, $n_{tc}$ = 29,400 rpm
Key: A. sec

the specific features of film cooling, and by the low thermal inertia of the peripheral sections of the disk. During the period when the mass flow of cooling air is low, the film presence on the disk surface is swept off by the main gas flow, whose velocity rises intensively with increase in rpm. During this time the disk periphery rapidly heats up and after the mass flow of cooling air reaches steady values, it cools off, since the efficiency of film cooling rises sharply.

It should be noted that film cooling proves to be highly sensitive to changes in the regime of gas flow in the blading. This can be easily seen in Fig. 36, where temperature drops between points 2 and 6 and between points 6 and 9 on the disk are shown. In the regime of diesel loading from idling to $N_d/N_{rat}$ = 0.87 (Fig. 36), during the first 15 sec the temperature drop reaches 65 deg, then it falls to zero in 20 sec, and thereupon rises with reverse sign to $\underline{1}60$ deg. Intensive disk cooling also spreads over shorter radii r = 0.7-0.75, indicated by the change in temperature drops between points 6 and 9.

The fact that mass flows of gas and cooling air, as well as rpm of turbocompressor rotor reached steady values already 5-10 sec after the beginning of loading, while at the same time heating of the bulk of the rotor takes 70-90 sec, enables us in calculations to look at the transient thermal process in the cooling system as thermal shock, during which the heat transfer boundary conditions in the rotor blading and on the cooling side change virtually instantaneously[6]. /59

[6] This is valid for turbocompressors operating in conditions akin to those of TKR-14-2b.

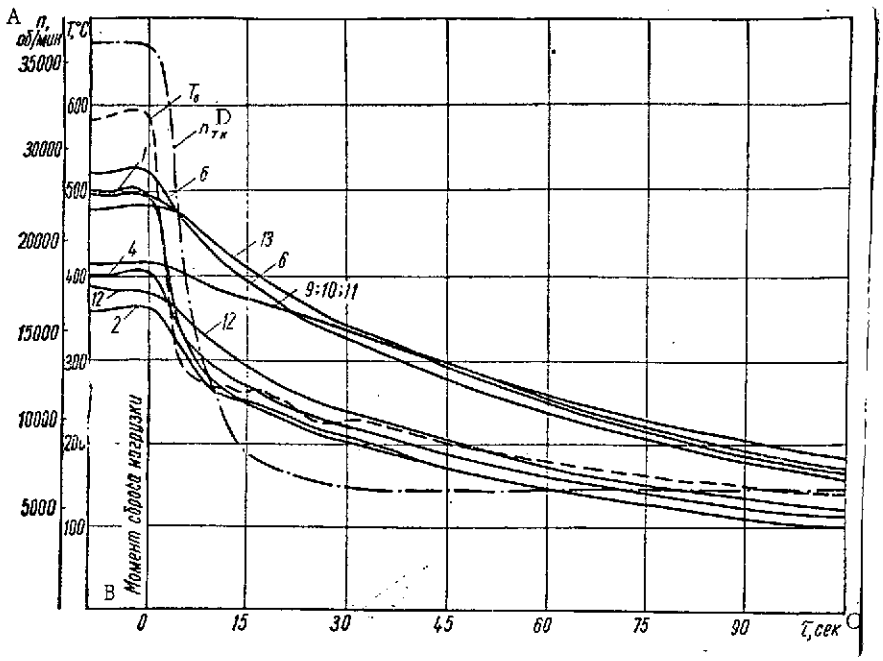


Fig. 37. Variation in temperatures at characteristic points of rotor of TKR-14-2b turbocompressor during relieving of loading from $N_{rat}$ = 184.5 kW to idling:
1. $\bar{r}$ = 1; 2. $\bar{r}$ = 0.98; 4. $\bar{r}$ = 0.85; 6. $\bar{r}$ = 0.71; 7. $\bar{r}$ = 0.60; 9. $\bar{r}$ = 0.43; 10. $\bar{r}$ = 0.33; 11. $\bar{r}$ = = 0.24 (1-11. Working side)
12. $\bar{r}$ = 0.85; 13. $\bar{r}$ = 0.60 (12-13. Back side)
Key: A. n, rpm
B. Instant of drop in load
C. sec
D. $n_{tc}$

When there is a sudden unloading, the nonsteady thermal process takes longer than in rapid loading, since with decrease in turbocompressor rpm the intensity of heat exchange between gas and rotor surface falls off. As follows from the data in Fig. 37, rotor temperatures reached steady values 4-5 min after unloading, while in the case of sudden loading the disk takes no longer than 1.5--2.0 min to heat up. The rpm of the turbocompressor rotor and the pressures $P_c$ and $P_{1g}$ become stabilized in 30 sec, not 5-10 /60 sec as in the case of sudden diesel loading.

During diesel unloading, the temperature drops along the rotor radius, in contrast to the loading regime, do not change their sign all the way up to the turbine rotor arriving at the steady thermal regime.

Axial temperature drops proved to be substantial for a very long time. The temperature drops at the points 12 and 4 on the back and working sides of the rotor (r = 60 mm) change sign 5 sec after unloading and reach 20-30 deg by 10-13 sec.

Results of experimental studies show that in centripetal turbines of turbocompressors the regimes of stopping and unloading are less thermally stressed than starting regimes.

## CHAPTER THREE

/61

# EFFECTIVENESS OF ROTOR COOLING SYSTEMS AND HEAT TRANSFER IN ROTOR ELEMENTS

## 1. Main Characteristics of Cooling Systems

In the earlier chapters we gave the main results of finding the effectiveness of rotor cooling systems experimentally in series-built turbocompressors. In this chapter we look at the performance of rotor cooling systems in centripetal turbines and give a comparative estimate of how effective each cooling system is. Experiments were run on a test stand with a combustion chamber; this allowed us to investigate rotor cooling systems under identical conditions.

TABLE 4

MAIN CHARACTERISTICS OF TURBOCOMPRESSOR TEST REGIMES

| Parameters | TKR-14-2a | TKR-23-1 |
|---|---|---|
| Initial gas temperature, °C | 500 | 500 |
| Mass flow of gas past turbine, kg/sec | 0.18-0.19 | 0.86-0.88 |
| Rotor revolutions per minute | 18,000 | 16,000 |
| Mass flow of oil to bearings, kg/sec | 0.04 | 0.065 |
| Mass flows of water to casing, kg/sec | 0.18 | 0.28 |

Radial blowoff of rotor back side with air is the simplest and so the most common way of cooling gas turbine rotors. It is used in particular in the turbocompressors TKR-14-2a and TKR-23-1.

The rotor cooling systems of these turbocompressors were experimentally studied over a wide range of cooling air mass flows at the same and at constant initial gas temperatures upstream of the turbine (Table 4).

Air was fed into the cooling line from an independent compressor unit through a control valve and a measuring diaphragm.

At the beginning experiments were run in which air was not delivered for rotor cooling. The temperature fields of the rotor obtained in this case were the starting values for comparing the different cooling methods. /62

Fig. 38 gives the temperature fields of uncooled and cooled rotors of the turbine in a TKR-14-2a turbocompressor[1]: the solid lines correspond to the temperature of rotor working side, while the dashed-dotted lines correspond to the temperature of rotor back side.

As the figure shows, the temperature field of the uncooled rotor is relatively uniform, and the overall rotor temperature level is 40-60 deg below the gas temperature in the blading. The decrease in the rotor temperature is accounted for by leakage of gas into the clearance between stator and rotor back side; here the gas gives off heat to the colder stator elements, by cooling the back side of the turbine rotor. In cooling systems of this type the pattern of gas flow in the relatively narrow clearance[2] between stator and back side of spinning rotor is strongly determined by the so-called pump effect.

As the disk spins, the fluid (gas) adjoining its working surface is ejected toward the periphery due to frictional forces, where an increased gas pressure zone forms. Correspondingly, close to the axis of rotation a zone of lower pressures builds up. The pressure drop thus produced causes the gas to flow along the immobile wall in the direction toward the rotor axis. Gas entering the clearance, on moving along the casing wall, is cooled and now at a lower temperature is sucked into the rotor surface along which it streams toward the peripheral part of the rotor.

---

[1] In the experimental installation the cavities of the TRK-14-2a casing and the oil block were joined by a pipeline and were hermetic. The pressure in this system was produced by the presence of the leakage of cooling air through the axial labyrinth and was regulated by a special valve on the oil block.

[2] In the TKR-14-2a the axial clearance between the rotor and the stator was 0.45-0.95 mm.

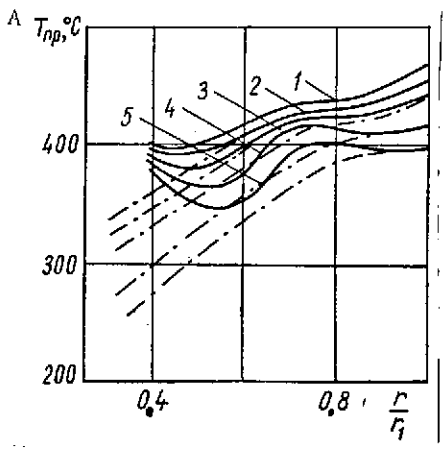


Fig. 38. Temperature fields of rotor of TKR-14-2a for radial blowoff and for various cooling air mass flows:
1. $g_{rad} = 0$, with gas leakage along radius of rotor back side
2. $g_{rad} = 0$, without leakage of gas along radius of rotor back side
3. $\bar{g}_{rad} = 0.44$ percent $G_{g.rat}$
4. $\bar{g}_{rad} = 0.9$ percent $G_{g.rat}$
5. $\bar{g}_{rad} = 1.4$ percent $G_{g.rat}$

Key: A. $T_{rd}$

If the mass flow of cooling air delivered to the clearance proves over this radius to be equal to the mass flow or else to exceed the flow caused by the pump effect of the spinning disk, the back (toward the axis of rotation) motion of the gas in the clearance halts and the entire clearance is filled with air moving toward the peripheral sections of the rotor [19, 38, 73, 79]. /63

An increase in the mass flow of air blowing off the rotor leads to a drop in air temperature level, but with this the nonuniformity of temperatures along rotor thickness and radius is caused to intensify. In this case it is virtually impossible to achieve a uniform rotor temperature field at suitable cooling air mass flows. The temperature drop along the rotor radius with increase in mass flows of cooling air becomes different for different rotor sections. Thus, over the rotor section in the $\bar{r} = 1.0$-$0.75$ interval, as the cooling air mass flow goes up from 0 to 1.2 percent $G_{g.rat}$, the temperature drop falls from 30 deg to zero, while over the rotor section in the interval $\bar{r} = 0.75$-$0.55$, it rises from 28 to 52 deg.

This pattern of change in the temperature field along rotor radius is caused by the combined action of radial blowoff of the rotor back side by air and the action of the air film leaking into the blading. The cooling effect of the air film on the rotor periphery at moderate air mass flows extends 8-12 mm along blading length.

It should be noted that for larger cooling air mass flows (of the order of 2.2-2.5 percent) a marked drop in the temperature of the gas flow at the outlet from the rotor is also evident, especially at the roots of the blades (Fig. 39). /64

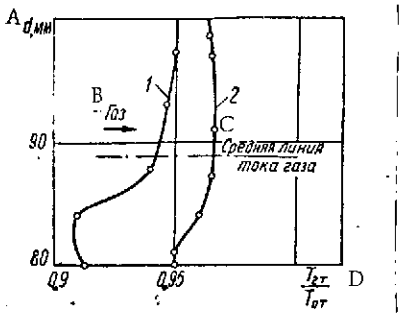


Fig. 39. Profile of gas temperature upstream of turbine rotor of TKR-14-2a turbocompressor when radial blowoff is used:

1. $\bar{g}_{i.a}$ = 0.0081 kg/sec
2. $\bar{g}_{i.a}$ = 0

Key: A. mm
B. Gas
C. Central line of gas flow
D. $T_{gt}/T_{0t}$ /gt = gas turbine; 0t = = inlet section of turbine/

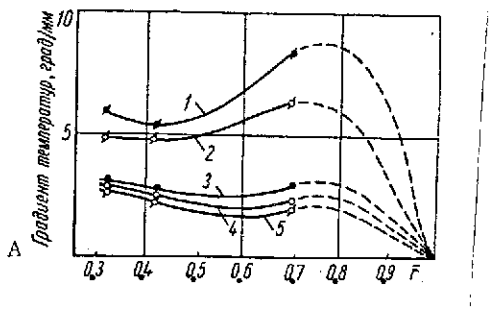


Fig. 40. Dependence of temperature gradients averaged over thickness of rotor of TKR-14-2a turbocompressor on mass flows of cooling air for radial blowoff:

1. Without delivery of cooling air and with gas leaking along rotor
2. Without delivery of cooling air and with absence of gas leaks along rotor
3. $\bar{g}_{i.a}$ = 0.97 percent $G_{g.rat}$
4. $\bar{g}_{i.a}$ = 1.62 percent $G_{g.rat}$
5. $\bar{g}_{i.a}$ = 2.5 percent $G_{g.rat}$

Key: A. Temperature gradient, deg/mm

Fig. 40 gives the axial temperature gradients measured in the rotor of the TKR-14-2a for different cooling air mass flows. The minimum temperature gradients, 1.7-2.0 deg/mm, occurred at the regime at which gas flowed in the axial clearance between casing and rotor. As the cooling air mass flow was raised to 1.1 percent $G_{g.rat}$, the minimum temperature gradients reached 6-8 deg/mm. The pattern of variation in the temperature gradients along the disk was such that the gradients reached their largest values over the rotor section $\bar{r}$ = 0.7-0.8, where the rotor thickness does not exceed 3-4 mm, and in addition, here also, on the back side of the disk, intensive heat rejection occurred. In passing to rotor /65 sections with greater disk thicknesses, there was a drop in the gradients and they remained nearly constant at $\bar{r}$ = 0.3-0.5.

[3] Here and in the following the mass flow of cooling air is presented with respect to the mass flow of gas in the rated regime.

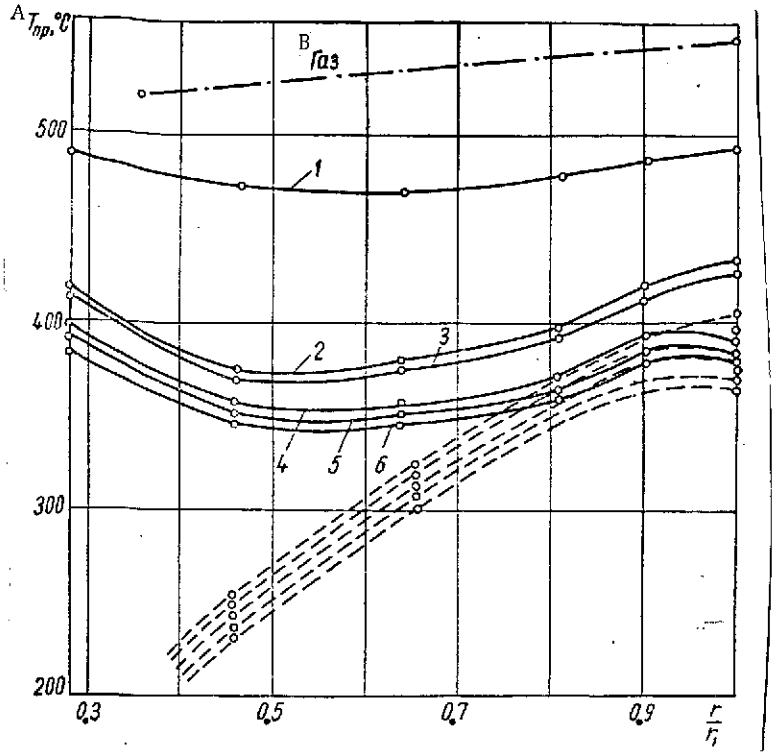


Fig. 41. Temperature fields of rotor TKR-23-1 turbocompressor for different cooling air mass flows:

1. $g_{i.a}$ = 0 kg/sec
2. $g_{i.a}$ = 0.013 kg/sec
3. $g_{i.a}$ = 0.014 kg/sec
4. $\bar{g}_{i.a}$ = 0.019 kg/sec
5. $g_{i.a}$ = 0.022 kg/sec
6. $g_{i.a}$ = 0.023 kg/sec

Key: A. $T_{rd}$
B. Gas

The temperatures of the rotor of a TKR-23-1 turbocompressor for different cooling air mass flows are shown in Fig. 41; the solid lines correspond to the working rotor side, and the dashed lines correspond to the back rotor side, while the dashed-dotted lines correspond to gas temperature. As in the TKR-14-2a turbocompressor, in the TKR-23-1 turbocompressor even without cooling air delivery heat is rejected from the disk (see Fig. 41, upper curve). When the cooling air delivery is 0.0105 kg/sec (0.78 percent $G_{g.rat}$), the disk temperature falls off most sharply (by 85-100 deg) at the sections $\bar{r}$ = 0.45-0.70. The region of highest disk temperatures at these mass flows shifts toward the disk periphery ($\bar{r}$ = 1.0) and toward the cooled rotor face on the exhaust side. As the mass flow of air is further intensified, this region shifts toward the axis of rotation ($\bar{r}$ = = 0.85-0.90), which, as in the case of TKR-14-2a, can be accounted for by the action of film cooling.

By comparing the curves of temperature distribution over the radius of the disks of the TKR-14-2a and TKR-23-1 turbocompressors, we can note that their similarity is retained over a fairly wide range of mass flows. Still, the temperature field of the rotor of the TKR-23-1 turbine is more uniform over the entire range of cooling air mass flows.

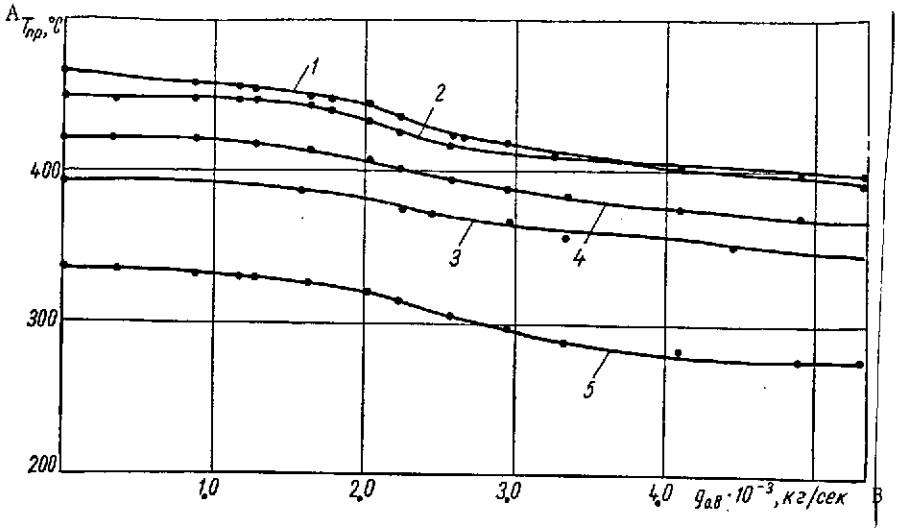


Fig. 42. Temperatures at characteristic points of rotor TKR-14-2a turbocompressor as function of cooling air mass flow in radial blowoff
1. $\bar{r} = 1$; 2. $\bar{r} = 0.90$; 3. $\bar{r} = 0.53$ (1-3. Working side of rotor); 4. $\bar{r} = 0.70$; 5. $\bar{r} = 0.40$ (4, 5. Back side of rotor).
Key: A. $T_{rd}$ /$\bar{r}$d = radius/
B. $g_{i.a} \cdot 10^{-3}$ kg/sec

These data permit estimating the lowest cooling air mass flow ensuring fairly high cooling efficiency. As follows from Figs. 42 and 43, the rate of the temperature drop over different intervals of mass flow values is the same. This is due to the suction into the clearance between the rotor and the casing of heated gas from the blading, typical for low cooling air mass flows. For both turbocompressors a weak drop in rotor temperature is observed in the 0-0.5 percent $G_{g.rat}$ range of cooling air mass flows. With further increase in the mass flow the metal temperature rises sharply. Curves of the rotor temperature as a function of cooling air mass flow above 0.5 percent $G_{g.rat}$ for the turbine are exponential and quite rapidly (already when $\bar{g}_{i.a}$ = 1.5 percent) approach a constant that characterizes the limiting capabilities of radial blowoff. So increasing the cooling air mass flow above 1.2-1.35 percent $G_{g.rat}$ through the turbine is not sensible and does not further lower rotor temperatures. /66

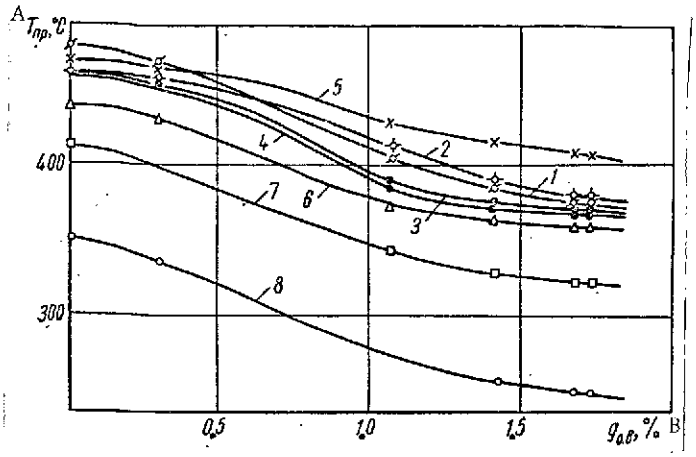


Fig. 43. Temperatures at characteristic points of rotor of TKR-23-1 turbocompressor as function of cooling air mass flows:
1. $\bar{r}$ = 0.98; 2. $\bar{r}$ = 0.81
3. $\bar{r}$ = 0.63; 4. $\bar{r}$ = 0.46
5. $\bar{r}$ = 0.29 (1-5. Working side of rotor)
6. $\bar{r}$ = 0.98; 7. $\bar{r}$ = 0.65
8. $\bar{r}$ = 0.46 (6-8. Back side of rotor)
Key: A. $T_{rd}$
B. $g_{i.a}$

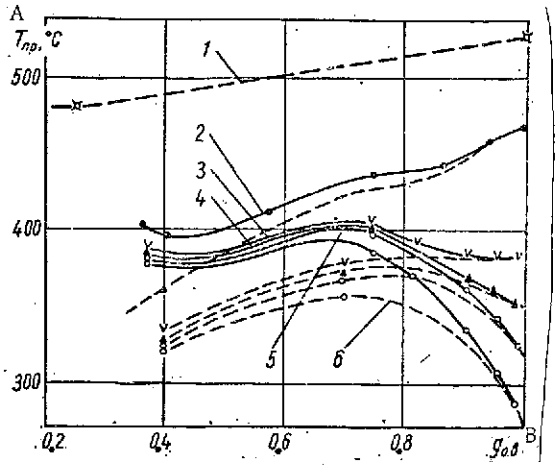


Fig. 44. Temperature fields of rotor of TKR-14-2a turbocompressor for film cooling:
1. Temperature of gas in rotor blading
2. $g_{i.a}$ = 0 (leakage of gas along rotor back side)
3. $g_{i.a}$ = 0.00186 kg/sec
4. $g_{i.a}$ = 0.00331 kg/sec
5. $g_{i.a}$ = 0.005 kg/sec
6. $g_{i.a}$ = 0.0084 kg/sec
Key: A. $T_{rd}$
B. $g_{i.a}$

Film cooling. The effectiveness of film cooling was studied on a reconstructed TKR-14-2a turbocompressor (see Chapter Two, Fig. 12). The test regime remained the same as for the investigation of radial blowoff. The experiments were conducted in three stages as to the number of thermalcouple connections to a ten-point current collector /slip ring/. The results are in Fig. 44; here the solid lines correspond to the working rotor surface temperature, and the dashed lines correspond to the temperature of the back side of the rotor. As expected, the greatest effect of film cooling is shown along the peripheral rotor sections. When the mass flows of cooling air were raised from 0 to 0.0084 kg/sec (0-2.22 percent $G_{g.rat}$) the rotor temperature at $\bar{r}$ = 1.0 /67 dropped from 470 to 289° C. The rate of the drop in rotor

temperatures slowed down sharply with increasing separation from the cooling air injection site. At $\bar{r} = 0.7$ the metal temperature for the same flow rates decreased from 430 to 395° C.

While a further rise in cooling air mass flows led to a relative drop in metal temperature at $\bar{r} = 1.0$-0.9, over the rotor sections with $\bar{r} = 0.6$ and less this decrease was slight. The film cooling system ensured a sharp drop in rotor temperature at relatively small flow rates. A further increase in cooling air flow rates did not lead to a marked drop in the temperatures of the turbine rotor metal. For instance, when the cooling air mass flow rate was up to 0.5 percent $G_{g.rat}$ at the turbine, the temperature of the peripheral part of the rotor dropped 100 deg, while a further rise in mass flow rates past 0.5 percent $G_{g.rat}$ lowered the rotor temperature within the limit of several degrees. The feature of the cooling system we are looking at is due to the fact that when cooling air was delivered into the clearance between the disk and the flange of the nozzle box even at relatively low mass flows there is a "cutting out" of the radial clearance, as a result of which gas cannot penetrate from the blading to the clearance. In this case the back side of the rotor is cooled with relatively cold air circulating in the clearance, which leads to a fairly uniform drop in the rotor metal temperature from the center to $\bar{r} = 0.78$-0.8. Over the rotor sections above $\bar{r} = 0.8$ cooling occurs because of the direct injection of air at the rotor working surface; here even small mass flows of air cause a perceptible lowering of metal temperature. Cooling of the rotor sections closer to the axis of rotation occurs mainly due to heat being rejected to the same air circulating in the clearance between the rotor back side and the stator; the amount of this air is virtually independent of total mass flow for cooling. So changes in the cooling air mass flow when film cooling is employed have a limited effect on the temperature of these rotor sections. The slight drop in the metal temperature observed in Fig. 43 over these rotor sections is due to the mixing of cold air into the stream of gas sweeping past the rotor surface. /68

A feature of the temperature field of the rotor when film cooling is present is the absence of a sharp drop in temperatures over the section $\bar{r} = 0.50$-0.65 that occurs during radial blowoff of the rotor. This evidently is linked to the slower heat removal in the area of the radial labyrinth seal. The temperature of the section $\bar{r} = 0.7$ was found to be the highest; when $g_{i.a}$ = 0-0.0084 kg/sec it fell only 40 deg. For moderate cooling air mass flows (0.5-0.6) percent $G_{g.rat}$, the rotor was found to be nearly evenly heated, and its mean temperature level was 335-400° C.

Rotor film cooling does not avoid large axial gradients. When cooling air is injected into the working duct the axial gradients rise and are 10-15 percent higher than the values under radial blowoff.

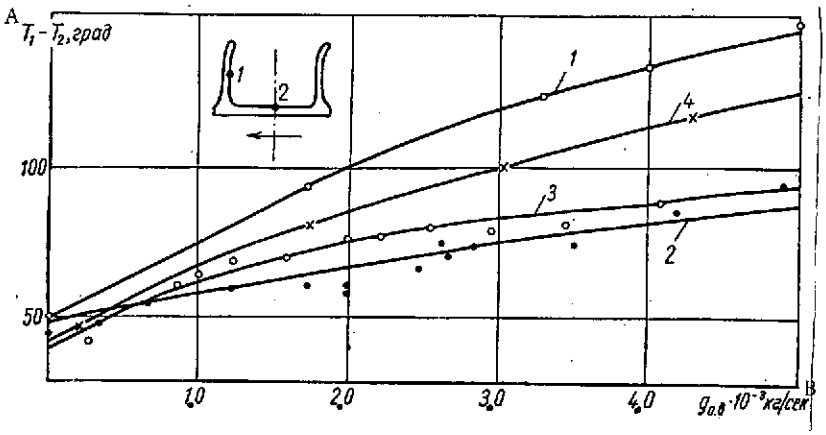


Fig. 45. Temperature drops between points 1 and 2 at the outer radius of rotor of TKR-14-2a turbocompressor for different cooling methods:
1. Film cooling
2. Film cooling together with radial blowoff (m = $= g_{rad}/G_{i.a} = 0.5$)
3. Radial blowoff together with shielded cooling
4. Radial blowoff

Key: A. $T_1-T_2$, deg B. $g_{i.a} \cdot 10^{-3}$ kg/sec

The presence of temperature drops over disk thickness for film cooling are caused to some degree by leakage of cooling air along the back side toward the rotor axis. Since the air will move from disk periphery to axial seal, its temperature at the peripheral sections proves to be less, in turn leading to larger temperature drops over rotor thickness. This is shown by the pattern of axial gradients along disk radii. Thus, the largest gradients show up at the section $\bar{r} = 0.6-0.75$ and, smoothly decreasing in the direction toward the center, reach 3.5-4 deg/mm. /69

The presence of cooling air mass flows above 0.54 percent $G_{g.rat}$, as stated, cause significant reverse radial temperature gradients to occur along the peripheral rotor sections (up to 3.5 deg/mm).

Fig. 45 (curve 1) shows the drop in temperatures of the metal between rotor and middle working ducting. As shown, with increase in air mass flows for cooling this drop also rises and can reach 150 deg when $\bar{g}_{i.a} = 2.7$ percent $G_{g.rat}$. In this respect film cooling is inferior to radial blowoff cooling, when for the same air mass flow this drop does not exceed 90-95 deg. Temperature drops in the root sections of the rotor blades in film cooling

experiments were not measured, however we can assume that they will be lower over the section $\bar{r}$ = 0.3-0.7 than for rotor radial blowoff, since the temperatures of rotor working surface when film cooling is used are 25-30 deg higher.

Overall, for the same mass flows of cooling air involving radial blowoff, film cooling (see Fig. 40) means a more uniform rotor temperature field at a somewhat higher (by 20-25° C) level in absolute temperatures.

Film cooling in conjunction with radial blowoff. Rotor cooling by radial blowoff gives the largest temperature drop at the sections $\bar{r}$ = 0.5-0.7. But film cooling makes it possible to considerably lower the temperatures of the peripheral rotor sections. Obviously, combining these cooling methods will mean a sharper drop in the overall temperature level of the rotor and achieve when necessary the uniform temperature field, or the temperature field desirable from strength considerations.

To check these hypotheses, we investigated the thermal state of the rotor of the TKR-14-2a turbocompressors swept by two air streams, one of which was delivered for radial blowoff of the disk back side, and the other was delivered as in film cooling (see Fig. 12). Both streams of cooling air mixed in the clearance between the nozzle box and the rotor rim and entered the rotor blading as a curtain.

The combined system of rotor air cooling of the turbocompressor was studied for different ratios of mass flows of air delivered for radial blowoff and for film cooling.

Fig. 46 shows the measurements of temperature fields of the rotor of the TKR-14-2a turbocompressor for two values of air mass /70
flow for radial blowoff and for five air mass flow values for film cooling.

As Fig. 46 shows, with combined cooling, rotor temperatures fall both because heat is removed from back side of rotor (dashed line), and because there is less heat removed from gas to rotor owing to the cooling air curtain on the rotor working surface (solid lines). Curves 1 in Fig. 46 characterize the rotor thermal state when there is a total absence of cooling air delivery. Here the gas enters the clearance between rotor and casing wall.

When cooling air is delivered along the disk blade in the amount of 0.00143 kg/sec (0.38 percent $G_{g.rat}$) and with minimum air mass flow for film cooling in amounts less than 0.15 percent $G_{g.rat}$, the rotor surface temperature falls from 470 to 430° C

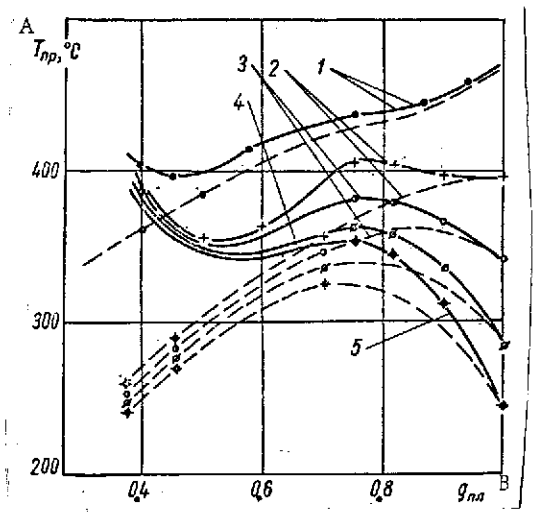


Fig. 46. Temperature fields of rotor of TKR-14-2a turbocompressor employing combined film cooling and radial blowoff
1. Without cooling
2. $\bar{g}_{fi}$ = 0.16 percent $G_{g.rat}$ /$\bar{f}i$ = film/
3. $\bar{g}_{fi}$ = 0.73 $G_{g.rat}$
4. $\bar{g}_{fi}$ = 1.3 percent $G_{g.rat}$
5. $\bar{g}_{fi}$ = 2.63 percent $G_{g.rat}$

Key: A. $T_{rd}$
B. $g_{fi}$

at the section $\bar{r}$ = 1.0. Over the section $\bar{r}$ = 0.7-0.85 the temperature drop is 35 deg. In this case the rotor temperature field corresponds to the field when rotor radial blowoff is used with low cooling air mass flows.

Raising the cooling air mass flow in film cooling sharply to $\bar{g}_{fi}$ = 0.73 percent $G_{g.rat}$ lowers the rotor rim temperature.

A further rise in air mass flow for injection results in the peripheral area temperature becoming 250° C while the initial gas temperature is 550° C. Axial temperature gradients appearing when mixed cooling is present intensify, as in the cases looked at earlier, with buildup in cooling air mass flows. Thus, when the ratios of mass flow cooling air sweeping the rotor back side to the total mass flow for cooling m = = 0-0.23, and for total mass flows of cooling air 0.38-1.7 percent $G_{g.rat}$, axial temperature gradients are 25-30 percent higher.

As Fig. 45 shows, the action of film cooling becomes strongly /71 evident over the section $\bar{r}$ = 1.0-0.75, while over the rest of the rotor its effect is slight.

Raising the cooling air mass flow for disk radial blowoff to 1.3 percent (see Fig. 46) results in an overall lowering of rotor temperatures and, besides, large temperature drops over the rotor section $\bar{r}$ = 0.5-0.65.

Rotor temperatures over the sections $\bar{r}$ = 0.5-0.38, both when the mass flow of air for radial blowoof $\bar{g}_{rad}$ = 0.38 percent as well as when $\bar{g}_{rad}$ = 1.3 percent, change by 10-12 deg with increase in mass flow of air for film cooling.

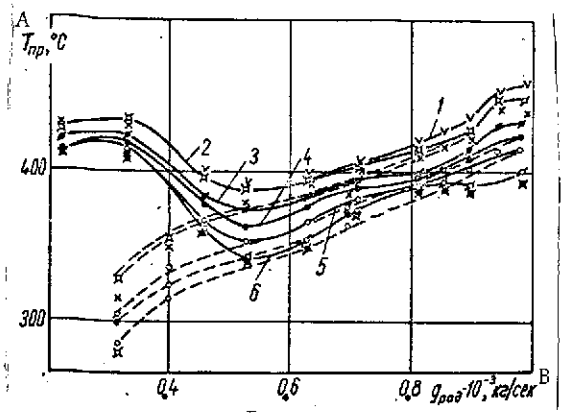


Fig. 47. Temperature field of rotor of TKR-14-2a turbocompressor when shielded cooling was combined with radial blowoff

1. $g_{rad} = 0$
2. $g_{rad} = 0.162 \cdot 10^{-3}$ kg/sec
3. $g_{rad} = 1.23 \cdot 10^{-3}$ kg/sec
4. $g_{rad} = 2.01 \cdot 10^{-3}$ kg/sec
5. $g_{rad} = 2.495 \cdot 10^{-3}$ kg/sec
6. $g_{rad} = 3.57 \cdot 10^{-3}$ kg/sec

Key: A. $T_{rd}$
B. $g_{rad} \cdot 10^{-3}$, kg.sec

The trend of the shape of the temperature curves of the rotor for different ratios of air mass flow through cooling lines allows us to state that fundamentally when combined cooling is used we can get virtually any temperature field. In particular, when the total air mass flow for radial blowoff and film cooling is of the order of 1.2-1.3 percent $G_{g.rat}$ and $m = 0.3$, the rotor temperature field will be near-uniform. Overall, combined cooling is quite effective when $m = 0.3$-$0.6$ and when total cooling air mass flows are 1.1-1.2 percent $G_{g.rat}$ through the turbine. In this case the total rotor temperature level will be 60-70 deg below the level of the uncooled rotor.

Radial blowoff together with shielded cooling. Water cooling of stator is used in some turbocompressors (for example, the TKR-14-2a). Water fed into the turbine casing from the diesel cooling system cools the casing wall, alongside which stands the rotor. The direct proximity of the cold casing wall has a marked effect on the rotor temperature field by removing heat from the cooling air in the clearance, as well as with small cooling air outflows because of heat being removed from the gases arriving from the blading in the clearance. Thus, the water-cooled casing wall acts as a water shield.

Special experiments were performed to estimate how effective shielded cooling of the rotor is in the TKR-14-2a turbocompressor in which rotor radial blowoff with air is provided. The turbine operating regime remained the same. /72

The mass flows of water and air for the cooling system in the experiments were varied broadly: from 0 to 1.13 percent $G_{g.rat}$ for cooling air, and from 0 to 0.2 kg/sec for water.

In these experiments an SK-13 twenty-point current collector was used; with it, the emf values of 19 thermocouples positioned on the rotor were transmitted to fixed instruments. Fig. 47 shows the rotor temperatures with constant mass flow of air through the stator part ($G_{i.a} = 5.32 \cdot 10^{-2}$ kg/sec) and several cooling air mass flows. Comparing these data with curve 1 in Fig. 46 corresponding to the regime without cooling air mass flow allows us to conclude that when water is delivered into the casing the maximum rotor temperature along the disk periphery is not above 460° C; this is 68 deg lower than the gas temperature upstream of the rotor. In contrast to the earlier-considered temperature distributions obtained for the rotor of the TKR-14-2a turbocompressor cooled by radial blowoff, over the working surface sections $\bar{r}$ = = 0.50-0.70 the zone of the lowest temperatures was found to be broader (solid lines). This doubtless stems from the shielded cooling effect.

When the cooling air mass flow for radial blowoff of the rotor was built up, the pattern of temperature distribution remained the same, but the absolute values of the metal temperatures along the rotor radius fell in proportion to the increase in the mass flows of cooling air. As Fig. 47 shows, the largest drop in temperatures relative to gas temperature was achieved over the rotor section $\bar{r}$ = 0.5-0.6 and is 50 deg in the interval of cooling air mass flow values 0-1.13 percent $G_{g.rat}$.

When the largest cooling air mass flow $g_{i.a}$ = 1.13 percent $G_{g.rat}$, the pattern of the temperature field is somewhat different: the rotor sections $\bar{r}$ = 1.0-0.85 are nearly uniformly heated; this can point to an air curtain forming in the rotor ducting.

The largest radial drops occurred over the section $\bar{r}$ = 0.5-1.0 and are 75 deg when $g_{i.a} = 0$, and 50 deg when $g_{i.a}$ = 1.13 percent.

The temperature of the rotor back side (dashed lines), as Fig. 47 shows, decreases smoothly from periphery to center; a sharp drop is observed over the interval $\bar{r}$ = 0.42-0.32. The temperature drop over this section is caused by heat being removed into the oil-cooled bearing.

Of special interest are data on the distribution of temperatures over rotor periphery and at the sites of blade insertion into disk (Fig. 48).

The drop in blade temperatures was 25-30 deg when the air mass flow was raised from 0.86 to 1.11 percent, and the decrease in rotor temperatures in the middle of the interblade channel was 35-40 deg. The point b temperatures were lower than in the middle of the channel, by 20-25 deg, but 70-75 deg lower than at point a /73

located on the blade. Thus, the temperature drop along the vertical extent of the blade at the disk face and over the section r = = 1.0 was much lower than in other disk sections.

When the effect of the water mass flow through the turbocompressor casing on the rotor temperature field was steadied, a series of experiments with constant mass air flow for radial blowoff and variable water mass flow was conducted. The experiments were performed for two cooling air mass flows -- minimum (0.16 percent $G_{g.rat}$) and maximum caused by the capacity of the cooling line (2.2 percent $G_{g.rat}$).

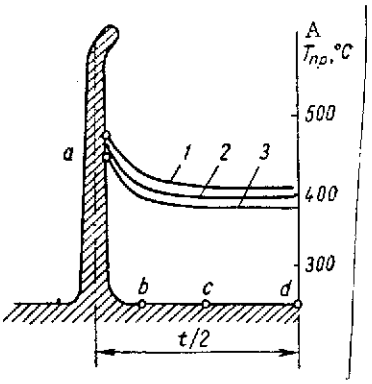


Fig. 48. Variations in temperatures of rotor blades in TKR-14-2a turbocompressor for different mass flows of cooling air delivered for radial blowoff:
1. $\bar{g}_{rad}$ = 0.864 percent $G_{g.rat}$
2. $\bar{g}_{rad}$ = 1.0 percent $G_{g.rat}$
3. $\bar{g}_{rad}$ = 1.11 percent $G_{g.rat}$
Key: A. $T_{rd}$

The temperatures of the characteristic points of the working and back rotor surfaces, with constant cooling air mass flow $\bar{g}_{i.a}$ = 0.16 percent and water mass flows from 0.0216 to 0.155 kg/sec, are shown in Fig. 49.

With an increase in water mass flows through the turbocompressor crankcase, there was a 20-25 deg temperature drop that was nearly the same for all sections; the drop was due to the lowering of the cooling air temperature owing to removal of heat into the "shield".

The level of temperatures and the uniform decrease over all rotor sections when the water mass flows were increased suggested the conclusion that for moderate mass flows of cooling air of 0.21-0.57 percent and water mass flows above 0.15 kg/sec, the same cooling effect can be achieved as for mass flows of air in radial blowoff $\bar{g}_{i.a}$ = 0.98--1.24 percent and water mass flows $G_w$ = 0.0216 kg/sec.

As these experimental data show, radial blowoff of the rotor with air together with water cooling of the stator raise large temperature drops over rotor thickness. The maximum temperature gradients correspond to large mass flows of cooling air for the same mass flows of water through the casing. For example, when the mass flow of cooling air $g_{i.a}$ = 0.672 percent $G_{g.rat}$ and

water mass flow 0.0532 kg/sec at $\bar{r}$ = 0.8, the temperature drop is 6 deg/mm. Over the rotor sections with $\bar{r}$ = 0.6 the temperature gradient is at a minimum, roughly 1.5-2 deg/mm, however its value again rises to 5.5 deg/mm at the rotor face ($\bar{r}$ = 0.3). /74

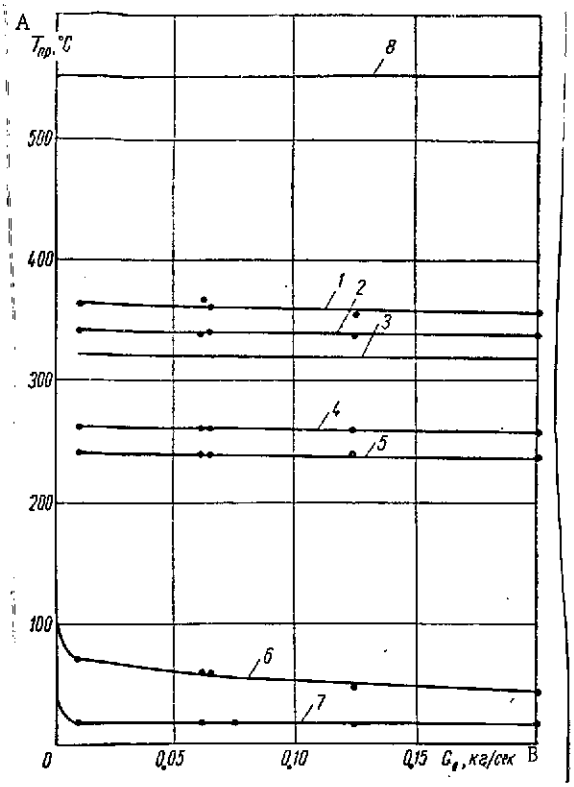


Fig. 49. Temperatures at characteristic points of rotor of TKR-14-2a turbocompressor as function of water mass flow for casing cooling:
1. $\bar{r}$ = 1.00
2. $\bar{r}$ = 0.742
3. $\bar{r}$ = 0.525
(1-3. Temperature of rotor working side)
4. $\bar{r}$ = 0.40
5. $\bar{r}$ = 0.325
(4,5. Temperature of rotor back side)
6. Temperature of casing wall facing rotor
7. Water temperature
8. Gas temperature
Key: A. $T_{rd}$
B. $G_w$, kg/sec

## 2. Estimating Effectiveness of Air-Cooling Methods Examined

As stated earlier, these characteristics can serve in quantitatively estimating how effective a given cooling method is:

a) overall temperature level of rotor metal;

b) temperature gradients in disk and rotor blades;

c) mass flow of cooling air; and

d) power losses due to use of cooling.

Comparison of these systems and cooling methods is usually conducted in the same turbocompressor operating regime.

Let us set up the approximate dependence of turbine power losses in a turbocompressor on the use of cooling[4].

The available power of the cooled turbocompressor turbine is

$$N = (G_g - g_{i.a} - g_{se}) \left( L_0 - \frac{\Sigma Q_{los}}{G_g} \right). \quad \text{(III.1)}$$

[4] /Footnote appears on following page./

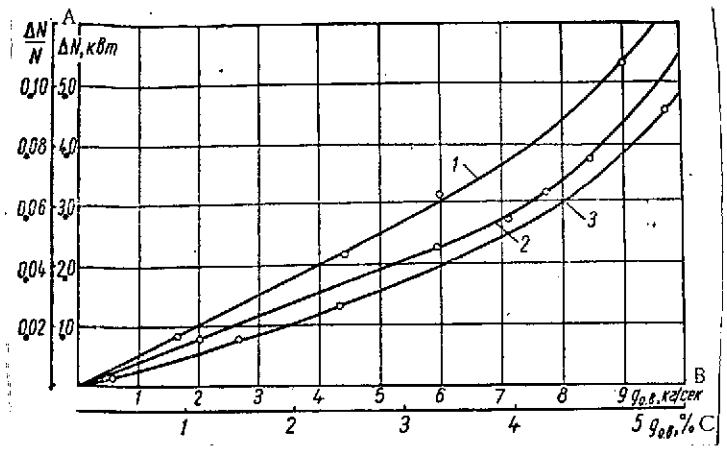


Fig. 50. Power losses of turbine due to rotor cooling being used:
1. Film cooling
2. Film cooling together with radial blowoff
3. Radial blowoff together with shielded cooling

Key: A. $\Delta N$, kW
B. $g_{i.a}$, kg/sec
C. $g_{i.a}$

relative drop in cooled turbine power:

$$\frac{\Delta N}{N_{rat}} = \frac{g_{ia} - g_{se}}{G_g}\left(1 + \frac{L'_{i.a}}{L_0}\right), \qquad \text{(III.3)}$$

where

$$L'_{i.a} = C_p(T_1 - T_{i.a}).$$

The dependence of relative power loss on mass air flow in disk cooling is shown in Fig. 50. Obviously, for uncooled turbines power losses in cooling are absent, but the temperatures of the /76

Here $\Sigma Q_{los}$ = losses associated with cooling /los = losses/,

$$\Sigma Q_{los} = Q_{sh} + Q_{inj}$$

/sh = shield; inj = injection/,

where $Q_{sh}$ = heat rejected from rotor to shield;

$$\frac{Q_{inj}}{G_g} = \frac{g_{ia} - g_{se}}{G_g} C_p(T_1 - T_{i.a}). \qquad \text{(III.2)}$$

Assuming the heat removed by air from the water to be returned to the gas and setting $C_p$ = = const, and also $Q_{sh} \ll Q_{inj}$, we get the

---

[4] In contrast to autonomous GTE, in turbocompressors power losses appearing with the introduction of cooling cannot be compensated by boosting gas temperature at turbine inlet.

uncooled rotor metal are much higher than the temperatures of the cooled rotor, and thus the strength characteristics of uncooled rotors are lower than for cooled rotors.(under otherwise equal conditions).

Let us first look at what effect different cooling methods (for the same cooling air mass flows) have on the thermal state of the rotor in a centripetal turbine, and then let us compare the thermal states of cooled and uncooled rotors as to the overall temperature level and maximum temperature drops.

Using radial blowoff of a disk with cooling air mass flow up to 1.25 percent $G_{g.rat}$ at the turbine on the average means a 110-120 deg drop in the rotor temperature level compared with an uncooled rotor. The maximum temperature drop, 80 deg, occurs between the rotor blade and the disk (see Fig. 45). Power losses in the turbine due to cooling for this mass flow of air for cooling are 1.8 percent (see Fig. 50).

But for the same cooling air mass flows and with film cooling, the power losses remain virtually the same, but the biggest temperature drops between the rotor blade and disk amount to 120-125 deg.

The mean temperature level of the rotor when film cooling is used turns out to be 20-25 deg higher compared to the temperature level of the rotor when radial blowoff is employed. Still, the temperature field of the rotor overall under film cooling is more uniform than under radial blowoff.

Combined cooling under the same overall air mass flows and m = 0.345 produces temperature drops between disk and blade of 115 deg, while the power losses here are 1.9 percent. The radial gradients in combined cooling are markedly reduced.

With combined cooling one can select the ratio of the mass flows of cooling air for radial blowoff and for film cooling such that the temperature flow of the rotor will be near-uniform. The total mass flow of air for cooling in this case can be kept equal to the mass flow for radial blowoff or purely film cooling.

If the total air mass flow for cooling is 1.25 percent $G_{g.rat}$ and $g_{fi}/g_{i.a}$ = 0.3-0.6, the temperature field of the rotor will be near-uniform, while the mean temperature level of the rotor will be 60-70 deg below that for the uncooled rotor (see Fig. 46).

The data from analysis allow us to state that using any one of the above-examined disk cooling systems much improves disk thermal and stressed states. The optimal cooling method and its /77

operating regime (air mass flow and parameters) can be selected only after a detailed analysis of the operating conditions of the cooling system throughout the range of the regimes that are practicable. In the first approximation, based on the temperature level and temperature gradients, it can be assumed that under otherwise equal conditions combined cooling will be most effective: a combination of film cooling with radial blowoff. From this same point of view jet-radial blowoff of the back side of the rotor in conjunction with film cooling is most promising. Jet blowoff of the back rotor side (with several blowoff zones) is intermediate between both of these combination variants.

## 3. Heat Transfer in Cooling System Elements

When calculating any rotor cooling system of a centripetal turbine, one must have data on the intense heat transfer at its surfaces.

The results of the experimental investigations of various cooling systems, given in earlier chapters, also permitted finding the heat transfer coefficients in the turbine rotor blading. Comparing these experimental data with the results of theoretical and experimental studies of other authors made it possible to weigh how suitable the functions they recommend are for calculating heat transfer processes in cooling systems, and in several cases also to revise them.

Earlier we noted that in any rotor cooling system of centripetal turbines heat is removed from the rotor back side. Therefore to calculate cooling systems we also have to have data on the heat transfer regularities both at this rotor surface as well as on the "shield" side, that is, at the fixed casing wall.

Highly involved circulatory currents of gas and air arise in the clearance between the rotor and the stator during turbocompressor running; their flow rates are amenable to direct measurement with great difficulty. Therefore calculating heat transfer in a clearance involves a number of difficulties.

Numerous experimental studies (a review of them is given, for example, in /197) showed that a number of boundary layers form in the clearance at wall and disk surfaces, and the flow core between them rotates with some angular velocity that in the general case varies along the radius. In the event of forced air (gas) delivery into the clearance between the disk and the wall, the flow core can be shifted toward the disk (as air is delivered toward the axis of rotation) or toward the fixed wall (when air is delivered toward the periphery of the clearance).

If the angular velocity of the disk is constant, the position of the flow core is determined by the ratio of the mass flows of delivered air and air bled by means of the so-called "pump effect" /78 (Fig. 51). If the flow of delivered air is directed from the axis of rotation and its flow rate is equal to or larger than the amount of air bled by the disk, air from the blading will not be delivered into the clearance. If it turns out that the mass flow of delivered air is less than the mass flow due to the pump effect, then along the fixed wall gas (air) from cavities adjoining the disk periphery will be sucked into the clearance.

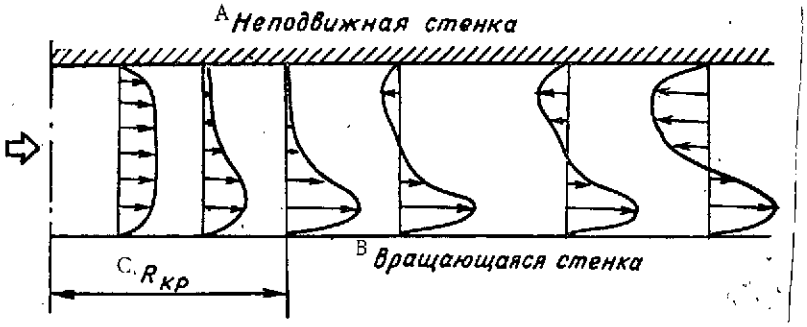


Fig. 51. Profiles of radial velocity components of gas in clearance between rotor back side and fixed wall
Key: A. Fixed wall
B. Rotating wall
C.. $R_{ed}$ /ed = edge/

Numerous theoretical and experimental studies have examined the heat transfer rate in these conditions /19, 38, 90, 115/. The results are presented as criterial equations, which describe with a given degree of reliability the effect of parameters on heat transfer regularities in the clearance between gas and rotating rotor. Results of experimental studies of the cooling systems of centripetal turbines for tests in stand conditions and directly in a diesel show that calculating heat transfer coefficients in the clearance between rotor and stator for turbocompressors of the types investigated is best conducted with functions given in Chapter Four.

Even more involved is the heat transfer process in the rotor blading. Here the heat transfer between gas and rotor working surface occurs in a curved duct when pressure gradients and a field of centrifugal force is directed opposite the motion of the gas flow are present.

Owing to the large number and indeterminacy of the parameters influencing heat transfer in the rotor blading of a centripetal

turbine, in the first theoretical investigations of the cooling systems, the heat transfer coefficients at the surface were determined from criterial equations describing heat transfer in the simplest cases (tubing and plate).

Thus, in the reference [106] local coefficients of heat transfer from gas to disk are found by the equation for longitudinal flow past a plane surface /79

$$\mathrm{Nu}_x = 0{,}0289\,\mathrm{Re}_x^{0.8}\,\mathrm{Pr}^{1/3}, \qquad \text{(III.4)}$$

where $x = r_1 - r$ is the distance from the leading edge along the rotor.

Heat brought to the disk by thermal conductivity along the blade tips in this case is taken into account according to the equation

$$\frac{\mathrm{Bi}_g^*}{\mathrm{Bi}} = 1 + \frac{\delta}{t}\left(\sqrt{\frac{2r}{\delta}}\cdot\frac{1}{\mathrm{Bi}_g} - 1\right). \qquad \text{(III.5)}$$

In [44, 45] the heat transfer coefficients averaged over the disk section, from the gas side, are calculated by the equation[5]

$$\mathrm{Nu} = 0{,}023\,\mathrm{Re}^{0.8}\mathrm{Pr}^{0.4}, \qquad \text{(III.6)}$$

where the Reynolds number is calculated from the mean relative gas flow in the ducting.

Heat brought to the disk by thermal conductivity along the tips of the rotor blades is taken into account in [44, 45] by means of the so-called conditional heat transfer coefficient; it is calculated by the formula

$$\mathrm{con} = \frac{\sqrt{\alpha f_1 B\lambda}\,\mathrm{th}\left(l\sqrt{\frac{\alpha B}{f\lambda}}\right) + \alpha_2 f_2}{f_1 + f_2}, \qquad \text{(III.7)}$$

[con = conditional]

[5] Eq. (III.6) characterizes heat transfer over the section of the stabilized flow, that is, the section more than 40-50 diameters from the inlet.

where $f_1$, B, and $\ell$ stand for the area and perimeter of root section, and the height of the blade at this section; $f_2$ is the area of the interblade disk surface.

Based on a solution of the momentum equation for a turbulent boundary layer in [5], with subsequent application of Reynolds analogy, a function was obtained for determining local coefficients of heat transfer between gas and rotor working surface:

$$\frac{Nu_x}{Re_x} = 0{,}0256\left(\frac{w}{w_1}\right)^{0.583}\left[\frac{w_1}{\nu}\int_{x_1}^{x}\left(\frac{w}{w_1}\right)^{3.94}dx\right]^{-0.2}. \qquad \text{(III.8)}$$

Removal of heat along blade tip to disk was allowed for by converting to the conditional heat transfer coefficient

$$\alpha_{con} = \alpha\left(1 - \frac{h}{t}\right) + \sqrt{\frac{2\alpha\lambda}{h}}\cdot\frac{h'}{t}. \qquad \text{(III.9)}$$

The necessity of allowing for specific heat transfer conditions in rotor bladings of centripetal turbines is the reason for arranging a number of special experimental studies.

In [5], heat transfer coefficients were determined in a model of the ducting of a centripetal gas turbine rotor. The experimental stand consisted of a fixed sector (one ducting) of a rotor along which gas flowed from the combustion chamber. The part of the rotor studied was cooled with water on the back side. Ahead of the inlet into the ducting was placed a cascade of rods, producing nonuniformity of velocity field at the inlet, to some extent simulating the action of axial eddy. /80

The distribution of velocities at the inlet into the ducting was provided in accordance with the condition $w_{ci} = -\omega t$.

Results of experimental studies shown in Fig. 52 and in [5] are generalized by the criterial equation

$$\overline{Nu} = 0{,}256\,Re^{0.63}\left(\frac{T_g}{T_d}\right)^{-1.2}\bar{w}^{0.92}, \qquad \text{(III.10)}$$

where $\bar{w} = (w_{av} + w_{ci})/w_{av}$ is the dimensionless velocity characterizing the effect on heat transfer of secondary flows in the interblade channel.

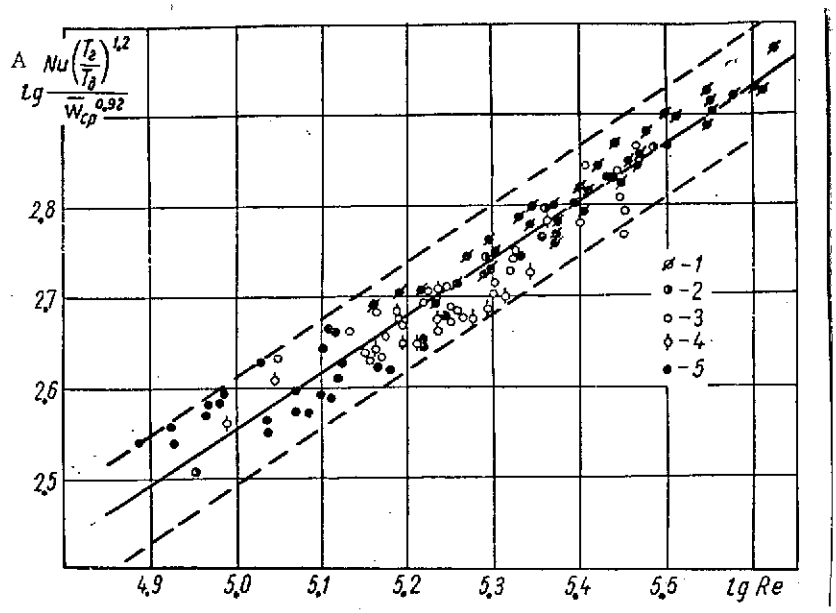


Fig. 52. Heat exchange in ducting of rotor of centripetal turbine [5]:
1. $\bar{w}_{av} = 1.0$; 2. $\bar{w}_{av} = 1.1$; 3. $\bar{w}_{av} = 1.2$;
4. $\bar{w}_{av} = 1.3$; 5. $\bar{w}_{av} = 1.4$; $\bar{w}_{av}$ is the relative gas flow rate in ducting
Key: A. $\lg [\bar{N}u(T_g/T_d)^{1.2}/\bar{w}_{av}^{0.92}]$

The equation is valid for the following ranges of the determining quantities appearing in it:

$$1 \cdot 10^5 \leqslant Re \leqslant 8 \cdot 10^5; \quad 1.1 \leqslant \bar{w} \leqslant 1.5; \quad 1.0 \leqslant \left| \frac{T_g}{T_d} \right| \leqslant 1.8.$$

It is shown in [5] that in the M number range 0.17-0.36 gas compressibility does not affect the intensity of heat transfer on the rotor heating side.

Eq. (III.10) allows for the rotor shape, however it does not altogether reflect the influence of centrifugal forces; their effect is disclosed in more than just the appearance of axial eddy [4], [6]. /81

Investigation of heat transfer in the rotor blading of high-speed centripetal turbines or on their rotating models that makes it possible to take into account all the specific features of the processes occurring in this case is an extremely involved technical problem.

In studies [56, 57], heat transfer was investigated between a flat spinning rotor, heated by a radiation furnace, where the rotor was made of a metal with good thermal conductivity, and air entering the clearance between the rotor and a fixed deflector via a felt belt spinning along with the rotor and producing total swirling of the flow along the peripheral sections. The installation also made it possible to investigate the film cooling of the disk, for which air at a different temperature was injected between the spinning disk and the air stream. In these same studies a function was obtained for determining the heat transfer coefficients averaged over the rotor when gas flowed toward the center without the injection of secondary air:

$$\mathrm{St}_1 \mathrm{Pr}^{0.4} \mathrm{Re}^{0.2} = \int_0^1 [\mathrm{St}_i \mathrm{Pr}^{0.4} \mathrm{Re}^{0.2}]\, d(\bar{r}^2). \qquad \text{(III.11)}$$

Results of calculation based on Eq. (III.11) agree quite closely with experimental data from the unit described. The following approximate criterial equation is recommended for practical use also in estimating changes in heat transfer when secondary air is injected, in [56, 57]:

$$\mathrm{St}_1 \mathrm{Re}^{0.65} = 66.0 + 30.0 \frac{\mathrm{Re}_\omega}{\mathrm{Re}}. \qquad \text{(III.12)}$$

Eq. (III.12) is obtained in experiments conducted over the ranges

$$2 \cdot 10^5 \leqslant \mathrm{Re} \leqslant 6 \cdot 10^5; \quad 0.3 \leqslant \frac{\mathrm{Re}_\omega}{\mathrm{Re}} \leqslant 1.3.$$

In contrast to studies of similar orientation [96, 117] in which the effect of injection when film cooling was used was estimated by the changes in the adiabatic temperature of the surface being projected, and where the coefficients of heat transfer to this surface with and without injection are usually assumed to be practically speaking unchanged, in [56, 57] the effective injection is taken into account by the complex

$$\Phi = \frac{\mathrm{St}_1 \mathrm{Re}^{0.65}}{(\mathrm{St}_1 \mathrm{Re}^{0.65})_{\theta^*=0}}, \qquad \text{(III.13)}$$

where $\theta^* = (T_{i.a} - T_1)/(T_d - T_1)$.

The complex $\Phi$ is the ratio of the mean heat transfer coefficient at the protected surface with and without injection for the same basic flow parameters. The empirical equation

$$\Phi = 1{,}0 - 7{,}70 G^{*0{,}6} \left(\frac{S}{r_0}\right)^{0{,}7}, \qquad \text{(III.14)}$$

is recommended for determining the complex $\Phi$ in [56, 57], where G* is the ratio of the mass flow rates of injected and main flow; $S/r_0$ is the relative inlet width.

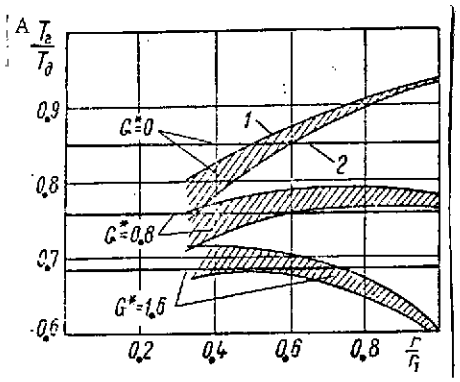


Fig. 53. Temperature fields when film cooling of rotor of centripetal gas turbine is used [56, 57]:
1. Temperature field in full-scale conditions
2. Temperature fields in model conditions

G* is air mass flow for cooling in percentages of gas mass flow into turbine

Key: A. $T_g/T_d$

Eq. (III.14) is valid for the following intervals of the determining quantities:

$$\begin{aligned} 10^5 \leqslant \mathrm{Re} \leqslant 10^6; \\ 10^5 \leqslant \mathrm{Re}_\omega \leqslant 10^6; \\ 0{,}2 \leqslant \frac{\mathrm{Re}_\omega}{\mathrm{Re}} \leqslant 1{,}0. \end{aligned}$$

Comparison of the results of calculations based on Eqs. (III.13) and (III.14) with the temperatures measured for a full-scale GTE (film cooling was used for the disk of this GTE) is shown in Fig. 53.

In [81], the effect of several design factors (reaction, relative length of interblade channel of rotor, angle of flow entry into rotor, and so on) on heat transfer from gas was investigated. The experiments were conducted in a full-scale turbine with rotating nozzle blades and hydraulic brake. This permitted observing kinematic similarity at low rpm. The study made use of the method of regular thermal regime using built-in $\alpha$-calorimeters. At constant rpm the gas temperature was varied discontinuously; the change in the temperatures of sensor (cylindrical copper insert) and gas were recorded; and the remaining turbine parameters directly or indirectly characterizing heat transfer were also measured.

To develop a measurement technique as well as to estimate the accuracy of determining heat transfer coefficients using $\alpha$-calorimeters, first control experiments on heat transfer of a

longitudinally-swept plate were conducted, that is, the body for which heat transfer at its surfaces is well known. The root-mean square relative error of finding the heat transfer coefficients using sensors 1.5-4.0 mm thick, determined by these experiments, were in the range ± 6-7 percent.

The relative errors in determining the Reynolds number, Nusselt number, and the angles of attack β are ± 1.4, 7.0, and 2.0 percent, respectively.

The following empirical equations were derived for heat transfer at the interblade surface of the disk, in /81/: /83

$$\mathrm{Nu} = \left(0{,}1 + \frac{1}{6{,}63\omega^2 - 8{,}42\omega + 27}\right) \mathrm{Re}^{0{,}65} \qquad \text{(III.15)}$$

or

$$\frac{\mathrm{Nu}}{\mathrm{Nu}_{\mathrm{N}}} = 0{,}73 + \frac{1}{0{,}907\omega^2 - 1{,}155\omega + 3{,}7}. \qquad \text{(III.16)}$$

The Nu and Re numbers were calculated over the length of the midline of the interblade disk surface.

Similar equations were derived in /81/ for heat transfer between gas and rotor blades:

$$\mathrm{Nu} = [0{,}137 - 0{,}0095\omega^{2{,}8} \exp(-0{,}67\omega)]\, \mathrm{Re}^{0{,}677 - 0{,}027 \exp(-1{,}64\omega)} \qquad \text{(III.17)}$$

or

$$\frac{\mathrm{Nu}}{\mathrm{Nu}_{\mathrm{N}}} = [1 - 0{,}0693\omega^{2{,}8} \exp(-0{,}67\omega)]\, \mathrm{Re}^{0{,}027[1 - \exp(1 - 1{,}64\omega)]}. \qquad \text{(III.18)}$$

Here and above $\mathrm{Nu}_{\mathrm{N}}$ is the Nusselt number obtained in the experiments on a fixed disk and defined by the equation

$$\mathrm{Nu}_{\mathrm{N}} = 0{,}137\, \mathrm{Re}^{0{,}65}. \qquad \text{(III.18a)}$$

Also presented in /81/ are graphical functions for determining the corrections that allow for the effect of angles of attack on the heat transfer to rotor blades. In the region of positive angle of attack heat transfer intensity rises, while for small negative and zero angles of attack the rate of heat transfer proves to be at a minimum and somewhat rises with increase in the negative angles.

In studying heat transfer in gas turbine blading, use can be made of the results of solving the inverse boundary value problems [17, 20, 30, 39, 44, 99] (in this case the thermal conductivity equations for the rotor). Here the problem boils down to finding the boundary conditions at the limits of the region (rotor) from the solution known for it, that is, the temperature field. The advantage of this method of determining heat transfer coefficients is that when use was made of the results of thermometry of the full-scale turbine rotor, allowance can be given to the features of virtually all processes influencing heat transfer.

In the ITTF AN UkSSR the results of solving the inverse thermal conductivity problem were applied in finding the heat transfer coefficients in the rotor blading of a centripetal turbine.

The problem was solved with EI-12 and MSM-I network integrators for the rotor of the centripetal turbine of a TKR-14-2a turbocompressor. Rotor and gas temperatures measured in the experiments served as the starting data.

All the calculations were made on two-dimensional electrical models, so the heat transfer values obtained in the ducting correspond to the so-called conditional heat transfer coefficients (Eqs. (III.7) and (III.9)). As shown by the temperature fields in the peripheral rotor sections given in Fig. 62, the errors associated with replacement of the bulk electrical model by a plane model are [84] 2.4-2.6 percent for the peripheral rotor sections and 2.0-2.2 percent for the rest. The same error values are indicated also in [44].

In determining the heat transfer coefficients averaged over the ducting for the plane electrical model, the values of the incremental resistances constant over the ducting length and modeling thermal resistance was found; these additional resistances for given gas temperatures made it possible to obtain the disk temperatures differing from the temperatures measured in the experiments by no more than $\pm$ 5 percent.

When the local heat transfer coefficients were determined with the electrical model, the values of the incremental resistances corresponding to it were determined at five-six points of the rotor working surface. In this case, total correspondence of model and full-scale temperatures was achieved by selection of the incremental resistances.

The heat transfer coefficients over the peripheral rotor section ($\bar{r}$ = 0.9-1.0) were found for regimes with the delivery of extremely low mass flows of cooling air, since for large mass flow values the film cooling effect shows up.

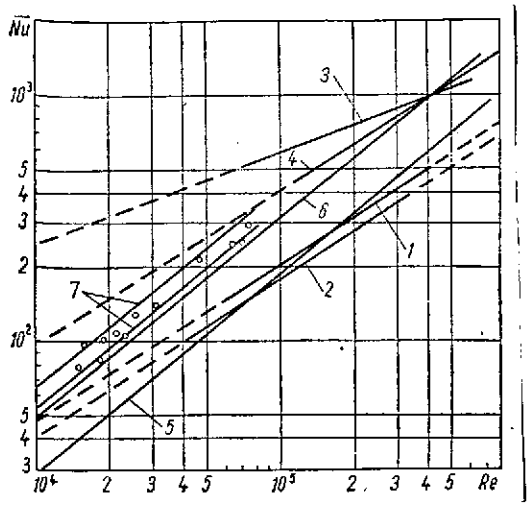


Fig. 54. Mean heat transfer in blading of rotor of centripetal gas turbine:
1, 2. Calculation based on /8/
3. Calculation based on /56, 57/
4. Calculation based on /5/
5. Calculation based on /45/
6. Calculation based on /97/
7. Calculation based on Eqs. (III.19) and (III.20) for Tu values of 12 and 18 percent

The calculations were conducted for 12 different regimes differing in rpm, mass gas flow, and gas temperature.

The mean heat transfer coefficients found by the above technique in the rotor blading of a TKR-14-2a turbine in all the test regimes conducted and treated in dimensionless form Nu = f (Re) are shown in Fig. 54. Here all the criterial equations were reduced to the same characteristic dimensions -- equivalent diameter and single determination temperature -- the temperature of the flow core. The experimental values of the Nusselt number plotted in Fig. 54 as experimental points differed from the calculated values obtained according to the indicated functions by 100-150 percent.

The Nusselt numbers determined in accordance with Eq. (III.12) for a smooth disk proved to be highest (Fig. 54, curve 3) and over the range of Reynolds numbers $10^4$ - $1.5 \cdot 10^5$ exceeded by 120-160 percent the values obtained in solving the inverse problem of thermal conductivity. This discrepancy evidently was due to the substantial difference between the air flow conditions in the interblade channels of a rotor of a centripetal turbine from those along the radius of a smooth turbine. In particular, in the latter case when the initial swirl of the flow was unity (experimental conditions given in /56, 57/), at smaller radii there was a marked difference between the tip speeds of disk and air, while in the turbine rotor the tip speeds of disk and gas were equal to each other for all radii. /85

Over the range of Reynolds numbers $10^4$ - $1.5 \cdot 10^5$, the smallest values of the Nusselt numbers were obtained for calculation relying on the criterial equation for steady flow in tubing used in /45/. Calculation by this equation gave results differing from the experimental values by 100 percent in the Re range $10^4$-$10^5$.

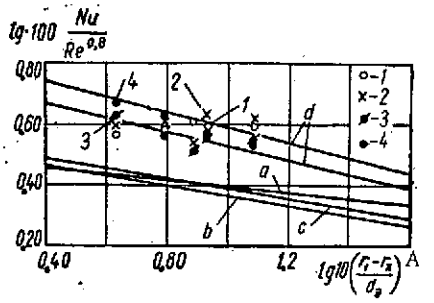


Fig. 55. Local heat transfer in blading of rotor of centripetal turbine:
1. $G_g$ = 0.37 kg/sec; $T_0$ = = 550° C; $n_{tc}$ = 520 rps;
2. $G_g$ = 0.18 kg/sec; $T_0$ = = 500° C; $n_{tc}$ = 300 rps;
3. $G_g$ = 0.15 kg/sec; $T_0$ = = 498° C; $n_{tc}$ = 275 rps;
4. $G_g$ = 0.1 kg/sec; $T_0$ = = 467° C; $n_{tc}$ = 182 rps;
a. Calculation based on /37/
b. Calculation based on /106/
c. Calculation based on /51/
d. Calculation based on Eqs. (III.19) and (III.21) for Tu equal to 12 and 18 percent

Key: A. $\lg 10 \left(\frac{r_1-r_x}{d_{ex}}\right)$; /ex = experimental/

A somewhat smaller difference between calculated and experimental Nusselt numbers (70-80 percent) was observed when criterial equations recommended in /81/ were used (Fig. 54, curves 1 and 2). These experimental data agreed best with the results of calculations based on the recommendations given in /5/ (Fig. 54, curve 4) found for experiments conducted with a fixed model of an interblade channel in the Reynolds number interval $10^4$-$10^5$. In this range the discrepancy of the calculated and experimental Nusselt numbers did not exceed 15-40 percent.

To raise the accuracy of temperature field calculations for rotors of centripetal turbines it is recommended that local heat transfer coefficients along the length of the rotor ducting be used /51, 105/. Local heat transfer coefficients in the rotor blading of the turbine of the TKR-14-2a turbocompressor were determined by the above-described method for plane electrical models. Experimental data interpreted in the form of the function Nu = f (Re) are shown in Fig. 55 by a group of points. Also given in this figure are analogous functions plotted based on Eqs. (III.4), (III.8), (III.19), and (III.21) recommended in /51, 97, 106/. As in the analysis of mean-heat transfer data, Eqs. (III.4) and (III.8) were reduced to unified characteristic parameters /54/: determining directions -- equivalent diameter and determining temperature -- temperature of flow core[6]. As shown by the data given in Fig. 55, the rate of heat /86

[6] When Eq. (III.8) was transformed, the linear law of variation of velocities in the rotor ducting $w_x/w = a\,(r/r_x)$ /48/ was assumed.

of heat transfer in the rotor ducting of a centripetal turbine proved to be somewhat higher than follows from Eqs. (III.4) and (III.8). Thus, the values of the Nusselt numbers based on experimental data are 30-35 percent higher than those obtained from Eq. (III.4). It should be noted that approximately the same difference between Nusselt numbers calculated by Eq. (III.4) from those found in experiments was noted also in the study /50/.

So the intensity of heat transfer in the rotor blading of a centripetal turbine, as shown by experimental results, differed markedly from the heat transfer rate described by the above-indicated empirical functions. The discrepancy of the experimental data with the results of calculations based on these functions is due first of all to the fact that they were obtained in each specific case for strictly specific conditions, which do not fully allow for processes occurring in a full-scale turbine. In recent studies it is shown that one of the key factors affecting the heat transfer intensity in actual turbines is the turbulence of the gas flow both at the inlet to the ducting under study as well as the ducting itself. From this standpoint, for nonshock gas entrance into the rotor ducting of a centripetal gas turbine the flow in the interblade ducting can to the first approximation be assumed similar to the flow in the initial section of a ducting with specific initial turbulence. In this case it appears possible to utilize, in determining heat transfer coefficients from gas to rotor, the criterial equations for the mean and local heat transfer in the initial tubing section:

$$\mathrm{Nu} = 0{,}023\,\mathrm{Re}^{0.8}\,\mathrm{Pr}^{0.4}\,\varepsilon_l. \qquad \text{(III.19)}$$

As shown in /97/, the coefficient $\varepsilon_l$ depends strongly on flow turbulence. A rise in inlet turbulence from 1 to 20 percent raises the heat transfer intensity in a tubing 1-10 diameters in length by 70-80 percent. For the possibility of using the empirical equations recommended /97/ we must have data on the turbulence in turbine blading. Since these data are lacking in the literature, profiles of the mean (with time) and pulsational velocities were measured in the ITTF AN UkSSR at characteristic elements of the air-gas ducting of the TKR-14-2a turbocompressor /25/. The measurements were made with a hot-wire anemometer operating by the direct current method with a single-filament, 40 μm diameter tungsten sensor. The method of measurements and the equipment used are described in detail in /97/. The hot-wire anemometer sensor was installed directly in front of the nozzle box of the turbine and downstream of the rotor. /87

In the studies /25, 97/ turbulence was estimated by the ratio of the root-mean pulsation of velocity to its mean (overtime) value:

$$\mathrm{Tu} = \frac{\sqrt{\overline{\omega_1^2}}}{\omega},$$

where $\sqrt{\overline{\omega_1^2}}$ is the root-mean value of the axial (in flow direction) component of velocity pulsation.

Since usually in a ducting local Tu values vary somewhat over the cross section, in heat transfer calculation ordinarily their value averaged over the mean flow is used.

As shown by the measurements, Tu = 8-12 percent in front of the inlet to the nozzle box of the turbine of a TKR-14-2a turbocompressor, while Tu = 20-25 percent at the outlet from the rotor. In both cases the Tu values were virtually independent of the Reynolds number, that is, the turbine operating regime[7].

To the first approximation can be assumed that in the rotor blading of the centripetal turbine Tu = 12-18 percent. For the mean heat transfer when $1 \leqslant \frac{r_1 - r}{d_{ex}} \leqslant 5$, the corrective factor for the ducting length is recommended to be determined by the equation given in /97/:

$$\bar{\varepsilon}_l = \frac{1{,}3 + 0.05\,\mathrm{Tu}}{\left(\frac{r_1 - r}{d_{eq}}\right)^{0{,}07 + 0{,}005\,\mathrm{Tu}}}, \qquad \text{(III.20)}$$

and for local heat transfer:

$$\varepsilon_l = \frac{1{,}35 + 0{,}04\,\mathrm{Tu}}{\left(\frac{r_1 - r}{d_{eq}}\right)^{0{,}17 + 0{,}006\,\mathrm{Tu}}}. \qquad \text{(III.21)}$$

Most data obtained by solving the inverse thermal conductivity problem based on averaged and local Nusselt numbers lie in the logarithmic system of coordinates between the corresponding straight lines plotted by Eqs. (III.20) and (III.21) for Tu values of 10 and 18 percent (see Fig. 54, curve 7, and Fig. 55 d). It should be noted that allowing for the buildup of heat transfer over the initial section based on the known recommendations in /37/ is inadequate in this case: experimental values of the Nusselt numbers here lie 20-25 percent below the calculated values.

---

[7] This fact is very essential, since the turbulence was measured as the turbine was operated with cold air ($T_g$ = 30-35° C).

Results of calculating the temperature fields of the rotors in centripetal turbines of the TKR-23-1 turbocompressors confirmed the suitability of the above-outlined method for determining the coefficients of heat transfer between rotor and gas. Only when the heat transfer rate is allowed for through increase in turbulence of the flow was it possible to ensure the fairly satisfactory agreement between calculated and measured temperature fields. /88

In the calculations of coefficients of heat transfer in rotor blading, usually the radial component of velocity is taken as the determining component. However, in noncalculated turbine operating regimes the relative gas velocity at the inlet to the ducting can differ appreciably in absolute value from its radial component. In principle this can introduce some error into the calculation of heat transfer coefficients.

The effect of the angle of gas entry into the interblade channel on the rotor temperature field was determined with a full-scale rotor of the TKR-14-2a. This effect, which is marked only at the peripheral rotor sections ($\bar{r} = 0.6$), in heat transfer calculation can be allowed for by determining the Reynolds numbers directly from the relative gas velocity.

The agreement of experimental data with data obtained according to Eqs. (III.19) - (III.21) permits recommending these functions for approximate calculations of the mean and local heat transfer coefficients in the rotor blading of the centripetal turbine.

The presence of film cooling complicates calculating the boundary conditions of heat transfer in the rotor blading of the centripetal turbine, since in this case we must allow for the change in thermal flows from the disk over the initial section of the ducting. Allowing for the effect of film cooling can be done either by correcting the coefficients of heat transfer from gas to rotor [56, 57], or by correcting the gas temperature [96] over the corresponding section of the ducting. The second method is more universal and at the present time is widely used in calculating boundary and combination cooling [24, 70, 91, 96].

In calculations along the section where the film cooling was in effect, instead of the gas temperature we used the so-called adiabatic temperature of the wall, $T_{w.ad}$, which was defined from the equation [96, 117]:

$$T_{w.ad} = \eta(T^*_{i.a} - T^*_g) + T^*_w \qquad \text{(III.22)}$$

The density of the local thermal flow toward the wall in combination cooling can be calculated using the equation

$$Q = \alpha \left[ \overline{T}_{w.ad} - T_d \right]. \qquad \text{(III.23)}$$

The heat transfer coefficient in the ducting is assumed in the first approximation to be identical with or without film cooling, according to [96].

Empirical functions in the literature for calculating the effectiveness of film cooling were derived for a plane surface with tangential injection of coolant [70, 96, 117]. Strictly speaking, they cannot be transferred directly to rotors of centripetal gas turbines owing to the axisymmetry of the flow and the difference in the coolant delivery conditions.

Functions obtained for the plate can be transformed suitably to conditions of centripetal turbines by the appropriate transformation of coordinates. The relationship of the coordinates is determined by the equations: /89

$$r = r_0(x) + y\cos\alpha;\ z = z_0(x) + y\sin\alpha. \qquad \text{(III.24)}$$

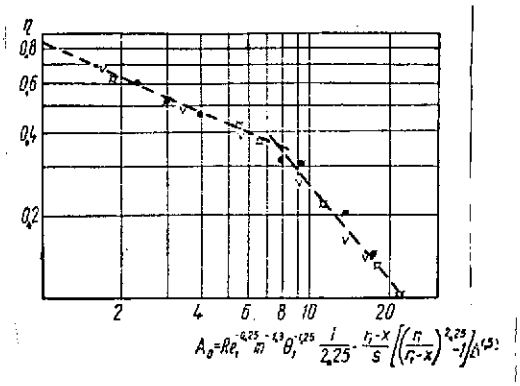


Fig. 56. Effectiveness of film cooling when cooling air is injected into the rotor blading of the TKR-14-2a. Experimental points correspond to injection coefficients 0.46-0.69.

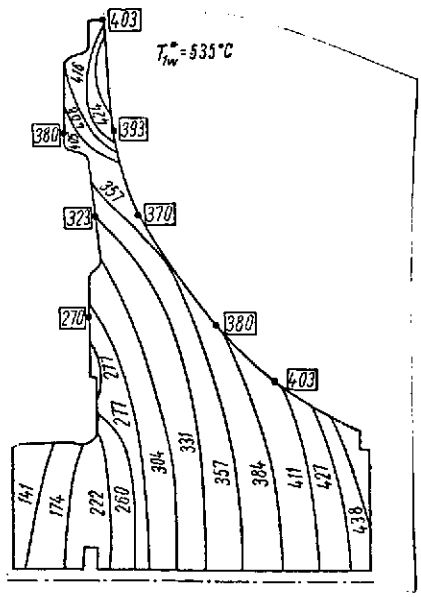


Fig. 57. Comparison of calculated (lines) and experimental (points) data on temperature fields of rotor of TKR-23-1.

To simplify the pattern of the flow in the rotor ducting, we must assume that the axisymmetric flow with number Pr ≈ 1 enters the ducting shockfree and travels further with complete twisting, that is, $v_{ci} = \omega r$.

In this case the motion of the flow relative to the rotor will be axisymmetric with the radial direction of the relative velocity, while the centrifugal forces will act in a direction opposite to the direction of the protective film. Thus, their action will be equivalent to the action of the pressure gradient directed along the surface being protected.

Results of analyzing[8] the integral equations for the boundary layer close to the working surface of the spinning rotor set up with reference to converting to the system of coordinates (III.24) enable us to derive an equation for calculating the effectiveness of rotor film cooling in a centripetal turbine:

$$\eta = f(A_0). \qquad \text{(III.25)}$$

Here, /90

$$A_0 = \Delta^{1.5}\,\mathrm{Re}_1^{-0.25} m^{-1.3} \theta_1^{-1.25} \frac{(r-x)}{2{,}25s}\left[\left(\frac{r_1}{r_1-x}\right)^{2.25} - 1\right], \qquad \text{(III.26)}$$

$$\text{where} \quad \Delta = \frac{s + h_{cr} + \delta^*}{s + 0{,}5h_{cr}}.$$

To check whether these relations are suitable for the conditions of a centripetal turbine, using an EI-12 network integrator, by solving the inverse problem of thermal conductivity using the measurements of metal temperature in the rotor blading, we calculated the effectiveness of film cooling of the turbine rotor of the TKR-14-2a turbocompressor. The calculation was performed on a two-dimensional network model of the rotor, on the back side which was assigned boundary conditions of the first kind and the metal temperatures measured in experiments.

In the model the heat transfer coefficients determined by the above-presented functions for the case when no coolant is injected into the rotor ducting are assigned for the blading.

In the rotor, the values of the potentials (proportional to gas temperature) that virtually ensure that the temperatures coin-

---

[8] A detailed analysis of the integral equations for the boundary layer close to the working surface of the spinning disk was made in /96/.

cide in the model blading and in temperatures measured on the full-scale rotor are selected on the heat removal side. The gas temperature thus determined along the section where film cooling is in effect was equal to the adiabatic wall temperature. Results of calculations for different cooling air regimes g = 0-0.0776 kg/sec and turbine operating regimes $T_g$ = 550° C, $n_{tc}$ = 245-300 rps and $G_g$ = 0.1745-0.18 kg/sec are shown in Fig. 56.

The values for film cooling effectiveness can be fitted, with the scatter of ± 12 percent, along curves approximated by the equations

$$\eta = \begin{cases} \left(1{,}516\,\frac{A_0}{\Delta^{1.5}}\right)^{-0{,}36} & \text{for } 1{,}5 \leqslant A_0 \leqslant 7{,}3; \\ \left(0{,}307\,\frac{A_0}{\Delta^{1.5}}\right)^{-1{,}2} & \text{for } A_0 \geqslant 7{,}3. \end{cases} \qquad \text{(III.27)}$$

The Reynolds number for calculating the coefficient $A_0$ in Eq. (III.26) was determined from the distance from the rotor leading edge and the relative gas velocity at the ducting inlet.

This method of allowing for the presence of film cooling in the ducting of a centripetal turbine was verified by the results of testing the cooling system of the TKR-23-1 turbocompressor.

Fig. 57 shows the temperature field of the turbine rotor of the TKR-23-1 turbocompressor in a near-rated regime. The mass flow of air for cooling was 0.013 kg/sec and provided for an air film in the rotor ducting. The effect of film cooling was allowed for by the method outlined, in accordance with Eq. (III.27). The discrepancy of experimental and calculated data was 4-4.6 percent of the difference between the gas temperature and the cooling air temperature, quite suitable for engineering purposes.

## CHAPTER FOUR

/91

## MAIN PRINCIPLES OF METHOD OF CALCULATING AIR-COOLING SYSTEMS OF ROTORS IN CENTRIPETAL GAS TURBINES

Generally rotors in centripetal gas turbines are cooled by blowoff of rotor back side in conjunction with injection of relatively cold air over the rotor surface swept by the gas. The air-cooling methods listed are used widely also in axial-type gas turbines. This makes it possible, when calculating air-cooling systems of rotors in centripetal turbines, to use the method of engineering calculations of cooling systems in axial-type gas turbines developed in the ITTF AN UkSSR and tested by the results of numerous investigations /21, 73/.

This method permits developing optimal designs of rotor air-cooling systems in gas turbines /21, 73/.

The problem of developing a cooling system for a newly designed turbine (direct problem) can be conditionally subdivided into two interrelated parts /21/.

1. Thermal calculation, in which one selects a cooling method and system operating regime, based on information obtained in some manner concerning the interrelationship of the thermal state of a particular assembly and mass flows and parameters of cooling air, where the cooling method and operating regime of the system ensure the appropriate temperature field of all parts for minimum coolant mass flows.

2. Hydraulic calculation in which one determines the configuration and dimensions of all components of the cooling line leading to obtaining the cooling system selected in the thermal calculation of the operating regime, that is, the distribution of mass flows of cooling air over all components, and reducing nonproductive coolant losses to a minimum.

The problem of determining the effectiveness (investigating) the cooling system of an existing gas turbine (inverse problem) can also be conditionally subdivided into the same two parts. In this case first the hydraulic calculation of the system is performed -- the mass flows and parameters of air in all components of the cooling line are determined. Then a thermal calculation is carried out, in which one finds the temperature fields of all parts of the particular assembly corresponding to this distribution.

So in developing and studying air-cooling systems we must first have sufficiently accurate methods of solving the thermal conductivity and hydraulic problems that arise and secondly, we must have reliable quantitative data on the conditions of uniqueness (boundary and initial conditions) for processes described by the related equations. /92

## 1. Hydraulic Calculation

The methods of hydraulic calculation of air-cooling systems currently in use /73/ are based on the fact that any, however complex cooling system can be represented in the form of suitably connected hydraulic drags of the so-called equivalent calculation scheme of the cooling system.

Setting up the equivalent scheme of a particular cooling system is done as follows /73/:

1) the system is divided into individual sections (standard elements) so that by selecting the appropriate coefficients (of drag, head, or volume flow) the fullest possible allowance for their interaction is ensured;

2) the connection sites of standard elements are replaced with nodal points. Here it is assumed that the merging and separation of flows at the nodal points occurs without pressure change; and

3) the standard elements are connected to each other and with the nodal points in the same sequence and in the order as the sections of the initial cooling system corresponding to them.

Usually, when separating standard elements in the system, an effort is made for the coefficient of hydraulic drag (head and mass flow) to be uniquely determined by flow geometry and regime. Here the availability in the literature of reliable data on the absolute values of these coefficients and their dependence on the parameters indicated above is vital.

For /given initial and final cooling air pressures, observing the conditions listed provide for corresponding points of the initial and equivalent schemes the equality of cooling air mass flows and parameters.

The distribution of air mass flows by hydraulic network elements is described by the following system of algebraic equations:

$$\left.\begin{aligned} P_i^* - P_j^* = \xi_{i-j}\rho\frac{w^2}{2} \end{aligned}\right\} \text{(a total of } z_1 \text{ equations);} \quad \text{(IV.1)}$$

$$\left.\begin{aligned} \Sigma g_{i-j} = 0 \end{aligned}\right\} \text{(a total of } z_2 \text{ equations)} \quad \text{(IV.2)}$$

or, using the continuity equation,

$$\left.\begin{aligned} P_i^* - P_j^* = \xi_{i-j}\frac{R}{2}\cdot\frac{T_{i(j)}}{\gamma P F^2}g^2; \\ \Sigma g_{i-j} = 0. \end{aligned}\right| \quad \begin{matrix} \text{(IV.3)} \\ \text{(IV.4)} \end{matrix}$$

Here the coefficient of hydraulic drag is determined by the difference of total pressures. /93

The number of equations $(z_1 + z_2)$ is due to the branching of the cooling system and usually does not exceed ten for rotors of centripetal gas turbines.

Coefficients of hydraulic drag in the general case can depend on mass flow of air through an element /component/, which makes the system of the above-presented algebraic equations nonlinear. Various methods of solving this system of equations are given in the literature: analytical, analytical-graphical, and using digital and analog computers. Advantages and drawbacks of each method are spelled out in /73/.

In devising and studying air-cooling systems of rotors in centripetal gas turbines, generally when used as analytical and analytical-graphical methods of hydraulic calculation detailed in /21, 73/. In particular, when solving the direct problem of hydraulic calculation, which boils down to solving the system of equations (IV.1) and (IV.2) for known $g_{i-j}$, $P^*_{con}$, $P^*_0$, and unknown $\xi_{i-j}$ and $F_{i-j}$, usually cooling air pressures at characteristic points of the cooling duct are assigned. Air temperatures at these points are determined by thermal calculation of the cooling system. This enables us to proceed from solving the system of equations (IV.1) and (IV.2) to solving the equations (IV.1) for branches of the cooling duct. Here each of the equations (IV.1) can be solved explicitly with respect to the unknown quantity $\xi_{i-j}/F^2_{i-j}$. The

desired quantity $F_{i-j}$ is found by using available literature data on the dependence of $\xi_{i-j}$ on standard element geometry and size.

When selecting pressures at characteristic points of the cooling system, one must allow for the following.

1. The pressure drop between cooling duct and blading must always be positive.

2. Elements of the cooling duct determining air mass flow in a given branch must have strictly specific dimensions unchanging during service of the installation.

3. The reduction in cooling air pressure at the above-indicated regulating elements must appreciably exceed pressure drops at the remaining elements of the given branch.

When solving the inverse problem of hydraulic calculation, reducing to solving the system (IV.1) and (IV.2) given known $P^*_0$, $P^*_{con}$, and $F_{i-j}$ and unknown $g_{i-j}$ and $\xi_{i-j}$, commonly the so-called analytical-graphical method is used /73/. In this case first by the analytical approach one calculates the air mass flow through each standard element and finds the quantitative relation between air mass flow and the pressure drop at this element, then graphically one determines for all standard elements the combined operating regime, that is, one finds the solution to the system of equations describing the distribution of air mass flows and parameters throughout the system.

The analysis of components of cooling systems in centripetal gas turbines in Chapter One singles out the following standard elements in these systems /49/: /94

1) ducting for bleeding and admission of cooling air (finite-length openings, bends, convergences, divergences, branches, and the like);

2) labyrinth seals; and

3) axial clearance between back surface of rotor and fixed wall of stator part of turbocompressor.

Standard elements of the first two kinds are passive, that is, the pressure change at them (pressure drop) is related only to the moving flow overcoming drag forces (friction and eddying). The air mass flow through these elements is calculated by Eq. (IV.3). Here the parameters of the medium at the characteristic section must be estimated with reference to acceleration of the stream up to the velocity in this section. When isothermal flow

is present in those cases in which the characteristic section lies ahead of the section at which the pressure loss occurs, the static pressure therein is determined by the equation /73/

$$P = \frac{P_i^*}{2} + \sqrt{\left(\frac{P_i^*}{2}\right)^2 - \frac{RT}{2F^2} g^2}, \qquad \text{(IV.5)}$$

or

$$P = \frac{P_j^*}{2} + \sqrt{\left(\frac{P_j^*}{2}\right)^2 - (1-\xi)\frac{RT}{2F^2} g^2}. \qquad \text{(IV.5a)}$$

If the characteristic section is selected beyond the section at which pressure losses are produced, the equations take the form /73/:

$$P = \frac{P_i^*}{2} + \sqrt{\left(\frac{P_i^*}{2}\right)^2 - (1+\xi)\frac{RT}{2F^2} g^2}, \qquad \text{(IV.6)}$$

or

$$P = \frac{P_j^*}{2} + \sqrt{\left(\frac{P_j^*}{2}\right)^2 - \frac{RT}{2F^2} g^2}. \qquad \text{(IV.6a)}$$

When using equations (IV.5) and (IV.6), the kind of standard element (short opening, bend, and so on) as well as its geometrical characteristics (ratio of areas, flow turning angle, shape of edge, and so on) are allowed for by selecting the coefficients of hydraulic drag ($\xi$). Determining $\xi$ as applied to standard elements in air-cooling systems of rotors in centripetal turbines will be examined somewhat further on.

Eqs. (IV.5) and (IV.6) are applicable only for calculations of standard elements in which total pressure losses occur in a single "characteristic" section.

In some standard elements, for example, channels of relatively long extent, the pressure drop is largely caused by air friction against walls. Pressure losses in this case proved to be uniformly distributed along element length. So in drags of this type the /95 characteristic section, strictly speaking, is absent, and Eq. (IV.1) is applicable only in differential form /73/:

$$-\bar{\lambda}\frac{dx}{D_g}\rho\frac{w^2}{2} = dP + d\left(\frac{\rho w^2}{2}\right). \qquad \text{(IV.7)}$$

Integrating Eq. (IV.7), for isothermal flows in constant-section ducting we get

$$P_i^2 - P_j^2 = \left(\bar{\lambda}\frac{L}{D_g} + \ln\frac{P_i}{P_j}\right)\frac{g^2RT}{F^2} \qquad \text{(IV.8)}$$

or

$$g = F\sqrt{\frac{1}{RT}\cdot\frac{P_i^2 - P_j^2}{\bar{\lambda}\frac{L}{D_g} + \ln\frac{P_i}{P_j}}}. \qquad \text{(IV.9)}$$

For convenience in calculations, Eq. (IV.8) can be represented as

$$\bar{\lambda}\frac{L}{D_g} = f(\bar{P}_i) - f(\bar{P}_j), \qquad \text{(IV.10)}$$

where

$$f(\bar{P}_j) = \frac{(\bar{P}_j')^2}{2} - \ln\bar{P}_j', \qquad \text{(IV.10a)}$$

$$f(\bar{P}_i) = \frac{(\bar{P}_i')^2}{2} - \ln\bar{P}_i'; \qquad \text{(IV.10b)}$$

$\bar{P}'$ is a dimensionless quantity proportional to the static pressure,

$$\bar{P}' = \frac{P}{\sqrt{P\rho\frac{w^2}{2}}}. \qquad \text{(IV.10c)}$$

The function $f(\bar{P}')$ is shown in Fig. 58 and is the same for all ducting. A table of the values of this function is in [73].

When estimating frictional losses, the coefficient of friction for laminar flow regime (Reynolds number for the ducting is smaller than $2\cdot10^3$) is calculated by the relation

$$\bar{\lambda} = \frac{K}{\mathrm{Re}}, \qquad \text{(IV.11)}$$

where K is a coefficient determined by ducting shape (K = 64 for a circle; K = 96 for an annular section; K = 57 for a square; k = 65-73 for an ellipse; and K = 96 for a thin slot).

In a turbulent flow regime (Reynolds number larger than $2.5 \cdot 10^3$) the coefficient of friction for channels of any configuration is

$$\bar{\lambda} = \frac{0.316}{\mathrm{Re}^{0.25}}. \qquad \text{(IV.12)}$$

Functions and data for finding $\bar{\lambda}$ in the transition region, in rough ducting, and in other cases more complex and seldom encountered are given in [35, 73]. Also presented there are recommendations about finding the coefficients of hydraulic drag of auxiliary elements in a cooling duct: tees, bends, bleed openings, and so on. /96

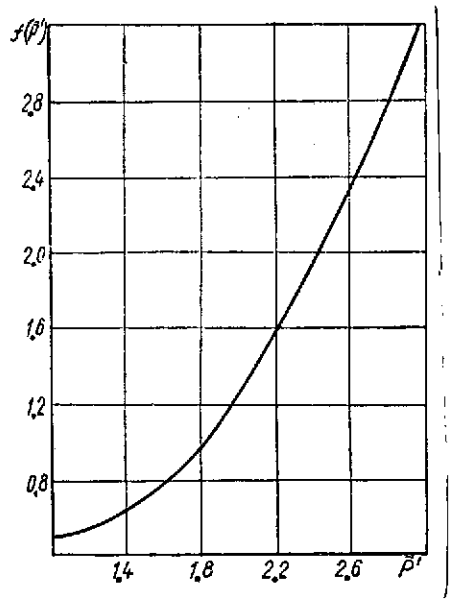


Fig. 58. Graphical solution of Eq. (IV.10c)

The mass flow of air or gas through a labyrinth seal in the studies [73, 76] is recommended to be determined by the equation

$$g = KF\sqrt{\frac{P_1^{*2} - P_2^{*2}}{iRT}}. \qquad \text{(IV.13)}$$

Coefficient K depends on the type of seal and is 0.7 for a stepped seal; K = 1.27 for a straight-flow seal; and K = = 1.15 for a straight-flow labyrinth with ridges inclined at an angle of more than 45° [76].

If the labyrinth seal lies at the face surface of the rotor (radial seal), air (gas) leakage is calculated by the formula

$$g_{se} = KF\sqrt{\frac{(P_1^* \pm \Delta P_{cf})^2 - P_2^*}{RT}}, \qquad \text{(IV.14)}$$

where $P_1^*$ and $P_2^*$ are the larger and smaller pressure at the seal boundaries. The plus sign in front of $\Delta P_{cf}$ allowing for the pressure rise due to the pump effect in the seal is present when the flow direction and the direction of centrifugal forces coincide.

All the above-presented working formulas characterize the pressure change for isothermal air flow through a standard element. The presence of heat transfer, primarily heat rejection to the cooling air, at each element has a definite effect on the element's hydraulic drag. This effect shows up in the change of air velocity along duct (element) length due to the change occurring in heat rejection in air density, and in several cases, primarily during viscosity flow regimes; this influence is also seen in the variation occurring in the coefficient of hydraulic drag of the element. An additional pressure loss owing to variation in air density during /97 heat rejection for an element with constant flow-through cross section is usually determined by the following equation /52, 73/:

$$\Delta P^*_{add} = {}^1/_2(\rho_i w_i^2 - \rho_j w_j^2). \qquad \text{(IV.15)}$$

When heat is rejected to the air, $\Delta P^*_{add}$ is always positive, that is, losses from overcoming frictional forces and heating add.

Relations for determining the frictional drag coefficient in nonisothermal viscosity (laminar) flow regime of air in ducting are presented in /52, 73/. Also indicated in /73/ are the main features of calculating hydraulic drag of standard elements when air flows through them at velocities close to the speed of sound.

In the hydraulic calculation of air-cooling systems of rotors in centripetal gas turbines, the greatest difficulties arise as part of the calculation of the air flow in the clearance between the spinning disk and the fixed casing wall opposing it. As already indicated, when the disk is rotating in this clearance an air flow caused by the action of viscosity forces is induced. Fluid particles directly adjoining the rotor surface are entrained into rotational motion and will travel from the axis of disk rotation to its periphery under the effect of centrifugal forces /19/. As a result, on the casing wall opposite the disk an air flow from periphery to center will develop, opposite in direction.

Owing to the pump effect a spinning disk ejects toward the periphery a quite specific (and radius-variable) amount of air. So in forced delivery into the clearance of cooling air the intensity of back currents, that is, the amount of suction gas, becomes smaller, while the depth of penetration of heated gases into the clearance decreases. When some, also quite specific

air mass flow is delivered into the clearance, the suction of heated gases into it halts completely and along the casing wall a flow from rotation axis to periphery is induced.

The rotational motion of air in the clearance leads to the initiation along the disk radius of a pressure drop; at high rotor tip speeds this pressure drop can markedly affect the hydraulic characteristics of the cooling system overall. So in hydraulic calculation of a rotor cooling system in a centripetal turbine the following must be determined:

a) the amount of heated air sucked into the clearance from the blading;

b) twisting of the air flow in the clearance over all of the rotor radii; and

c) pressure drop over the disk radius.

Data on the amount of gas sucked into the clearance and on the twisting of the flow in the clearance are also needed to calculate the heat transfer in the clearance, that is, for the thermal calculation of the cooling system.

Large numbers of experimental and theoretical studies deal with the flow of air into the axial clearance between the side surface of the rotor and its casing; they are reviewed, for example, in [19, 90]. /98

In [73] engineering methods are proposed for calculating flow in the clearance under conditions that are most common in gas turbines. These methods, whose main principles are outlined below, are based on generalizing several experimental studies, which are given in [73].

When there is an absence of forced air delivery into the clearance, the amount of fluid (air or gas) sucked in by the spinning disk is recommended to be determined by the following equation, in [73]:

$$g = q\omega r_1^3 \rho; \qquad \text{(IV.16)}$$

$$q = 0{,}1 \lg\left(100 \frac{s}{r_1}\right)\left(\frac{r}{0{,}87 r_1}\right)^{2{,}3} \mathrm{Re}_\omega^{-0{,}2}. \qquad \text{(IV.16a)}$$

Eq. (IV.16a) was derived by generalizing experimental data of several authors in the range of relative clearances ($s/r_1$) 0.02-0.1; for larger $s/r_1$ values, the calculation is based on the equation:

$$q = 0{,}1\left(\frac{r}{0{,}87r_1}\right)^{2{,}3} \mathrm{Re}_\omega^{-0{,}2}. \qquad \text{(IV.16b)}$$

If there is no forced delivery of air into the clearance, one can assume approximately that in the clearance there is a flow core spinning at constant angular velocity. In this case all velocity changes occur in thin layers at the disk and casing. In /73/ the twisting of the flow core is recommended to be calculated by the equation

$$z_{\varphi_0} = \frac{v_{\varphi_0}}{\omega r} = 0{,}338\left(\frac{s}{r_1}\right)^{-0{,}1}, \qquad \text{(IV.17)}$$

where $v_{\varphi_0}$ is the peripheral velocity component in the core at radius r obtained by generalizing the results of experiments of a number of authors in the range $0.025 \leqslant s/r \leqslant 0.3$.

When air is delivered into the clearance, the flow pattern in the clearance becomes markedly complicated and a reliable enough calculation is possible only for relatively simple cases. This circumstance is dictated, first, by the fact that twisting of the flow core when air is delivered into the clearance becomes radius-variable. In the case of radial blowoff of the disk with air being fed into the clearance at the minimum radius and with zero initial twisting of the air flow, flow twisting in the middle of the clearance width can be determined by the results of the theoretical calculation /79/ presented in Fig. 59, satisfactorily agreeing with experiments. Here the parameter needed in the calculation is

$$\beta = \frac{0{,}167}{q_r (r_1/r_0)^{2.6} \mathrm{Re}_\omega^{0.2}}, \qquad \text{(IV.18)}$$

where $q_r = g_{i.a}/\rho\omega r_1 s$ is the dimensionless air mass flow for radial blowoff; $r_0$ is the radius at which cooling air is delivered into the clearance; and $g_{i.a}$ is the absolute mass flow of air for radial blowoff. /99

For forced delivery of cooling air into the clearance, the amount of medium sucked in by the spinning disk is recommended in /73/ to be determined by the empirical relation

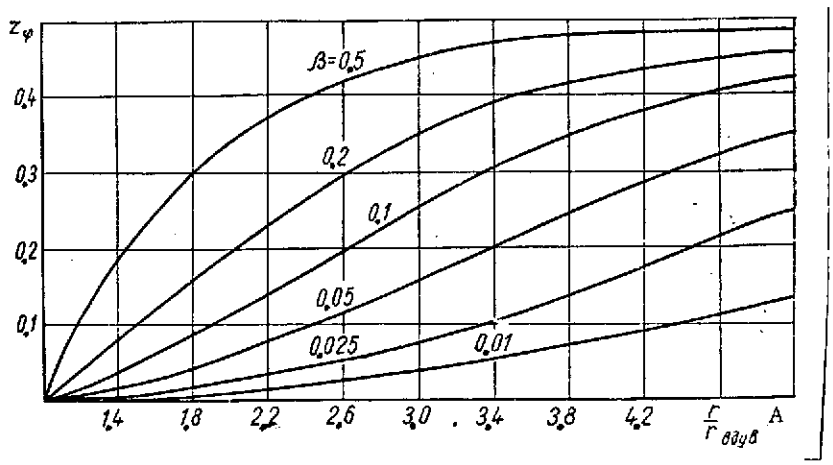


Fig. 59. Dependence of relative flow twisting $z_\phi = v_\phi / \omega r$ in the middle of the clearance on $\bar{r} = r/r_0$ for different values of parameter β when the initial twist of the flow at the radius at which air is fed into the clearance is zero.
Key: A. $r/r_{inj}$

$$\frac{q}{q_0} = \frac{z_\varphi}{z_{\varphi_0}} - 10\left(\frac{1}{K_v}\right), \qquad \text{(IV.19)}$$

where $q_0$ is the dimensionless volumetric flow of the reverse stream without air delivered into the clearance; q is the same as above, when air is delivered into the clearance; $z_\phi$ is the twisting of the flow in the middle of the clearance at the given radius when air is being fed into the clearance; $z_{\phi_0}$ is the same, without air being delivered into the clearance; $K_v = \omega r / v_{2_{av}} = 2\pi r^2 s\ (\omega r)/g_{i.a}$ is the kinematic factor at the given radius; $v_{2_{av}} = g_{i.a}/2\pi r s \gamma$ is the radial velocity at the given radius averaged over the mass flow.

If $z_\phi / z_{\phi_0} \leqslant 10\ 1/K_v$, the back flow along the wall or the casing, that is suction of heated gases into the clearance, is not observed.

To the first approximation, the above relations can be used also in calculating flow in the clearance when disk jet blowoff is used /73/. In this case, outside the zone of action of the jets, beginning at radius r = R - (10-20)d and below (R = radius

of arrangement of nozzles for jet blowoff organization; and d = /100
= nozzle diameter), the motion of the medium can be assumed to be entirely subject to the above-presented functions for calculating flow in the clearance without forced air delivery. Beginning with the radius r = R + (10-20)d and above, the flow of air in the clearance can to the first approximation be calculated from the relations for calculating the flow in radial blowoff.

For jet-radial disk blowoff, the currents at radii greater and smaller than the jet delivery radius are calculated from the relations for the flow in the clearance in radial blowoff. Naturally, at the radii smaller than the jet delivery radius the mass flow of air is assumed to be equal to the mass flow of air supplied into the clearance for radial blowoff, and at larger radii -- equal to the total mass flows in radial and jet blowoff. The pressure change along the radius of the clearance between disk and casing /73/ is recommended to be calculated by the equation

$$P - P_0 = \frac{1}{2}\rho_{av}\omega^2 r^2\left\{\frac{2}{\bar{r}^2}\int_1^{\bar{x}} z_\varphi^2 \bar{r}\,d\bar{x} + \eta_{dif}\left(\frac{1}{K_{v_0}^2\bar{r}^2} - \frac{1}{K_v^2}\right)\right\}, \qquad \text{(IV.20)}$$

where $\eta_{dif} \approx 0.5$; $K_{v_0}$ are the values of the kinematic factor at radius $r_0$; $K_v$ is the instantaneous value of the kinematic factor at radius r. Beginning with the radius of back current formations and above, $_{dif} = 0$. In the absence of air delivery into the clearance, we have

$$P - P_0 = \frac{1}{2}\rho_{av}\omega^2 r^2 z_\varphi^2\left(1 - \frac{1}{\bar{r}^2}\right). \qquad \text{(IV.21)}$$

In the remaining cases, Eq. (IV.20) is solved by numerical or graphical integration for flow twisting along the clearance radius determined by the methods described above. The calculation is performed from periphery to center, and at radius $r_1$ the pressure in the clearance between the disk and casing is assumed to be equal to the pressure in the clearance between the nozzle vanes and the rotor.

## 2. Thermal Calculation

As already stated, it is the task of thermal calculation of the cooling system to find the temperature fields of the rotor in an existing turbine from air mass flows, known from hydraulic

calculation, in all the elements of the cooling duct (inverse problem of thermal calculation), or else to determine the method of cooling and the mass flow of cooling air ensuring that a given temperature field of the rotor is achieved (direct problem of thermal calculation). To perform the thermal calculation in any formulation, one must have the solution to the differential equation of thermal conductivity for a rotor with suitably formulated boundary conditions.

The thermal calculation of air-cooling systems of rotors in centripetal gas turbines at the present time can be done either analytically, or else with means of mathematical simulation, primarily electrical models of continuous media, resistance networks, and their combinations. /101

The analytic solution of the problem of determining temperature fields of a rotor in a centripetal gas turbine is hindered both by the existing variability along the rotor radius of disk thickness and the heat transfer coefficients over both surfaces (gas-heated and air-cooled), as well as by the abrupt difference in the temperature of the media at both of its side surfaces. The latter factor accounts for the solution of the axisymmetric thermal conductivity problem in a two-dimensional formulation. This leads to a sharp rise in the labor involved in the solution.

Usually when using analytical methods the problem is solved in two stages: first one finds the solution to the thermal conductivity problem in the case when temperature drops along disk thickness are neglected, and then from the temperature distribution along the radius that is known for the middle line, one finds the temperature drops in the axial direction.

In solving the first problem, one uses the differential equation of steady thermal conductivity of the gas turbine disk in the form /90/:

$$\frac{d^2T}{dr^2}+\left(\frac{1}{r}+\frac{1}{y}\cdot\frac{dy}{dr}\right)\frac{dT}{dr}-\frac{2\alpha_{av}}{y\lambda}(T-T_{eq})=0, \qquad \text{(IV.22)}$$

where $T_{eq}=\frac{\alpha_w T_{i.a}+\alpha_g T_g}{\alpha_{i.a}+\alpha_g}$ is the equivalent temperature in going from asymmetric to symmetric rotor cooling.

The general solution of equation (IV.22) for a variable-thickness rotor with radius-varying boundary conditions is difficult to arrive at /90/. Therefore usually the rotor of a centripetal turbine is subdivided into concentric rings of constant thickness, within each of which the heat transfer coefficients and the temperature of the medium are assumed constant.

The temperature field of a rotor is calculated by the successive transition from ring to ring, and at their junction temperatures and thermal flows, that is, temperature gradients in the radial direction, are assumed to be equal.

The temperature distribution within a single ring is determined by Eq. (IV.22) for radius-constant values of y, $\alpha_{av}$, and $T_{eq}$. In this case /90/

$$T = T_{eq} + A_i I_0(m_i r) + B_i K_0(m_i r), \qquad \text{(IV.23)}$$

where $I_0$ is the zero-order Bessel function of the first kind in the imaginary argument; $K_0$ is the zero-order Bessel function of the second kind in the imaginary argument; $m = \sqrt{\frac{2\alpha_{av}}{y_i \lambda}}$ is the parameter characterizing disk cooling intensity.

To find the constants of integration $A_i$ and $B_i$ the following /102 boundary conditions are used in each ring. If at the outer radius $T = T$ and $\frac{dT}{dr}\Big|_{r=r_1} = 0$, then

$$A_1 I_0(m_1 r_1) - B_1 K_1(m_1 r_1) = 0; \qquad \text{(IV.24)}$$

at the junction of the first and second (counting from the disk periphery) rings, we have

$$T_{r_2} = T_{r_1} \text{ and } \frac{dT_{r_2}}{dr} = \frac{dT_{r_1}}{dr} \qquad \text{(IV.25)}$$

or

$$A_1 I_0(m_1 r_2) + B_1 K_0(m_1 r_2) = A_2 I_0(m_2 r_2) + B_2 K_0(m_2 r_2); \qquad \text{(IV.25a)}$$

$$m_1 A_1 I_1(m_1 r_2) - m_1 B_1 K_1(m_1 r_2) = m_2 A_2 I_1(m_2 r_2) - m_2 B_2 K_1(m_2 r_2); \qquad \text{(IV.25b)}$$

at the disk hub radius

$$T_{r_{n-1}} = T_{r_n} \text{ and } \frac{dF}{dr}\Big|_{r=r_n} = 0 \qquad \text{(IV.26)}$$

or

$$A_{n-1}I_0(m_{n-1}r_n) + B_{n-1}K_0(m_{n-1}r_n) = A_nI_0(m_nr_n) + B_nK_0(m_nr_n); \quad \text{(IV.26a)}$$

$$m_{n-1}A_{n-1}I_1(m_{n-1}r_n) + m_{n-1}B_{n-1}K_0(m_{n-1}r_n) = m_nA_nI_1(m_nr_n) - m_nB_nK_1(m_nr_n) = 0. \quad \text{(IV.26b)}$$

To find the constants $A_n$ and $B_n$, we have to solve a system of 2n equations (IV.23) containing the same number of unknowns. Since in the general case this is a quite laborious operation, usually in the analytic calculation of temperature fields the rotor is subdivided by radius into not more than 3-4 sections.

In solving the second part of the problem the temperature change over the disk thickness is assumed to obey a linear law. In this case the temperature at the outer (side) surface on the side swept by the gas will be

$$T_{d.g} = \frac{T_g\alpha_g + T\frac{2\lambda}{y}}{\frac{2\lambda}{y} + \alpha_g}; \quad \text{(IV.27)}$$

and similarly on the sides swept by air,

$$T_{d.a} = \frac{T_{i.a}\alpha_{i.a} + T\frac{2\lambda}{y}}{\frac{2\lambda}{y} + \alpha_{i.a}}, \quad \text{(IV.27a)}$$

where T is the temperature at the disk mid-thickness for a given radius and y is half the disk thickness at the given radius.

The workload and the inadequately high accuracy of the above-described analytic method of thermal calculation promoted the wide acceptance in actual practice of methods based on electrical models [21, 44, 79, 80]. When these methods are used, thermal calculation of a cooling system when the inverse problem of thermal calculation is being solved reduces to setting up an electrical model of the rotor, assigning boundary conditions on it that allow for the parameters and mass flows of the media sweeping the rotors, and determining the field of potentials equivalent to the temperature field [21]. When solving the direct problem of thermal calculation, the boundary conditions ensuring that a given rotor temperature field is attained are selected for the electrical model [21]. /103

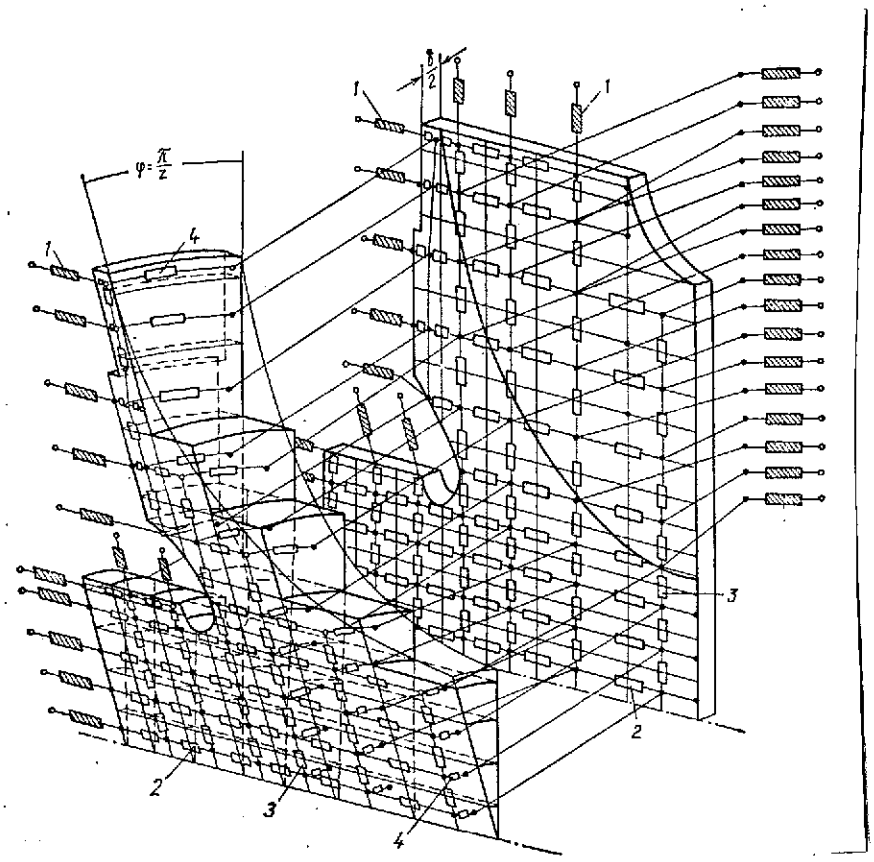


Fig. 60. Schematic diagram of three-dimensional electrical model of rotor of TKR-23-1 turbocompressor:
1. Resistances of network simulating boundary conditions
2. Resistances of network in axial direction
3. Resistances of network in radial direction
4. Resistances of network in tangential direction

Problems arising in solving the thermal conductivity equation for turbine parts using devices of electrical simulation are treated in detail in specialized literature /17, 20, 31, 39, 46, 73, 79, 90, 93/. Therefore below we present only several features of this method used in thermal calculation of air-cooling systems of rotors in centripetal turbines. /104

Most often network and combination electrical models /73, 21/ are used in the thermal calculation of rotor cooling systems in gas turbines. In the latter case, a model of the rotor body is made of electrically conductive paper, and the boundary resistances are variable ohmic resistances. The method of constructing both the first and second kinds of models as applied to turbine rotors is outlined in detail in /21, 73, 93/.

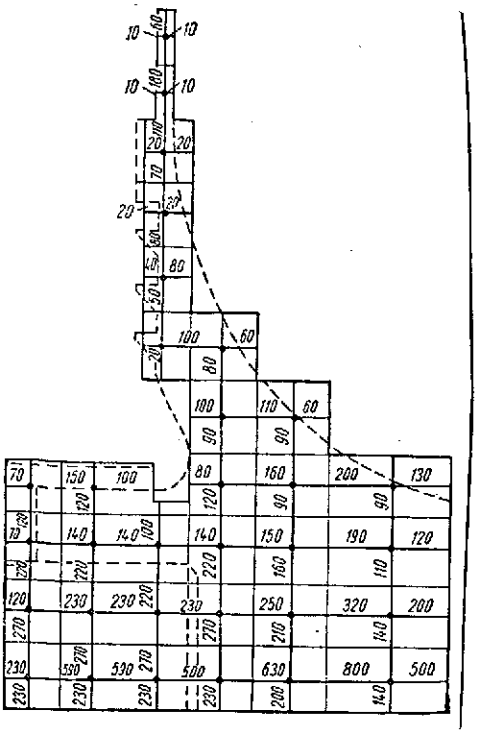

Fig. 61. Schematic diagram of plane electrical model of rotor of TKR-23-1 turbocompressor. The contour of the rotor section is indicated with the dashed line, and the numbers give the electrical resistances of the network.

In the investigations on the thermal calculation of air-cooling systems of rotors in centripetal gas turbines, use was made of electrical network models built on series-produced EI-12 and MSM integrators. The network parameters were calculated based on relations recommended in /21, 44, 93/.

To illustrate, in Fig. 60 is shown a three-dimensional model of a rotor made from two plane models connected at nodal points by the resistances $R_\phi$ proportional to the thermal resistance in the peripheral direction. One of the model components corresponded to the sectoral part of the rotor without blade, while the other refers to the plate whose thickness is equal to half the average thickness of the rotor blade.

Potentials corresponding to the temperatures of the air and gas sweeping the rotor were fed to the boundary points of both models through supplementary resistances inversely proportional to the heat transfer coefficients.

Fig. 61 shows a plane electrical model of the same rotor. Building axisymmetric plane models requires a much smaller volume of the network and is less laborious.

The rotor element was subdivided into blocks in accordance with the recommendations in /17, 79, 93/. The absolute error arising in solving the thermal conductivity problems by a finite-difference approximation was estimated by the function recommended in /39/: /105

$$E = -\frac{\Delta x}{2}\left(\frac{\partial^2 u}{\partial x^2}\right), \quad \text{(IV.28)}$$

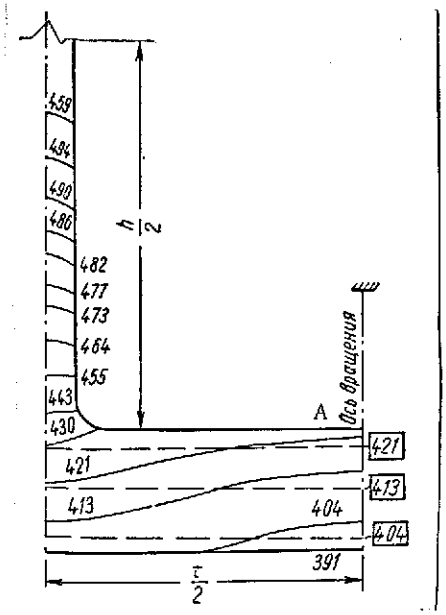


Fig. 62. Results of calculating rotor temperatures with an axisymmetric model
Key: A. Axis of rotation

where $\Delta x/2$ is the spacing of the network over the section of the model for which the error is being determined; $\left|\frac{\partial^2 U}{\partial x^2}\right|$ is the second derivative of the potential /39/,

$$\left|\frac{\partial^2 u}{\partial x^2} = \frac{u_1 - u_2 - 2u_0}{\Delta x^2}\right|; \qquad \text{(IV.29)}$$

$u_1$, $u_2$, and $u_0$ are the values of the potentials at the network points $x_0 - \Delta x$, $x_0 + \Delta x$, and $x_0$, respectively.

Subdividing the element of the rotor being simulated into blocks determines the largest error $E/\dot{u}\cdot 100$ percent, which was $\pm$ 1.65 percent during the present investigations.

The temperature field of the rotor in the centripetal turbine in the general case is three-dimensional; however, one can perform thermal calculations of cooling systems with two-dimensional axisymmetric electrical models with an accuracy suitable for engineering calculations. Here the boundary conditions at the heating side are assigned with allowance for the inflow of heat to the rotor from the rotor blades.

To find whether it is possible to convert from a spatial rotor model to a plane model, the temperature fields determined with these two kinds of models were compared at the ITTF AN UkSSR. Fig. 62 presents the temperature field of a rotor in the meridional section at the relative radius $r/r_1 = 0.76$ calculated for the axisymmetric (dashed lines) and three-dimensional (solid lines) electrical models. As we can see from the figure, the results of calculating the temperatures agree quite closely.

In thermal calculations of air-cooling systems of rotors in centripetal gas turbines, boundary conditions of the third kind are used on the side of the gas and cooling air: the values of the heat transfer coefficients and the temperatures of the corresponding media.

On the side of heat delivery usually local values of the heat transfer coefficients are assigned, calculated according to the criterial relations (III.19) and (III.21) given in Chapter Three. /106

When a film of relatively cold air is present in the rotor blading, instead of the gas temperature along these sections the adiabatic surface temperature is assigned, determined by the so-called effectiveness of film cooling (Eqs. (III.26) and (III.27)).

In all cases, when assigning the boundary conditions on the gas side, one must take into account the variation in gas parameters along the length of the interblade channel of the rotor [59, 92, 99, 108].

The local temperatures and relative gas velocities in the working ducting needed in calculating boundary conditions can be obtained by solving the system of the following main equations [26, 48, 77]:

$$\left.\begin{aligned} &2\frac{k}{k-1}R(T_{g_1}-T_{g_x})=w_{r_x}^2-w_{r_1}^2+u_1^2-u_x^2;\\ &w_{r_x}F_x=G_gV_x;\\ &P_1v_1^m=P_xv_x^m=\text{const}, \end{aligned}\right\} \qquad \text{(IV.30)}$$

where $m=\frac{\lg P_1-\lg P_2}{\lg v_2-\lg v_1}$ is the polytropic index.

The system of equations (IV.30) can be reduced to the relation

$$w_1^2\left[\frac{F_1}{F_x}\left(\frac{T_{r_1}}{T_x}\right)^{\frac{2}{m-1}}-1\right]-\frac{2k}{k-1}R(T_{g_1}-T_x)+(\omega r_1)^2-(\omega r_x)^2=0. \qquad \text{(IV.31)}$$

The results of calculation based on Eq. (IV.31) show that the thermodynamic gas temperature along the rotor radius varies virtually linearly, that is,

$$T_x=T_{g_1}-\frac{T_{g_1}-T_{g_2}}{r_1-r_2}(r_1-r_x). \qquad \text{(IV.32)}$$

The change in the total temperatures along the length of the ducting here can be described by the equation

$$T_{1_w}^*-T_{x_w}^*=\frac{u_1^2-u_x^2}{2\frac{k}{k-1}R}, \qquad \text{(IV.33)}$$

which can be approximated by the following straight line, to an error not more than ± 0.5 percent for turbine rotors of turbocompressors:

$$T^*_{x_w} = T^*_{1_w} - \frac{T^*_{1_w} - T^*_{2_w}}{r_1 - r_2}(r_1 - r_x). \qquad \text{(IV.34)}$$

The relative gas velocity at the midline of the stream in the ducting is

$$w_x = \psi \sqrt{\frac{w_1^2}{2} + C_P(T_{g_1} - T_x) - \pi^2 d_0^2 n^2_{tc}\left(1 - \frac{d_x^2}{d_0^2}\right)}, \qquad \text{(IV.35)}$$

where $d_0$ and $d_x$ are the largest and instantaneous rotor diameters.

The radial component of the relative velocity at the inlet to the ducting here is determined from the parameters at the inlet to the turbine rotor: /107

$$w_{1_r} = \frac{G_g R T_{g_1}}{\rho_1 \pi d_0 h}. \qquad \text{(IV.36)}$$

The temperature of the gas upstream of the nozzle cascade is

$$T_{g_1} = T_0 - \Delta T_{1ad} + \Delta T_I - \Delta T_{II}, \qquad \text{(IV.37)}$$

where $\Delta T_{1ad}$ is the isentropic drop in the nozzle cascade,

$$\Delta T_{1ad} = \rho T_0 \left[1 - \left(\frac{P_2}{P_0}\right)^{\frac{k-1}{k}}\right]; \qquad \text{(IV.37a)}$$

$\rho$ is the turbine reaction; $\Delta T_1$ is the rise in the gas temperature due to irreversible losses in the nozzle cascade,

$$\Delta T_I = \Delta T_{1ad}\left(\frac{1}{\varphi^2} - 1\right); \qquad \text{(IV.37b)}$$

$\Delta T_{II}$ is the drop in gas temperature owing to heat rejection in the nozzle cascade,

$$\Delta T_{II} = \frac{Q_n}{G_g C_P}; \qquad \text{(IV.37c)}$$

$$Q_n = \lambda_{i.a} F \frac{T_{wa} - T_{cor}}{\delta}; \qquad \text{(IV.37d)}$$

F is the surface of the nozzle cascade flange facing the stator; $Q_n$ is the amount of heat rejected to the stator; and $\delta$ is the size of the axial clearance, or the thickness of the heat insulation layer between the nozzle rim and the bearing housing.

In calculations of heat-physical characteristics of the gas flow, one can take the actual gas temperatures in the ducting allowing for heat losses due to employment of cooling as the determining temperatures. In this case the temperature of the gas downstream of the rotor is found by the equation

$$T^*_{g_2} = T^*_{g_0}\left[1 - \left(\frac{P_2}{P_0}\right)^{\frac{k-1}{k}}\right] + \Delta T_I - \frac{Q_I}{G_g C_P} + \Delta T_{III}, \qquad \text{(IV.38)}$$

where $Q_I$ are heat losses due to rejection to the ambient medium; $\Delta T_{III}$ is the drop in the gas temperature upon mixing of cooling air,

$$\Delta T_{III} = T_{g_1} - \frac{g_{i.a} T_{i.a} + G_g T_{g_1}}{G_g + g_{i.a}}. \qquad \text{(IV.38a)}$$

The quantities $Q_I$ and $\Delta T_{III}$ at the present time are not amenable to calculation and must be found experimentally. As shown by tests of the TKR-14-2a and TKR-23-1 turbocompressors tested in the ITTF AN UkSSR, at regimes of 80 and 100 percent power rating the drop in gas temperature due to heat rejection and mixing of cool air is commensurable with the thermal drop induced in the turbine. So as a first approximation, when calculating cooling systems of centripetal turbines that have an air capacity close tothe value considered, we can assume /29/ /108

$$\frac{Q_I}{C_P G_g} + \Delta T_{III} = (0{,}85 - 1{,}05)(T^*_{g_0} - T^*_{g_2}). \qquad \text{(IV.39)}$$

In this equation the larger value of the correction cofactor corresponds to regimes with smaller mass flow of working gas.

The reliability of this approximate approach of calculating temperatures in rotor ducting in accordance with which the change in the temperatures averaged over the orthogonal sections are assumed to be linear from the initial to the terminal radius, this reliability was verified from results of thermometry of rotor blades of the turbocompressors tested.

Since at a thin and long enough rotor blade heat flows along blade length, that is, heat rejection into the disk, are small, the blade temperature is virtually the same as the stagnation temperature of the gas in the duct in the corresponding sections.

Fig. 63 gives the temperature field of an uncooled rotor blade of a TKR-14-2a turbocompressor obtained by calculation using a three-dimensional electrical network model. Boundary conditions of the first kind were assigned on the side of heat rejection (temperatures of disk back surface measured experimentally). This permitted avoiding errors in assigning coefficients of heat transfer from disk to cooling air in final calculation results. Gas temperatures in the ducting were calculated according to Eq. (IV.34) for experimentally known gas temperatures upstream and downstream of the turbine. Also given in this figure are the experimentally measured temperatures of the rotor blade. As Fig. 63 shows, the discrepancy between calculated and experimental data is not more than 6-8 deg for the initial gas temperature upstream of the turbine of the order of 550° C.

Somewhat larger difficulties arise when determining boundary conditions of heat exchange with the back, air-swept, rotor side.

In thermal calculation of air-cooling systems of rotors in centripetal turbines, local heat transfer coefficients are assigned on the disk back side, which in the absence of forced delivery of cooling air to the clearance can be found by the equation /73/

$$\overline{\mathrm{Nu}} = 0{,}0118\,(n + 2{,}6)^{0.2}\,\mathrm{Re}_{\omega}^{0.8}. \qquad \text{(IV.40)}$$

where n is the exponent in the equation determining the distribution of the temperature head over the disk radius ($\Delta T = T_1 - T_2 = cr^n$); usually $n \approx 2$-4, less often n is smaller.

In Eq. (IV.40) the temperature of the air in the clearance is the determining temperature.

To find the local coefficients of heat transfer from disk side surface to air when radial blowoff was used, we can employ the criterial equation recommended in /73/: /109

$$\mathrm{Nu} = 0{,}022\,(1 - z_{\tau})^{0.75}\,\mathrm{Re}_{\omega}^{0.75}\left(\frac{s}{r}\right)^{0.25}. \qquad \text{(IV.41)}$$

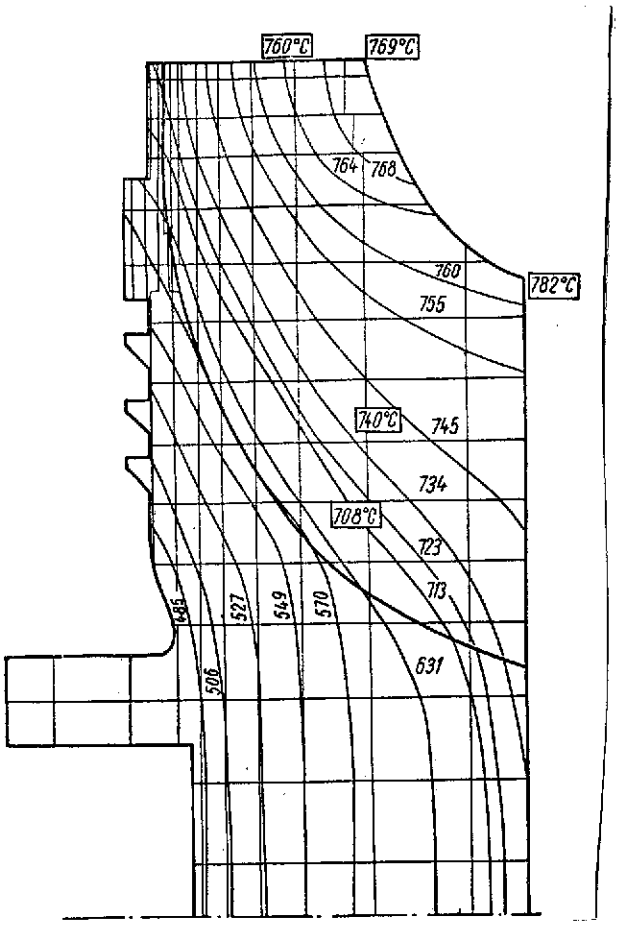


Fig. 63. Temperature field of uncooled rotor blade (the lines correspond to calculations based on the electrical model; experimental temperature values are given in the rectangles).

The twist $z_\phi$ needed for calculations by Eq. (IV.41) at a given radius is found from the recommendations presented in Section 1 of this same chapter (Eqs. (IV.17)-(IV.19)).

The generalized criterial function for determining local coefficients of heat transfer at the disk side surface swept by circular jets uniformly distributed over the periphery and also by continuous and discontinuous annular jets is of the form /73/ /110

$$\overline{\mathrm{Nu}} = [a^{2,5}\,\mathrm{Re}_0^2 + b^{2,5}\,\mathrm{Re}_\omega^2]^{0,4}. \qquad \text{(IV.42)}$$

Over sections larger than the radius R of jet blowoff, for circular jets with diameter d and spacing t and for discontinuous annular jets, we have

$$a = 0{,}22\left(\frac{z_C t}{2\pi R}\right)^{0,7}\left(\frac{x}{d}\cdot\frac{r}{P_1}\right)^{-n}; \qquad \text{(IV.43)}$$

$$n = 0{,}31\exp\left(\frac{0{,}66 z_C t}{2\pi R}\right); \qquad \text{(IV.43a)}$$

$$b = 0{,}022, \qquad \text{(IV.43b)}$$

and for continuous annular jets of height h, we have

$$a = 0{,}22\left(\frac{x}{h}\cdot\frac{r}{R}\right)^{-0,6}; \qquad \text{(IV.44)}$$

$$b = 0{,}022. \qquad \text{(IV.44a)}$$

Over the sections of radius smaller than the jet blowoff radius, we have

$$a = 0{,}22\left(\frac{z_C t}{2\pi R}\right)^{0,7}\left(\frac{x}{d}\right)^{-n}; \qquad \text{(IV.45)}$$

$$n = 0{,}8\left(\frac{z_C t}{2\pi R}\right)^{0{,}15}; \qquad \text{(IV.45a)}$$

$$b = 0{,}022; \qquad \text{(IV.45b)}$$

$$a = 0{,}22\left(\frac{s}{h}\right)^{0{,}4}\left(\frac{x}{h}\right)^{-1{,}1}; \qquad \text{(IV.46)}$$

$$n = 100\left(\frac{x}{h}\right)^{-1{,}15}; \qquad \text{(IV.46a)}$$

$$b = 0{,}022\left(1 + \frac{\mathrm{Re}_0}{\mathrm{Re}_\omega}\right)^{-n}, \qquad \text{(IV.46b)}$$

For $r > R$, $x = r - R$, while for $r < R$, $x = R - r$. For blowoff with a discontinuous annular jet having height h, d in the reduced equations is replaced by h. The limits of the applicability of these equations are indicated in /73/ and cover virtually all cases possible in centripetal turbines.

In Eq. (IV.42), the temperature of air in the axial clearance (mean-mass) at the given radius is the determining temperature.

From the data in /73/, auxiliary radial blowoff of the disk influences only the temperature of the air in the clearance. Therefore when jet-radial disk cooling is used, in the range of $g_{rad}/g_{jet}$ values 0 to 0.63, the coefficients of heat transfer from rotor side surface (below the zone of jet blowoff and above it) to the first approximation must be determined by Eq. (IV.41). In this case over the sections of the radius smaller than the zone of action of the jets, by 10-20 jet diameters, $g_{i.a} = g_{rad}$, while at larger radius sections, $g_{i.a} = g_{rad} + g_{jet}$. /111

Local values of coefficients of heat transfer at the side wall of the turbine casing opposite the rotor side surface can be calculated by the following equation, to the first approximation:

$$\mathrm{Nu} = 0{,}022 z_\Phi^{0{,}75}\mathrm{Re}_\omega^{0{,}75}\left(\frac{s}{r}\right)^{0{,}25}, \qquad \text{(IV.47)}$$

in which the twist of the flow $z_\phi$ is determined by the recommendations given in Section 1 of this same chapter (Eqs. (IV.17) and (IV.19)).

In assigning the boundary conditions of heat transfer at the rotor surface facing the casing, special attention must be given to finding the mean-mass temperature of the medium in the axial clearance. Here the following must be taken into account: heat delivery to medium from rotor side surface; delivery (or removal) of heat to medium (or from it) at the casing surface opposite the rotor side surface; and the possibility of the arrival into the axial clearance of a certain amount of heated gas from the blading due to the pump effect.

In the latter case, the amount of suction gas is determined by the recommendations given in Section 1 of this chapter, while its temperature at the outer radius of the clearance can be assumed to be equal to the thermodynamic temperature of the gas in the near-wall section of the clearance between the nozzle vanes. The temperature of the gas sucked into the clearance at the other radii is determined both with allowance for its displacement with the medium flowing from center to periphery, as well as with allowance for heat transferred from it to the turbine casing.

Therefore, for a sufficiently precise thermal calculation of the cooling system of a rotor in a centripetal turbine, we must specify or else determine, by additional calculation, the temperature of the surface of the turbine casing facing the rotor back side.

## 3. Examples of Calculations

To illustrate the main principles of the above-outlined calculation method and to test it with experimental data, below are given some results of calculations of cooling systems of turbocompressors tested in the ITTF AN UkSSR. These calculations were conducted in the course of appropriate investigations, and not during the preparation of the manuscript of this book. They show some discrepancies from the recommendations of the preceding sections. These discrepancies, due for the most part to the appearance in recent years of more advanced and less laborious methods of solving individual problems, are not of fundamental importance. This is also true of the volume of calculations, which as a rule were much smaller, for several organizational reasons, than is regarded as necessary at the present time.

In the TKR-14-2a turbocompressor cooling air (see Fig. 7) is bled from the outlet section of the vaneless diffuser of a centrifugal pump, delivered through axial and radial passages in the casing to the rotor back side of the turbine, and then through the slit between the outer rim of the rotor and the flange of the nozzle box -- to the blading. Leakage of air to the bearing case is possible through the axial labyrinth. /112

The following data were used in the hydraulic calculation and in determining the mass flow of cooling air: pressure and temperature at inlet to intake pipe (passage); pressure in clearance between nozzle boxes and rotor; and air pressure in turbocompressor casing.

In this case the hydraulic calculation of the cooling system was based on the analytical-graphical methods. Essentially, it

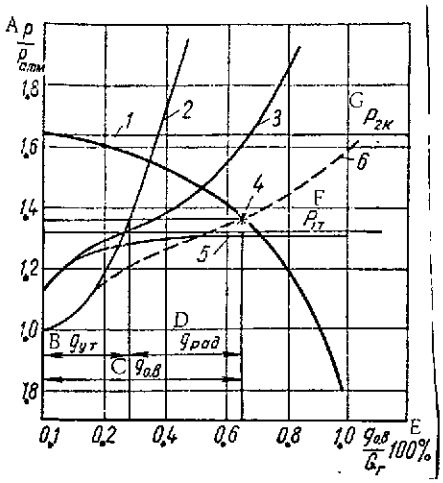


Fig. 64. Results of hydraulic calculation of rotor cooling system in a centripetal turbine by the analytical-graphical method:

1. Characteristic of delivery branch, $P_{nod}/P_{atm} = f(G_{i.a})$
2. Characteristics of first discharge branch (axial labyrinth seal), $P_{nod}/P_{atm} = f(G_{se})$
3. Characteristics of second discharge branch (clearance between disk and casing wall), $P_{nod}/P_{atm} = f(g_{rad})$
4. Working point
5. Variation in pressure drops due to centrifugal forces in clearance between disk and casing wall as a function of mass flows of cooling air in clearance, $P_{cf} = f(g_{i.a})$
6. Overall characteristic of discharge branches, $P_{nod}/P_{atm} = f(G_{i.a})$

Key: A. $P/P_{atm}$; B. $g_{nod.pt}$ /nod.pt = nodal point/ C. $g_{i.a}$; D. $r_{rad}$ E. $g_{i.a}/G_g$; F. $P_{1t}$ G. $P_{2c}$

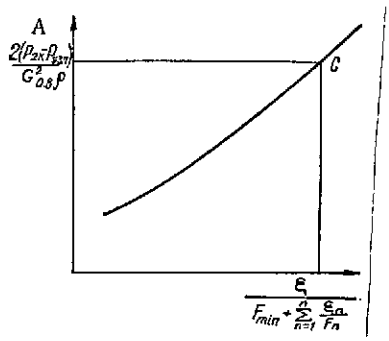


Fig. 65. Pressure losses in branch as function of overall coefficient of hydraulic drag

Key: A. $\frac{2(P_{2c} - P_{nod})}{G^3_{i.a}\rho}$

reduces to calculating the flow in a tee-piece with a nodal point (point of branching of flows) in the so-called seal chamber -- -- at rotor hub (see Fig. 7). Hydraulic characteristics of individual branches of the ducting were determined according to the recommendations given in Section 1 of this chapter (Eqs. (IV.2), (IV.7), and (IV.8)). This made it possible to plot the function $g_{i.a\ i} = f(P_{nod})$ (Fig. 64). Combined solutions of the equations graphically linking mass flow in inflow and discharge branches with pressure at nodal point are represented by the point of intersection of the consolidated curves for the inflow and discharge branches (point 4). By this point the overall mass flow of cooling air in the cooling system is determined. Mass

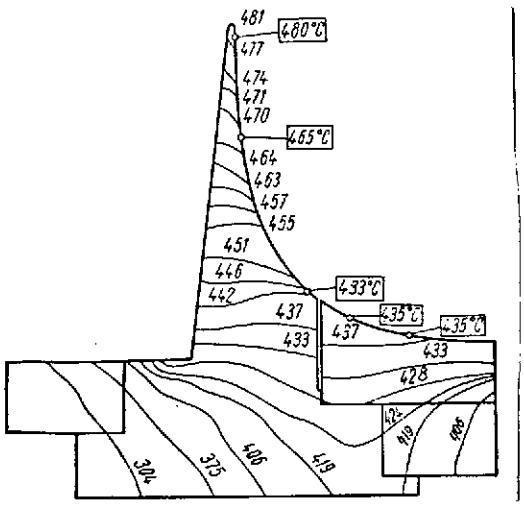


Fig. 66. Temperature field of rotor of TKR-40 turbocompressor at the 80 percent power regime (lines correspond to calculation with electrical model; experimental temperatures are given in boxes)

flows of air along the discharge branches of the cooling line were determined by the points with ordinate $P_{nod}/P_{atm}$ at the corresponding curves. /113

Above we examined the inverse problem in which, from known initial and final air parameters and geometrical characteristics of the ducting, we were required to find the mass flows of cooling air.

Let us examine a specific case (a tee-piece with a single inflow and two discharges) of the solution of the direct problem, when from the mass flow of cooling air known from thermal calculation and initial and terminal air parameters we are required to determine the flow-through sections of the ducting. Here the configuration of the ducting, and its general design data are assumed to have already been chosen. By calculating and graphically representing the hydraulic drag values as functions of mass flows for the discharge branches and by plotting the overall characteristic for the discharges

$$P_{nod} = f\left(\sum_{1}^{n} g_i\right)$$

from the overall mass flow of cooling air

$$G_{i.a} = g_{i.a} + g_{se}, \qquad \text{(IV.48)}$$

let us find the calculated point $(P_{nod}, G_{i.a})$. Here the drag of the inflow branch is determined from the equation

$$\sum_{1}^{n} \frac{\xi_n}{F_n^2} = \frac{2(P_{2c}^{*} - P_{nod}^{*})}{G_{i.a}^2 \rho}. \qquad \text{(IV.49)}$$

Since the inflow branch is a series of successively connected hydraulic drags, then by assigning the ducting sections $F_n$ as appropriate for the design overall and determining for them, in accordance with /35/, the coefficients of hydraulic drags $\xi$, let

us find the overall drag of the branch as a function of the area of the smallest cross section in the ducting. Fig. 65 also shows this quantity as a function of the dimensions of the determining cross section producing the highest drag in the line. The dimensions of this section are determined after plotting point C with ordinate $\frac{2(P_{2C}-P_{nod})}{G^2_{i.a}\rho}$. on the curve. If the section of the entire ducting is constant, the solution of Eq. (IV.49) is unique: /114

$$F=\sqrt{\frac{\sum_1^n \xi G^2_{i.a}\rho}{2(P^*_{2C}-P^*_{nod})}} \qquad \text{(IV.50)}$$

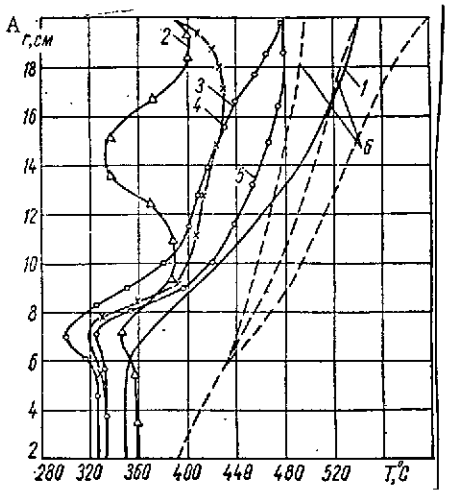


Fig. 67. Mean temperatures over thickness of disk in TKR-40 turbocompressor, in full-power regime, as functions of various cooling methods:

1. Jet cooling through system of concentrically arranged openings in deflector, $\bar{g}_{i.a}$ = = 0.20 percent
2. As above, with $\bar{g}_{i.a}$ = 2.24 percent
3. Radial blowoff
4. Film cooling
5. Shielded cooling with gas leakage, $\bar{g}_{i.a}$ = 0.3 percent
6. Optimal distribution of disk temperatures

Key: A. r,cm

When solving either the direct or the inverse problem, we must allow for the deviations in the dimensions of the flow-through sections of the elements of the cooling line that are possible during manufacture or service, compared to the rated values. In this case the calculation is performed for the largest and smallest flow-through sections. Graphically, a characteristic of each cooling duct branch will be represented by two curves.

Since the results of testing cooling systems of the TKR-14-2a turbocompressor were used in revising the regularities of heat transfer at the gas and air sides for rotor film cooling, their verification was based on results of experiments on the TKR-23-1 and TKR-40 turbocompressors.

Fig. 57 shows the temperature field of a rotor in a TKR-23-1 turbocompressor in the "control" regime close

to the rated regime. The mass flow of cooling air is determined experimentally and is 0.013 kg/sec. This mass flow of cooling air permitted a curtain to be produced in the rotor ducting. Allowing for the film cooling effect was done in accordance with the above-presented method. The divergence of calculated and experimental values averaged 4-4.6 percent of the difference between the gas temperature and the cooling air temperature.

Results of calculating the temperature field of the TKR-40 turbocompressor when jet blowoff was present are shown in Fig. 66. The calculation was based on the 80 percent power regime at which the mass flow of cooling air determined in the hydraulic calculation was 0.0194 kg/sec (0.45 percent $G_{g.rat}$). Part of the cooling air (0.00482 kg/sec) flowed through the axial labyrinth seal into /115 the compressor part of the engine. As is clear from Fig. 66, heat flows to the rotor faces, compressor impeller, and turbine bearing proved to be the most intense. This pattern of the temperature field was due largely to the design features of this particular turbocompressor (see Fig. 9).

The presence of the clearance between the main part of the turbine rotor and the inset hub of the straightening cascade (HSC) led to some heating (by 30-35° C) of the latter, even without allowing for the thermal resistance at the point of mating of the HSC hub and the rotor shaft. As follows from Fig. 66, rotor temperatures measured in the experiment exceeded calculated values by no more than 12 deg. In this case the film cooling effect proved insufficient owing to gas being sucked from the blading, and the amount of this gas at the outer radius was more than 2.5 times (0.0682 kg/sec) than the mass flow of air fed for cooling. So allowing for the film cooling effect in this case is not mandatory.

As shown by the results of the studies, the above-outlined approximate method of calculating rotor cooling systems in centripetal gas turbines enables us, with sufficient reliability, not merely to determine the temperature field of an existing turbine, but also to select the cooling system and its operating regime that ensure the desired (from strength considerations) disk temperature field. As an example, in Fig. 67 are presented the results of these calculations for the rotor of a TKR-40 turbocompressor in the full-power regime for various cooling methods. Also given in this figure are curves 6, determining the temperature field that is optimal from strength requirements. As we can see from the figure, only curves 1 and 5 satisfy the desired distribution of temperatures averaged over disk thickness with inaccuracy sufficient for practical uses[9].

---

[9] In this rotor the temperature drops over disk thickness most strongly affect the stressed state and strength.

# CHAPTER FIVE

## STRESSED STATE AND STRENGTH OF ROTORS OF CENTRIPETAL TURBINES AND OF CENTRIFUGAL COMPRESSORS WHEN ACTED ON BY CENTRIFUGAL FORCES

### 1. Background on the Stressed State of Rotors of Radial Turbo-Machines

Selection of the alloy for fabricating a unit-cast or unit-milled rotor of a centripetal turbine is determined by the temperature of the blade metal that is not specifically cooled. The temperature of this blade is usually somewhat lower than the gas sweeping it owing to the removal of heat into the cooled disk. The temperature of the latter depends to a greater extent on the method of cooling and the operating regime of the cooling system employed in the turbine. Cooling systems of the TKR-23-1 and TKR-14-2a turbocompressors provide the maximum disk temperature that is 150 deg below the initial gas temperature upstream of the turbine, while the mean disk temperature is 250 deg below the initial gas temperature upstream of the turbine.

Locomotive diesels with gas turbine supercharging operate for much of their service life under variable load regimes. On the average, the turbocompressor operates with a gas temperature of 570-600°C, and with rated rpm levels for not more than 20% of its service life. The rest of the time the load and rotor temperature are much lower than in the rated regime.

The temperature and stress fields in the turbine rotors of the TKR-14-2a and TKR-23-1 turbocompressors made of austenite steel EI-572L are such that in service conditions substantial creep of metal must not be anticipated. The absence of marked creep of rotors in service is confirmed also by the results of inspecting turbocompressors after different accrued operating times. It can be assumed that these rotors operate in the regime of elastic, and possibly, low elastico-plastic stresses without appreciable residual deformations overall for considerable time intervals.

As indicated, these turbocompressors operate mainly in conditions of nonsteady thermal stresses arising in frequent starts and stops of the engine. Therefore when devising methods of calculating thermal stresses in rotors of centripetal turbines and estimating their strength, one must take into account the action of nonsteady temperature regimes. In several cases temperature stresses not in steady turbine operating conditions, but in variable turbine service regimes pose the main danger to the strength of turbine rotors.

Plastic deformations set in earlier in a rotor loaded with centrifugal forces and temperature stresses, that is, at smaller rotor rpm than in a rotor present in isothermal conditions, but the relative influence of thermal stresses decreases with increase in load from centrifugal forces [38, 67]. Therefore, during short bursts of rpm increase the effect of thermal stresses can be insubstantial. This factor is vital in estimating the effect of temperature stresses of a steady kind on the short-term (time-independent) static strength of rotors of turbocompressors in service conditions. /117

Temperature fatigue of metal caused by heat-cyclic loading can in several cases lead not only to the appearance in turbine rotors of thermal cracks in the action zone of maximum tensile stresses, but also appreciably below the static strength of the rotor owing to the unfavorable action of low-cycle fatigue on metal strength.

Owing to the foregoing, when carrying out the present investigations, the emphasis was placed on studying short-term static strength of disks acted on by centrifugal forces and their resistance to thermal fatigue in nonsteady thermal loading.

Behavior during failure and not during working load is decisive for designing. Therefore the allowable working load must be determined with respect to the failure load. Breakdown of an element of a structure is associated either with excessive inelastic strain or with failure. As a rule, failure is always preceded by general or local plastic strain of the metal: the failure load for a stable design is due to the plastic yield load. Realization of this principle for semishrouded rotors of radial turbo-machines is hindered by the fact that thus far the problem of design determination of stresses in a rotor in the elastico-plastic and plastic stages of metal performance has not been solved. So in design practice one has to use the results of calculating the elastic stresses arising in a part in order to determine its bearing capacity.

Analysis of methods of calculating elastic stresses in semishrouded rotors of radial turbo-machines published in the literature afford the conclusion that methods in which a one-sided rotor is regarded as a design-orthotropic disk without symmetry plane and where the algorithm for solving the fundamental equations suitable for existing computers are promising techniques. In this study, the method described in [56] was used for calculating on a computer stresses in semishrouded rotors with radial or slightly twisted blades.

A theoretical analysis of the strains in an actual rotor and its comparison with the scheme of deformation of a design-orthotropic disk shows several important features of the design schematization of the natural rotor. In the transition to the

plastic state of strain the rotor can behave differently, depending /118
on the kind of strains in the material, its ability to become strengthened, and the redistribution of stresses resulting from plastic strain.

Tip nonuniformity of rotor strain strongly increases the importance of radial stresses when determining the strength of a natural rotor, compared to what is given by a calculated analysis based on a scheme of a design-orthotropic disk. If the rotor material has adequately high plasticity preventing the premature buildup of local plastic strains in zones between blades, the effect of plastic strain on equalizing the stresses is shown not only in the radial, but also the peripheral directions. As a result, stresses equalized over the periphery correspond more closely to the axial symmetry adopted in rotor schematization than the stresses differing from each other along and between the blades in the elastic calculations for which this schematization was carried out. This factor, with reference to the slight redistribution of radial stresses along rotor radius in the plastic stage, enables us to determine the yield stresses in the rotors all the way up to their failure based on calculating elastic stresses in the design-orthotropic disk.

Radial stresses are determining for solid turbine rotors, while peripheral stresses at the bore are decisive for compressor rotors [impellers] with central bore. Since for a plastic material in the elastico-plastic stage of rotor strain the peripheral stresses in the disk are substantial, while the radial stresses are very slightly redistributed along the radius, even for rotors with central bore radial stresses can be at yield values.

If the rotor material is incapable in the early stages of plastic deformation of withstanding the buildup of local strains along the periphery, the perturbing action of discrete blades leads to the premature, compared with the outcome predicted from calculating the design-orthotropic disk, failure of an actual rotor. Here increasing the number of blades in a rotor can have an undesirable effect: it can lower its strength and the accuracy of determining the failure number of revolutions. In the general case calculating yield stresses in the rotor must be done with reference to the perturbing action of blades.

## 2. Survey of Methods of Stress Calculation

In calculating stresses due to centrifugal forces in a disk and the blades of a rotor in a centripetal turbine (with radial blades), three main methods are used in the design schematization of an actual rotor in the elastic stage of deformation.

The first method is the so-called method of attached blade mass. Here the rotor is viewed as a symmetrical disk with a radius-variable specific weight of metal, blade stiffness is not considered, while blade mass is assumed uniformly distributed along rotor periphery at the appropriate radii. /119

The second method of calculation is based on rotor schematization in the form of a symmetric disk with the presence on the disk of a layer formed by the blades. Here the tensile strains are taken into account not only in the disk, but also in the blades. This method of schematization is inappropriate for calculating thermal stresses since it is impossible to take into account the actual difference in temperatures along the rotor axis caused mainly by the difference between the disk and blade temperatures.

Under the third method, the turbine rotor is schematized in the form of a design-orthotropic disk without a symmetry plane. In this case tensile and flexural strains of the disk and the blades are taken into account.

The discreteness of application of loading from blade to disk characteristic of actual rotors is not taken into account in any of the calculation methods indicated. The "exact" solution of the problem, consisting in satisfying the conditions of plate and fillet contact [8, 88], involves major difficulties.

The first method, whose basis is the simplest and least plausible assumption that the blades only load the disk operating in tension (even if the rotor is one-sided) was proposed as early as 1936 in [83].

At the present time studies have appeared [2, 27, 28, 36, 119] that essentially indicate the total inapplicability for turbine-building practice of viewing blades as an attached mass.

The second group of calculation methods, based on allowing for the effect of blade stiffness on disk tension in the case when flexion of the axisymmetric rotor is neglected includes a large number of studies differing mainly by the method of solving the primary starting equations [3, 13, 82]. At the present time, owing to the use of computers the methods of the second group do not correspond to the present level of turbo-machine design; however, 10-15 years ago these calculation methods in plant practice promoted higher reliability for rotors of radial turbo-machines.

All methods of the third group are based on schematization of an actual one-sided rotor in the form of a design-orthotropic disk without a symmetry plane.

The disk is viewed as a slightly twisted plate with radially disposed ribbing -- blades. The blades are calculated by the rod calculation scheme; edge flare was neglected.

When the number of blades $z \geq 10$-12, the problem was regarded as axisymmetric.

In the third-group methods the following two hypotheses of plate and shell theory were used:

1) cylindrical sections of an unloaded disk in axisymmetric loading become conical (so-called hypothesis of plane sections or untwisted normals);

2) normal stresses in sections perpendicular to the rotor axis of rotation are negligibly small compared with the normal stresses in the cylindrical and radial sections. /120

Among the studies in subgroup 1 examining jointly flexion and tension of a rotor without assuming an arbitrary or hypothetical assumptions on the arrangement of the neutral rotor surface (the surface with zero flexural stresses) are included, for example, the studies [27, 36, 119]. In [87] dealing with calculating the blades of centripetal turbines, they are regarded as plates rigidly inserted into the disk.

In the studies [2, 94, 95, 105] are examples of the method in subgroup 2, in which the stresses in the rotor due to flexion and tension are determined separately.

The ideas of the method outlined in [36] will be clear from the below-presented calculation technique. In [27] the same calculation scheme is used as in [36]. Along with allowing for the nonuniform heating of the rotor, the former method also takes into account the change in the elastic characteristics of the material over disk thickness and radius. The problem is solved in force terms. The method of successive approximations is used in solving the basic integral equations.

In the method [94, 95] of separate determination of flexural and tensile stresses in semishrouded rotors, the problem's solution reduces to solving linear equations for $\sigma_r$ and $\sigma_\phi$ like those that were used for axial turbo-machines. As indicated in [95], this calculation method does not differ formally from the method of calculating the disk of an axial turbo-machine. The only difference is that the coefficients $\alpha_r$, $\alpha_t$, $\alpha_C$, $\beta_r$, $\beta_\phi$, and $\beta_C$ in the equation

$$\left.\begin{aligned} \sigma_r &= \alpha_r \sigma_{r_0} + \alpha_\varphi \sigma_{\varphi_0} + \alpha_C T_C; \\ \sigma_t &= \beta_r \sigma_{r_0} + \beta_\varphi \sigma_{\varphi_0} + \beta_C T_C \end{aligned}\right\} \qquad \begin{aligned} &\text{(V.1)} \\ &\text{(V.2)} \end{aligned}$$

for disk tension are calculated by formulas differing from the formulas for disks of axial turbo-machines. The coefficients in

these equations were calculated in advance and the appropriate plots were constructed from them [94, 95].

A similar method and procedures were used in [95] also in determining stresses arising from flexion of a disk, where in [95] the validity of applying the hypothesis of untwisted normals, the soundness of finding the position of the neutral surface, and allowing for stiffness characteristics in rotors were verified by strain gauge measurements. Here, the geometrical locus of points where radial displacements during bending were equal to zero, that is, the neutral surface, was found from the peripheral strains measured at the side surfaces of the rotor and along the inner diameter of the hub.

The results of investigating bending of rotors and a plate with different stiffness characteristics confirmed the soundness of the hypothesis that the normals were untwisted and made it possible to propose a simple method of finding the neutral surface. In particular, this made is possible to bypass the necessity of /121
using the highly arbitrary boundary condition at the site of blade transition into hub.

Since the magnitudes of the calculated and experimental stresses were in satisfactory accord, in [95] it was concluded that the method of calculating rotor stiffness during bending bears practical suitability.

One of the advantages of the method of calculating stresses in semishrouded rotors outlined in [95] is its suitability for manual computation. In this respect it differs advantageously from other methods in the third group. However, the formulation of the problem of finding the neutral surface of the rotor is less correct than in [27, 36], and this represents a disadvantage of this method.

## 3. Main Premises of the Method of Calculating Stresses in Rotors Using Computers

Rotors of a centripetal turbine and a centrifugal compressor have considerable asymmetry, which inevitably causes bending of the disk and blades. Therefore in their calculation one must consider the interaction of disk and the blade in the case of tension and of bending.

Let us dwell in more detail on the features of the effect of blades on rotor strength and selection of material for blade manufacturing.

During rotor loading, owing to the presence in the rotor of blades, discrete forces are induced, conveying perturbations into the stresses and strains determined without allowance for the

actual interaction of blades and disk. In the region of elastic deformations the perturbing forces of the blades lead to the initiation of stresses that are variable over the disk periphery. If the local stresses here exceed the creep limit, plastic strain arises "relieving" the stress peak and equalizing the stresses along the periphery. Measured residual elongations of a rotor along its blades in this case proved to be smaller than between the blades. The higher the availability of the rotor material to redistribute the stresses resulting from plastic strains, the lower the influence on rotor strength exerted by the perturbing action of blades. In the ideal case in plastic strain a kind of actual "smearing out" of the blades over the disk takes place in accordance with the assumptions of the method of calculating the actual rotor as a design-orthotropic disk without a symmetry plane.

Thus, realization of the scheme of a design-orthotropic disk when an actual rotor is being deformed corresponds more closely to the elastico-plastic and plastic stages of metal functioning than to the purely elastic stage.

It should be noted that the strain of a rotor along the periphery is complex owing to the cyclic symmetry of the stiffness rotor characteristics and the forces acting on the rotor and this strain is complicated by structural inhomogeneity and inhomogeneity /122
in the properties of the metal along the disk.

The effect of blade spacing t on the stress state of a disk is contradictory. On the one hand, the smaller the blade spacing, the smaller must be the difference of displacements along the blade and between them $\Delta u_i$, since the action of the blade on the metal disk span rises, while their action along the radii of application remains the same. In the elastic stage of performance of the rotor material, one can regard as valid the conclusion drawn in [72, 85, 119] to the effect that the more numerous the blades in the rotor, the closer to reality are the stress calculations based on assuming rotor axial symmetry. However, one cannot use as the characteristic parameter only the number of blades, since in this case one omits from consideration such a most important design factor as blade spacing (or some other more suitable characteristic that is proportionally dependent on spacing). For example, the ratio $z/D_c$ including the number of blades and diameter is a suitable characteristic.

In the elastico-plastic and plastic stages of the functioning of rotor metal, the effect of blade spacing and rotor strength becomes more involved because to the positive influence of small spacings in added their adverse effect on the nature of plastic strain: owing to an increase in nonuniformity of strain within a spacing localization of strain intensifies.

For small spacings, the quantity $\delta u_i = \Delta u_1/t$ will increase until the denominator diminishes faster than the numerator with increasing z.

Large values of $\delta u_i$ for small spacings lead to greater localization of plastic strains, which lowers the rotor strength when the metal had inadequate capacity to become strengthened and redistribute stresses in conditions of high stress gradient along the spacing.

Since for the rotors investigated a relatively high peripheral stress nonuniformity is typical, the metal for rotor manufacture must exhibit the ability to become strenghtened with increase in its plastic deforming. In rotors made from a metal incapable of becoming strenghtened, nonuniformity of strains in the elastic region will become more aggravated as the loading builds up by the ever-mounting localization of plastic strain at the weak points with subsequent failure of the rotor at relatively low rotor rotative velocity. The lower the ability of the metal to become strengthened, the less the volume of the metal involved in resisting strain and failure. In [64] it is shown that the ability of a metal to become strengthened not only during tension, but also in a complex stressed state is characterized by the uniform elongation of the metal during tension $\delta$. Most important for the metal used in semishrouded rotors of radial turbomachines is the requirement of high uniform elongation of the specimen when in tensile testing. Under otherwise equal conditions /123 a larger $\delta$ is needed for rotors with a larger number of blades. The requirement of the high ability to become strengthened is a necessary condition, but of itself it does not yet ensure that the metal has the ability to implement this property optimally for a given stiffness of the stressed state of the rotor. This realization will be carried out if the specimen strain curve during tensile tests will be gently sloping, and $\sigma_{0.2}/\sigma_B$ will be less than some critical value that depends on the ratio of the principal stresses in the rotor [69].

Selecting the method of calculating stresses in rotors and the calculation scheme must be based on allowing for the effect of blades on rotor stressed state. It is particularly necessary to allow for the perturbing action of blades for the elastico-plastic and plastic stages of rotor metal deformation. Therefore below we present initially the method of calculating stresses in rotors in the elastic stage of metal functioning. Here the rotor is schematized as a design-orthotropic disk without a symmetry plane. Then we set forth the method and results of the experimental investigation of rotor strength and, finally, we examine the method of calculating yield stresses in an actual rotor based on the results of "elastic" calculation of the design-orthotropic disk and the calculation-experimental determination of the perturbing action of blades during plastic deformation.

The ratio $(\varepsilon_\phi/\varepsilon_r)_{a.d} = [(u/r)/(du/dr)] = B$ (where $u$ is the radial displacement of an actual disk along the radius $r$) can be used as a characteristic of the blade perturbing effect [16].

To determine B, we used a unique modification of the method of two disk calculations: with zero and with calculated orthotropic layers, let us assume that the calculated orthotropic layer is conventionally formed of two parts: "smeared-out weightless blades" with stiffness ensuring deforming of the actual disk as the design-orthotropic disk (with preservation of nontwisting status of normals and other hypotheses), and "smeared-out material blades," whose stiffness is equal to the difference between the total stiffness of the blades of the schematized rotor and the stiffness of the weightless blades.

Let us denote the relative elongations of rotor with weightless blades (with orthotropic layer of zero thickness) by $\varepsilon_{\phi_d}$ and $\varepsilon_{r_d}$, and the relative elongations of a blade involving the calculated orthotropic layer -- by $\varepsilon_{\phi_c}$ and $\varepsilon_{r_c}$. The ratio $(\varepsilon_{\phi_c} - \varepsilon_{\phi_d})/(\varepsilon_{r_c} - \varepsilon_{r_d})$ can be represented as $\varepsilon_\phi/\varepsilon_r$ due to the "smeared-out material blades." If in the $\varepsilon_{\phi_c}/\varepsilon_{r_c}$ ratio we allow for the effect of the thickness of the "smeared" layer," we get the ratio $(\varepsilon_{\phi_c}/\varepsilon_{r_c})_{a.d}$, which then is the first approximation for determining the relative tip and radial elongations in the disk of /124
and actual rotor:

$$B = \frac{\varepsilon_{\phi_c}}{\varepsilon_{r_c}} - \frac{\varepsilon_{\phi_c} - \varepsilon_{\phi d}}{\varepsilon_{r_c} - \varepsilon_{r_d}} \qquad (V.3)$$

Let us express B in terms of stresses obtained from two calculations,

$$B = \frac{\sigma_{\varphi_c} - \mu\sigma_{r_c}}{\sigma_{r_c} - \mu\sigma_{\varphi_c}} \cdot \frac{(\sigma_{\varphi_d} - \mu\sigma_{r_d}) - (\sigma_{\varphi_c} - \mu\sigma_{r_c})}{(\sigma_{r_d} - \mu\sigma_{\varphi_d}) - (\sigma_{r_c} - \mu\sigma_{\varphi_c})}. \qquad (V.4)$$

Eq. (V.4) is suitable for the calculated estimate of the perturbing action of blades. Use of B in the calculations is dictated by the following restrictions: when $\sigma r_c \leq \mu\sigma_{\phi_c}$ and $(\sigma r_d - \sigma r_c) \leq (\sigma_{\phi_d} - \sigma_{\phi_c})$, the value of B is not determined, that is, in the calculations we exclude the appearance of its negative values close to the rotor edges, and the possibility of the denominators being equal to zero and we also do not consider the effect of the perturbing action of blades in zones where the influence of radial stresses in rotor strength is so diminished that the correction for them is insubstantial.

In 1962, a program for calculating stresses in centripetal turbines using a computer was drawn up and tested [14]. Since 1963 calculations based on this program have been carried out in the Urals University imeni A.M. Gor'kiy. They are used for design investigations of the stressed state of rotors in centripetal turbines and for practical designing of rotors of turbocompressors.

In this program, calculations are conducted for the projection of the blade (without allowing for flare of edges) on the assumption that the blade thickness is variable only along the radius; the blade thickness is averaged in the axial direction for each radius.

Stresses due to tension and flexion are calculated jointly and are found as the overall radial and tangential stresses at the points $z_1$, $z_2$, $z_3$, and $z_0$ of the disk sections (Fig. 68). The finite-difference method is used in solving the main equations. Hypotheses of plate and shell theory are used in the calculation. Under the first hypothesis, cylindrical sections of an unloaded disk in the case of axisymmetric loading become conical (hypothesis of plane sections). Under the second hypothesis, normal stresses in sections perpendicular to the axis of rotation are negligibly small compared with stresses in the cylindrical and radial sections. The discreteness of the inertial and temperature loading caused by blades is not taken into account in the program.

The modulus of elasticity and Poisson's ratio are assumed constant and are selected based on the mean rotor temperature in the rated regime. The network method of calculating stresses in a centripetal turbine was proposed in [36] (in the presentation of this method outlined below, the specific features of computer use are taken into account).

Using the hypothesis of plane sections, we assume that the deformation in the disk section consists of the purely radial displacement u and rotation about some fixed point z with angle $\vartheta$. /125
In this case strain at any point of the disk section can be written as

$$\zeta = u + \vartheta (z_0 - z). \qquad (V.5)$$

The relation between u and $\vartheta$, as we can see from Eq. (V.5), depends on selection of coordinate $z_0$. If plastic strain is inevitable, which often is the case for nonsteady thermal loading, and if the region of plastic strain is small, then the characteristics of the stressed state in it very weakly affect the

stressed state in the rest of the rotor. Therefore we can make an elastic calculation, assuming it to be conditional in the region of plastic strain.

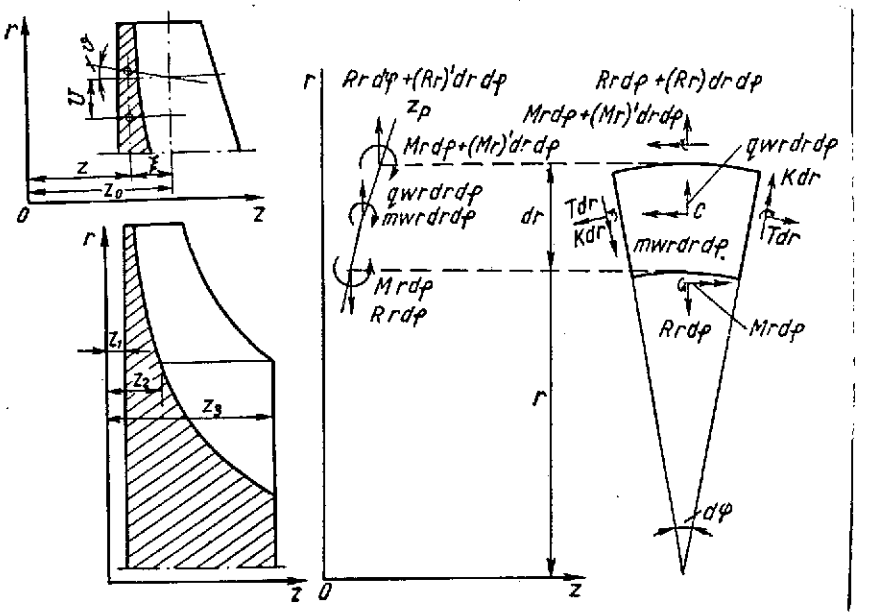


Fig. 68. Scheme for calculating stresses and displacements in design-orthotropic disk.

In the elastic state, deformation is caused by stresses obeying Hooke's law, which as applied to the disk can be given in the form:

$$\left.\begin{aligned}
\sigma_r &= \frac{E}{1-\mu^2}\left(\frac{d\zeta}{dr}+\mu\frac{\zeta}{r}\right)-\frac{E}{1-\mu}\alpha T_d;\\
\sigma_t &= \frac{E}{1-\mu^2}\left(\frac{\zeta}{r}+\mu\frac{d\zeta}{dr}\right)-\frac{E}{1-\mu}\alpha T_d;\\
\sigma_{rb} &= E\frac{d\zeta}{dr}-E\alpha T_d,
\end{aligned}\right\} \qquad (V.6)$$

where $\sigma_{r_b}$ are radial stresses in blade.

Introducing Eq. (V.5) into Eq. (V.6), we get the final expressions for stresses in the disk: /126

$$\left.\begin{aligned}
&\sigma_r = \frac{E}{1-\mu^2}\left[u' + \vartheta(z_0' - z) + \vartheta z_0' + \frac{\mu u}{r} + \frac{\mu\vartheta(z_0 - z)}{r}\right] - \\
&- \frac{E}{1-\mu} aT_d; \\
&\sigma_\varphi = \frac{E}{1-\mu^2}\left[\mu u' + \mu\vartheta(z_0 - z) + \mu\vartheta z_0' + \frac{u}{r} + \vartheta\frac{z_0 - z}{r}\right] - \\
&- \frac{E}{1-\mu} aT_d; \\
&\sigma_{r_b} = E[u' + \vartheta(z_0 - z) + \vartheta z_0'] - EaT_d.
\end{aligned}\right\} \qquad (V.7)$$

The derivatives with respect to the radius denoted with the stroke are taken for a fixed chord at z, therefore z' = 0. Let us determine the forces and moments acting in the disk sections. The radial force in the peripheral section of the disk, per unit peripheral length, is

$$R = \frac{1}{2\pi r}\int_{F_d} \sigma_r dF + \frac{1}{2\pi r}\int_{F_b} \sigma_b dF. \qquad (V.8)$$

The moment relative to coordinate $z_0$ effective in the peripheral section of the disk, given per unit peripheral length, is

$$M = \frac{1}{2\pi r}\int_{F_d} \sigma_r (z_0 - z)\, dF + \frac{1}{2\pi r}\int_{F_b} \sigma_b (z_0 - z)\, dF. \qquad (V.9)$$

The tangential force in the radial section given per unit radius length is

$$T = \int_{z_d} \sigma_\varphi dz. \qquad (V.10)$$

The tangential moment in the radius section given per unit radius length is

$$K = \int_{z_d} \sigma_\varphi (z_0 - z)\, dz. \qquad (V.11)$$

Using Eqs. (V.7), we can write expressions for the forces and moments in the displacements. After integration, we get

$$\left.\begin{aligned}
R &= \frac{E}{1-\mu^2}\left[(F_d + F_b)u' + (F_d + F_b)\vartheta z_0' + F_d\frac{\mu u}{r} + S_d\frac{\mu\vartheta}{r}\right] - \\
&- R_{td} - R_{tb}; \\
M &= \frac{E}{1-\mu^2}\left[(I_d + I_b)\vartheta + S_d\frac{\mu u}{r} + I_d\frac{\mu u}{r}\right] - M_{td} - M_{tb}; \\
T &= \frac{E}{1-\mu^2}\left[\mu F_d u' + \mu\vartheta S_d + \mu\vartheta z_0' F_d + \frac{u}{r}F_d + \frac{\vartheta}{r}S_d\right] - R_{td}; \\
K &= \frac{E}{1-\mu^2}\left[\mu u' S_d + \mu\vartheta z_0' S_d + \frac{u}{r}S_d + \frac{\vartheta}{r}I_d + \mu\vartheta' I_d\right] - M_{tb};
\end{aligned}\right\} \qquad (V.12)$$

where $F_d$, $F_b$, $S_d$, $S_b$, $I_d$, and $I_b$ are the areas, static moments, and moments of inertia relative to disk coordinates and blade coordinates of the rotor, respectively, given per unit length in the tangential direction. /127

The equations of equilibrium of forces acting on the disk element are

$$\left.\begin{aligned}
rR' + R - T + \frac{\gamma}{g}r^2\omega^2(F_b^* + F_d) &= 0; \\
rM' + M - K - rz_0' R + \frac{\gamma}{g}r^2\omega^2(S_b^* + S_d) &= 0,
\end{aligned}\right\} \qquad (V.13)$$

where $F_b^* = \frac{F_b}{1-\mu^2}$; $S_b^* = \frac{S_b}{1-\mu^2}$.

After putting expressions for M, R, T, and K into the equilibrium equations, we get two second-order differential equations in u and $\vartheta$:

$$\left.\begin{aligned}
A_{10}u'' + A_{11}u' + A_{12}u + B_{10}\vartheta'' + B_{11}\vartheta' + B_{12}\vartheta &= \Phi_{1\omega} + \Phi_{1t}; \\
A_{20}u'' + A_{21}u' + A_{22}u + B_{20}\vartheta'' + B_{21}\vartheta' + B_{22}\vartheta &= \Phi_{2\omega} + \Phi_{2t}.
\end{aligned}\right\} \qquad (V.14)$$

Selection of the coordinate $z_0$ can be arbitrary; we can take the intersection of the plane of the perpendicular axis with the radial section as this coordinate. In the method presented, the coordinate is

$$z_0 = \frac{1}{F_d + F_b}\left[\int_{z_d} z\,dz + \frac{(1-\mu^2)\,\bar{z}\delta}{2\pi r}\int_{z_b} z\,dz\right]. \qquad \text{(V.15)}$$

Assignment of the coordinate according to Eq. (V.15) leads to $A_{20} = B_{10} = 0$, which somewhat simplifies the calculation. Section characteristics are:

$$\left.\begin{aligned} &F_d = z_2 - z_1; \quad F_b = (1-\mu^2)\frac{\delta\bar{z}}{2\pi r}(z_3 - z_2);\\ &S_d = z_0 F_d - K_1; \quad S_b = z_0 F_b - K_2;\\ &I_d = z_0^2 F_d - 2z_0 K_1 + 1/3\,(z_2^3 - z_1^3); \end{aligned}\right\} \qquad \text{(V.16)}$$

where

$$\left.\begin{aligned} &I_b = z_0^2 F_b - 2z_0 K_2 + \frac{1/3\,(1-\mu^2)\,z\delta}{2\pi r}(z_3^3 - z_2^3);\\ &K_1 = 1/2\,(z_2^2 - z_1^2); \quad K_2 = \frac{(1-\mu^2)\,\bar{z}\delta}{4\pi r}(z_3^2 - z_2^2);\\ &z_0 = \frac{K_1 + K_2}{F_d + F_b}; \quad S_d + S_b = 0. \end{aligned}\right|$$

Surfaces with coordinates $z_1$, $z_2$, $z_3$ are shown in Fig. 95.

The constant coefficients of Eq. (V.14) are found by the formulas

$$\left.\begin{aligned} &A_{10} = r(F_d + F_b); \quad A_{11} = [A_{10}]'; \quad A_{12} = \mu F_d' + \frac{F_d}{r};\\ &B_{11} = A_{10}z_0'; \quad B_{12} = A_{11}z_0' + A_{10}z_0' - \mu z_0' F_d' - \frac{S_d}{r} + \mu S_d';\\ &A_{21} = -A_{10}z_0'; \quad A_{22} = S_d'\mu + \frac{1}{r}S_d - z_0' F_d\mu;\\ &B_{20} = r(I_d' + I_b'); \quad B_{21} = [B_{20}]';\\ &B_{22} = -(z_0')^2 A_{10} + I_d'\mu - \frac{I_d}{2r} - 2\mu z_0' S_d';\\ &\Phi_{1t} = \frac{1-\mu^2}{E}[r(R_{td}' + R_{tb}') + R_{tb}];\\ &R_{td} = \frac{aE}{1-\mu}\int_{z_1}^{z_2} T_d\,dz; \quad R_{tn} = \frac{aET_{avb}}{1-\mu^2}F_b;\\ &\Phi_{1\omega} = -\frac{1-\mu^2}{E}\cdot\frac{\gamma}{g}r^2\omega^2(F_b' + F_d');\\ &\Phi_{2t} = -\frac{1-\mu^2}{E}[r(M_{td}' + M_{tb}') + M_{tb} - Rz_0'(R_{td}' + R_{tb}'); \end{aligned}\right| \qquad \text{(V.17)}$$

/128

$$\Phi_{2\omega} = -\frac{1-\mu^2}{E} \cdot \frac{\gamma}{g} r^2\omega^2 (S^*_b + S_d);$$

$$M_{td} = \frac{aE}{1-\mu}\left[z_0 \int_{z_1}^{z_2} T'_d dz - \int_{z_1}^{z_2} T'_d z dz;\right];$$

$$M_{tb} = \frac{aET_{av.b'}}{1-\mu^2} S_{b'}$$

The derivatives denoted with the stroke are replaced with the ratios of finite differences during computation.

The mean blade temperature is calculated by one of the methods outlined in Chapter Four, or else is determined from testing centripetal turbines of similar designs.

With the boundary conditions at the disk axis (zero section) for a rotor with a bore are

$$R_0 = 0; \quad M_0 = 0; \tag{V.18}$$

for a rotor without a bore in its center, they are

$$M_0 = K_0; \quad T_0 = M_0. \tag{V.19}$$

If in the radial rotor the blades are arranged in sections somewhat distant from the zero section, for a disk without a bore the boundary conditions at the axis can be written as:

$$u' = \frac{u}{R} - z'_0\vartheta; \quad \vartheta' = \frac{\vartheta}{R}. \tag{V.20}$$

The zero section is assumed to be two cascade spacings from the axis.

Angles of rotation, displacements, and their derivatives are calculated in the successive transition from section to section, based on Eqs. (V.14).

For the zero section the values of u and $\vartheta$ are assigned, u' and $\vartheta'$ are calculated by Eq. (V.20), and u" and $\vartheta''$ are calculated by Eq. (V.14).

To get the conversion expressions, let us use the Taylor expansion of the functions: /129

$$\left.\begin{aligned} u_n &= u_{n-1} + 2\varepsilon u'_{n-1} + \varepsilon^2 u''_{n-1} + \varepsilon^2 u''_n; \\ \vartheta &= \vartheta_{n-1} + 2\varepsilon \vartheta'_{n-1} + \varepsilon^2 \vartheta''_{n-1} + \varepsilon^2 \vartheta''_n; \\ u'_n &= u'_{n-1} + \varepsilon u''_{n-1} + \varepsilon u''_n; \\ \vartheta'_n &= \vartheta_{n-1} + \varepsilon \vartheta''_{n-1} + \varepsilon \vartheta''_n; \\ \varepsilon &= \frac{h}{2}. \end{aligned}\right\} \qquad \text{(V.21)}$$

Using these formulas, by moving from section to section we can find the boundary conditions at the periphery of the rotor $R_n$ and $M_n$ that depend on u and $\vartheta|$ in the zero section.

To obtain the necessary values of u and $\vartheta|$ in the zero section satisfying the assigned $R_n$ and $M_n$ (boundary conditions at the disk periphery), let us use the rule of four miscalculations [proschety]. We can easily show that expressions relating $R_n$ and $M_n$ with u and $\vartheta|$ are linear and can be written as follows:

$$\left.\begin{aligned} R_n &= A_1 u + B_1 \vartheta + \Phi_1; \\ M_n &= A_2 u + B_2 \vartheta + \Phi_2. \end{aligned}\right| \qquad \text{(V.22)}$$

Let us make the three miscalculations:

First miscalculation. Assigning arbitrarily the values of u and $\vartheta|$ and making the calculation for $\Phi_{1\omega} + \Phi_{1t} \neq 0$ and $\Phi_{2t} + \Phi_{2\omega} \neq 0$, we get the values of $R_{n1}$ and $M_{n1}$ at the boundary.

Second miscalculation. The values of u and $\vartheta|$ are the same, but $\Phi_{1\omega} + \Phi_{1t} = 0$; $\Phi_{2t} + \Phi_{2\omega} = 0$. Then we get the values of $R_{n2}$ and $M_{n2}$.

Third miscalculation. $u = \vartheta| = 0$. When $\Phi_{1\omega} + \Phi_{1t} = 0$; $\Phi_{2\omega} + \Phi_{2t} = 0$, we get the values of $R_{n3}$ and $M_{n3}$.

Solving this system of equations (V.22) for the three miscalculations, we find the values of the constants:

$$\left.\begin{aligned} \Phi_1 &= R_{n1} - R_{n2}; \quad \Phi_2 = M_{n1} - M_{n2}; \\ A_1 &= \frac{R_{n2} - B_1\vartheta}{u}; \quad A_2 = \frac{M_{n2} - B_2\vartheta}{u}; \\ B_1 &= \frac{R_{n2} - R_{n3}}{\vartheta}; \quad B_2 = -\frac{M_{n3} - M_{n2}}{\vartheta}. \end{aligned}\right| \qquad \text{(V.23)}$$

The correct values of u and $\vartheta$ we find from Eq. (V.22) and then, making the last, and fourth miscalculation, we find the values of u and $\vartheta$ and their derivatives in each section.

From Eqs. (V.7) we find that the stresses from the displacements and angles of rotation. For the disk of a centripetal turbine, usually centrifugal loading on the disk periphery is absent ($R_n = M_n = 0$). We should point out that the boundary conditions are assigned integrally ($-R_n = M_m = 0$, and not $\sigma_r = \sigma_{rb} = 0$), which leads to an error in calculating the stresses in the disk sections close to the periphery. /130

In assigning the numerical material, we must see that the radii of the sections, as well as the geometrical characteristics $F_0$ and $F_b$ varied by no more than 30% from section to section. Failure to observe this condition leads to considerable calculation error.

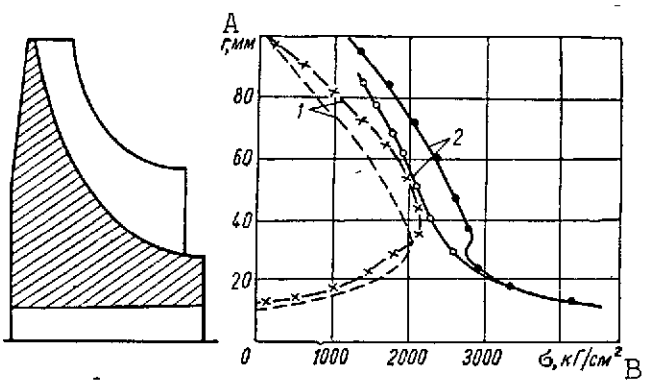


Fig. 69. Comparison of calculated and measured stresses in rotor of centrifugal compressor:
1. radial stresses
2. peripheral stresses.

Key: A. mm
B. kg/cm$^2$

The correspondence to actual stresses determined by the above-outlined method was estimated by comparing the calculated and experimental stresses in a compressor impeller [rotor] [102] (Fig. 69). Radial stresses calculated by the TMZ [Turbomotor Plant] method agree satisfactorily with the stresses found experimentally. The calculated peripheral stresses exceed the stresses obtained experimentally. Calculated values of the peripheral strains proved to be higher than the measured strains, especially close to the bore, as this occurred also in the experiment [36] on shrouded model rotors.

## 4. Design Study of Stressed State of Rotors

The outlined method of calculating stresses in rotors of centripetal turbines and centrifugal compressors (without allowing for the perturbing effect of blades), owing to the use of computers, made it possible to conduct a calculated investigation of the effect of design and geometrical characteristics of rotors on their stressed state.

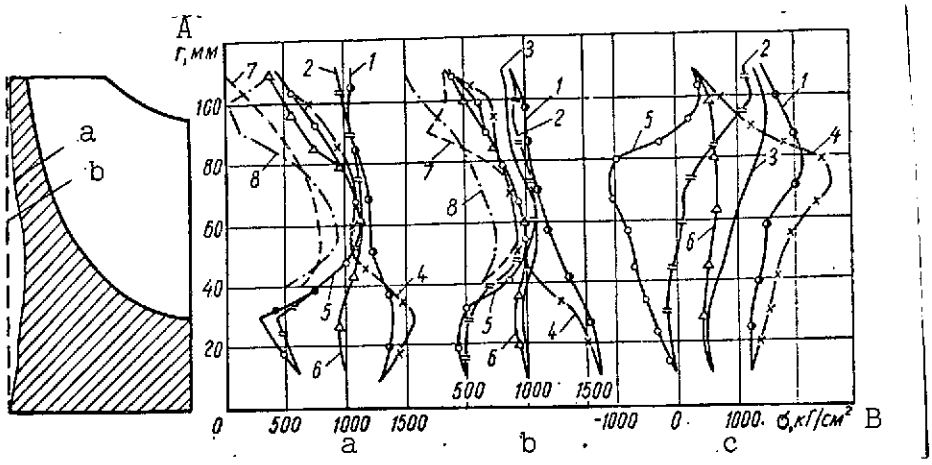


Fig. 70. Dependence of stresses in turbine rotor on thickness of disk rim:
a. initial rotor design
b. thickened disk
c. disk of initial rotor without blades.
The symbols of the curves are given in the text.

Key: A. mm
B. kg/cm$^2$

The results of this investigation are shown in Figs. 70-73, where the following notation is used: corresponding to curve 1 are the peripheral stresses on the back side of the disk, $\sigma_{\phi 1}$; 2. peripheral stresses at working side of disk $\sigma_{\phi 2}$; 3. the mean peripheral stresses in disk (corresponding to the initial surface $z_0$), $\sigma_{\phi_0}$; 4. radial stresses on back side of disk, $\sigma_{r_1}$; 5. radial stresses on working side of disk $\sigma_{r_2}$; 6. mean radial stresses in disk $\sigma_{r_0}$, corresponding to surface $z_0$; 7. radial stresses in blade at fastening, $\sigma_{rb_2}$; 8. radial stresses in blade at trailing and intermediate edges, $\sigma_{rb_3}$. The maximum stresses in the disk depend on the degree of disk asymmetry. The rotor symmetry can be generally increased by the appropriate profiling of the back side of the disk, for its working side is profiled with reference to gas dynamic conditions. /131

The effect of changes in the outer profile and the thickness of the rotor disk on the stressed state of the disk and the turbine blades in the TKR-23 turbocompressor is shown in Fig. 70.

The calculations were made for $n_{tc}$ = 22,000 rpm. From Fig. 70 it follows that when the disk was thickened and when the blade thickness was kept unchanged, stresses in the latter rose.

The transition to a disk of tapered profile reduces the rotor asymmetry, and, as a result, rotor flexion. As a result, the maximum stresses in the disk are somewhat reduced.

Stresses in the rotor hub of a centripetal turbine, as a rule, are distributed extremely unevenly. The maximum radial and tip stresses usually are induced at the back side of the rotor, that is, where the largest stresses due to tension and flexion are added together. The main reason for bending is the intrinsic asymmetry of the disk. Blades, in contrast, in most cases unload the back side of the disk, since $\omega$ gives a bending moment with an opposite sign compared to the thin part of the disk. The maximum stresses in a standard disk without blades are much higher than in a disk with blades. From Fig. 70 it is clear that the blades unload the upper part of the disk and load its hub.

Fig. 71 gives the results of calculations for determining the /132
effect of blade thickness and number on the stressed state of rotor. For this purpose, with rotor size kept unchanged, in the calculation the thickness and number of blades were varied, where the blades remained geometrically similar in terms of thickness distribution in all cases, and only the absolute value of the thickness was changed. From the figure it is clear that thickening of the blades for the same blade number causes a reduction in flexural stresses and an increasing in tensile stresses in the disk. Whereas for blades thickened 1.5 times only the mean stresses (at the surface $z_0$) are increased, while the maximum stresses remain nearly unchanged, thickening of blades by a factor of 3 leads to a considerable increase in both the mean and maximum stresses. The stresses in the blades themselves intensify especially appreciably. Thus, an increase in the blade thickness causes an increase in the tensile stresses in the disk itself and, especially, in the blades. Increasing blade thickness lead to a /133
corresponding rise in the bending moment of the blades. The maximum stresses at the back side of the rotor proved to be the same, since simultaneous, nearly identical increase in stresses occurs at the outer side of the rotor owing to a buildup in the tensile forces and a decrease -- owing to a drop in the overall bending moment from disk and blades.

Thus, from Figs. 70 and 71 it is clear that increasing the rotor symmetry is best done by improving disk configuration, and not by increasing blade mass.

A reduction in the number of rotor blades for fixed rotor blade thickness reduces stresses just as a decrease in blade thickness does for fixed blade number.

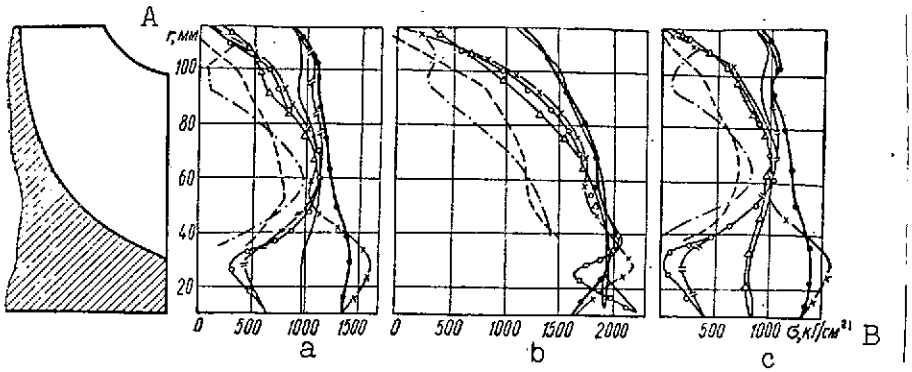


Fig. 71. Dependence of stresses in turbine rotor on blade thickness and number:
a. initial rotor z = 19
b. rotor with $\Delta = 3\Delta$
c. rotor identical to initial rotor, z = 13

Key: A. mm
B. kg/cm$^2$

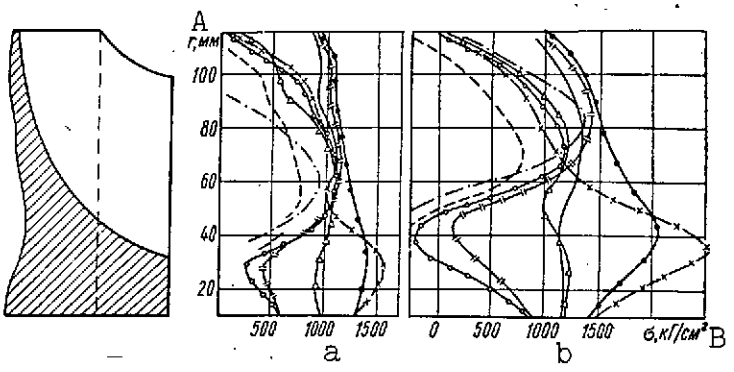


Fig. 72. Effect of rotor thickness on rotor stresses:
a. initial rotor
b. rotor of reduced thickness

Key: A. mm
B. kg/cm$^2$

Fig. 72 shows the distributions of stresses in rotors of the turbine of the TKR-23 turbocompressor, differing only in the axial size of the disk and blade.

From a comparison of the curves we can establish the dependence of the stresses in the disk and blade on the axial sides of the rotor for the designs in which the HSC [hub of straightening cascade] is made in one piece with the radial disk, and we can also see how much advantage in strength is obtained from a rotor design with separate HSC compared with a rotor in which the HSC and the disk are fabricated as one piece.

In turbines operating in severe conditions, that is, at high tip speeds and high temperatures, we can use rotors "without rim," that is, rotors in which the blades are virtually unshrouded on both sides along the periphery for an extent of approximately

15-20% of their radius. Results of tests conducted at the TMZ [Ural'sk Turbomotor Plant] on the heat endurance of these rotors showed that they can withstand a much larger number of heat cycles until the first cracks appear than ordinary semishrouded rotors [15].

As follows from Fig. 73, removal of the rim from the initial rotor makes it possible to markedly reduce the maximum and mean stresses in the disk. However, the maximum stresses in the blades of this rotor proved to be 25% higher than in the blades of the initial rotor.

A reduction of weight at the rotor periphery leads to appreciable lightening of the rotor and, which is the main thing, a reduction in its moment of inertia, that is, an increase in the turbine accelerating ability, very vital for light GTE and turbocompressors used in diesel supercharging.

The transition to an unshrouded rotor causes an abrupt rise in stresses both in the disk and the blades compared to the initial rotor and is therefore undesirable.

A similar design study was made also for compressor rotors with central bore. Results of calculating these rotors are close to the conclusions obtained for turbine disks. The differences were due to the different effect of blades on stressed disk state and stresses in the blade themselves. The latter are appreciably smaller in compressor rotors than in the disk, therefore the change in blade thickness has a relatively slight effect on stresses in the disk on the back side.

## 5. Method of Investigating Strength of Rotors in Acceleration Tests of Full-Scale Turbocompressors /135

Special acceleration tests were conducted of rotors of centripetal turbines to verify the above-presented design method and results of design studies, as well as to gather information on the behavior of rotors when large plastic strains and failures are present.

These test results may also be used in arriving at design strength criteria for semishrouded rotors, one of the most important problems in boosting the reliability of turbocompressors operating at speeds of 20,000-50,000 rpm and for temperatures of gas upstream of the rotor of 600-650°C.

Based on acceleration tests at the TMZ, the effect of the scaling factor was found, since the diameter of the rotor of the TKR-23 turbocompressor is larger than that for the TKR-14, by 1.65 times. Tests of the rotors of the TKR-11 turbocompressor

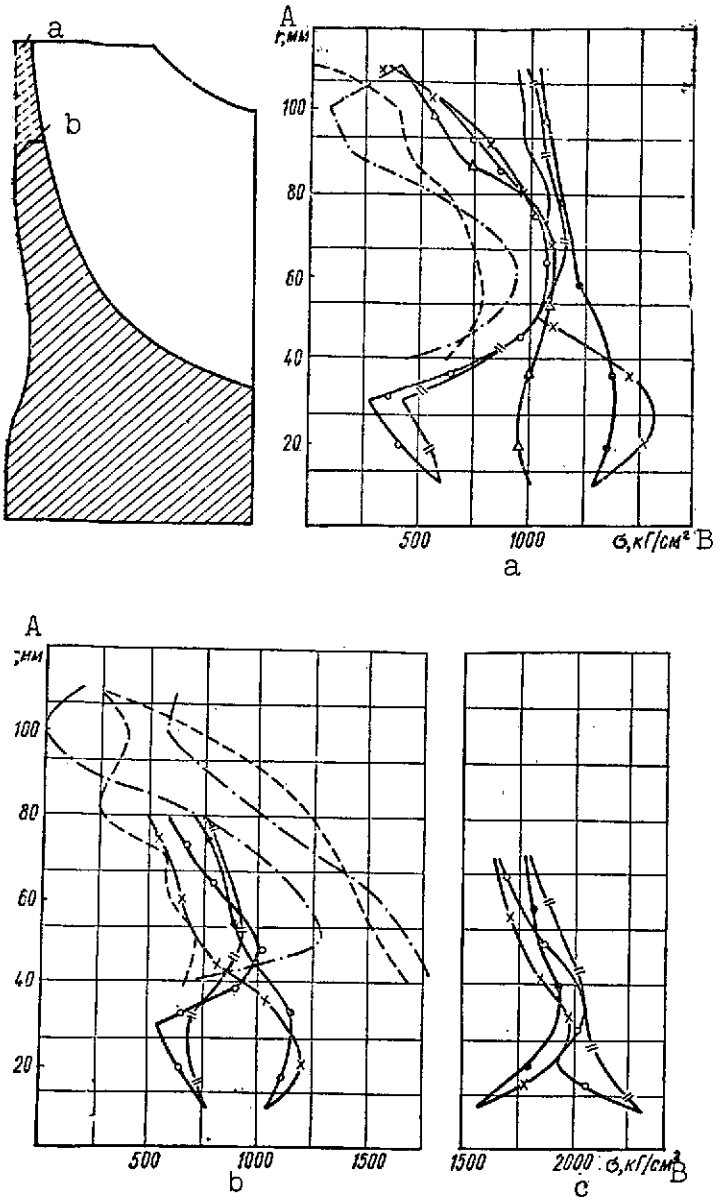


Fig. 73. Dependence of stresses in turbine rotors of different designs with the same blades:
a. initial rotor
b. rimless rotor
c. unshrouded rotor

Key: A. mm
B. kg/cm$^2$

built at the Chelyabinsk Turbine Plant [ChTZ] extended the range of the rotor type classes studied.

Turbine altogether different in design and function were investigated: turbine and compressors. The former were built solid, while the latter had a central opening. The difference in the properties of austenite steels and aluminum alloys was so large that the strength criteria obtained for these alloys evidently will virtually cover most of the metal groups used in turbine-building.

In order to make the examination of the problems of strength and gas dynamics solved in designing of radial turbomachines more comprehensive, the accleration tests of full-scale rotors were supplemented with studies of rotors differing only in the number of blades.

At the present time growing acceptance is being won by semishrouded rotors of small centrifugal compressors that have a large number of radial blades (z = 18-26), promoting higher efficiency and higher pressure head of turbocompressors [112]. Therefore, determining the effect of increasing the number of blades on a disk, and, therefore, reducing their spacing on rotor strength is a most important and urgent problem.

Besides, investigating correlations of strain and failure of rotors with different blade spacings is of paramount importance in solving several fundamental problems arising in estimating and calculating rotor strength, in particular, when developing strength criteria. Above it was already pointed out that included among the most important design factors determining largely the nature and degree of redistribution of stresses along the periphery must be blade spacing. It was also noted that for compressor rotors changing the number of blades does not make a marked change in the design stressed state in the substitute design-orthotropic disk. /136

Thus, the effect of the number of blades (spacing) is best checked with compressor rotors, since changing the number of blades (spacing) must be reflected explicitly in the number of revolutions required to produce failure in these rotors. Actually, given the same design stresses in the same disks with z and 2z blades, the values of B along the radius of the rotors being compared will also be the same. Therefore, a system of forces equivalent in consolidated effect will act on the disks.

If studying the strength of rotors with different numbers of blades bears both practical and theoretical importance, acceleration testing of a bladeless rotor has its own purpose, chiefly to establish only the qualititative effect of blades on the kind of disk strains.

To estimate the design and actual influence of the balancing collar on the stressed state of rotors, acceleration tests of rotors were conducted, differing from each other only by the presence or absence of the collar. The question of the actual role of the collar is of major practical importance for manufacturing. Increasing collar dimensions simplifies the conditions of rotor balancing. A counterindication to this is a considerable increase in design radial stresses below the collar. Here stresses in the compressor disk change very markedly in calculating the design-orthotropic disk. So the effect of the collar was verified experimentally for compressor rotors.

Also conducted was an experimental check of the validity of the "thin" disk hypothesis for relatively broad rotors. The values $D/B \geq 4$ were typical of most full-scale rotors tested. Since sometimes even broader rotors have to be used in turbo-machines, acceleration tests were run on experimental turbine rotors with $D/B = 3$ ($D_s = 180$ mm) and $D/B = 3.3$ ($D_s = 200$ mm) obtained from series rotors of the TKR-23-1 turbocompressor by cutoff of the peripheral part. These rotors differ in their D/B ratio compared with series rotors and are characterized by somewhat different geometrical ratios.

Residual elongations of rotors along the radius and tip were measured directly after tests of each rotor modification.

Calculations and measurements were made for the back side of the rotor, that is, with allowance for bending. The yield strength $\sigma_B$ was used as the limiting characteristic of the material. Yield stresses at the instant of failure were compared with the static value of $\sigma_B$ to develop design criteria of rotor strength.

The broad diversity of structures and the mechanical properties of cast metal impeded the analysis and the generalization of the resulting experimental data, while at the same time it permitted studying the effect of changing the strength and plastic properties of the metal, its purity, and several other factors on rotor bearing capacity. /137

Acceleration tests were run on a turbocompressor placed in a protective housing at a 600°C gas temperature at the turbine inlet (Fig. 74). Air was delivered to the combustion chamber from the plant air line, from the compressor of the test set, or from both sources simultaneously. During the experiments the rotor rpm ($n_{TC}$) was measured to an error ±0.5%. For this, an electronic tachometer developed at the TMZ with measurement range $10^4$-$10^6$ rpm was used. The gas temperature was measured with a chromel-alumel thermocouple in a set with a ZPP-M1 single-point instrument (measurement limits 0-800°C).

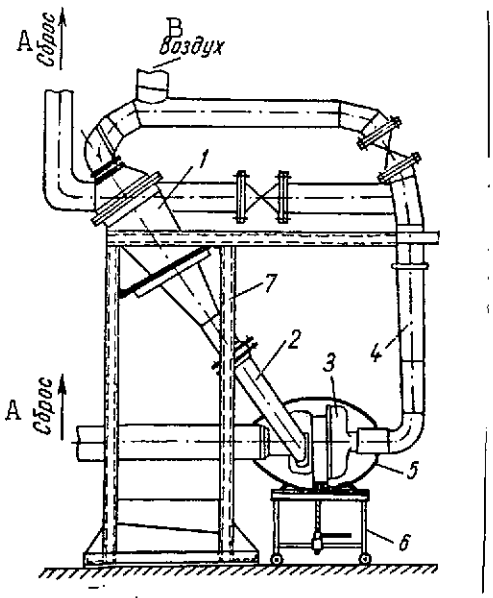


Fig. 74. Arrangement of TMZ stand for accelerated testing of turbocompressor rotors: 1. combustion chamber; 2. gas ducting; 3. turbocompressor; 4. air ducting; 5. spherical armored housing; 6. support; 7. bearing structure.

Key: A. Discharge; B. Air

From the results of the experimental studies of the strength of disks of axial turbo-machines it can be concluded that disk failure sets in when the largest normal stress $\sigma_1$ becomes equal to or greater than the yield strength of the material $\sigma_B$ (that is, $\sigma_1 \geq \sigma_B$). It is shown in [67] that this failure condition can be obtained for the biaxial stress state when three strength theories are used: 1) theory of greatest normal stress; 2) greatest tangential stress; and 3) Mohr's theory. Thus, the above-presented failure condition does not depend on the kind of failure (without appreciable plastic strain or when this condition is in fact present).

As shown by calculations, depending on rotor design and geometry, radial stresses in the disk or blades (usually for solid turbine rotors) or peripheral stresses (usually for compressor rotors with

central bore) will be at a maximum. It should be expected that it is precisely these stresses that can become the limiting values for the rotor, that is, can predetermine the nature of its failure and the number of revolutions required ($n_{fa}$) [fa = failure]. The specific features of the stressed state of semishrouded rotors of radial turbo-machines, as well as the characteristic of calculating stresses therein due to schematizing of rotors in the form of a design-orthotropic rotor make it possible to expect the successful use of results of "elastic" calculation of a rotor in determining the yield stresses in a rotor at the instant of failure. /138

As a rule, radial stresses can be the yield values for turbine rotors. From calculations and tests of disks of axial turbo-machines we know that the rate of stresses therein are only slightly redistributed due to plastic strain and failure sets in when $\sigma_{r_{max}} \geq B$. For semishrouded rotors in contrast to symmetric disks of axial turbo-machines, we must additionally expect flexural stresses to be redistributed along rotor thickness, and we must also anticipate overall stresses along the rotor periphery at a given radius in the event of plastic strain. However, the change in $\sigma_{r_{l_{max}}}$ in the even of plastic strain owing to a reduction in $\sigma_{fle_{max}}$ for a given flexural moment is relatively small and can be allowed for in approximate terms.

Determining the conditions under which rotors fail from peripheral stresses is a more complicated matter. The main reasons for this include the following:

1. The above-presented method gives a large error in maximum $\sigma_{\phi_1}$ at the rotor bore compared with the experimental (toward the side of overstated design stresses). From the center of the rotor to its periphery the discrepancy of the calculated experimental stresses becomes smaller.

2. If we must allow for the effect of plastic strain on redistribution (equalizing of $\sigma_{r_1}$ along rotor periphery in order to choose the correct value of the design yield radial stresses, for a similar selection in terms of peripheral stresses we must, in addition to redistributing $\sigma_{\phi_1}$ along the periphery, also take into account their redistribution along the radius.

3. If we even assume that owing to the high capacity for stress redistribution the rotor material completely equalizes the actual $\sigma_{\phi_1}$ along the radius, then even in this case averaging of $\sigma_{\phi_1}$ is made difficult, since we must average individually the flexural and tensile stresses.

Owing to the foregoing it is clear that it would be scarcely advisable and possible to solve the problem of selecting the yield peripheral stresses and the corresponding strength criteria, with all the conditions and the problems satisfied stringently.

## 6. Main Results of Investigating Rotor Strength

Figs. 75-81 give the most interesting and characteristic cases of rotor failure; rotor failure sets in chiefly due to the action of radial stresses $\sigma_{r_1}$ and occurs approximately along cylindrical or conical surfaces. Sometimes commencing from the surfaces, failure progresses further in the radial direction. /139

The rupture of turbine rotors due to the action of radial stresses as a rule begins in the action zone of maximum or near-maximum design stresses at the disk back side (Fig. 82). Rupture of turbine rotors due to the action of peripheral stresses occurred only in a number of experiments when the structure of the hub metal was unfavorable (casting defects, porosity, pores, slag inclusions, and so on).

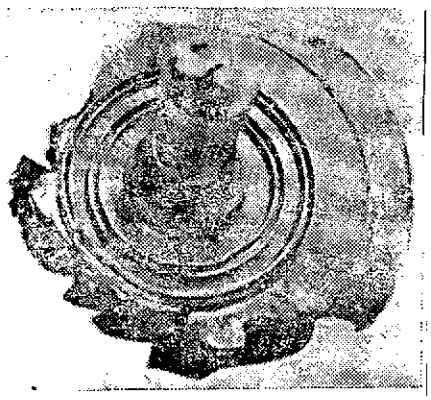

Fig. 75. Rotor of turbine of TKR-23-1 turbocompressor after acceleration tests at $n_{tc}$ = 39,150 rpm.

All compressor rotors of series-built TKR-23-1 turbocompressors, in contradiction to the results of calculation based on the scheme of the design-orthotropic disk, failed not due to peripheral, but radial stresses. Failure occurred not in accordance with the classical scheme along the radial direction from the bore, but by rupture of part of the rotor rim above the lower fillet of the balancing collar. Below it will be shown that the "anomalous" character of the rupture of these rotors can be accounted for by the perturbing action of blades given the restricted ability of the series-built rotors to redistribute the stresses resulting from plastic strain.

Compressor rotors of the TKR-14 turbocompressors failed from the bore under the effect of peripheral stresses.

Impurities strongly affect the ability of the metal to be plastically strained. The presence in metal of dissolved gases, especially hydrogen, lowers the creep area. In aluminum alloys hydrogen is present in dissolved form and virtually speaking forms no chemical compounds with aluminum. It is the reason for gaseous

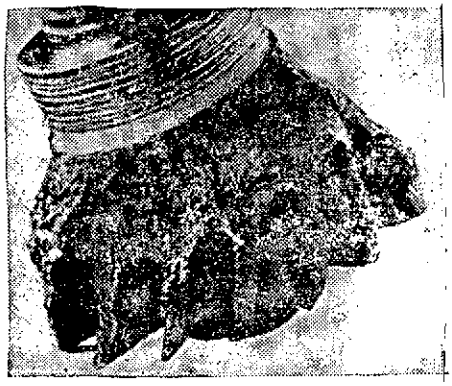

Fig. 76. Rotor of turbine of TKR-23-1 turbocompressor after acceleration tests at $n_{tc}$ = 74,000 rpm.

Fig. 77. Turbine rotor of TKR-23-1 turbocompressor after acceleration test with $n_{tc}$ = = 32,000 rpm.

porosity in rotors. Oxygen present in the AL-9 alloy in the form of aluminum oxide forms solid metallic inclusions, which can be called slag inclusions [1, 74, 75].

Reducing gas porosity and the amount of slag inclusions in metal is one way of increasing design strength of compressor rotors. The effect of improvement in rotor metal structure (resulting from refining processing) on rotor bearing capacity was checked from the results of comparative acceleration tests of compressor rotors of the TKR-23-1 turbocompressor made from the same melt. Half of the melt metal was processed by the series technology, while the other was additionally treated with No. 3 all-purpose flux. /140

The improvement in the metal structure of compressor rotors of the TKR-23 turbocompressors achieved through the refining action of No. 3 flux, expressed in less porosity of metal and increased metal compactness, led not only to a rise in the number of $n_{fa}$ but also to a change in the nature of rotor failure.

Series-melt rotors of TKR-14 turbocompressors, made of AL-9 alloy, exhibited porosity of scale rating 2-3 (higher at the hub), while series rotors of TKR-23 turbocompressors had porosity scale readings of 3-4. These differences are the manifestation of the processing scaling effect. TKR-23 turbocompressor rotors made from modified metal had a denser structure (first porosity scale level) and thereby exceeded in strength the rotors of TKR-14 and TKR-23 turbocompressors made from series-produced metal. /141

From these data and comparisons we can conclude that the unsatisfactory strength of compressor rotors of the TKR-23 turbocompressors of series production is a consequence of inadequate metal purity, primarily the significant metal porosity impeding plastic strain and the attendant stress redistribution.

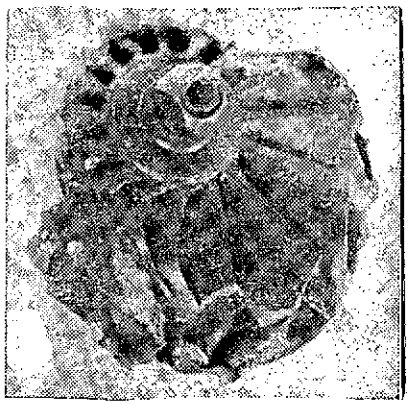

Fig. 78. Turbine rotor of TKR-14-2 turbocompressor after acceleration tests at $n_{tc}$ = = 68,000 rpm.

Fig. 79. Turbine rotor of TKR-23-1 turbocompressor after acceleration tests at $n_{tc}$ = = 37,450 rpm.

From the testing it was found that for turbine rotors $P = \sigma'_{r01}/\sigma_B$ varies in the range 0.89-1.18, while for series compressor rotors it varies in the range 0.25-0.60 ($\sigma'_{r01}$ is the limit radial stress at the danger point and of the design-orthotropic disk replacing the actual disk calculated for $n_{fa}$). The broad range of variation in P can be accounted for only by the different manifestation of the perturbing effect of blades for turbine and compressor rotors not allowed for in the calculation.

The strong perturbing effect of blades on the disk for compressor rotors can be readily seen by comparing the nature of strain and failure of comparative rotors in the rim zone. Rupture of part of the disk rim in the case of compressor rotors, depending on the features of the material in each of them, is accompanied by a different strain pattern. In some cases no residual rotor elongations were found, while in others nonuniundulating strain of the rotor was found, especially in the rim zone, not only by exact measurements, but also easily seen with the unaided eye.[1] /142

Besides the wave in the disk place (let us call it the radial wave), one often observes also a wave associated with residual flexion of the rim between the blades in the direction perpendicular to the disk plane (let us call it the flexural wave). In some rotors undulating deformation of the rim in both directions is observed. The sag of the flexural wave for the TKR-23 compressor rotors tested was 1-5 mm. The flexural wave also was present for other turbine rotors (Fig. 84), but the sag did not exceed 1 mm for them. No marked radial wave at the rim of turbine rotors was detected.

[1] We are referring to the large difference of residual elongation of disk fibers along blades and between them and the formation of unusual arches between blades, visible in Fig. 83.

Fig. 80. Turbine rotor of TKR-23-2 turbocompressor after acceleration tests at $n_{tc}$ = = 40,500 rpm.

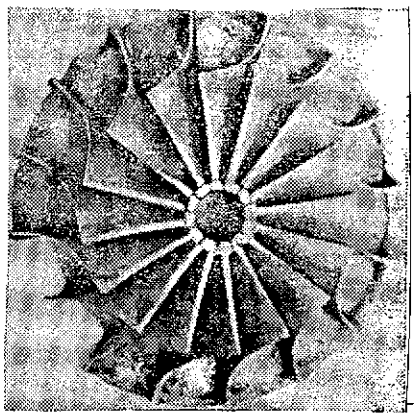

Fig. 81. Compressor rotor of TKR-23-1 turbocompressor after acceleration tests at $n_{tc}$ = 40,500 rpm.

Rim rupture occurred differently in turbine and compressor rotors of TMZ turbocompressors. In the case of turbine rotors with a high level of design radial stresses in the design-orthotropic disk, all or most of the rim, always together with blades, was ruptured. In the case of compressor rotors in which there was a relatively low level of radial design stresses in the design-orthotropic disk and relatively high stresses due to the perturbing action of blades, nonuniformity of strains and stresses showed up much more strongly not only along the blade spacing, but also along all of the rotor periphery. This led to the rupture of the rim of these rotors only over several spacings, as well as to considerable differences in the flexural and radial deformation waves for different interblade channels. Generally one to two channels were broken off. As a rule, the rupture of part of the rim occurred with separation of the disk and the blades in the prefracture stage. The blades usually did not rupture, indicating low stresses in them from centrifugal forces of their own masses. /143

Increasing rotor stiffness with blades sets up conditions for localizing plastic strains in the middle part of the interblade channel, leading after depletion of the metal's ability to equalize radial stresses along the spacing, to the premature rupture of the rim. The profile of the metal rupture between the blades is near-rectangular or semicircular. If a rotor is made with fillets along the profile of the possible rupture, then obviously not only will it be made easier (with smaller moment of inertia), but also the nonuniformity of strains and stresses along the separation will be markedly reduced. By selecting for each standard rotor the optimal fillet depth, one can significantly boost its bearing capacity.

Making fillets along the rim in several cases is desirable also for turbine rotors, in spite of the lower perturbing effect

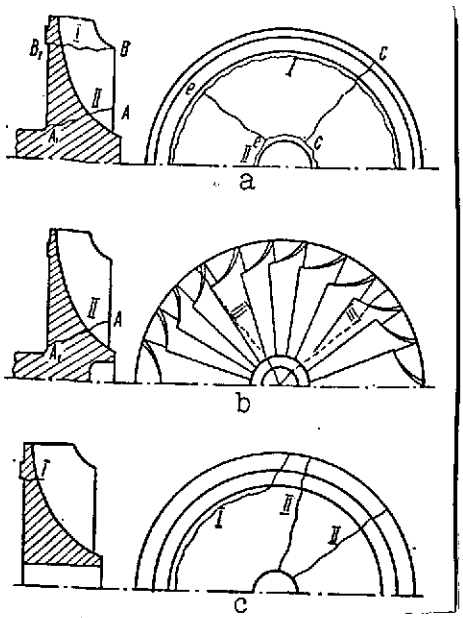

Fig. 82. Typical failure schemes of centripetal turbine rotors:
a. failure of turbine rotors acted on by radial yield stresses $\sigma_{r_1}$ (along the lines I and II) and due to combined action of $\Delta\sigma_{r_1}$ and $\sigma_{\phi_1}$ along the lines II, cc, ee
b. Combined failure of turbine rotors independently of $\sigma_{r_1}$ (line II) and $\sigma_{\phi_1}$ (line III)
c. Failure of compressor rotors due to $\sigma_{r_1}$ (line I) or $\sigma_{\phi_1}$ (line II)

of blades; removal of metal between the blades substantially increases the heat endurance of the rotor and has a smaller effect on efficiency than in the case of compressor rotors [15]. An experimental test of these assumptions by accelerating the TKR-23 compressor rotor with fillets along the rim (Fig. 85) confirmed their favorable effect. /144

Fig. 86 shows the experimental dependence of $P = \sigma'_{r_{01}}/\sigma_B$ on B. Clearly, characteristic of compressor rotors is larger B values than for turbine rotors, and the fact that as B is increased, P becomes smaller. The value of B determines not only the theoretical comparability of the selected design yield stress with the yield characteristic of metal strength, but also how closely the schematization of the rotor in the form of a design-orthotropic disk comes close to actuality.

The lower relative strength of compressor rotors as compared with turbine rotors is thus accounted for not only by differences in metal properties, but also by the greater perturbing effect of blades on the disk in the case of compressor rotors.

From Fig. 86 we can clearly see the influence of properties and characteristics of the metal of each specific rotor of a given type class (B = const) on the scatter of P values. From the physical point of view, this scatter is predictable, since it is associated for cast rotors with the greater diversity of metal quality.

From acceleration tests of rotors failing due to the action of radial stresses it follows that there are no fundamental differences between compressor and turbine rotors with respect to the manifestation therein of the perturbing action of blades, in spite of the overall large differences in material and design. Acceleration tests of the vaneless compressor rotor of a TKR-23

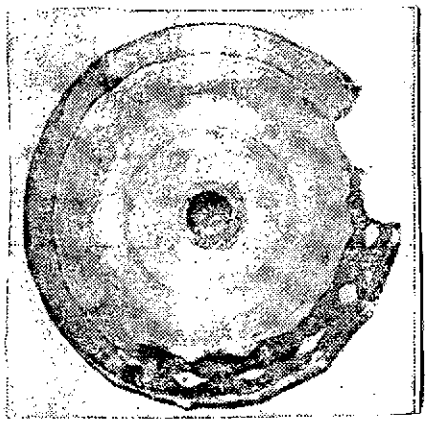

Fig. 83. Compressor rotor of TKR-23 turbocompressor after acceleration tests at $n_{tc}$ = 29,200 rpm.

turbocompressor showed that it was not possible to make the disk fail, since when $n_{tc}$ = 40,500 rpm the turbine rotor of the TKR-23-1 turbocompressor serving as the drive with diameter D = 200 m failed first.

The series compressor rotor of the TKR-23 turbocompressor with z = 16 behaves, in plastic deformation, not in accordance with the design scheme of the design-orthotropic disk and fails when $n_{tc} < n_{fa}$ in accordance with our theory, while the disk (without blades) of this same rotor proves to be stronger than followed from the theory based on schematizing of the actual rotor with a design-orthotropic disk.

This comparison shows the appreciable effect of blades on rotor deformation and failure. It should be expected that given an intermediate number of blades (between zero and 16), the results of acceleration tests and calculations should agree more closely. Of definite interest is an analysis of strain and comparison of rotor failure not only for rotors with 8-10 blades which according /145 to the statements of several authors [3, 72, 85, 119], can be assumed to be axisymmetric, but also with a smaller number of blades.

Some of the rotor castings from the experimental melt were used to establish what effect the number of blades has on rotor strength with identical metal properties. Calculation of stresses

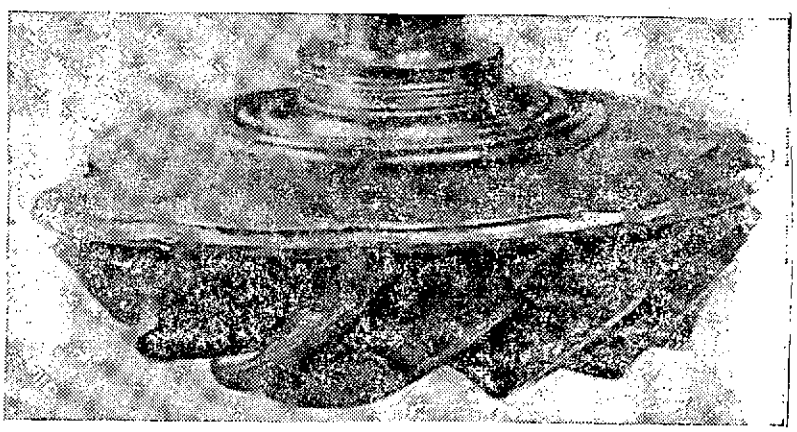

Fig. 84. Turbine rotor of TKR-23-2 turbocompressor after acceleration tests at $n_{tc}$ = 41,300 rpm.

Fig. 85. Compressor rotor of TKR-23 turbocompressor with fillets at rim after acceleration tests with $n_{tc}$ = = 45,000 rpm.

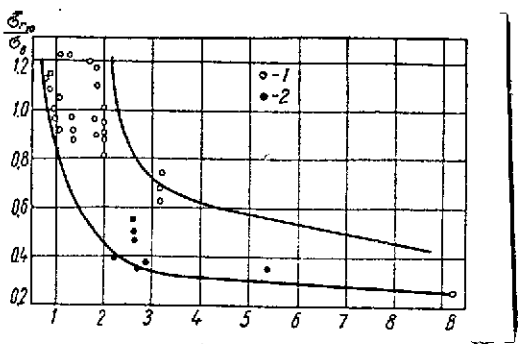


Fig. 86. $\sigma'_{r_{10}}/\sigma_B$ as function of perturbing effect of blade B, from experimental data:
1. turbine rotors of TKR-23, TKR-14, TKR-12, and TKR-11 type turbocompressors
2. compressor rotors of TKR-23, TKR-14, and TKR-11 type turbocompressors.

in the TKR-23 rotors with 16, 8, and 4 blades showed virtually identical stresses. Acceleration tests of these rotors made from the same melt with identical design stresses calculated without allowing for the discreteness of blade fastening also revealed under comparable conditions the manifestation of the perturbing action of a finite number of blades in relation to blade number. Rotors with 8 or 4 blades were made from the last series 16-blade rotors to be constructed by milling off the excess blades while preserving the axisymmetric arrangement of the remaining blades. In contrast to the series-built rotor with z = 16, rotors with z = 8 and z = 4 failed due to peripheral stresses after virtually the same number of revolutions as did the modified rotor with z = 16. From the experiments with different modifications of compressor rotors of the TKR-23 turbocompressors, the following functions were plotted:

$$v_{fa} = f(\Delta u_1)_y \overline{z} \quad [y = \text{yield}],$$

where $(\Delta u_1)_y = (\Delta u_1)_{cal}(n_{fa}/n_{cal})^2$ [cal = calculated]; $v_{fa}$ is the peripheral rotor velocity at $n_{fa}$). Plotted along the X axis is the dimensionless parameter proportional to $(\delta u_1)_y$ = = $(\Delta u_1)_y/z$. Actually, $(\delta u_1)_y$ = = $(\Delta u_1)_y z/\pi$. For all the rotors represented in the diagram, $(\Delta u_1)_{cal} \approx$ ≈ const. The plot in Fig. 87 graphically illustrates the effect on rotor strength of the strain gradient along the spacing for assigned values of $(\Delta u_1)_{cal}$ and B in relation to the number of blades and the quality of rotor material. Although the plot was constructed for a specific group of rotors, it characterizes some general regularities. The diagram shows in which cases the value of $v_{fa}$ is virtually independent of the yield strain gradient attained $(\delta u_1)_y$ and when increasing $(\delta u_1)_y$ causes $v_{fa}$ to become smaller.

Line AB corresponds to the values of $(\delta u_1)_{lim}$ for which the change in porosity of the AL-9 alloy from the first to the fourth scale division is not reflected in $n_{rup}$ and in the nature of failure. /146

The value $(\delta u_1)_{lim}$ at point B we call the critical value. When $(\delta u_1)_{lim} > (\delta u_1)_{cr}$, the curve $v_{rup} = f[(\delta u_1)_{lim}\bar{z}]$ breaks down into several branches as a function of the quality of the AL-9 alloy with the transition to failure due to radial stresses for series-built rotors. Branch BC corresponds to rotors made of modified alloy, branch BE corresponds to rotors made of better-quality series alloy, and branch BM corresponds to rotors made of poorer-quality series alloy. In order to increase the resistance of rotors to the action of radial stresses beyond the critical point and the retain the level of $v_{rup}$ attained when $z \leqslant 8$, it proved necessary to markedly improve the ability of the AL-9 alloy to redistribute the stresses resulting from plastic deformation. Lines AC, AE and AM correspond to z = var. Line MC is the relationship between $(\delta u_1)_{lim}$ and $v_{rup}$ when z = 16 = const. In this case only a difference in the properties of the metal determine the change in the value of $v_{rup}$. The higher the material quality when z = const, the more the gradient $(\delta u_1)_{lim}$ is in a position to be "smoothed out" by the plastic deformation and to attain large values of $n_{rup}$. The line AC corresponds to rotor failure from the bore, lines BE, BM and MC correspond to failure by rupture of the rim under the action of radial stresses. Point C in the diagram characterizes $(\Delta u_1)_{lim}\bar{z}$ for which the rotor fails at the same peripheral and radial stresses.

Results of these studies permit several important conclusions to be drawn on the regularities of the combined effects of the number of blades and the properties of the rotor material on rotor strength.

The disparity with the failure of series-built compressor rotors of TKR-23 turbocompressors with the scheme of the design-orthotropic disk is accounted for by the incapacity of the AL-9 alloy, when contaminated with third-scale division pores, to "smooth out" their perturbing action on the rim in rotors in which the relative number of blades $z/D = \bar{z} = 0.7$. For the same rotor metal quality with $\bar{z} = 0.35$ and $\bar{z} = 0.175$, failure occurs from the rotor bore, which corresponds closely to the results of calculations.

In contrast to elastic straining, elastico-plastic deformation in the case when the rotor material has inadequate ability during plastic deformation to redistribute the stresses along the periphery leads to a greater error in the replacement of the actual rotor by the design-orthotropic disk, the denser the blade cascade. From the foregoing it also follows that the number of blades without indication of rotor diameter in general cannot be /147

accepted as a criterion for the admissibility or inadmissibility of the schematization of the rotor in the form of the design-orthotropic disk.

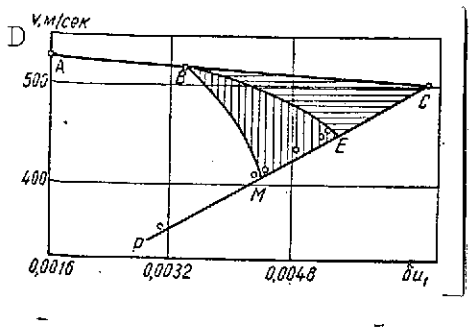


Fig. 87. Plot of limit peripheral velocity of compressor rotors of TKR-23 turbocompressors as a function of $u_1$ and metal quality:
A. z = 4 B. z = 8
C, E. M. P. z = 16
(z = number of rotor blades)
Key: D. v, m/sec

It is convenient to take as the integrated characteristic of the blade spacing the relative number of blades, which is the ratio of the number of blades z to the outer rotor diameter. Above it was shown that the effect of the blade spacing is contradictory and depends on $\delta u_1 = \Delta u_1/t$. Therefore it is best to use in general purposes precisely the ratio $z/D = \bar{z}$ and in specific calculations of different rotor sections, to use $\delta u_1$.

Thus, the manifestation of the perturbing effect of blades and its influence on rotor deformation and strength depends on three jointly acting principal factors.

1. Ratios of stresses (strains) described by the complex B, that characterizes the overall influence of the blades independently of their number, that is, only the influence of their overall mass and dimensions is taken into account in the calculated scheme by the thickness produced by the blades of the orthotropic layer.

2. The thickness of the blade cascade, that is, the relative number of blades $\bar{z}$.

3. The ability of the material to distribute stresses along the periphery in the event of plastic deformation.

For small $\bar{z}$, the influence of B is much smaller than for large $\bar{z}$, and in addition the effect of B depends on the material. For a plastic material the value of $\bar{z}$ has a small effect on the influence of B, while for a low-plasticity material, $\bar{z}$ has a marked effect. Therefore, the influence of B depends on the combination of $\bar{z}$ and material plasticity. The poorer the metal plasticity, the smaller must be the number $\bar{z}$ for the same B values.

These experiments with the failure of rotors differing only in the number of blades permitted not only ascertaining the influence of blade spacing on the manifestation of blade perturbing action, but also confirmed the above-presented results of design

studies. In particular, this is true of the conclusion that blades have a weak influence on stresses in the design-orthotropic disk replacing an actual compressor rotor. The significance of this conclusion for compressor building practice is that with a proper selection of a metal for compressor rotors and with a well-defined observance of the optimal technological process of rotor manufacture, there are no obstacles for using compressor rotors with a large number of blades all the way up to $\bar{z} = 1.5$, that is, up to the limits of the region investigated, in order to improve the principal gas-dynamics indicators.

A small blade number is not an obstacle for schematization of these rotors when calculations are made of limit yields due to centrifugal forces by a design-orthotropic disk. In contrast, for rotors with $\bar{z} \leq 0.4$, schematization is advisable even when the material has a limited capacity to redistribute stresses and to reduce their nonuniformity due to plastic deformation. When $\bar{z} > 0.4$, analysis of the stressed state of the design-orthotropic disk must be supplemented for a natural rotor by analysis of the perturbing action of blades. /148

From experiments with specialized rotors, it can be concluded that the use of the scheme of the design-orthotropic disk is admissible, including all main hypotheses on the nature of deformation assumed usually in calculation of disks (nontwisting of normal, "thin" disk and so on) and for rotors with $D/B = 3$.

Removal of the rim of a disk in the case of the compressor rotor of the TKR-23 turbocompressor by 10% of the radial length increased its failure revolutions in accordance with calculation predictions from 42,000 to 45,000 rpm. Also confirmed were the conclusions of the calculated study of the effect of the more favorable profiling of the rotor back side on rotor strength.

Results of acceleration tests confirmed the soundness of the calculated investigations given the condition that the rotors are made of plastic material without serious structural defects. If the material does not fully measure up to these requirements, premature failures of compressor rotors due to radial stresses and mixed failures of turbine rotors are possible. Based on these considerations and the outlined method of calculating the limit radial stresses in a rotor, one can predict the strength of compressor and turbine rotors.

In spite of the large volume of acceleration tests (a total off 60 rotors were operated to failure as the result of acceleration, with a considerable diversity of rotor design), it was not possible to arrive at criteria of blade strength. This was accounted for by many factors, the principal of which are the following:

1) calculation of stresses in blades where according to the method given in [36] the calculation is less reliable for the roots than in the disk;

2) as a rule, stresses in blades for the turbine rotors investigated and, especially, for the compressor rotors, are lower than the maximal radial stresses in the disk. This circumstance is very important: satisfying the strength conditions for disks essentially is a means also of guaranteeing blade strength, but naturally this factor leaves few opportunities to uncover true blade strength in experiments; and

3) for rotors fabricated by the proper technology of casting and heat treatment, the yield strength of blade material is much higher than for disk material.

The results of studying the stressed state of rotor blades in a centripetal turbine are given in [111]. Fig. 88 shows the stress distribution in the blades of a rotor without a rim obtained from an experiment, in the elastic stage of metal deformation. /149

## 7. Calculation of Limit Stress. Criteria and Margins of Safety

By analyzing experimental data and variant calculations, it was possible to develop an engineering method of calculating limit radial stresses in a disk, that allows for the perturbing action of blades, the actual properties of metal, and the design feature of the semishrouded rotor.

From Fig. 86 it is clear that as D is increased, P decreases more slowly. Let us assume that the radial limit stresses are an irrational power function of B. We produce the so-called reduced radial limit stresses in the disk that allow for the actual perturbing action of the blades:

$$\sigma^*_{r_1} = \sigma'_{r_1} B^{1/m}. \qquad \text{(V.24)}$$

Let us use K to stand for $B^{1/m}$, which we can call the coefficient of reduction of the calculated limit stresses to the experimental values or the coefficient of increasing the calculated stresses owing to the perturbing action of blades. When B = 1, $\sigma^*_{r_1} = \sigma'_{r_1}$ for any values of m, the value of $B^{1/m}$ will tend to unity also in the event that the combination of properties of metal and z is such that 1/m tends to zero. If m = 1, then a linear relationship will exist between K and B. The exponent m for specific rotors can be found from the condition $\sigma^*_{r_{10}}/B = 1$, that is, the equality of the instant of failure of the reduced /150

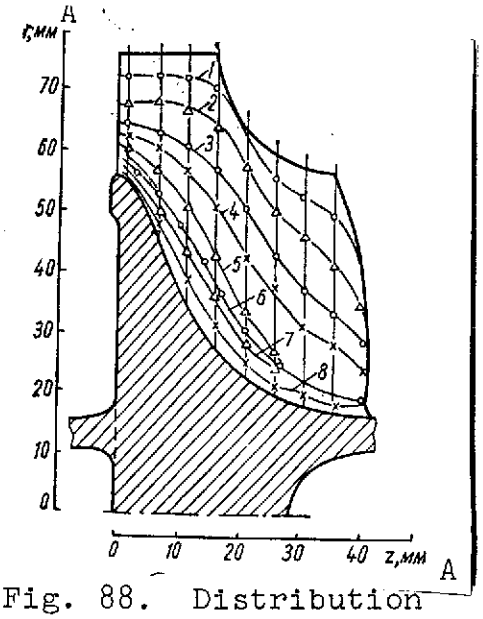


Fig. 88. Distribution of experimental stresses in blade of rotor without rim:
1. $\sigma_1$ = 500 kg/cm$^2$
2. $\sigma_1$ = 1000 kg/cm$^2$
3. $\sigma_1$ = 1500 kg/cm$^2$
4. $\sigma_1$ = 1700 kg/cm$^2$
5. $\sigma_1$ = 1900 kg/cm$^2$
6. $\sigma_1$ = 2000 kg/cm$^2$
7. $\sigma_1$ = 2000 kg/cm$^2$
8. line of maximum values

Key: A. mm

stress at the danger point of the rotor to the yield strength of its material at this same point. Physically, the quantity m is a function of the metal's ability to redistribute stresses resulting from plastic deformation for an assigned deformation gradient along the blade spacing. Fig. 89 presents a plot of K as a function of B for different m. Knowing the value of B from the calculations and determining m, from the plot in Fig. 89 we can find K and the reduced stresses.

Let us introduce a formula for $n_{rup}$ with allowance for the closeness to the actual values not of the calculated, but of the reduced radial stresses. We set $\sigma^*_{r10}/\sigma_B = N$.

Since $\frac{\sigma_{r_{10}}}{\sigma_B}\left(\frac{n_{rup}}{n_{cal}}\right)^2 = P^4$, then $N = KP$

where $\sigma_{r10}$ is the calculated stress at the danger point for an assigned rotor speed). In the event that we have properly chosen (calculated) K, we can assume N = 1. Then

$$\frac{\sigma_{r_{10}}K}{\sigma_B}\left(\frac{n_{rup}}{n_{wor}}\right)^2 = 1;$$

$$n_{rup} = n_{wor}\sqrt{\frac{\sigma_B}{K\sigma_{r_{10}}}}. \qquad (V.25)$$

Let us examine several variants of the use of the plot in Fig. 89.

1. A group of rotors of different type classes made of melt of the same grade with approximately the same quality (for example, milled rotors) is in production. We must determine the value of $n_{rup}$ for rotors of all type classes. After calculation based on the proposed method, let us find the dangerous sections for each of them and determine B in these sections. Then we perform rupture tests for a minimum of two rotors: the largest and the smallest. From the values of $n_{rup}$ found in the experiment, let us determine m for the larger and smaller rotors. The

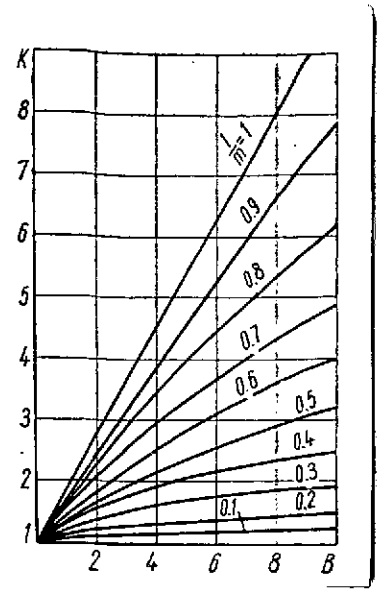

Fig. 89. Functions for calculating limit radial stresses with allowance for perturbing action of blades.

value of m for other type classes can be determined by interpolation with reference to z of each rotor.

2. The same conditions, but owing to the rotor manufacturing technology adopted (for example, casting rotors with a not very stable technological process), the quality of the metal changes more appreciably than in the former case as we move from one type class to another, and from rotor to rotor.

Based on preliminary studies of the specimens, we can test at least two rotors for acceleration (correspondingly, of the maximum and minimum type classes) with poorest and best metal quality. Further, the sequence of calculation is analogous to that examined in the first case. /151

For these variants, the plot $K = f(B)$ was used for solving the direct (calculated determination of $n_{rup}$) and the inverse (determination based on the known value $n_{rup}$ of the integrated characteristic 1/m) problems.

3. The problem conditions are the same as in the first and second cases, but owing to the absence of an acceleration stand we cannot test even isolated rotors.

In this case we cannot of course solve the inverse problem, and the direct problem can be solved from determining m for the rotor material from the data of mechanical tests of specimens, studies of metal structure, analysis of strain plots, comparison of the properties of the test material with the material for which the value of 1/m is known, comparison of $\bar{z}$, and so on.

Based on this investigation of the cast rotors made of austenite steel and aluminum alloy, we can regard as acceptable the values of $1/m \leq 0.3$ in manufacturing semishrouded rotors from similar alloys. The use of the proposed method of determining the rotor bearing capacity will not only be effective for rotors of these materials, but also relatively simple: the differences in metal quality of the individual rotors will have a relatively little effect on both the actual rotor strength and on the calculated failure revolutions. As a result, the operating reliability of the rotors will be increased not only through the better ability of the metal to neutralize, through classic deformation, the perturbing action of blades, but also due to the

the possibility of the more proper selection of the rotor safety margin. The soundness of this statement is well illustrated by Fig. 89, for which it follows that as the 1/m values are reduced, the dependence of K on B is appreciably diminished. Therefore errors in the calculated determination of B will be less influential on the calculated value of $n_{rup}$ found by the proposed method, the lower 1/m. From Fig. 89 we also see that the error in the calculated determination of $n_{rup}$ caused by the inaccuracy of assigning 1/m for specific rotors will be the greater, the larger the B values of the characteristic rotor sections. The dependence of K on B for fixed 1/m values decreases with increase in B. The substantial influence of B on K is observed for $B \leq 5$. A further rise in B has a weak effect on the value of K. Properly designed rotors must have $B \leq 2$. In this zone, especially for an insufficiently plastic metal, we can achieve a considerable increase in the rotor bearing capacity owing to the small change in B, toward its lesser values.

When $B \geq 5$, a substantial rise in $n_{rup}$ of rotors can be achieved mainly through the transition to a more plastic material. /152
If a reduction in B is achieved, but the resulting B exceeds 5, the increase in bearing capacity will be relatively small.

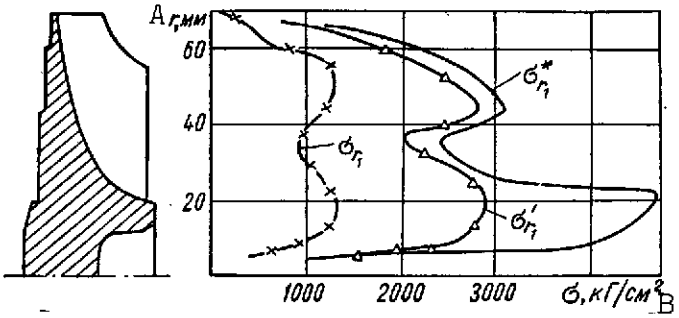


Fig. 90. Radial stresses at back side of rotor of TKR-14-11 turbocompressor turbine.

Key: A. mm
B. kg/cm$^2$

To illustrate the methods used in determining the stressed state of semishrouded rotors, in Figs. 90 and 91 are presented plots of the calculated stresses at the back side of turbine and compressor rotors at working and limiting rotative speeds. For the turbine of the TKR-14-11 turbocompressor, only a comparison of the curves of $\sigma'_{r1}$ (limit stresses without allowing for perturbations due to blades) and $\sigma'_{r_1}$ (as above, but with allowance for blade perturbation) established the actual dangerous rotor cross section. It is precisely where $\sigma^*_r$ values are at a maximum that rotor rupture begins on attainment of limit rpm values.

In the general case to determine the rotor danger sections one must calculate the reduced stresses over the rotor radius, not be limited to determining the values of $\sigma^*_r$ for points where the calculated stresses $\sigma_{r_1}$ in the design-orthotropic disk are at a

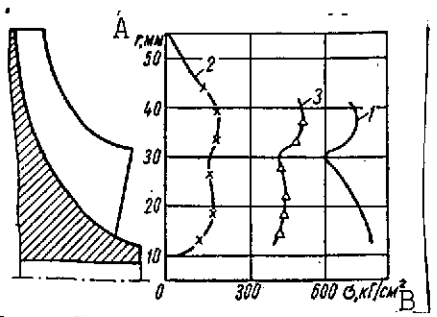


Fig. 91. Radial stresses at the back side of compressor rotor of TKR-11 turbocompressor:
1. $\sigma^*_{r_1}$; 2. $\sigma_{r_1}$; 3. $\sigma'_{r_1}$

Key: A. mm
B. $kg/cm^2$

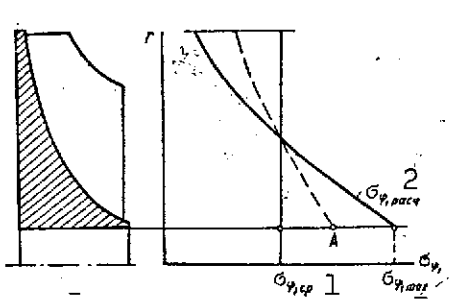


Fig. 92. Total and partial stress redistribution over rotor radius resulting from plastic deformation.

Key: 1. $\sigma_{\phi_1}$av
2. $\sigma_{\phi_1}$cal

maximum or approach the maximum values. As shown by calculations and experimental studies, in most cases one can be limited to determining the reduced stresses only for several of the most dangerous points on the rotor back side.

The effectiveness of the proposed method can be readily seen also in the example of the compressor rotor of the TKR-23 turbocompressor without balancing collar. Removal of the balancing collar eliminates the stress concentration focus and lowers the calculated $\sigma_{r_1}$ at the diameter 180 mm from 4 to 2.5 $kg/mm^2$, that is, virtually to the stress level in the compressor rotor of the TKR-14 turbocompressor (at the same point and at the same tip speeds). It seemed that all of this must lead to an appreciable rise in $n_{rup}$. However, actually this did not take place owing to an increase in the perturbing action of blades, expressed in a substantial rise in B. /153

As a result of the studies, strength criteria were found for semishrouded rotors of radial turbomachines with radial and slightly twisted blades suitable for practical use.

If the rotor strength is determined primarily by the resistance to the action of radial stresses ($\sigma^*_{rmax} \geq \sigma_{\phi_1}$av) failure occurred when the largest overall local reduced stress $\sigma^*_1$ became equal to the yield strength of the rotor material in simple tension and when the specimen temperature was equal to the temperature of the rotor metal at the rupture site.

The failure condition is as follows: $\sigma^*_{rmax} \geq \sigma_B$; the strength condition is: $\sigma^*_{rmax} < \sigma_B$.

Satisfying the disk strength conditions for radial stresses virtually ensures also the strength of blades when the casting

technology and the heat treatment of the rotors are properly selected.

If the rotor strength is determined by the resistance to the action of peripheral stresses ($\sigma_{\phi 1 av} > \sigma^*_{r_1 max}$), then depending on the deformability of the material, the relative number of blades $\bar{z} = z/D$, and the requirements imposed on rotor operating reliability, we can use one of the following strength conditions:

1) $\sigma'_{\phi av} < \sigma_B$ predominately for rotors with $l/m \leq 0.3$; and

2) $\frac{3\sigma'_{\varphi av} + \sigma'_{\varphi max}}{4} < \sigma_B$ for rotors with $l/m > 0.3$,

where $\sigma'_{\phi av}$ is the arithmetic mean of $\sigma'_\phi$ along the radius and $\sigma'_{\phi max}$ is the maximum local $\sigma'_\phi$ (Fig. 92), which are selected for the side of the disk where the calculated stresses are higher, that is, where the left-hand side of the inequality is larger.

When determining the limit stresses and $n_{rup}$ of rotors made of plastic materials, one need not take into account the effect of ordinary stress concentrators (of the fillet type). When $n_{rup} = n_{wor}$ [wor = working], one can obtain a reserve of rotor bearing capacity in terms of rupture rpm as follows /154

$$\frac{n_{rup}}{n_{wor}} = \sqrt{\frac{\sigma_B}{K\sigma_{r_{10}}}} = K_n. \qquad \text{(V.26)}$$

To ensure reliable rotor performance in service conditions, the following condition must be satisfied

$$K_n \geq K_{n\ add} \quad [add = addition] \qquad \text{(V.27)}$$

Selection of the values $K_{n\ add} = n_{rup.add}/n_{wor}$, that is, the allowable rotor safety margins in terms of bearing capacity, can be done with reference to their design features, production, and service characteristics. Selection of the safety margin for cast semishrouded rotors depends on several factors: operating regime, extent of dispersion of metal properties, reliability with which l/m was determined, distribution of stresses over disk radius and thickness, value of parameter B and rotor diameter (scaling effect). When designing rotors similar to those already experimentally verified made of the same materials and with the same stable manufacturing technology, that is, if the coefficients of the perturbing action of blades K can be assigned reliably,

it is expedient to use the following strength conditions for turbocompressors operating in locomotive diesels and in conditions similar to them [16]:

for turbine and compressor rotors, respectively:

$$K_n = \sqrt{\frac{\sigma_B}{K\sigma_{r_{10}}}} \geqslant 1{,}6; \qquad \text{(V.28)}$$

$$K_n = \sqrt{\frac{\sigma_B}{K\sigma_{r_{10}}}} \geqslant 1{,}5. \qquad \text{(V.29)}$$

If a considerable dispersion of values of rotor metal quality from melt to melt is possible or if there is limited information on the possible scatter of 1/m values, then for these cases as applied to turbocompressors of locomotive diesels, a unified strength condition was obtained for turbine and compressor rotors [16] $K_n \geq 1.85$.

Selection of $K_{n\ add}$ for rotors of turbocompressors made of materials differing widely from those investigated and manufactured by another method (for example, integrally-milled), and also intended for service conditions other than those considered, must be done with manditory allowance for the specific features of production and service. A similar approach is desirable also for semishrouded rotors of small gas turbine engines and other radial turbo-machines.

## 8. Approximate Determination of Rupture Revolutions for Rotors

In design practice, sometimes one must determine approximately $n_{rup}$ of an in-design or operating rotor with a detailed calculation that requires computer use. When a rotor fails along /155
a diametral section due to the action of peripheral stresses, the method proposed in [4] can be used.

Below is derived an approximate formula for $n_{rup}$ of semishrouded rotors with radial blades without allowing for the bending of rotor and the perturbing action of blades for the case when the radial stresses are the limit stresses. The recommended functions for both types of failure give the best results for symmetric two-sided rotors made of plastic materials. However, they can be used also in estimating the strength of one-sided rotors.

Let us assume that the stresses $\sigma_\phi$ and $\sigma_r$ over rotor thickness and periphery at a given radius are constant and that rotor

failure occurs along one of the cylindrical surfaces when $\sigma'_{r\ max\ cal} = \sigma_B$. It is shown in [36] that the stress $\sigma_r$ and at the surface $z_0$ ($\sigma_{r_0}$ and $\sigma_{\phi_0}$) and stresses in the rotor without allowing for rotor flexion virtually coincide. Therefore, it is precisely stresses $\sigma_{r_0}$ and $\sigma_{\phi 0}$ that characterize the stresses in a symmetric and in an asymmetric rotor with negligibly small flexion. Generalization of the results of calculating large numbers of semishrouded rotors, as well as calculations of two-sided and one-sided rotors with allowance for blade deformation only in tension showed that we can adopt $\sigma_{r_0} \approx \sigma_{\phi 0}$ for solid rotors below $\bar{r} = 0.7$-$0.75$. For rotors with a bore, this condition can be used up to the lower limit $\bar{r} = 0.2$-$0.3$; when $\bar{r} > 0.75$, it can be used for rotors with or without a bore; for $\bar{r} < 0.3$, it can be used for rotors with a bore $\sigma_r < \sigma_\phi$. However, this is not of special importance in the derivation of the formula owing to the smallness of the radial stresses in these zones. In addition, as shown by the results of acceleration tests as well as service experience, the failure of rotors due to radial stresses as a rule occurs in the zone from the disk hub to $\bar{r} = 0.75$ with the mandatory participation of blades in resisting the rupture. We can assume for this part of the rotor that $\sigma_{r_0} = \sigma_{\phi_0} = \text{const}$ with an error adequate for practical purposes.

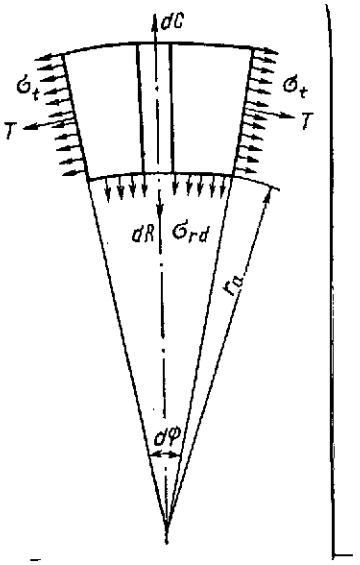

Fig. 93. Element of rotor rim with stresses acting on it during rotation.

Let us divide a rotor element by two meridional planes at the angle $d\phi$ and by the cylindrical surface $r = r_a$. In Fig. 93 we use the following notation: T is the force produced by the peripheral stresses; $F_d$ is the cross-sectional area of the disk (without the orthotropic layer) above $r = r_a$; dR is the force produced by the radial stresses, /156

$$dR = h^*_a r_a \sigma_{r_a} d\varphi; \qquad \text{(V.30)}$$

$h^*_a = h_{da} + h_{ba}$ is the thickness of the design-orthotropic disk when $r = r_a$; $\sigma_{r_a}$ are the radial stresses in the disk when $r = r_a$; dC is the centrifugal force of the isolated rotor element (with orthotropic layer),

$$dC = \frac{C d\varphi}{2\pi}; \qquad \text{(V.31)}$$

$$C = C_d + C_\ell \qquad (V.32)$$

We can easily calculate C by knowing the disk dimensions and the dimensions of the orthotropic layer. Let us set up the conditions for the equilibrium of the isolated rotor element, by projecting all forces in the radial direction. Assuming $\sin d\phi/2 \simeq d\phi/2$, we get

$$\frac{C}{2\pi} = h_a^* r_a \sigma_{r_a} + F_d \sigma_{\varphi_a},$$

whence

$$\frac{C}{2\pi r_a h_a^*} = \sigma_{r_a} + \frac{F_d}{h_a^* r_a} \sigma_{\varphi_a}.$$

As the second condition, let us use $\sigma_{r_0} = \sigma_{\phi 0}$ and let us write $\sigma_{\phi_a}$ in terms of $\sigma_{r_a}$. Adopting this condition leads to an increase in the stress $\sigma_{r_a}$ compared with the actual stresses, since above $\bar{r} = 0.75$ $\sigma_{\phi_0} > \sigma_{r_0}$. However, this area is not of significant importance for $\bar{r}_a \leq 0.75$ owing to the relative smallness of $F_d$ above $\bar{r} = 0.75$. As a result, we get

$$\frac{C}{2\pi r_a h_a^*} = \sigma_{r_a}\left(1 + \frac{F_d}{h_a^* r_a}\right). \qquad (V.33)$$

The centrifugal force of the part of the rotor lying above this cylindrical section $r = r_a$ is

$$C = \rho\omega^2 \int_{r_a}^{r_b} 2\pi r h^* dr; \qquad (V.34)$$

where $n = n_{rup}$

$$C_{rup} = \rho\omega_{rup}^2 \int_{r_a}^{r_b} 2\pi r h^* dr, \qquad (V.35)$$

where $\int_{r_a}^{r_b} rh^* dr = I^* = I_d + I_\ell$ is the moment of inertia of the annular section of the rotor above the rupture section.

Assuming with reference to the foregoing the rupture condition $\sigma_{r_a} = \sigma_B$, we get in the transition to the instantaneous section r,

$$\sigma_B\left(1 + \frac{F_d}{rh^*}\right) = \frac{\rho\omega_{rup}^2 I^*}{rh^*}. \qquad \text{(V.36)}$$

Transferring the term at $\sigma_B$ to the right-hand side of the and performing the transformations, we find /158

$$\sigma_B = \frac{\rho\omega_{rup}^2 I^*}{2h^* + F_d}. \qquad \text{(V.37)}$$

Let us determine from (V.36) the rupture angular speed of the rotor:

$$\omega_{rup} = \sqrt{\frac{\sigma_B(rh^* + F_d)}{\rho I^*}}, \quad 1/\text{sec};$$
$$n = 9{,}55\sqrt{\frac{\sigma_B(rh^* + F_d)}{\rho I^*}}, \quad \text{rpm}. \qquad \text{(V.38)}$$

In order to estimate to what loss of accuracy the simplifications adopted in deriving Eq. (V.38), let us compare $n_{rup}$ found from Eq. (V.38) with the value found from calculating the design-orthotropic disk. In order to reduce the computational work, let us represent approximately the cross section of the disk above $\bar{r} = 0.50$ as the area of a triangle, and from $\bar{r} = 0.5$ to $r_b$ -- as the area of a trapezium. Then above $\bar{r} = 0.5$ $F_d = (h/2)(r_b - r)$. Putting this value of $F_d$ into Eq. (V.38), we find

$$\omega_{rup} = \sqrt{\frac{\sigma_B rh^*\left(1 + \frac{r_a}{r}\frac{h}{h^*}\right)}{\rho I^*}}. \qquad \text{(V.39)}$$

TABLE 5. RESULTS OF CALCULATIONS OF LIMIT NUMBER OF REVOLUTIONS OF TURBOCOMPRESSOR ROTORS BASED ON DIFFERENT METHODS

/157

| Turbocompressor | Rotor type | Rupture velocity $n_{rup}$, rpm: Based on formulas in [4] | Based on Eqs. V.39 & V.40 | Based on calculation of design-orthotropic disk | | Relative error of approximate formula, % $\Delta = \frac{n_{rup} - n_{rup\,appr}}{n_{rup}} 100\%$ (appr = approximate) | | |
|---|---|---|---|---|---|---|---|---|
| | | In terms of $\sigma_\phi$ | In terms of $\sigma_r$ | In terms of $\sigma_\phi$ | In terms of $\sigma_r$ | Dangerous section ($\bar{r}$) | In terms of $\sigma_r$ | In terms of $\sigma_\phi$ |
| TKR-23-1 | Turbine (with bore) | 43 800 | — | 39 800 | — | — | — | 10,0 |
| | Turbine | 47 800 | 41 600 | 46 800 | 38 200 | 0.696 | 9.4 | 2,1 |
| | | | — | | — | 0.565 | 6,1 | |
| | | | — | | — | 0,26 | 11.2 | |
| | Compressor | 46 600 | 55 000 | 48 300 | 55 000 | 0,696 | 0 | —3,5 |
| | | | — | | — | 0.348 | 9.8 | |
| TKR-23-2 | Turbine (with bore) | 4500 | 44 200 | 44 000 | 44 600 | 0.696 | —0.9 | 2,3 |
| | | | — | | — | 0.435 | —0,84 | |
| | | | — | | — | 0.269 | 7.4 | |
| | Turbine | 50 000 | — | 48 800 | — | — | — | 2,5 |
| TKR-18-2 | Turbine | 60 800 | 66 000 | 63 700 | 68 000 | 0,777 | —2.9 | —4,5 |
| | | | — | | — | 0.722 | 0 | |
| | | | — | | — | 0.333 | 8.8 | |
| | Compressor | 64 300 | 68 000 | 69 500 | 72 000 | 0.666 | —2.9 | —7,5 |
| | | | — | | — | 0.556 | —1 | |
| TKR-14-11 | Turbine | 79 500 | — | 85 800 | — | — | — | —7,4 |
| | Turbine (with bore) | 73 000 | 83 600 | 81600 | 82 400 | 0,786 | 1.5 | —10,5 |
| | | | — | | — | 0.643 | 0 | |
| | | | — | | — | 0.286 | —7 | |
| | Compressor | 74 600 | 95 200 | 79 000 | 107 200 | 0.644 | 11.2 | —5,6 |
| | | | — | | — | 0.679 | —12,4 | |
| | | | — | | — | 0,428 | —6.7 | |
| TKR-14-2a | Turbine | 75 200 | 79 200 | 82 500 | 69 200 | 0.572 | 14.0 | —8,8 |
| | | | — | | — | 0.357 | 15,2 | |
| | | | — | | — | 0.308 | 10,5 | |
| | Compressor | 76 200 | 99 000 | 76 400 | 105 400 | 0.572 | —6.0 | —0,3 |
| | | | — | | — | 0,428 | —10.5 | |
| | | | — | | — | 0.286 | —14.0 | |

The term $r_{av}h/rh^*$ reflects the effect of $\sigma_\phi$ on the number $n_{rup}$ (unloading). For the sections lying below $\bar{r} = 0.5$ and above $r_{wt}$, the cross-sectional area of the disk will be

$$F_{\underline{d}} = h_{0,75} 0,5 r_{wt} + (0,5\, r_{wt} - r)\left(\frac{h_{0,5} + h}{2}\right).$$

Substituting the expression for $F_{\underline{d}}$ into Eq. (V.38) and performing simple transformations, we find

$$\omega_{rup} = \sqrt{\frac{\sigma_B\left[rh^* + \frac{r_W}{2}\left(h_{0,5} + \frac{h}{2}\right) - r\left(h_{0,75} + \frac{h}{2}\right)\right]}{\rho I^*}}. \qquad (V.40)$$

Table 5 gives the values of $n_{rup}$ found in failure due to $\sigma_r$ based on Eqs. (V.39) and (V.40) and due to failure from $\sigma_\phi$

$$n_{rup} = 9,55\sqrt{\frac{\sigma_B F_M}{\rho I^*_M}},$$

where $F_M$ is the area of half of the meridional section of the disk; $I^*_M$ is the moment of inertia of half the meridional section of the disk with the orthotropic layer relative to the axis of rotation.

The expression $\sigma_{\phi_0} = \sigma_B$ was adopted as the condition for failure due to peripheral stresses in the design-orthotropic disk. For the case in which the rotor fails due to the action of radial stresses, the error of the approximate formula is presented for the two-three dangerous rotor sections.

# CHAPTER SIX

## STRESSED STATE AND STRENGTH OF ROTORS IN CENTRIFUGAL TURBINES WHEN STEADY AND NONSTEADY TEMPERATURES FIELDS ARE PRESENT

/159

### 1. Stressed State of Rotors When Acted on by Thermal Stresses and Stresses Induced by Centrifugal Forces

Thermal stresses arise due to the action of thermal strains in a body. In the event that a material is deformed elastically, thermal stresses are proportional to the modulus of elasticity, E, the coefficient of linear expansion $\alpha$, and the pressure drop $T_d$. In "elastic" calculation, it is convenient to introduce the dimensionless thermal stresses $\nu_S$:

$$\nu_S = \frac{\sigma}{\alpha E (T_g - T_{i.d})}, \qquad \text{(VI.1)}$$

where $T_{i.d}$ is the initial disk temperature.

In elastic deformation, the force and thermal actions obey the principle of superpositioning. In the case when the mechanical characteristics of a material change significantly with change in temperature, we can also use the principle of superpositioning and assume the thermal and force actions separately. However, it is convenient to combime, calculating the temperature field with the calculation of stresses using a computer. In inelastic deforming stresses must be assumed concomitantly, since in this case the superpositioning principle is not observed.

Since thermal stresses are self-equalizing, along with tensile stresses, in a body compressive stresses always arise, and the total moment and total force due to thermal stresses in any section is equal to zero. A property of self-equalizing can serve as a good method of verifying the correctness of calculations.

To estimate the strength of a structure, we must examine the thermal stresses and the stresses due to centrifugal forces jointly in time and not limit ourselves simply to their arithmetic addition.

Let us examine a case when thermal exposure is separate in time from the action of centrifugal forces. We assume that during intensive heating or cooling centrifugal forces are absent or are small. The thermal stresses arising during heating or cooling can lead to cracks appearing in the disks or blades of the rotor of a centrifugal turbine. Let us determine the conditions under which cracks may appear. In estimating rotor strength, let us use the techniques of thermoplastic adaptation. /160

The general theory [47] on adaptation reduces to the following statement: if we can find a distribution of residual stresses independent of time such that their sum with conditional elastic stresses at each point of a body forms a safe-stressed state in which the stresses are smaller than the creep limit, the structure has become adapted to the distribution of residual stresses and in subsequent changes of loading within the indicated limits its behavior will be wholly elastic.

Since residual stresses must not exceed the creep limit $\sigma_0$, the safe conditional elastic stresses $\sigma_{el}$ can be found from the inequality:

$$\sigma_{el} - \sigma_0 < \sigma_0 , \qquad (VI.2)$$

whence,

$$\sigma_{el} < 2\sigma_0$$

Thus, if the conditionally elastic stresses do not exceed double the creep limit, the structure exhibits the property of adaptation.

In the case when the conditional elastic stresses during the thermal loading cycle change sign (heating and cooling cycle), the total amplitude of change in stresses is substituted into Eq. (VI.2).

If the condition of adaptation is not observed, then sign-alternating plastic deformation arises after a certain number of cycles of thermal loading, cracks appear, which will spread from the surface into the rotor body. The appearance of cracks leads to the annihilation of elastic bonds in the body, and so the growth of cracks beyond a certain number of cycles is altered.

Thermal stresses of themselves do not cause the total failure of the rotor. The rule of thermoplastic adaptation makes it possible in some way to judge thermal strength having only the results of elastic calculation, which naturally is very convenient.

Let us proceed to analyzing the loading of a rotor due to the action of centrifugal forces. If thermal loading causes cracks to appear, this means that the bearing area of the body has been reduced and, therefore, stresses have arisen due to the centrifugal force. When stresses due to centrifugal forces are large enough, the increased stresses can exceed the yield strength and the rotor wheel fails. If the temperature of loading and loading due to centrifugal forces are combined in time, then instead of the conditional elastic thermal stresses, one must substitute the total stresses in Eq. (VI.2).

The condition of adaptation is obtained for the tension-compression plot without strengthening, with the total absence of plastic deformation in the elastic stage. The true deformation curve can differ from the ideal curve; in particular, some plastic deformation can also occur in the elastic region.

In practice cracks were observed to be formed in thermal fatigue when the stresses were lower than twice the creep limits. If minor preliminary imperfections are present in a part (for example, microscopic cracks caused by welding or heat treatment), cracks can also develop even at lower thermal stresses. In cooled rotors, thermal stresses arise also in the steady regime. /161

## 2. Thermal stresses in rotors of centrifugal turbines

The combined examination of temperature field and thermal stresses induced in the rotor of a centrifugal turbine during heating is conveniently begun with uncooled disks, since the pattern of thermal loading in this case is the simplest, and the behavior of nonsteady stresses generally is retained also for cooled rotors.

Let us assume in the first approximation that the intensity of heat transfer in the uncooled rotor from the blade side and from the smooth side of the disk is approximately the same and constant contour-wise, that the change in gas temperature along the radius is small, and that the heat-physical properties of the material do not depend on temperature.

This examination is more than of methodological interest. Heating and cooling of rotors at a constant temperature and heat transfer coefficient contour-wise is carried out in testing disks for thermal shock count; the same conditions are observed during heat treatment of discs, and also in the rapid startup of a turbine with uncooled rotor when the period of the temperature rise compared to the heating time is small.

In the above-indicated case, the temperature and stress changes occurring during heating are fully determined by the Biot criterion.

Calculation of thermal stresses preceeded by the method outlined in Chapter Five, while the geometrical ratios of the rotor corresponded to the rotor of the centripetal turbine of a TKR-14 turbocompressor.

The stresses induced in the disk can be conditionally subdivided into stresses caused by nonuniformity of temperatures of the disk as such, and stresses arising due to a difference between the mean disk temperature and the blade temperature.

Fig. 94 shows the stresses in the rotor of a centripetal turbine when the disk has a constant temperature $T_D$ and the blades have the constant temperature $T_G$ ($T_G > T_D$) and thus, the stresses are caused only by the difference between the disk temperature and the blade temperature. As we can see from Fig. 94, the structure experiences intense thermal flexion, the result of which radial and tangential stresses that the back and working disk surfaces have different signs.[1] Stresses in the blades are different in sign; at the fastening site, they are negative, while along the free edge they are positive. The value of the stresses in the blades near the disk depends significantly on temperature change in the area of transition from disk to blade. /162

In the calculations performed, it was assumed that the blade temperature is constant and equal to the mean temperature in the axial direction. This has almost no effect on the result of calculating stresses at all points of the disk and the blades, except for the fastening site. For an exact calculation of stresses in the sites at which the blades are fastened to the disk, we must take into account the process of heating the disk-blade system. Compressive stresses of the blades at the fastening sites prove to be close to tensile stresses at the free end.

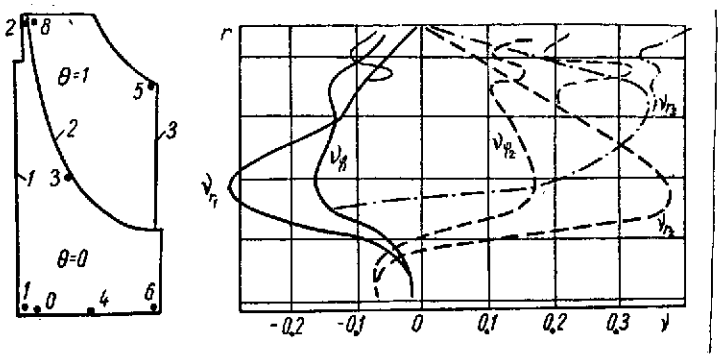


Fig. 94. Thermal stresses in rotor of centripetal turbines or constant disk temperature: $\nu_{r_1}$, $\nu_{\phi_1}$ are stresses at disk back side; $\nu_{r_2}$ and $\nu_{\phi_2}$: are stresses on disk working side; $\nu_{r_2}$ are stresses in blade.

The boundary conditions at the surfaces of the maximum disk radius are given integrally: R = 0 and M = 0. Actually, the boundary conditions at the surface are: $\sigma_r = 0$ and $\sigma_{r\ell} = 0$.

The stresses in the disk hub are caused by two factors: on the one side by the above-indicated thermal bending, and the other -- by compression of the hub caused by heated blades. Obviously, in the disk the radial stresses are the largest, which arise in the section $\bar{r} = 0.45$. In the blades, the largest stresses occur in the section $\bar{r} = 0.75$.

[1] Here and in the following $\theta = (T - T_{i.d})/(T_g - T_{i.d})$.

To find the actual stresses in the section $\bar{r} > 0.8$, we can use the superpositioning method. If we apply to the free surface the stresses obtained from thermoelastic calculation, but with the opposite side and if we calculate the stresses in the disk, summing up the resulting stresses with the results of calculating thermal stresses gives the true pattern of the stressed state.

An exact calculation of stresses arising in a rotor due to contour loading must be based on methods of elasticity theory and involve difficulties that are nearly insurmountable at the present time. An approximate calculation based on plate theory with the introduction of the above-listed hypotheses is based on integral relations at the boundary and therefore is also unsuitable for our problem. /163

In estimating the stresses in the boundary sections of a disk, let us use a method based on reducing the actual structure to some simple model. Here we will not take into account the tangential stresses in the disk, whose average value at the moment the maximum radial stresses appear in the upper disk sections is small. This method gives a rough estimate of the magnitude of the tangential stresses acting along the margin of the plate that can simulate the balde. As a result, for the approximate estimate we have:

$$\tau \approx \sigma_2, \quad \text{(VI.3)}$$

where $\sigma_2$ are the conditional stresses at the stress-free disk margin obtained by thermoelastic calculations with the assignment of integral conditions at the boundary $R = 0$, $M = 0$. The derivation of relation (VI.3) is detailed in /6/ and is not presented here.

As we can see from Fig. 94, the fictitious radial stresses in the upper sections are large, and therefore the tangential stresses $\tau_2$ are also considerable.

Let us make a qualitative analysis of the temperature field and stresses when the rotor is heated with constant Biot numbers and constant heating gas temperature over the contour. The blade temperature is equal to the gas temperature.

Let us examine the case in which a disk is heated with mean number Bi = 2 (the most realistic heating conditions). As we can see from Fig. 95 a, in part of the hub the isotherms have a lyre-shaped form, while in the thin part of the disk the temperature gradient is generally radial. Axial temperature differences in the hub lead to the appearance of additional compressor stresses, which are summed with the compressor stresses induced by blade expansion.

The radial difference between the temperatures in the disk show up due to its nonuniform heating owing to the substantial change in thickness radiuswise. The radial temperature difference leads to the appearance of compressive stresses in the upper disk sections. As a result of the gradual heating of the disk, radial stresses in it and in the blades become smaller, and here the stresses in the blades decrease faster owing to the more rapid heating of the upper disk sections.

From Fig. 95 b it is clear that radial stresses in this case, compared with stresses when Fo = 0.01 are reduced less, while stresses in blades are appreciably reduced; stresses in the hub are hearly unchanged. As the Fourier criterion is increased to 0.031, tensile stresses in the disk in the upper disk section increase even further (Fig. 95 c). The temperature of the upper sections approach the gas temperature, therefore the stresses in the blades were small. Radial stresses also diminished. The isotherms in the thick part of the hub became more gradual, which led to a decrease in the axial temperature differences in the hub; /165
Fig. 95 d shows the thermal and stressed state of the rotor for Fo = 0.0725. By this time the upper disk sections were heated nearly to the gas temperature, therefore the stresses in the blades were small. As a result of the decrease in the differences between the disk temperature and the blade temperature, stresses in all sections were reduced, approaching zero.

Let us examine the nonsteady temperatures and stresses in the case Bi = 0.4, that is, when the heat transfer intensity is four times smaller than in the above-considered case. Here the disk is heated slowly and therefore temperature differences in it are small. The stresses are mainly caused by the difference between the disk temperature and the blade temperature, since only for a very low heating rate are the blade and disk temperatures able to become equalized. As we can see from Fig. 96 a, the axial temperature differences in the disk hub are small and the tensile stresses of the smooth surface arise mainly owing to the radial temperature drop.

Now let us examine disk heating for very large Biot numbers /166
(Bi = 20), which corresponds either to a very intense heat transfer, or to the large rotor dimensions. As we can see from Fig. 96 b, axial gradients in this case are very sizable and the maximum stresses (compressive) arise in the hub. The maximum peripheral stresses in the upper disk sections increase, but slightly. As a result of weakening of the influence of thermal flexion in the blades, compressive stresses arise at the free edge.

As follows from the above-presented data, for different Biot numbers, the maximum stresses arise at several characteristic points: at the disk surface and at the free edge of the blades.

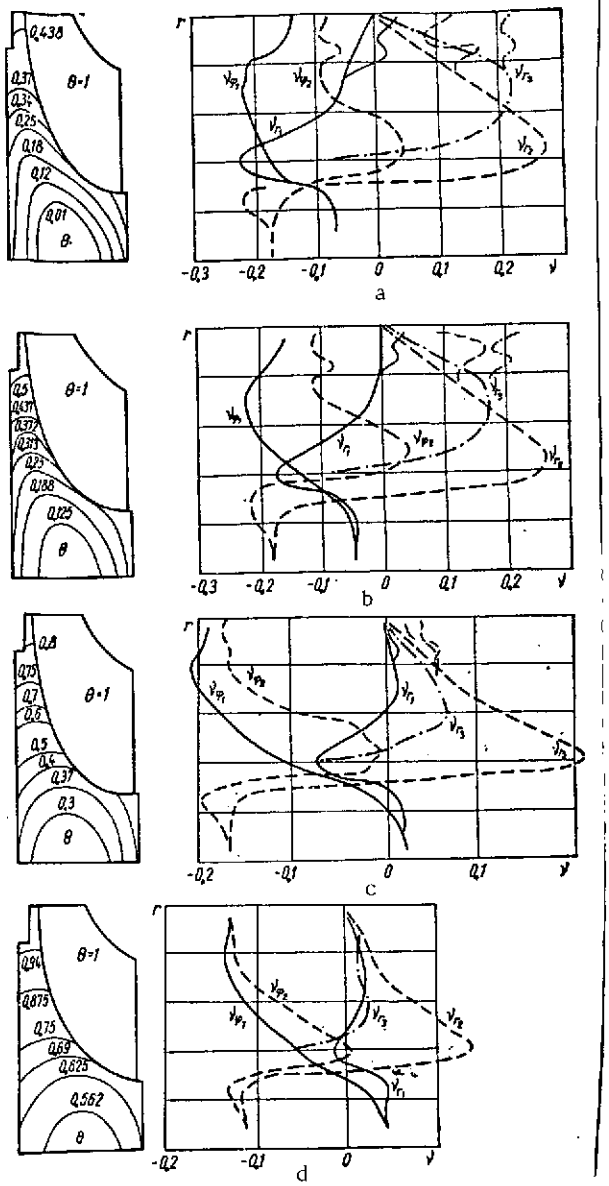


Fig. 95. Field of temperatures and stresses when Bi = 2 and Fo = 0.01 (a), Fo = 0.0125 (b), Fo = 0.031 (c), and Fo = 0.0725 (d). The symbols by the curves are the same as in Fig. 94.

These sites are shown in Fig. 94: point 1, back surface, r = 0, stresses are tangential and radial; point 2, $\bar{r}$ = 1, stresses are tangential, $\nu_\phi$; point 3, working surface, $\bar{r}$ = 0.45, stresses are radial, $\nu_r$; point 5, free side of blade, stresses are radial; and point 8, blade fastening site, stresses are tangential. /164

The lifetime of thermal stresses at different points differs, which influences their danger for thermal failure. The maximum radial stresses in the blade and in the disk vary little with change in Biot numbers, since they are mainly determined by the difference between the disk temperature and the blade temperature. At the moment they arise, the blade temperature is close to the gas temperature, while the disk temperature is close to the initial temperature.

Fig. 97 shows the variation in thermal stresses with time at characteristic rotor points for different Biot numbers (solid lines: Bi = 0.4; dashed lines: Bi = 2). From Fig. 97 we can conclude that the maximum tangential stresses at point 2 (see Fig. 94) depend weakly on the Biot criterion.

Maximum tangential stresses at the upper sections of the disk in an uncooled axial gas turbine when Bi < 10 depend strongly on the Biot number, which is accounted for by the delay in heating /167

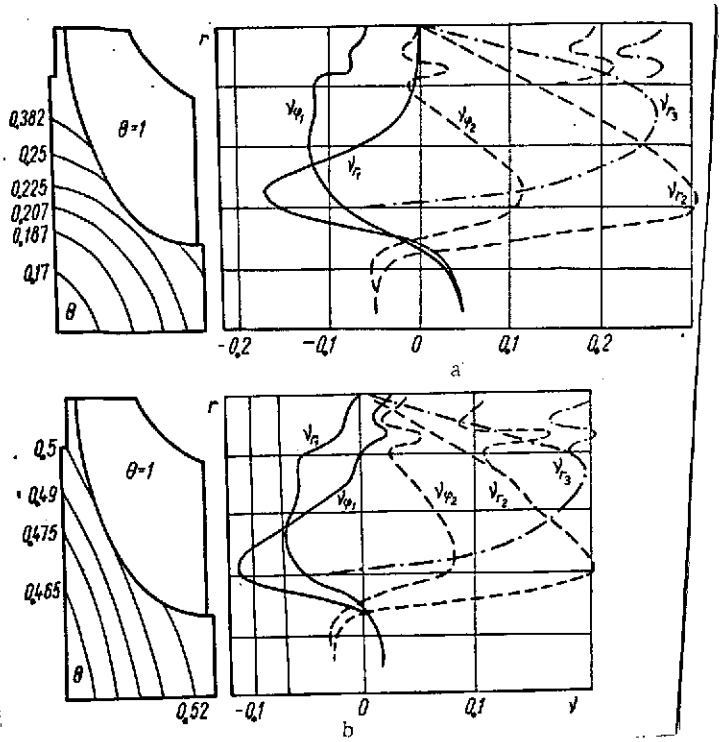


Fig. 96. Field of temperatures and stresses for Bi = 0.4, Fo = 0.155 (a), and Bi = 20, Fo = 0.0075 (b). The symbols by the curves are the same as in Fig. 95.

of the middle disk sections compared to the upper. The delay and, thus, the value of the maximum temperature is the greater, the larger the Biot criterion.

When a disk is heated with a large change in thickness radiuswise and when heat is brought to the face surfaces, the maximum temperature difference is determined mainly by the difference in thicknesses. This can be seen directly from the analysis presented below.

We will assume the heat flow to be only axial, which is approximately satisfied when $R \gg a$ (a = axial dimension of disk variable over disk radius), while the annular element at different radii is cooling according to Newton's law (radial temperature gradients are absent). Then the change in temperature with time for each annulus can be described as follows:

$$\Theta = e^{-\frac{m}{a}}, \quad \text{where} \quad m = \frac{2\alpha\tau}{C\rho}.$$

We assume that the maximum tangential stresses arise at the moment when the maximum difference is established between the temperatures of the upper and lower disk sections and are a function of this difference: /168

$$\Delta\Theta = e^{-\frac{m}{a_1}} - e^{-\frac{m}{a_2}}. \qquad \text{(VI.4)}$$

Let us find the maximum of the function (VI.4) by differentiating it in time and by setting the derivative equal to zero:

$$\frac{m}{a_2} e^{-\frac{m}{a_2}} - \frac{m}{a_1} e^{-\frac{m}{a_1}} = 0,$$

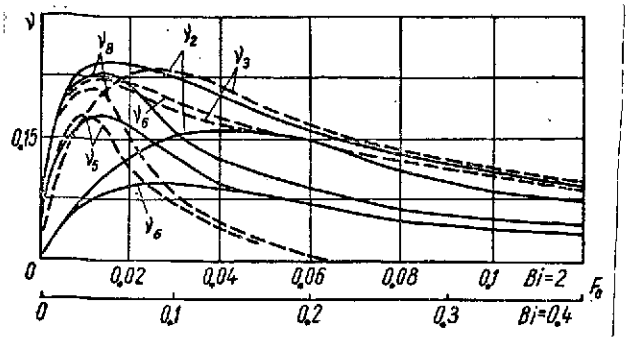


Fig. 97. Change in temperature stresses with time

whence

$$m = \frac{a_1 a_2 (\ln a_2 - \ln a_1)}{a_1 - a_2} \qquad \text{(VI.5)}$$

and, therefore,

$$\Delta\Theta_{\max} = e^{\frac{-a_2(\ln a_2 - \ln a_1)}{a_2 - a_1}} - e^{\frac{-a_1(\ln a_2 - \ln a_1)}{a_2 - a_1}}. \qquad \text{(VI.6)}$$

Clearly, the maximum temperature difference does not depend on heat transfer rate, and therefore, neither does it depend on the Biot number, but only on the ratio of thicknesses. Eq. (VI.5) shows that the time required for maximum thermal stresses to be established in a disk having assigned configuration is inversely proportional to the Biot criterion, which can be readily confirmed by comparing the curves for stresses at point 2 in Fig. 97. Since in actual cases the above-presented assumptions are observed only in part, as can be seen from Fig. 97, some increase in the maximum stresses at point 2 with increase in Biot number is observed.

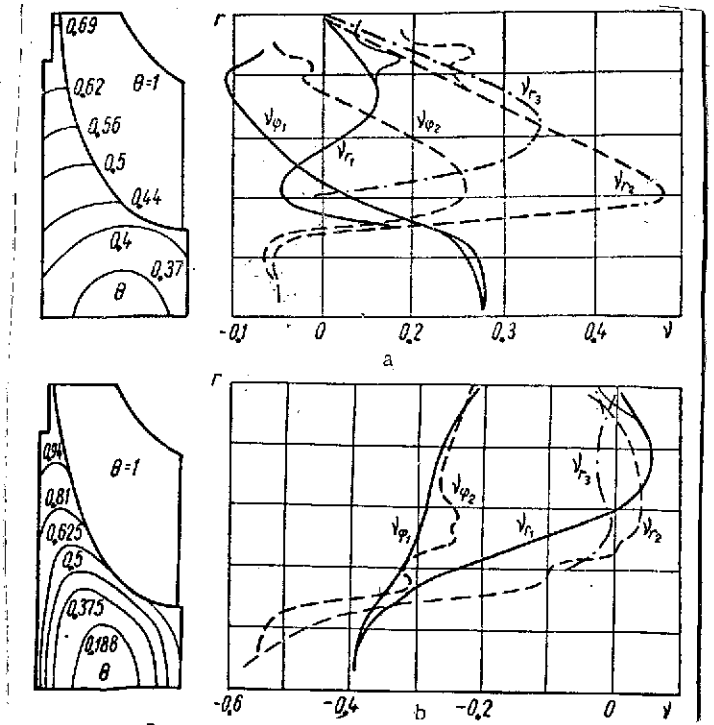


Fig. 98. Field of temperatures and stresses in cooled rotor when Bi = = 0.4; $\theta_{i.a}$ = 0.1; Fo = 0.108 (a) and Fo = 0.432 (b)

Stresses in the hub caused mainly by the axial differences between temperatures will increase considerably with increase in Biot number, as must occur when the plate undergoes surface heating.

Now let us examine the stressed state of a rotor in a centripetal turbine when cooling is present. As shown in the preceding chapter, the nature of the temperature field in the rotor is determined by the design of the cooling system and its operating conditions. Therefore, on these same conditions will also depend the thermal stresses in the rotor of a cooled turbine.

To analyze the thermal strength of rotors and to estimate the rotor cooling system effectiveness, we must have data on the temperature distributions in the rotor. These data can be obtained by calculation using the technique detailed in Chapter Four of this book. In principle, calculating temperature fields can proceed also by other methods. It would be optimal to combine stress calculation with temperature field calculation.

In a cooled rotor the rotor temperature is below the gas temperature, and the blade temperature is close tothe temperature of the heating gas. Rotor cooling has a dual effect on rotor strength: on the one hand, strength characteristics of the material are improved, and on the other this leads to the formation in the material of additional steady (in time) thermal stresses. /169

Fig. 98 a and b show the temperatures and stresses in a cooled rotor for the same heat transfer coefficient values over the contour (Bi = 0.4). Temperatures of the heating gas and the cooling air are unchanged over the rotor ($\theta_g = 1$, $\theta_{i.a} = 0.1$). Fo = 0.432 corresponds to arrival at the steady regime. When Bi = 0.4, the temperature differences in the cooled rotor are relatively small, and therefore the temperature stresses are determined mainly by the difference between the disk temperature and the blade temperature. The distribution of stresses remains similar in different instants of time, all the way up to the steady regime. The rotor is apparently heated by the gas at a temperature that is the average between the gas temperature and the air temperature, and therefore the temperature differences in the cooled disk are much smaller (dashed lines) than in the uncooled disk (solid lines) for the same Biot criterion (Bi = = 0.4) (Fig. 99).

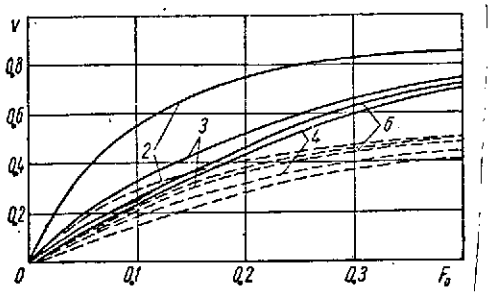


Fig. 99. Variation in disk temperature at characteristic points, with time (the arrangement of the points is shown in Fig. 94).

But the difference between disk temperature and blade temperature is larger and persists at the steady regime.

From numerous calculations of cooled and uncooled rotors, an approximate formula was derived for calculating thermal stresses at point 2 (Fig. 94) from the known temperatures in the disk

$$\nu_n = \frac{\theta_0 - \theta_g}{2},$$

where $\theta_o$ is the temperature at the intersection of disk axis with the plane drawn through the middle of its upper section.

Cooling of the disk does not reduce, but somewhat increases the stresses induced by the difference between the disk temperature and the blades, since at the moment heating of the blades ends, due to cooling the disk has a lower temperature than without cooling. However, the increase in stresses is relatively small, since in any case blade heating ends at a low disk temperature. Therefore the difference between disk temperature and blade temperature will vary only slightly due to rotor cooling. An essential point is the fact that the stresses induced by thermal flexion persist also on attainment of the steady rotor thermal regime. The maximum temperature stresses at characteristic points are close to the stresses in the steady regime. /170

The above-presented conclusions will also be valid for the case when a rotor is heated with variable heat transfer coefficient values and for variable gas and air temperatures in time if a smooth variation in their values is observed. If during heating a sudden rise in temperatures is observed, the stressed state must be studied separately.

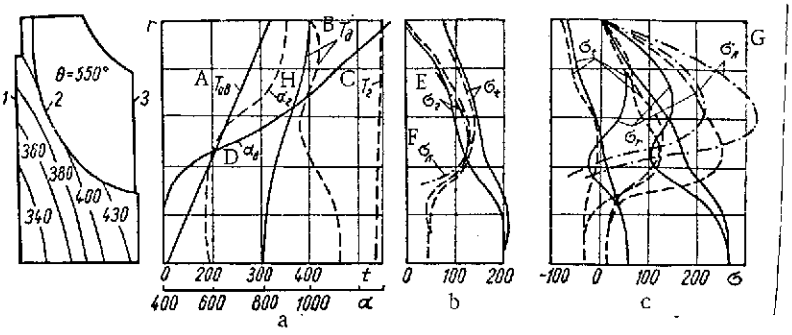


Fig. 100. Temperature field and stresses in cooled rotor of turbine of TKR-14 turbocompressor (solid lines refer to temperature and stresses at surface 1; dashed lines refer to these quantities at surface 2; dashed-dotted lines refer to these quantities at surface 3):
a. Variation in temperature at disk surface $T_d$, gas temperature $T_g$, and cooling air temperature $T_{i.a}$, and also variation in heat transfer coefficients $\alpha_g$ and $\alpha_{i.a}$
b. Stresses due to centrifugal forces
c. Variation in thermal and overall stresses ($n_{tc}$ = = 30,000 rpm; $R_0$ = 7 cm)

Key: A. $T_{i.a}$; B. $T_d$; C. $T_g$; D. $\alpha_{i.a}$; E. $\sigma_g$; F. $\sigma_b$; G. $\sigma_g$; H. $\alpha_g$

During engine stopping times, nonsteady thermal stresses in the cooled disk will be much smaller than in an uncooled disk, since the initial disk temperature is lower. Fig. 100 shows the distribution of temperatures and stresses in the rotor of a TKR-14 turbocompressor in the steady regime. The temperature distribution was obtained at one of the regimes in full-scale tests of the cooling system of a rotor in a centripetal turbine, therefore the boundary conditions correspond to the actual conditions; the stresses were calculated on a BESM-2M computer.

## 3. Experimental Studies of Rotor Thermal Fatigue

Since none of the methods of calculating thermal stresses proposed in the literature underwent experimental testing, experimental studies of rotor thermal strength are especially vital. Investigations at the TMZ consisted of analyzing the design heat endurance of turbine rotors in turbocompressors and determining ways of increasing it, as well as finding the sites of maximum thermal stresses and strains in the rotor, establishing the dependence of thermal strength of a rotor on temperature drops /171 along the radius, maximum and minimum cycle temperatures, exposure time at $T_{max}$, and other regime parameters, and also thermal strength as a function of mechanical properties and structure of the metal.

Progress in methods of estimating the design thermal strength of a part based on related model and full-scale tests is most vital. Since similarity theorem as applied to thermal fatigue testing has scarcely been elaborated, major interest centers in investigating design thermal strength of full-scale parts, above all assemblies differing by complex conditions of interaction of individual elements during heating and cooling.

The rotor of a centripetal turbine is an example of a structure whose thermal endurance cannot be ensured merely by selection of metal. In studying the design thermal strength of a rotor, it is important to select an effective method of testing that can reveal with the simplest possible means the most essential features and properties of the rotor structure influencing the thermal endurance of turbine disk and blade. Obviously, in addition to rotor geometry and design, the difference in the operating conditions of cooled and uncooled rotors must be taken into account.

In the testing of full-scale rotors, the principal problem in test procedures is to ensure temperature fields such that would be similar in character to those prevailing during service under all turbocompressor operating regimes.

Results of exposure to heat cycles of a rotor that are close to those observed in service could be obtained directly by testing turbines in characteristic regimes. In this case carrying out the combined exposure to stresses from temperature drops and centrifugal forces is particularly valuable. However, thermal fatigue testing in full-scale or near-full-scale conditions has a number of key disadvantages. These tests are expensive and are fraught with the possibility of significant turbine failures. The possibilities of testing rotors of different configurations in identical conditions are becoming increasingly narrower; it is very difficult to determine the number of cycles before the first cracks appear and to conduct observations of changes in the induced cracks and the formation of new cracks, since this requires continuous dismantling and re-assembly of the turbo-compressor, which leads, besides all else, to very lengthy testing.

Thus, studies of thermal fatigue of large numbers of diverse rotor structures of centripetal turbines under near-full-scale conditions are not highly productive. Full-scale tests are desirable obviously as control monitoring for verifying the results of laboratory tests on the thermal fatigue of stationary rotors.

This method of studying rotor thermal fatigue has, also, certain methodological advantages, since it makes it possible to uncover not only the combined effect of heat cycles and centrifugal forces, but also to determine the separate action of each factor. /172

In the investigation of rotor thermal endurance in laboratory conditions, heat-cyclic loading must be produced by alternating appropriate temperature fields; these temperature fields must be similar to those occurring in full-scale turbines. Each complete temperature field in the turbine consists of heating (starting), exposure at maximum temperature (steady operation), and cooling (shutting down).

For an approximate simulation of temperature fields from the standpoint of studying rotor thermal fatigue it is important to establish which transient regimes are determining in terms of stresses and strains. Numerous literature data state that in this case the regime of thermal stresses -- startup -- is the most hazardous.

Starting regimes are usually considered as hazardous regimes for centripetal turbines /12, 106/. Results of thermometry of rotors of the TKR-14-2a and TKR-14-2b turbocompressors (see Figs. 33 and 36) confirm the conclusion of the determining significance of starting regimes in the heat-cyclic loading of a disk.

From the above-presented data it follows that in laboratory investigations of the thermal endurance of rotors in centripetal turbines, one must chiefly simulate the temperature fields during starting. This conclusion as a rule pertains to both air-cooled and nonair-cooled rotors. Therefore roughly two thirds of all experiments with nonrotating rotors of turbocompressors were carried out in the "dangerous starting" conditions /157.

In the general case, considering the diversity of the functions and service conditions of centripetal turbines, one must not be limited only to examining variants of the "dangerous start." When setting up the general methodology of an investigation, it is desirable to provide for the possibility of studying the thermal endurance of rotors also during "dangerous shutdown."

As follows from the results of calculations and experiments, rotor thermal strength is determined mainly by three temperature factors:

1) by the maximum disk temperature (for rotors with air cooling, except for intensive film cooling, this is the rim temperature $T_{rm}$);

2) by the maximum (mean) temperature drop between blade and disk, that is, by the drop that is usually present in the sections where the temperature of the latter is at a minimum: $\Delta T_1 = T_b - T_{rm}$; and

3) By the maximum radial temperature drop over the disk, $\Delta T_2 = T_{rm} - T_{av}$.

Basically, on the differences $\Delta T_1$ and $\Delta T_2$ depends the relative role of the different kinds of strain (flection, tension, and compression) of a rotor in its stressed state, and dependent on $T_{rm}$ is the resistance of the metal in the elastic and plastic stages, and also curing creep. As a rule, ensuring the equality /173
of the quantities $\Delta T_1$, $\Delta T_2$, and $T_{rm}$ in the heating-cooling cycle for fixed uncooled rotors is impossible in the simulated and full-scale conditions.

Let us assume that turbine shutdown is hazardous. Then for an approximate simulation of the temperature field in the cooling half-cycle, the following must be provided in the heating half-cycle:

equality of maximum temperatures of model rim and full-scale rotor rim $T_{rm.m} = T_{rm.f}$;

equality for both model and full-scale unit of temperature drops in the steady regime prior to cooling $\Delta T_{2m} = \Delta T_{2f}$; and

equality for model and full-scale unit of the difference between the blade temperature and the disk temperature prior to cooling $\Delta T_{1m} = \Delta T_{1f}$.

Meeting the conditions $T_{rm.f} = T_{rm.m}$ and $\Delta T_{1m} = \Delta T_{1f}$ in the cycle does not permit during testing to heat the rotor hub fully and thus reduces the temperature drop in the disk owing to the cooling half-cycle ($\Delta T_{2}$). By satisfying the second condition $\Delta T_{2m} = \Delta T_{2f}$ in the cycle, one cannot satisfy the first and third conditions.

Similar conclusions can be obtained also for the testing conditions during "dangerous starting."

Practical solutions to the problem lie in rejecting simulation (even approximate) based on all three conditions and in proceeding to partial simulation with respect to the "hazardous factors" using two series of heat-cyclic tests of stationary rotors. Thus, radial cracks at the disk rim are chiefly a consequence of the unacceptable values of $\Delta T_2$, while cracks at the edges of blades are a consequence of exceeding the allowable values of $\Delta T_1$. Each of the differences $\Delta T_1$ and $\Delta T_2$ can become a hazardous factor for rotor thermal endurance and depend on rotor geometry and design, the methods of rotor cooling, and turbine operating regimes.

Experience in running TMZ turbocompressors showed that cracks in the fastening sites and at the edges of blades do not in general develop, while radial cracks in the disk rim are observed in a number of cases. Therefore to verify rotor thermal fatigue in these operating conditions, during testing one must maintain the equality in the model and the full-scale unit of the second and third conditions. But if there is an increased hazard of cracks arising from large values of $\Delta T_1$, then during modeling one must adhere to the equality of the first and third conditions.

A drawback of this method is the failure to allow for the interaction of strains induced by $\Delta T_1$ and $\Delta T_2$ that are present in an actual full-scale unit.

Dangerous values of $\Delta T_1$ can occur both in cooled as well as uncooled rotors. The fundamental difference is that for the former large $\Delta T_1$ values persist even in the steady turbine operating regime owing to deep cooling of the disk.

Intensive cooling of the disk rim increases its thermal endurance owing to a reduction in $\Delta T_{rm}$ and $\Delta T_2$ compared with the uncooled rotor. Therefore it is desirable for a disk, however when this cooling is used one must not permit excessive increase in $\Delta T_1$ and an exceeding of the limits allowable for it. The allowable values of $\Delta T_1$ can be established from the first series of experiments on the thermal endurance of blades in fixed rotors with simulation with respect to $\Delta T_1$. As the result of the second series of heat-cyclic tests of stationary rotors with modeling in $\Delta T_2$ and $\Delta T_{rm}$ with the safe $\Delta T_1$ value selected from the first series, one can determine the thermal endurance of the disk attained by using the appropriate cooling system. /174

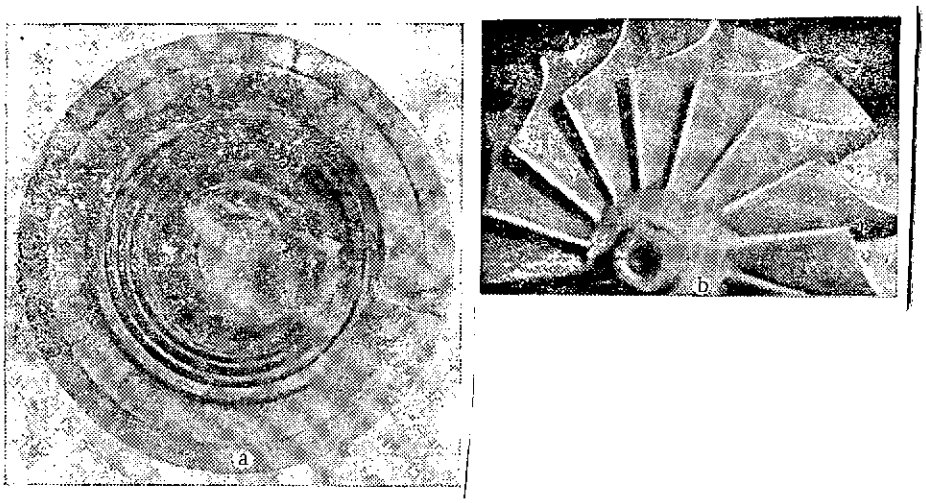


Fig. 101. Appearance of cracks at back (a) and working (b) sides of turbine disk

For uncooled rotors, one must select the allowable time and startup rate of the turbine. In this case it is not required to conduct tests separately for the hazardous factors, but one must find which if the factors $\Delta T_1$ or $\Delta T_2$ for the anticipated regimes of starting and stopping are more dangerous, that is, cause cracks in the rotor and loss in its thermal endurance. Increasing the number of cycles until the first cracks appear can be provided by the directed correction of the starting and stopping regimes, and when necessary, also rotor geometry. Tests of various rotor modifications were conducted at the TMZ under a program providing for both laboratory and full-scale investigations of thermal fatigue.

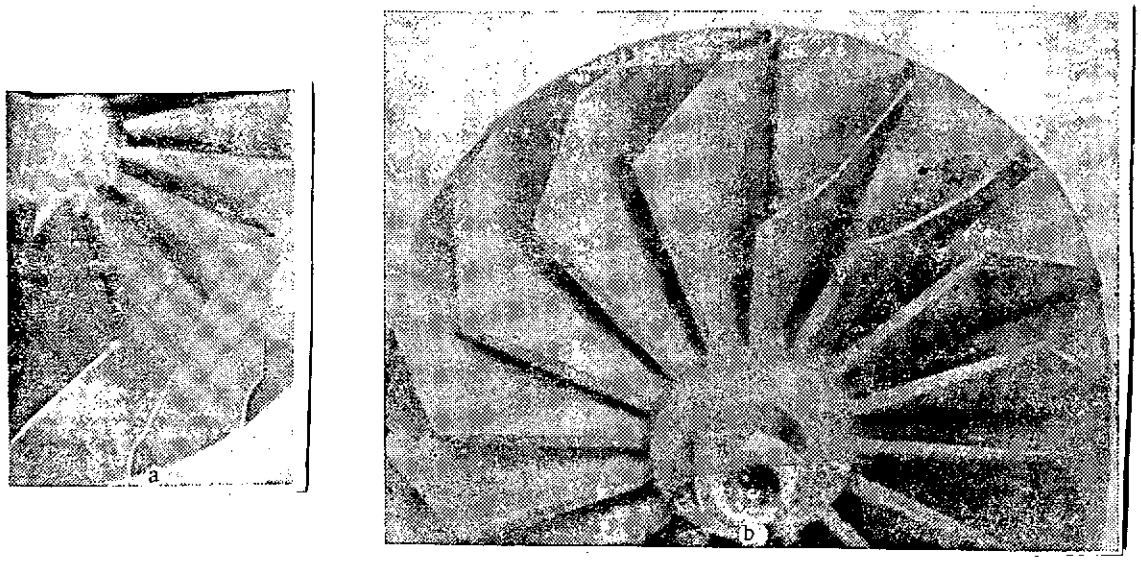


Fig. 102. Rotor of turbine with cracks at leading (a) and trailing (b) edges of blade

Experiments on fixed rotors were conducted in a laboratory with different heating and cooling methods, and also for different cycles of change in rotor temperature varying by loading severity. The experiments on rotating rotors were conducted on stands in conditions that were as close as possible to service conditions.

The procedure of conducting experiments with fixed rotors, the method of treating the results, and the main findings are given in /4/.

Below are presented the results of investigating the thermal fatigue of full-scale cast rotors of centripetal gas turbines (60 fixed rotors of TKR-14 turbocompressors and several spinning rotors of the TKR-14 and TKR-23 turbocompressors). /175

As a rule, rotor failure began at the disk rim from its very periphery. In all cases cracks ran radially and were exposed, that is, tensile peripheral stresses $\sigma_\phi$ were their cause. At the thick and unstepped rim of a disk the cracks often appeared close to the fittings of blades into rim.

Rotors with characteristic cracks, warping of disk rim, and cracks on blades are shown in Figs. 98-104.

Under conditions of high temperature drops occurring in most tests of fixed rotors, as to be expected, rotors made of materials with higher plasticity (independently of strength indicators) proved to be more crack-resistant.

The effect of the maximum cycle temperature (disk rim temperature $T_{rm}$) on rotor thermal endurance in the case when no exposure /176 at $T_{max}$ was present depends on the ratio of thicknesses of rim, disk, and blades. For the same thicknesses of these elements, increasing $T_{max}$ lowered the number of heat cycles withstood by the rotor. When there was a major difference between the thickness of the disk rim and blade thickness, the effect of $T_{max}$ became contradictory because at high $T_{max}$ values the cracks developed at the disk rim, while at relatively low $T_{max}$ values the cracks developed in the blades. Clearly, for each specific rotor of given geometry and design there is some optimal disk rim temperature $T_{rm}$ at which the optimal thermal endurance of the rotor is attained. This factor must be taken into account when developing cooling systems for centripetal turbines.

Fig. 103. Warping of turbine rotor.

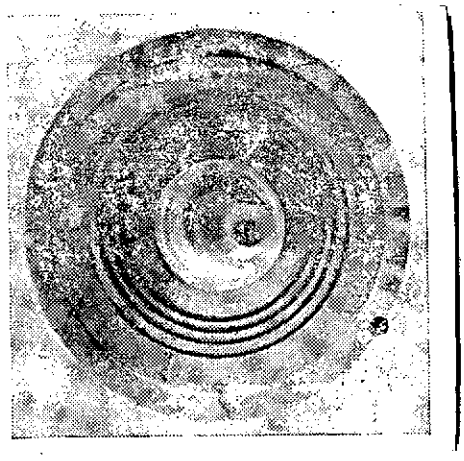

Fig. 104. Rotor of turbine in TKR-14 turbocompressor after 3000 hours of operation on plant stand

Upon analysis of the chemical composition of the materials of the rotors tested, no substantial deviations from the type properties was detected. Results of microscopic inspection of the metal after cyclic tests showed that the microstructure was

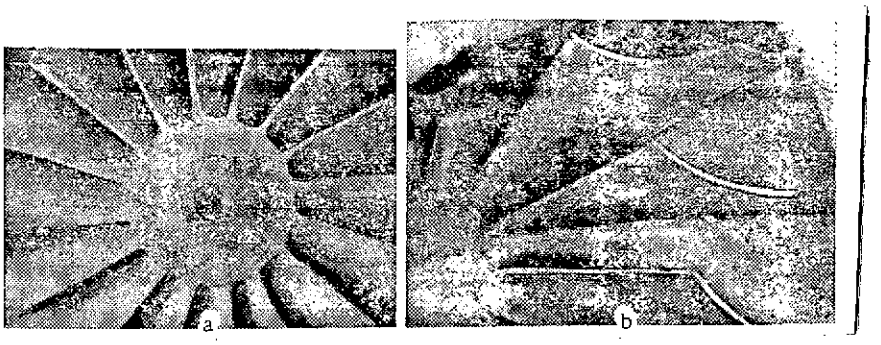

Fig. 105. Network of cracks at face of hub (a) and cracks running from hub (b) of rotor of TKR-23 turbocompressor (after heat treatment)

virtually analogous for all rotors. A difference in metal structure between individual rotors consisted in the different grain sizes. In the rotors examined, no segregations of a secondary phase were detected. Grain size was found to adversely affect rotor thermal endurance. Coarse-grained metal had much lower thermal endurance. It was found that the cracks ran predominantly along grain boundaries. And this was most graphically revealed in the coarse-grained structure. Introduction of semicircular and especially oblong grooves at the rotor rim considerably increased the number of cycles before the first cracks appeared.

The advantage of plant stand tests, in addition to bringing the operating conditions of turbocompressors close to service conditions, is the possiblity of monitoring the regimes and the status of the equipment at virtually any time. /177

The operating conditions of turbocompressors on the TMS test stands and in service in diesel locomotives are virtually analogous with respect to the number of startups and shutdowns and their periodicity, and also as to the main regime factors. One startup occurred for an average of 10-11 hours of operation. In the event that rotors failed on stands after a total accrued operating time of 2500-3000 hours, the turbocompressors had thus 250-270 startups and shutdowns (Fig. 104).

In service conditions and in plant tests, thermal fatigue cracks at the rim developed only in several rotors when the metal structure was unfavorable, namely: when the grain size was larger than the first scale division as standardized by GOST /State Standard/ 5039-51. Rotors made of metal with normal structure and normal mechanical properties (grain at scale division four) under quite analogous service conditions did

not suffer any visible damage. Coarse-grained metal had a severely lowered resistance to thermal fatigue. This and other regularities established from laboratory testing were confirmed by experience with stand tests and service of turbocompressors. The experimental work permits a qualitative verification of the results of the design study of nonsteady thermal stresses in rotors of centripetal gas turbines.

Generally, results of calculations were confirmed by experimental data, that is, cracks developed in rotors where the corresponding calculated stresses were at a maximum for similar testing and calculating regimes (based on the Biot and Fourier criteria). When Bi = 0.4-2, cracks were observed at the disk rim (due to the action of $\sigma_\phi$), at the trailing edges of the blades, and at the sites of blade fastening to disk, in both the leading and trailing edges. When the rotors were heated in a furnace (Bi $\approx$ 0.4), numerous cracks were observed at the trailing edges of the blades (due to the action of $\sigma_{r.b}$), and these cracks, with decrease in the heating time, often appeared first (see Fig. 103). When salt- /178 bath heating was used, no cracks appeared at the trailing edges. High values of the Biot numbers and small Fourier numbers characteristic of these tests in several cases led to the forming of large numbers of cracks in the rotor in the area of the hub both due to the action of $\sigma_{r_2}$ as well as $\sigma_{\phi_2}$. For example, Fig. 105 a shows a network of cracks at the face of the hub. Similar cracks developed also in other turbines. As a rule, turbines with cracks forming after heat treatment in the hub region are characterized by very coarse-grained metal. The rotor shown in Fig. 105 b had all the mechanical properties, with the exception of impact toughness $a_c$, above the TU /State Specifications/ requirements:

$$a_c \approx 2\text{-}2.3 \text{ kgm/cm}^2 \text{ (according to TU, } a_c \geqslant 3 \text{ kgm/cm}^2\text{).}$$

In contradiction to the calculation data, in test regimes when Bi $\leqslant$ 2, no cracks were detected in the area in which maximum calculated radial stresses were operative in the disk at the relative radius $\bar{r}$ = 0.45. These cracks were also not observed in service conditions of the TKR-14 and TKR-23 turbocompressors in marine and locomotive diesels.

## REFERENCES


1. Al'tman, M. B., Nemetallicheskiye vklyucheniya v alyuminiyevykh splavakh /Nonmetallic Inclusions in Aluminum Alloys/, Metallurgizdat, Moscow, 1965. /179

2. Birger, I. A., Kruglyye plastinki i obolochki vrashcheniya /Circular Plates and Shells of Revolution/, Oborongiz, Moscow, 1961.

3. Birger, I. A. et al., in the book: Prochnost' i dinamika aviatsionnykh dvigateley /Strength and Dynamics of Aircraft Engines/, No. 1, "Mashinostroyeniye" Press, Moscow, 1964.

4. Birger, I. A., Shorr, B. R., and Shneyderovich, E. M., Raschet na prochnost' detaley mashin. Spravochnoye posobiye /Strength Calculations of Machine Parts, A Reference Text/, "Mashinostroyeniye" Press, Moscow, 1966.

5. Bogoslavskiy, Ye. G., Sbornik nauchnykh statey Rostovskogo-na-Donu instituta zheleznodorozhnogo transporta /Collection of Scientific Articles of the Rostov-na-Donu Institute of Railroad Transportation/, p. 32, Rostov-na-Donu, 1961.

6. Boli, B., and Weiner, J., Teoriya temperaturnykh napryazheniy /Theory of Thermal Stresses/, translated from the English, "Mir" Press, Moscow, 1964.

7. Bondarenko, K. R. et al., in the book: Dvigateli vnutrennego sgoraniya /Internal Combustion Engines/, edited by L. K. Kollerov, "Mashinostroyeniye" Press, Moscow-Leningrad, 1965.

8. Vaynberg, D. V., Raschet prostranstvennykh konstruktsiy /Calculation of Spatial Structures/, No. 5, Gosstroyizdat, Moscow, 1959.

9. Vansheydt, V. A., Sudovyye dvigateli vnutrennego sgoraniya /Marine Internal Combustion Engines/, Sudpromgiz, Leningrad, 1962.

10. Vasil'chenko, G. S., in the book: Trudy TsNIITMASh /Transactions of the Central Scientific Research Institute of the Machine Building Industry/, No. 30, TsNIITMASh Press, Moscow, 1961.

11. Gazoturbinnyye ustanovki. Voprosy teorii i praktiki /Gas Turbine Installations, Problems of Theory and Practice/ translated from the English, edited by A. G. Kurzon, Sudpromgiz, Leningrad, 1959.

12. Gokhfel'd, D. A., and Kononov, K. M., in the book: Teplovyye napryazheniya v elementakh konstruktsiy /Thermal Stresses in Structural Members/, No. 5, "Naukova dumka" Press, Kiev,

13. Gusak, Ya. M., in the book: Teplovyye napryazheniya v elementakh konstruktsiy, No. 5, "Naukova dumka" Press, Kiev, 1965.

14. Gusak, Ya. M., in the book: Energeticheskoye mashinostroyeniye /Power Machine Building/, No. 9, NIIinformtyazhmash Press, Leningrad, 1966.

15. Gusak, Ya. M., and Tsigel'nik, G. I., in the book: Teplovyye napryazheniya v elementakh konstruktsiy, No. 5, "Naukova dumka" Press, Kiev, 1964.

16. Gusak, Ya. M., "Study of the stressed state and the strength of semishrouded rotors of radial turbo-machines," Candidate Degree Dissertation, TsKTI, Leningrad, 1968.

17. Gutenmakher, L. I., Elektricheskoye modelirovaniye (elektrointegrator) /Electrical Simulation (Electrical Integrator)/, USSR Academy of Sciences Press, Moscow-Leningrad, 1943.

18. Dizeli i gazovyye dvigatelya. Katalog-spravochnik /Diesels and Gas Engines, A Catalog-Handbook/, "Mashinostroyeniye" Press, Moscow, 1968.

19. Dorfman, L. A., Gidravlicheskoye soprotivleniye i teplootdacha vrashchayushchikhskya tel /Hydraulic Drag and Heat Transfer of Rotating Bodies/, Fizmatgiz, Moscow, 1960.

20. Druzhinin, N. I., Metod elektrogidrodinamicheskikh analogiy i yego primeneniye pri issledovanii fil'tratsiy /Method of Electrohydrodynamic Analogy and Its Used in Filtration Research/, Gosenergoizdat, Moscow-Leningrad, 1956.

21. Dyban, Ye. P., "Study of rotor air cooling systems in gas turbines," Doctoral Dissertation, LPI /Leningrad Polytechnic Institute/, Leningrad, 1964.

22. Dyban, Ye. P. et al., Energomashinostroyeniye, 1, (1969). /180

23. Dyban, Ye. P. et al., in the book: Energeticheskoye mashinostroyeniye, No. 5, KhPI /Khar'kov Polytechnic Institute/ Press, Khar'kov, 1968.

24. Dyban, Ye. P. et al., IFZh 15/5, (1968).

25. Dyban, Ye. P., Kolesnichenko, A. F., and Epik, E. Ya., Izv. vuzov. Energetika, 1, (1969).

26. Zhiritskiy, G. S. et al., Gazovyye turbiny dvigateley letatel'nykh apparatov /Aircraft Engine Gas Turbines/, "Mashinostroyeniye" Press, Moscow, 1971.

27. Zavartseva, N. A., in the book: Trudy NAMI /Transactions of the Central Scientific Research Institute of Motor Vehicles and Automotive Engines/, No. 55, NAMI Press, Moscow, 1967.

28. Zavartseva, N. A., in the book: Teplovyye napryazheniya v elementakh konstruktsiy /Thermal Stresses in Structural Members/, No. 3, UkSSR Academy of Sciences Press, Kiev, 1963.

29. Zaydel', G. R., Turbodetandery kislorodnykh ustanovok /Turbo-compressed Gas Motor of Oxygen Installations/, Mashgiz, Moscow, 1960.

30. Zaychenko, Ye. N., Aboltin, E. V., and Kriger, V. A., in the book: Trudy NAMI, No. 58, NAMI Press, Moscow, 1963.

31. Zarubin, V. S., Temperaturnyye polya v konstruktsii letatel'nykh apparatov /Temperature Fields in Aircraft Structures/, "Mashinostroyeniye" Press, Moscow, 1966.

32. Zaryankin, A. Ye., Zatsepin, M. F., and Nikitin, V. N., Izv. vuzov. Energetika, 8, (1961).

33. Zaryankin, A. Ye., and Sherstyuk, A. N., Radial'no-osevyye turbiny maloy moshchnosti /Low-Power Centripetal Turbines/, Mashgiz, Moscow, 1963.

34. Ivanchenko, N. N., and Korsakov, N. V., in the book: Dvigateli vnutrennego sgoraniya /Internal Combustion Engines/, edited by L. K. Kollerov, "Mashinostroyeniye" Press, Moscow-Leningrad, 1965.

35. Idel'chik, I. Ye., Spravochnik po gidravlicheskim soprotivleniyam /Handbook on Hydraulic Drag/, Gosenergoizdat, Moscow, 1960.

36. Il'yin, L. O., Prikladna mekhanika 6/1, (1960).

37. Isachenko, V. L., Osipova, V. A., and Sukomel, A. S., Teploperedacha /Heat Transfer/, "Energiya" Press, Moscow, 1969.

38. Kapinos, V. M., IFZh 6/8, (1963).

39. Kozlov, I. A., Issledovaniye nesushchey sposobnosti elementov rotorov turbomashin /Investigation of Bearing Capacity of Elements of Turbo-Machine Rotors/, "Naukova dumka" Press, Kiev, 1969.

40. Kovalenko, A. D., Teoriya rascheta na prochnost' koles turbomashin /Theory of Strength Calculations of Turbo-Machine Rotors/, UkSSR Academy of Sciences Press, Kiev, 1950.

41. Kovalevskaya, A. Ye., and Perel'man, R. G., Izv. AN SSSR, OTN, 11, (1958).

42. Kovalevskiy, M. M., Dembo, Ya. M., and Gusak, Ya. E., Energomashinostroyeniye, 9, (1962).

43. Kazanevich, Z. Ya., in the book: Khimicheskoye mashinostroyeniye, 2. Tekhnika /Chemical Machine Building, No. 2, Equipment/, 1965, pp. 4-5.

44. Kozdoba, L. A., Izv. vuzov. Energetika, 10, (1961).

45. Kozdoba, L. A., Energomashinostroyeniye, 4, (1962).

46. Kozdoba, L. A., Elektromodelirovaniye temperaturnykh poley v detalyakh sudovykh energeticheskikh ustanovok /Electrical Modeling of Temperature Fields and Parts of Marine Power Plants/, Sudpromgiz, Leningrad, 1964.

47. Koyter, V. T., Obshchiye teoremy teorii uprugoplasticheskikh sred /General Theorems of the Theory of Elasticoplasticity of Media/, Vol. 1, translated from the English, IL, Moscow, 1961.

48. Kolesnichenko, A. F., in the book: Teploobmen v energeticheskikh ustanovkakh /Heat Transfer in Power Plants/, "Naukova dumka" Press, Kiev, 1967.

49. Kolesnichenko, A. F., "Heat transfer in cooling systems of centripetal turbines," Candidate's Degree Dissertation, ITTF AN UkSSR, Kiev, 1968.

50. Kostyuk, A. G., and Sokolov, V. S., in the book: Doklady nauchno-tekhnicheskoy konferentsii po itogam nauchno-issledovatel'skikh rabot za 1964-1965 gg. Sektsiya energomashinostroitel'naya /Papers Presented at the Scientific-Technical Conference on the Results of Scientific Research for 1964-1965, Power Machine Building Section/, Gosenergoizdat, Moscow, 1965.

51. Kostyuk, A. G., in the book: Trudy MEI /Transactions of the Moscow Power Institute/, No. 47, Gosenergoizdat, Moscow, 1963.

52. Kutateladze, S. S., and Borishanskiy, V. M. Spravochnik po teploperedache /Handbook on Heat Transfer/, Gosenergoizdat, Moscow-Leningrad, 1959.

53. Lantsa, Henri, Gazovyye turbiny maloy moshchnosti /Low-Power Gas Turbines/, translated from the French, Mashgiz, Moscow, 1958.

54. MacAdams, William H., Teploperedacha /Heat Transfer/, Metallurgizdat, Moscow, 1961.

55. Makarov, A. N., and Sherman, M. Ya., Raschet izmeritel'nykh i reguliruyushchikh drossel'nykh ustroystv /Calculation of Measuring and Regulatory Throttle Devices/, Metallurgizdat, Moscow, 1953. /181

56. Metzger, D. E., and Mitchell, D. W., Teploperedacha /Heat Transfer/ (Russian translation) 87/1, (1966).

57. ibid., 88/4, (1965).

58. Mikheyev, M. A., Osnovy teploperedachi /Heat Transfer Fundamentals/, Gosenergoizdat, Moscow-Leningrad, 1956.

59. Mitsumati, N., Issledovaniye radial'nykh gazovykh turbin /Investigation of Radial Gas Turbines/, translated from the Japanese, Mashgiz, Moscow, 1961.

60. Moiseyev, A. A., Topunov, A. M., and Tikhomirov, B. A., Energomashinostroyeniye, 10, (1966).

61. Morgulis, P. S., and Perfilov, V. G., Turbokompressory teplovoznykh dvigateley /Turbocompressors of Locomotive Engines/, "Mashinostroyeniye" Press, Moscow, 1965.

62. Mokrushin, S. A., in the book: Teplovyye napryazheniya v elementakh konstruktsiy, No. 5, "Naukova dumka" Press, Kiev, 1965.

63. Odivanov, L. N., and Tunakov, A. P., Izv. vuzov. Aviatsionnaya tekhnika, 1, (1964).

64. Pashkov, P. O., Razryv metallov /Metal Rupture/, Sudpromgiz, Leningrad, 1960.

65. Perel'man, R. G., and Polikovskiy, V. I., Izv. AN SSSR, OTN, 10, (1958).

66. Petukhov, B. S., Opytnoye izucheniye protsessov teploperedachi /Experimental Study of Heat Transfer Processes/, Gosenergoizdat, Moscow-Leningrad, 1962.

67. Rabinovich, V. P., in the book: Trudy TsNIITMASh, No. 12, TsNIITMASh Press, Moscow, 1960.

68. Rabinovich, V. P., Energomashinostroyeniye, 3, (1959).

69. Rabinovich, V. P., Prochnost' turbinykh diskov /Strength of Turbine Disks/, "Mashinostroyeniye" Press, Moscow, 1966.

70. Repukhov, V. M., "Investigation of Effectiveness of Film Cooling of Flat Surfaces," Candidate's Degree Dissertation, ITTF AN UkSSR, Kiev, 1967.

71. Rozenberg, G. Sh., Sudovyye tsentrostremitel'nyye gazovyye turbiny /Centripetal Marine Gas Turbines/, "Sudostroyeniye" Press, Leningrad, 1964.

72. Rubach, O. M., and Agranovich, V. M., Prikladna mekhanika 3/1, (1957).

73. "Design and experimental methods of determining the thermal state of main assemblies of gas turbines with air cooling," Rukovodyashchiye ukazaniya ITTF AN USSR-TsKTI /Guideline Instructions of the ITTF of the UkSSR Academy of Sciences and the Central Scientific Research, Planning, and Design Boiler and Turbine Institute imeni I. I. Polzunov/, No. 29, Vols. I and II, Leningrad, TsKTI imeni I. I. Polzunov Press, 1970-1972.

74. Spravochnik po svoystvam staley, primenyayemykh v kotloturbostroyenii /Handbook on Properties of Steels Used in Boiler and Turbine Building/, Mashgiz, Moscow-Leningrad, 1958.

75. Spravochnik po mashinostroitel'nym materialam /Handbook on Machine Building Materials/, edited by G. I. Pogodin-Alekseyev, Vol. 2, Mashgiz, Moscow-Leningrad, 1959.

76. Skubachevskiy, G. S., Aviatsionnyye gazoturbinnyye dvigateley. Konstruktsiya i raschet detaley /Aircraft Gas Turbine Engines; Design and Calculation of Parts/, Mashgiz, Moscow, 1969.

77. Stechkin, B. S., Teoriya reaktivnykh dvigateley. Lopatochnyye mashiny /Theory of Jet Engines, Bladed Machines/, Oborongiz, Moscow, 1956.

78. Stradomskiy, M. V., Gusak, Ya. M., and Kolesnichenko, A. F., in the book: Energeticheskoye mashinostroyeniye, No. 9, KhPI Press, Khar'kov, 1970.

79. Teplovoye sostoyaniye rotorov i tsilindrov parovykh i gazovykh turbin /Thermal State of Rotors and Cylinders of Steam and Gas Turbines/, edited by K. P. Seleznev et al., "Mashinostroyeniye" Press, Moscow-Leningrad, 1964.

80. Teoriya dvigateley vnutrennego sgoraniya /Theory of Internal Combustion Engines/, edited by N. Kh. D'yachenko, "Mashinostroyeniye" Press, Moscow-Leningrad, 1965.

81. Tkachev, N. M., "Investigation of heat transfer in rotor of centripetal gas turbine," Candidate's Degree Dissertation, LPI, Leningrad, 1967.

82. Traupel', V., Teplovyye turbomashiny /Thermal Turbo-Machines/, Gosenergoizdat, Moscow-Leningrad, 1961-1963.

83. Turmarkin, S. A., in the book: Trudy TsAGI /Transactions of the Central Institute of Aerohydrodynamics imeni N. Ye. Zhukovskiy/, No. 262, TsAGI Press, Moscow, 1936.

84. Tunakov, A. P., Izv. vuzov. Aviatsionnaya tekhnika, 3, (1960).

85. Umanskiy, E. S., and Vaynberg, D. V., Napryazhennoye sostoyaniye sostavnykh diskov i plastin /Stressed State of Disks and Plates/, UkSSR Academy of Sciences Press, Kiev, 1952.

86. Khanin, N. S. et al., Nadduv i nagnetateli avtomobil'nykh dvigateley /Supercharging and Compressors in Automotive Engines/, "Mashinostroyeniye" Press, Moscow, 1965. /182

87. Chernin, V. M., in the book: Teplovyye napryazheniya v elementakh konstruktsiy /Thermal Stresses in Structural Members/, No. 3, UkSSR Academy of Sciences, Kiev, 1963.

88. Chernykh, K. F., and Chestyakova, K. N., Uchenyye zapiski LGU im. A. A. Zhdanova 280/35, Leningrad, (1960).

89. Chekhonadskiy, N. A., in the book: Trudy VNII im. Mendeleyev /Transactions of the All-Union Scientific Research Institute of Metrology imeni D. I. Mendeleyev/, No. 57 (117), Standartgiz, Moscow, 1962.

90. Shvets, I. T., and Dyban, Ye. P., Vozdushnoye okhlazhdeniye rotorov gazovykh turbin /Air Cooling of Gas Turbine Rotors/, Kiev State University imeni T. G. Shevchenko, Kiev, 1960.

91. Shvets, I. T. et al., in the book: Trudy I Respublikanskoy konferentsii po aerogidromekhanike, teploobmenu i massoobmenu /Transactions of the First Republican Conference on Aerohydromechanics, Heat Transfer, and Mass Transfer/, KGU, Kiev, 1969.

92. Sherstyuk, A. N., in the book: Trudy MEI, No. 47, Gosenergoizdat, Moscow, 1963.

93. Shpet, N. G., "Investigation of Air Cooling Systems of Multistage Rotors of Gas Power Turbines," Candidate's Degree Dissertation, ITTF AN UkSSR, Kiev, 1965.

94. Shustorovich, L. A., Energomashinostroyeniye, 11, (1963).

95. ibid., 10, (1965).

96. Ekkert, E. R., and Drake, R. M., Teoriya teplo- i massoobmena /Theory of Heat and Mass Transfer/, Gosenergoizdat, Moscow-Leningrad, 1961.

97. Epik, E. Ya., "Effect of Turbulence of Air Flow on Heat Transfer in Initial Ducting Section," Candidate's Degree Dissertation, ITTF AN UkSSR, Kiev, 1967.

98. Grun, M., MTZ, 9, (1965).

99. Dettmering, W., B.W.K. 8/18, (1966).

100. "Low-Power BMW-6002 Gas Turbine," MTZ, 6, (1959).

101. Due, H. E., Trans. ASME 88A/2, (1966).

102. Egli, H., Preprint SAE 1-157, presented at a meeting of the Metropolitan Section of SAE, 10 March 1959.

103. "Development of a Deutz Gas Turbine," MTZ, 6, (1959).

104. "125 kW Gas Turbine -- the Allen Sonst-Gas Turbine," MTZ, 12, (1959).

105. Jaburek, F., Osterreichische Ingenieur-Archiv 7/3, (1953).

106. Jaggi, H., MTZ, 5, (1961).

107. Judge, A. W., Small Gas Turbines and Free Piston Engines, London, 1960.

108. Katsanis, T., Trans. ASME 88A/2, (1966).

109. Kres, H., MTZ, 9, (1960).

110. Leist, K., MTZ, 6-7, (1969).

111. Nill, B., MTZ, 10, (1968).

112. Penny, Noel, SAE Trans. 72, (1964).

113. Nuell, W., MTZ, 6, (1959).

114. Oberlander, G., MTZ, 10, (1964).

115. Patrick, E. N., and Smith, K. D., ASME Paper 54-A-245.

116. Kress, H., MTZ, 10, (1960).

117. Seban, R. A., Trans. ASME 82C/4, (1960).

118. Ruti, M., Brown Boveri Mitteilungen ; 52/3, (1965).

119. Schilhansl, M. I., J. Eng'g for Power [no date given].

120. "Efficient exhaust gas turbine charging, 50-700 HP," MTZ, 6, (1959).